Annual Report

Leibniz-Institut für Kristallzüchtung

im Forschungsverbund Berlin e.V.

2016

Annual Report

Leibniz-Institut für Kristallzüchtung

im Forschungsverbund Berlin e.V.

2016

Preface

Liebe Leserinnen und Leser, liebe Kolleginnen und Kollegen,

in diesem Bericht finden Sie einen Überblick über die wichtigsten wissenschaftlichen und technologischen Ergebnisse des Jahres 2016 der Abteilungen und Gruppen am IKZ. Ein Highlight des vergangenen Jahres sind die Ergebnisse zur Züchtung von Aluminiumnitrid-Einkristallen mit hoher struktureller Qualität. Sie sind die Voraussetzung für spezielle Anwendungen, die mit weniger perfektem Material schlicht nicht möglich wären. Dank der am IKZ entwickelten Züchtungsmethode entstehen Aluminiumnitrid-Kristalle mit weltweit einzigartiger Transparenz im UV-Bereich, die für Leuchtdioden, beispielsweise zur Wasser- oder Luftdesinfektion, benötigt werden.

Die Kristalle des IKZ sind die Grundlage für die Entwicklung neuer Technologien und ermöglichen Innovationen. Sie stehen am Anfang der Wertschöpfungskette und der daran anschließenden Forschungsaktivitäten. Von besonderer Bedeutung ist daher die Vernetzung mit Partnern aus Forschung und Industrie. Über die Projektarbeit hinaus tauschten sich Wissenschaftler und Vertreter aus der Wirtschaft 2016 in Workshops zu verschiedenen Themen aus. Im September diskutierten sie unter anderem über die Herstellung und Anwendung von Galliumoxid und die Chancen des Halbleitermaterials für das neue Forschungsfeld Oxidelektronik. Bislang wurden diesbezüglich grundlegende Forschungsarbeiten durchgeführt, die zu ersten Demonstratoren und Bauelementen weiterentwickelt wurden und damit einen weiteren Schritt in Richtung Anwendung gehen. Das Institut ist mit diesen Arbeiten auch in den 2016 gestarteten Leibniz WissenschaftsCampus GraFOx – Growth and fundamentals of oxides for electronic applications eingebunden. Das umfassende Know-how des IKZ, von der Züchtung der Substratkristalle über die Abscheidung kristalliner Schichten bis hin zur Charakterisierung, wird in den Forschungshighlights der jeweiligen Abteilungen beschrieben.

Auch 2016 war die Züchtung von hochperfekten Kristallen für die Neudefinition der Avogadro-Konstante und damit auch des Kilogramm ein wichtiges Thema für das IKZ. Mit dem Aufbau einer Reinigungs- und Züchtungstechnologie hat das Institut zudem die Voraussetzungen für die Züchtung von (isotopenangereichertem) Germanium geschaffen. Diese Arbeiten sollen in Zukunft helfen, die Natur und Eigenschaften von Neutrinos zu bestimmen, die bis heute noch nicht vollständig erforscht sind. Auch hier ist die kristalline Qualität ein entscheidender Faktor.

Eine besonders erfreuliche Nachricht für uns ist, dass der Aufbau des Zentrums für Lasermaterialien am IKZ in 2016 bewilligt wurde, mit dem Lasermaterialien künftig umfassend erforscht werden können. Dieser Bereich wird damit weiter an Bedeutung gewinnen – mit dem Potenzial, eine tragende Rolle der Forschung am IKZ einzunehmen.

Diese erfreulichen Ergebnisse wären ohne die engagierte Arbeit aller Mitarbeiterinnen und Mitarbeiter nicht möglich, Ihnen gilt mein besonderer Dank. Ebenso möchte ich mich beim Land Berlin und dem Bund bedanken, die mit ihren Zuwendungen und den Förderprogrammen die Forschung des Instituts ermöglichen.

Ich wünsche Ihnen eine unterhaltsame Lektüre,

Ihr

Günther Tränkle

Preface

Dear readers, dear colleagues,

in this report you will find an overview of the most important scientific and technological results of the year 2016 for the departments and groups at IKZ. One highlight of the past year has been the growth of high structural quality aluminium nitride single crystals. They are the prerequisite for special applications that would simply not be possible with less perfect material. The growth technology for aluminium nitride, developed at IKZ, allows us to prepare crystals with worldwide unique transparency in the UV range for light emitting diodes, needed for example for water or air disinfection.

The crystals of the IKZ are literally the basis for the development of new technologies and enable innovations. They are at the beginning of the value-added chain and the subsequent research activities. Therefore, networking with partners from research and industry is particularly important. In addition to the project work, scientists and company representatives exchanged views in workshops on various topics in 2016. In September, they discussed the production and application of gallium oxide and the opportunities of semiconductor materials for the new research field of oxide electronics. To date, fundamental research has been carried out in this respect, which has been developed into the first demonstrators and components, thus taking a further step towards application. The Institute is also involved in the Leibniz WissenschaftsCampus GraFOx – Growth and fundamentals of oxides for electronic applications, which has been launched in 2016. The comprehensive know-how of the IKZ, from growth of the substrate crystals to deposition of crystalline layers and characterization, is described in the research highlights of the respective departments.

In 2016, the growing of highly perfect crystals for the redefinition of the Avogadro constant and thus also the kilogram measure has been an important topic for the IKZ. With the development of a purification and growth technology, the institute has established the prerequisites for the growth of (isotope-enriched) germanium. In the future, this work will help to determine the nature and properties of neutrinos that have not yet been fully understood. Crystalline quality is also a decisive factor here.

We are particularly pleased to have received the approval to set up the Center for Laser Materials at the IKZ in 2016, which will enable us to carry out comprehensive research into laser materials in the future. This area will thus continue to gain in importance – with the potential to play a major role in research at the IKZ.

These encouraging results would not have been possible without the dedicated work of all our employees, and I wish to thank you for your commitment. I would also like to thank the State of Berlin and the Federal Government, whose grants and funding programs enable the Institute's research.

I wish you an enjoyable reading,

Yours sincerely,

Günther Tränkle

Content

The Institute

Foto: Lothar M. Peter

Leibniz-Institut für Kristallzüchtung im Forschungsverbund Berlin e.V.

FOUNDED 1992
PART of Forschungsverbund Berlin e.V.
MEMBER of the Leibniz Association

STAFF	110
Scientists	47 (external funding: 18)
Ph.D. students	16 (external funding: 8)
Technicians	45 (external funding: 15)
Trainees	2
BUDGET 2016	13.4 Mio €
Basic funding	10.4 Mio €
Third-party funding	3.0 Mio €

The Institute

Das Leibniz-Institut für Kristallzüchtung (IKZ)

ist eine in Europa einzigartige Forschungs- und Service-Einrichtung, die sich experimentell und theoretisch mit den wissenschaftlich-technischen Grundlagen des Wachstums, der Züchtung, der Bearbeitung und der physikalisch-chemischen Charakterisierung von kristallinen Festkörpern beschäftigt. Dies reicht von der Grundlagenforschung bis hin zum Vorfeld industrieller Entwicklung. Die zurzeit entwickelten Materialien finden vorwiegend Verwendung in der Mikro-, Opto- und Leistungselektronik, der Photovoltaik, in Optik und Lasertechnik, in der Sensorik und Akustoelektronik. Das Forschungsgebiet des IKZ umfasst Volumenkristalle, kristalline Schichten und Nanostrukturen sowie die Entwicklung von materialübergreifenden Kristallzüchtungstechnologien.

Arbeitsschwerpunkte des Institutes sind:

- *Entwicklung von Züchtungs-, Bearbeitungs- und Charakterisierungsverfahren für Massivkristalle sowie kristalline Gebilde mit Abmessungen im Mikro- und Nanometerbereich sowie von materialübergreifenden Kristallzüchtungstechnologien*
- *Bereitstellung von Kristallen mit besonderen Spezifikationen für Forschungs- und Entwicklungszwecke*
- *Modellierung und Erforschung der Kristallwachstums- und Kristallzüchtungsprozesse*
- *Experimentelle und theoretische Untersuchungen zum Einfluss von Prozessparametern auf Kristallzüchtungsvorgänge und Kristallqualität*
- *Erforschung von Verfahren zur Kristallbearbeitung und der dabei ablaufenden Vorgänge*
- *Physikalisch-chemische Charakterisierung kristalliner Festkörper und Entwicklung geeigneter Methoden bis hin zur atomaren Ebene; Aufklärung des Zusammenhangs zwischen Struktur und Eigenschaften kristalliner Materialien*
- *Entwicklung und Bau von Anlagenkomponenten für die Züchtung, Bearbeitung und Charakterisierung von Kristallen*

Als Züchtungsverfahren werden Methoden der Züchtung aus der Schmelze, aus der Lösung, aus der Gasphase und davon abgeleitete Verfahren zur Herstellung kristalliner Schichten verwendet.

Durch die mögliche Synergie zwischen Volumenkristallzüchtung und der Abscheidung von Schichten verfügt das Institut über ideale Voraussetzung zur Herstellung von Substrat/Schicht-Kombinationen mit maßgeschneiderten Eigenschaften.

Materialien

- *Halbleiter mit großem Bandabstand (Oxide, Aluminiumnitrid) für Hochtemperatur-, Leistungs- und Optoelektronik*
- *Oxidische und fluoridische Kristalle für Lasertechnik, Optik, Sensorik und Akustoelektronik*
- *Silizium-Kristalle für Mikro- und Leistungselektronik und Photovoltaik*
- *Silizium/Germanium Kristalle für Strahlungsdetektoren und Beugungsgitter, kristalline Si/Ge-Schichten für thermoelektrische Anwendungen*
- *Silizium Schichten auf amorphen Unterlagen für die Photovoltaik*
- *Ferroelektrische und halbleitende Oxidschichten für die Mikro- und Leistungselektronik, Sensoren und Datenspeicher*

The Leibniz Institute for Crystal Growth

is a unique research and service institute in Europe, which is theoretically and experimentally investigating the scientific-technical fundamentals of crystal growth, processing and physico-chemical characterisation of crystalline solids. This ranges from explorative fundamental research to pre-industrial development. The materials presently in development are of fundamental importance in micro-, opto- and power electronics, in photovoltaics, in opto- and laser technology, in acousto-electronics and sensor technology as well as for fundamental research. The research activities of the institute include bulk single crystals as well as crystalline layers and nanostructures, but also the development of comprehensive crystal growth technologies.

The research and service tasks of the institute include:

- Development of technologies for growth, processing and characterization of bulk crystals and of crystalline structures with dimensions in the micro- and nanometer range and of comprehensive growth technologies
- Supply of crystals with non-standard specifications for research and development purposes
- Modelling and investigation of crystal growth processes
- Experimental and theoretical investigations of the influence of process parameters on crystal growth processes and crystal quality
- Development of technologies for the chemo-mechanical processing of crystalline samples and scientific investigation of related processes

The Institute

- Physico-chemical characterisation of crystalline solids and development of suitable methods; investigation of the correlation between crystalline structures and properties
- Development and construction of components for growth, processing and characterization of crystals

Crystals are grown from the melt, from solutions and from the vapour phase and new techniques are developed and improved for the preparation of crystalline layers.

With the combination of bulk crystal growth and layer deposition, the institute possesses ideal conditions to produce customized substrate/layer-combinations.

Materials presently in development:

- Wide band gap semiconductors (aluminium nitride, oxides) for high temperature, power- and opto-electronics
- Oxide and fluoride crystals for acousto-electronics, laser-, opto- and sensor technology
- Silicon for micro and power electronics and photovoltaics
- Gallium arsenide for wireless communication and in high-frequency technology
- Silicon/germanium-crystals for radiation detectors and diffraction gratings, crystalline Si/Ge layers for thermoelectric devices
- Silicon layers an amorphous substrates for photovoltaics
- Ferroelectric and semiconducting oxide layers for micro and power electronics, sensor applications or data storage

Organisation Chart/Organigramm

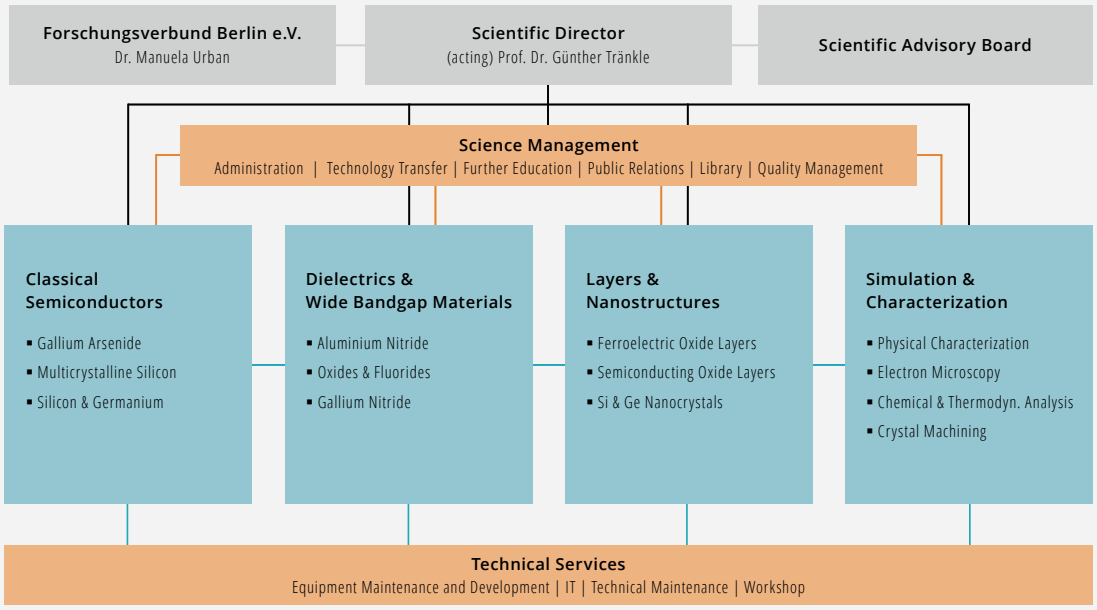

The Institute

Scientific Advisory Board 2016
Wissenschaftlicher Beirat 2016

apl. Prof. Dr.-Ing. Michael Heuken (chair)
Faculty of Electrical Engineering and Information Technology,
RWTH Aachen University & Vice President of Research and Development AIXTRON SE, Aachen

Dr. Lothar Ackermann
Forschungsinstitut für mineralische und metallische Werkstoffe, Edelsteine/Edelmetalle – FEE GmbH, Idar-Oberstein

Dr. Hubert Aulich
SC Sustainable Concepts GmbH, Erfurt

Prof. Dr. Saskia Fischer (vice chair)
Department of Physics, Humboldt-Universität zu Berlin

Prof. Dr. Michael Kneissl
Institute of Solid State Physics, Technische Universität Berlin

Prof. Dr. Götz Seibold
Brandenburgische Technische Universität Cottbus-Senftenberg

Dr. Ulrich Steegmüller
Head of Research and Technology OSRAM Opto Semiconductors GmbH, Regensburg

Representative of the State of Berlin

Marie Trappiel
Senatsverwaltung für Wirtschaft, Technologie und Forschung, SenWTF Berlin

Representative of the Federal Republic

Dr. Anne Parge
Bundesministerium für Bildung und Forschung, BMBF Bonn / Berlin

Guest

Dr. Manuela Urban
Forschungsverbund Berlin e.V.

Events

IKZ Sommerschule 2016

Die seit nunmehr 9 Jahren fest etablierte, jährlich stattfindende IKZ-Sommerschule wurde in diesem Jahr vom 12. – 14. Oktober 2016 abgehalten. Als internationaler Experte referierte Herr Prof. Elias Vlieg vom Institut für Moleküle und Materialien der Radboud Universität in Nijmegen (Niederlande) zum Thema: „Kristallwachstum im atomaren Maßstab verstehen".

Prof. Elias Vlieg ist vor allem im Kreis der Kristallzüchter berühmt für seine exzellenten Forschungsartikel und Konferenzvorträge. Sein didaktischer und anregender Vorlesungsstil sowie seine humorvollen Einlagen machten es zu einem Vergnügen seinen Themen zu folgen. Obwohl Prof. Vlieg eher ein Theoretiker ist, gelang es ihm auf bemerkenswerte Art und Weise den Fokus auf die Anwendungen zu legen.

Da Kristallwachstum stets an der Grenzfläche zwischen Wachstumsmedium und Kristall, d. h. demnach nahezu immer Atom an Atom stattfindet, ist es unumgänglich über Kenntnisse der atomaren Prozesse und Strukturen an der Grenzfläche zu verfügen. Nur so ist es möglich, ein Verständnis über das Kristallwachstum und eine anschließende Kontrolle der Kristalleigenschaften zu erlangen. Herr Prof. Vlieg stellte insbesondere die entscheidende Frage „Warum Kristalle wachsen?" und ging damit auf eine Reise durch den Kristall auf atomarer Ebene.

Einen Teil seiner Referate widmete Herr Prof. Vlieg dem kürzlich verstorbenen Prof. Pieter Bennema, welcher ein Spezialist auf dem Gebiet der Morphologie-Vorhersage war und 1995 mit dem Frank-Preis der Internationalen Organisation für Kristallzüchtung (IOCG) ausgezeichnet wurde.

Auch in diesem Jahr war die IKZ Sommerschule ein persönlicher Gewinn für jeden Teilnehmer, nicht zuletzt aufgrund eines äußerst talentierten Dozenten, welcher es verstand, komplexe Inhalte einfach und anschaulich, auf amüsierende Weise, darzustellen.

IKZ Summer School 2016

The IKZ Summer School has been well established now for nine years. In 2016, from 12–14 October, the internationally known expert Prof. Elias Vlieg from the Institute of Molecules and Materials of the Radboud University in Nijmegen (Netherlands) gave a lecture on "Understanding crystal growth on the atomic scale".

Prof. Elias Vlieg is well known for his excellent research articles and conference presentations, especially in the crystal growth community. His didactic and stimulating presentation style as well as his entertaining interludes made it a pleasure to follow his lecture. Although Prof. Vlieg is more of a theoretician, he managed to put the focus on applications in a remarkable way.

Since crystal growth always occurs at the interface between growth medium and the crystal, i.e. almost always atom for atom, a deep understanding of the atomic processes and structures at the interface is essential. This understanding provides the basis for crystal growth and allows to control the growth process as well as the crystal properties, eventually.

Prof. Vlieg dedicated a part of his lecture to the late Prof. Pieter Bennema, an expert in the field of morphology prediction, who was awarded the Frank Prize of the International Organization for Crystal Growth (IOCG) in 1995.

This year again, the Summer School was a personal gain for every participant, not least because of this outstanding lecturer, who was able to present complex content in an amusing, simple and intuitive way.

Events

Das IKZ als familienfreundlicher Arbeitgeber

Das IKZ möchte seinen Beschäftigten ein offenes, kooperatives und familienfreundliches Arbeitsumfeld bieten. Das Institut unterstützt daher seine Mitarbeiterinnen und Mitarbeiter bei der Vereinbarkeit von Arbeit und Familie, z.B. durch flexible Regelungen zur täglichen Arbeitszeit oder durch variable Regelungen zu Teil- und Vollzeitbeschäftigung.

Seit 2015 ist das Institut zertifiziert durch das audit berufundfamilie. Damit verbunden hat es Ziele einer familienbewussten Personalpolitik definiert und sich verpflichtet, entsprechende Maßnahmen in den nächsten drei Jahren umzusetzen und weiterzuentwickeln. Das audit steht unter der Schirmherrschaft der Bundesfamilienministerin und des Bundeswirtschaftsministers, nähere Informationen finden sich unter www.beruf-und-familie.de

IKZ as family-friendly employer

The institute intends to create a co-operative and open working environment for all employees. It places special emphasis on the reconcilability of job and family, offering flexible working time models as well as full or part-time employments. In 2015, the institute has been awarded the audit berufundfamilie certificate for its family-friendly human resources policy. The objectives defined in this process will be implemented in the next three years.

The certificate is issues under the auspices of the German Federal Minister for Families and the German Federal Economics Minister. More information is available under www.beruf-und-familie.de

Zertifikat seit 2015
audit berufundfamilie

Girl's Day 2016

2016 bot das IKZ interessierten Schülerinnen erneut die Möglichkeit, sich über die verschiedenen Berufsbilder im Bereich der Kristallzüchtung zu informieren. Wissenschaftlerinnen und Wissenschaftler, sowie wissenschaftliche-technische Mitarbeiterinnen und Mitarbeiter gaben den Schülerinnen einen Einblick in unsere Forschungsaktivitäten und die Arbeit am Institut. Die Teilnehmerinnen besuchten unsere Züchtungshalle und konnten sich selbst in kleinem Maßstab als Kristallzüchterinnen versuchen.

Girl's Day 2016

In 2016, the IKZ once again offered interested schoolgirls the opportunity to find out more about the different professions in crystal growth. Scientists and members of the scientific-technical staff gave the students an insight into our research activities and the work at the institute. The participants visited our crystal growth hall and were able to pull a lab scale crystal out of the melt themselves.

Events

5. Deutsch-Französischer Oxid-, Dielektrika- und Laserkristall-Workshop 2016

Das jährliche Treffen des DGKK-Arbeitskreises „Kristalle für Laser und Nichtlineare Optik" mit den französischen Kolleginnen und Kollegen wurde 2016 von Prof. M. Bickermann am IKZ organisiert. Über 40 Teilnehmer aus Deutschland, Frankreich, Tschechien, Schweden, Polen, Italien und China nutzten den Workshop für den fachlichen Austausch und die Vernetzung von Forschung und Industrie.

Die Palette an Materialien umfasste Kristalle für optische und Szintillatoranwendungen sowie Ferroelektrika und Supraleiter. Die Themen im Workshop reichten von der Herstellung und kontrollierten Dotierung von Volumenkristallen, der Bestimmung der strukturellen, physikalischen und optischen Eigenschaften solcher Kristalle bis hin zur Herstellung und Charakterisierung von Wellenleitern und Lasereigenschaften. Aspekte der Grundlagenforschung wurden in den Vorträgen von L. Schmack (IKZ) über die Bestimmung des Phasendiagramms von $LiNbO_3$-$LiTaO_3$ oder von S. Schwung (FEE) über Lumineszenzübergänge in seltenend-dotierten Einkristallen adressiert. Anwendungsorientierte Vorträge kamen z. B. von A. Sottile (Univ. Pisa, Italien) über Pr^{3+}-dotierte Faserlaser und M. Klejch (Crytur) zur kommerziellen Züchtung von Bleiwolframat für Kalorimeter in der Teilchenphysik. Als Highlight kann auch der Vortrag von P. Leisching (Toptica Photonics) gelten, der die Schwierigkeiten und Perspektiven der Nutzung neuer Materialien in der kommerziellen Anwendung ausführlich beleuchtet hat.

5th Franco-German Oxide, Dielectrics and Laser Crystal Workshop 2016

In 2016, the annual meeting of the DGKK working group "Crystals for Laser and Nonlinear Optics" with its French colleagues had been organised by Prof. M. Bickermann at the IKZ. More than 40 participants from Germany, France, the Czech Republic, Sweden, Poland, Italy and China took advantage of the workshop to exchange expertise as well as network research and industry.

The range of materials included crystals for optical and scintillator applications as well as ferroelectrics and superconductors. The topics covered in the workshop ranged from growth and controlled doping of solid crystals, determination of the structural, physical and optical properties of such crystals to the production and characterization of waveguides and laser properties. Aspects of basic research were addressed in the lectures given by L. Schmack (IKZ) on the determination of the phase diagram of $LiNbO_3$-$LiTaO_3$ or of S. Schwung (FEE) on luminescence transitions in rarely doped single crystals. Application-oriented presentations were given by A. Sottile (Univ. Pisa, Italy) via Pr^{3+}-doped fiber lasers and M. Klejch (Crytur) for the commercial cultivation of lead tungsten for calorimeters in particle physics. One of the highlight of the workshop was the presentation by P. Leisching (Toptica Photonics), who gave a detailed insight into the difficulties and perspectives of using new materials in commercial applications.

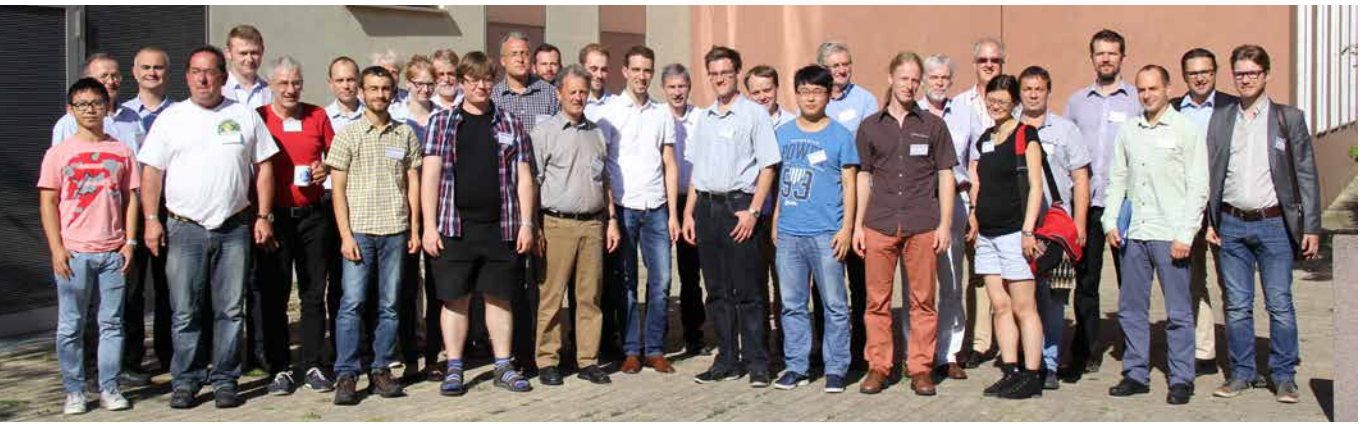

Events

Deutsch-Japanisches Galliumoxid-Technologie-treffen 2016

Vom 7. – 9. September 2016 veranstaltete das IKZ ein internationales Expertentreffen zur Technologie des neuen Halbleitermaterials Galliumoxid (β-Ga_2O_3). Knapp 40 Wissenschaftler und Technologen aus den führenden einschlägigen Forschungsinstituten und Industrieunternehmen waren zusammengekommen, um über den aktuellen Status sowie die anwendungsorientierten Perspektiven der Materialherstellung, Epitaxie, Charakterisierung und der Bauelementtechnologie von Galliumoxid zu diskutieren.

Das IKZ erforscht sowohl die Herstellung von Galliumoxid-Kristallen als auch von Epitaxieschichten auf diesen Kristallen im Rahmen des Leibniz-WissenschaftsCampus „Growth and Fundamentals of Oxides for Electronic Applications (GraFOx)". Diese Aktivitäten werden in diesem Jahresbericht an anderer Stelle ausführlich beschrieben. Das Material ist aufgrund der hohen Bandlücke und der Verfügbarkeit großer Kristalle ein vielversprechender Kandidat für die Leistungselektronik (z.B. Leistungskonverter bei 600 V und 1200 V) und kann dort – potentiell noch besser als Siliciumcarbid oder Galliumnitrid – zur weiteren Miniaturisierung und Effizienzsteigerung beitragen.

Ziel des Expertentreffens war es, die anwendungsorientierten Aktivitäten zu stärken, sowie die Vernetzung mit Industriepartnern. Vortragende aus Japan, den USA und Deutschland berichteten über verschiedene Methoden zur Kristallzüchtung des Substratmaterials oder zur Abscheidung von kristallinen Schichten, sowie über geeignete Charakterisierungsmethoden. Vertreter von Infineon und dem Ferdinand-Braun-Institut stellten den Status und die Perspektiven des konkurrierenden Halbleitermaterials Galliumnitrid vor. Schließlich stellten die Galliumoxid-basierten Bauelement-Demonstratoren der Cornell Universität (USA), des Air Force Research Laboratory (USA), und dem National Institute of Information and Communications Technology (Japan) die Stärken und Möglichkeiten des neuen Materials in den Fokus.

Die vorgestellten ersten Ergebnisse waren für alle Teilnehmer sehr ermutigend und das Expertentreffen wurde von den Anwesenden als voller Erfolg und als wichtiger Schritt zur Anwendung von Galliumoxid bezeichnet. Es darf mit Spannung in die Zukunft dieses neuen Materials geblickt werden.

German-Japanese Gallium Oxide Technology Meeting 2016

From September 7–9 2016, IKZ hosted an international expert meeting on gallium oxide technology. Nearly 40 scientists and technologists from the leading research institutes and industrial companies came to discuss the current status and application-oriented perspectives of material preparation, epitaxy, characterization and device technology of this new semiconductor.

In the frame of the Leibniz ScienceCampus GraFOx – Growth and Fundamentals of Oxides for Electronic Applications – the IKZ investigates the growth of gallium oxides single crystals as well as epitaxy of crystalline layers. These activities will be described in more detail later in this annual report. Due to the large band gap and the availability of large crystals, gallium oxide is a promising candidate for power electronics (e.g. power converters at 600 V and 1200 V) and could contribute – probably even better than silicon carbide or gallium nitride – to further miniaturization and efficiency increase.

The aim of this expert meeting was to strengthen application-oriented activities as well as networking with industrial partners. Lecturers from Japan, USA and Germany presented different crystal growth methods for bulk material or the deposition of crystalline layers as well as characterization techniques. Representatives from Infineon and the Ferdinand-Braun-Institut presented the status and prospects of the competing semiconductor material gallium nitride. Finally, the gallium oxide based device demonstrators of Cornell University (USA), the Air Force Research Laboratory (USA) and the National Institute of Information and Communication Technology (Japan) focused on the advantages and the potential of this new material.

The first results presented were very encouraging for all participants and the meeting was described by those present as a success and an important step towards the application of gallium oxide. We can look forward to the further development of this interesting material.

Highlight

M. Bickermann, K. Irmscher

Die Herstellung von UV-transparenten Aluminiumnitrid-Substraten

Der Siegeszug der LED-Beleuchtung im privaten und gewerblichen Bereich, der sich in den letzten Jahren vollzogen hat, wurde erst durch die Massenfertigung von Galliumnitrid-basierten LEDs möglich. Bei diesen LEDs handelt es sich um eine der wichtigsten neueren Entwicklungen auf dem Gebiet der Halbleitertechnik. Neben der erheblichen Energieeinsparung besticht die LED durch einen nutzerfreundlichen Betrieb (Versorgung mit Niedrigspannung, sofort volle Lichtleistung, lange Lebensdauer), ein stoßfestes Gehäuse, die punktförmige Abstrahlung und die Lichtqualität. Deshalb ist es naheliegend, LED-Strahler auch für den ultravioletten (UV) Wellenlängenbereich zu entwickeln.

Ein Forschungsthema am IKZ ist die Herstellung von AlN-Substraten, die für optoelektronische Bauelemente (LEDs, Laser, Sensoren) im tiefen Ultraviolett (UVC-Bereich) bei 220–300 nm genutzt werden. Dieser Wellenlängenbereich ist besonders interessant für die Wasserreinigung und die Luftdesinfektion. Diese Anwendungen stellen bereits heute einen beachtlichen kommerziellen Markt dar, bislang werden hier Gasentladungs- und Lichtbogenlampen eingesetzt. Aber auch die Detektion chemischer Substanzen (z.B. NO oder NH_3 im Abgas, Aminosäuren in der Luft oder Verunreinigungsspuren in aufbereitetem Wasser), die Flammendetektion oder die optische Nahkommunikation sind potentielle Anwendungsfelder für UVC-LEDs [1]. Dazu müssen jedoch AlN-Substrate mit den geforderten Eigenschaften zur Verfügung stehen. AlN ist ein Halbleitermaterial, deshalb werden wesentliche Eigenschaften von Punktdefekten und Verunreinigungen bestimmt.

UVC-LEDs sind aus $Al_xGa_{1-x}N$-Epitaxieschichten aufgebaut. Mit einem steigenden Aluminiumgehalt in diesen Schichten steigt auch die Bandlücke von 3.4 eV (GaN) bis auf etwa 6.0 eV (AlN) an. Gleichzeitig sinkt die Emissions-/Detektionswellenlänge von 360 nm auf etwa 210 nm. Somit sind AlN-Substrate insbesondere wichtig für $Al_xGa_{1-x}N$-Schichten mit hohem Al-Gehalt. Ihr Einsatz führt neben der hohen Wärmeleitfähigkeit und chemischen Kompatibilität des Substrats auch zu einer hohen strukturellen Qualität und Rissfreiheit der Epitaxieschicht aufgrund der geringen kompressiven Verspannung als Resultat der verbleibenden Gitterfehlpassung.

Preparation of deep-UV transparent aluminum nitride (AlN) substrates

The "lighting revolution", i.e. the pervasive use of LED lighting during the last years, is the result of one of the recent, most disruptive inventions in semiconductor technology, the invention of gallium nitride based LEDs. Notwithstanding the great contributions in energy saving, also low voltage, instant-on and long lifetime operation, small size, rugged design as well as point source behavior and light quality are associated with LED lighting. What would be more intriguing than to apply LED lighting also in the UV wavelength domain?

The IKZ works on the preparation of AlN substrates to be used for deep-UV optoelectronic devices (e.g. LEDs, lasers, sensors) in the 220–300 nm wavelength range. Such wavelengths are particularly important for water purification and air disinfection, a quite considerable business, as well as chemical sensing (e.g. NO or NH_3 in exhaust gases, amino acids, ions in water), solar-blind flame detection and near-field communications. The advantages of LEDs as detailed above are also a main driver for replacing existing gas discharge and arc lamps in those applications [1]. For this, providing AlN substrates with suitable properties is a key prerequisite. As in every semiconductor, these properties strongly depend on the point defects and impurities in the material as shown below.

Deep-UV optoelectronic devices consist of multiple $Al_xGa_{1-x}N$ epilayers. With increasing Al content in the $Al_xGa_{1-x}N$ active layers such as quantum wells, the band-gap can be tuned from 3.4 eV (GaN) to about 6.0 eV (AlN), which corresponds to emission/detection wavelengths from 360 nm to 210 nm, respectively. Realization of deep-UV emitters that feature $Al_xGa_{1-x}N$ layers with high Al content would strongly benefit from the use of AlN single-crystalline substrates due to their high structural quality, high thermal conductivity, chemical compatibility, and a lattice mismatch yielding compressively strained layers resistant to cracking.

Highlight

Trotzdem nutzen die meisten kommerziellen Anbieter Saphirsubstrate und nehmen dabei eine hohe Dichte an Strukturdefekten in den Bauelementschichten – und damit auch eine niedrige Quanteneffizienz – in Kauf. Denn AlN-Substrate sind aufgrund des noch nicht ausreichend gut verstandenen und beherrschten Herstellungsverfahrens teuer, klein und auch nicht ohne weiteres kommerziell verfügbar. Doch auch die mangelnde optische Transmission bei der Einsatzwellenlänge ist ein großes Problem. Das LED-Licht muss nämlich durch das Substrat hindurch geleitet werden, da die auf der anderen Seite liegende p-leitende $Al_xGa_{1-x}N$-Kontaktschicht das UVC-Licht stark absorbiert und der LED-Aufbau in seiner Stapelreihenfolge nicht ohne weiteres änderbar ist.

Aufgrund der hohen Bandlücke sollte AlN das in der aktiven $Al_xGa_{1-x}N$-Schicht generierte UVC-Licht durchlassen, wie das auch im Saphirsubstrat der Fall ist. Doch erzeugen Punktdefekte (z.B. Verunreinigungen oder Leerstellen im Kristallgitter) elektronische Übergänge in der Bandlücke, die das UVC-Licht absorbieren. Die resultierende optische Absorption kann man einfach messen, aber die Identifikation der zugrundeliegenden Punktdefekte ist nicht auf direktem Wege möglich und daher schwierig. Im Folgenden berichten wir über die Fortschritte, die wir beim Verständnis der UVC-Absorption in AlN erzielen konnten. Dadurch, und mit Hilfe einer verbesserten Kontrolle des Einbaus von Verunreinigungen während der AlN-Kristallzüchtung, können wir „UVC-transparente" und damit für die UVC-Optoelektronik besonders geeignete AlN-Kristalle und -Substrate herstellen.

Punktdefekte und optische Absorption von AlN

AlN-Volumenkristalle werden mittels physikalischem Gasphasentransport (PVT) bei Temperaturen von mehr als 2000°C hergestellt [2]. Am IKZ werden AlN-Kristalle mit hoher struktureller Qualität und niedriger Versetzungsdichte gezüchtet [3]. Jedoch gelangen Verunreinigungen aus dem Züchtungsaufbau, dem Ausgangsmaterial und der Gasatmosphäre während der Züchtung in den wachsenden Kristall. Bei unserem Züchtungsprozess werden Sauerstoff und Kohlenstoff in Konzentrationen zwischen 10^{18} cm^{-3} und 10^{19} cm^{-3}, Silizium in Konzentrationen von einigen 10^{16} cm^{-3} eingebaut.

Sauerstoff wird auf dem Stickstoffplatz im AlN-Kristallgitter eingebaut. Während Sauerstoff in GaN elektrisch als flacher Donator auftritt, bildet sich in AlN ein sogenanntes DX-Zentrum aus, das ein weiteres Elektron von einem benachbarten Sauerstoffatom (oder einer anderen Verunreinigung) aufnimmt [4] und so die Leitfähigkeit in AlN drastisch reduziert. Wie bei jeder Störstelle gibt es auch hier eine Aktivierungsenergie, mit der das Sauerstoffatom in den flachen Donator-Zustand gebracht werden kann.

However, still many companies use sapphire substrates as the basis of their devices, even if the resulting high concentration of structural defects in the active layers limit their quantum efficiency. The main reasons are the remaining challenges in AlN crystal growth and the accompanying issues of price and availability of AlN substrates. But another considerable problem is the optical transmittance of the substrate. The stacking order of the epilayers is fixed due to issues in nitride epitaxy, and with the nontransparent p-type $Al_xGa_{1-x}N$ contact on top, the light outcoupling must happen through the substrate.

Due to its high band-gap energy, AlN should be transparent to deep-UV light just as sapphire. But point defects (e.g., impurities or vacancies) provide transition levels in the band-gap that may lead to optical absorption at the desired emission/detection wavelength. While optical absorption measurements are straightforward, the nature of the causative defects is often difficult to identify. In the following, we report on our progress of understanding deep-UV absorption in AlN. In conjunction with advances in the control of impurity incorporation during crystal growth, we were able to develop "deep-UV transparent" AlN crystals and substrates for beneficial use in deep-UV optoelectronics.

Point defects and optical absorption in AlN

AlN bulk single crystals are grown by physical vapor transport (PVT), a sublimation-recondensation technique, at temperatures above 2000°C [2]. AlN crystals grown at IKZ show high structural perfection and low dislocation densities [3]. However, during growth impurities from the growth set-up, the starting material, and the gas atmosphere are incorporated in the growing crystals. In our process, the resulting concentrations in the crystals are in the 10^{18}–10^{19} cm^{-3} range for oxygen and carbon and in the 10^{16}–10^{17} cm^{-3} range for silicon.

Oxygen is incorporated on the nitrogen site in the lattice. In contrast to GaN where it behaves like a normal shallow donor, it forms a so-called *DX* center in AlN. As such, it captures the electron of a second oxygen atom or other (shallower) donors [4], effectively reducing the electrical conductivity in AlN. As for any trap, there is an energetic barrier for letting the oxygen revert to a shallow donor state. Temperature-dependent measurements of the free carrier absorption in the near infrared range (see Fig. 1a) yielded activation energies in the range of 0.5–1.0 eV in oxygen dominated samples, in accordance to theoretical calculations.

Highlight

Durch temperaturabhängige Messungen der Absorption freier Ladungsträger im nahen Infrarot (siehe Abb. 1a) wurde die Aktivierungsenergie zu 0,5–1,0 eV bestimmt, in Übereinstimmung mit ab-initio-Modellrechnungen. Silizium wird gezielt zugegeben (dotiert), um n-leitfähige $Al_xGa_{1-x}N$-Schichten zu erhalten. Bei sehr hohem Al-Gehalt (> 85%) steigt die Aktivierungsenergie des Siliziumdonators jedoch stark an. In Modellrechnungen sagen die Bildung eines DX-Zentrums mit einem Umladungsniveau 0,15–0,4 eV unterhalb der Leitungsbandkante voraus [4,5]. Es ist aber genauso gut möglich, das Silizium als flacher Donator von Verunreinigungen (Sauerstoff, Kohlenstoff) oder durch die Bildung von Stickstoffleerstellen elektrisch kompensiert wird. Jedenfalls zeigen siliziumdotierte AlN-Proben eine deutlich höhere Restleitfähigkeit als AlN mit einem hohen Sauerstoffgehalt.

Silicon is the predominant *n*-type dopant in $Al_xGa_{1-x}N$. But for very high Al contents (> 85%), its activation energy steeply increases. Recent theoretical work tend to predict a *DX* center formation with the transition level 0.15–0.4 eV below the conduction band minimum [4,5]. But it is also possible that silicon forms shallow donors that can be compensated by oxygen, carbon, or nitrogen vacancies. Anyway, the residual *n*-type conductivity of Si-doped AlN is clearly higher than for oxygen dominated AlN.

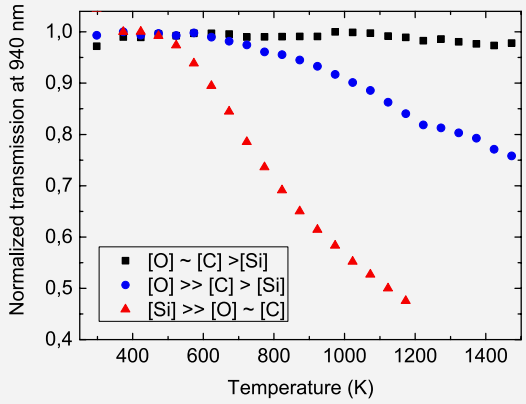

a)

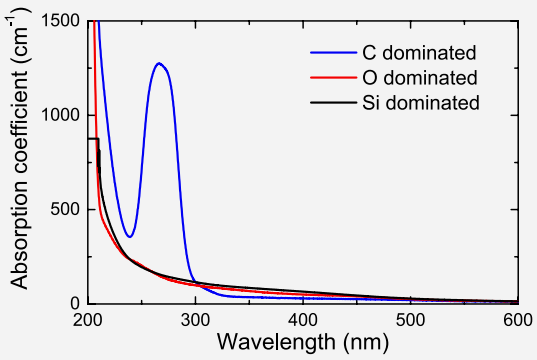

b)

Abb. 1
a) Temperaturabhängige Infrarot (IR)-Transmission von AlN-Proben mit unterschiedlichen Verunreinigungskonzentrationen. Die Abnahme der IR-Transmission wird durch die Absorption freier Ladungsträger verursacht, eine höhere Ladungsträgerkonzentration führt somit zu einer verringerten IR-Transmission.
b) Optische Absorption dieser AlN-Proben. Die kohlenstoffdominierte („C dominated") Probe zeigt eine starke UVC-Absorption bei 4,7 eV (265 nm). Weil diese Probe im blauen Wellenlängenbereich (400–500 nm) eine geringere Absorption als die beiden anderen Proben aufweist, erscheint sie dem Betrachter als farblos, während die anderen beiden Proben eine Gelbfärbung aufweisen.

Fig. 1
a) Temperature-dependent near infrared transmission of AlN samples with different concentrations of impurities. The decrease in IR transmission is caused by free carrier absorption, thus a higher carrier concentration in the sample leads to a decrease in transmission.
b) Optical absorption of the same AlN samples. The "carbon dominated" sample shows a strong deep-UV absorption peaking at about 4.7 eV (265 nm). Note that this sample has a lower optical absorption in the 400–500 nm range, thus it appears colorless by the eye, whereas the other samples appear yellowish.

Highlight

Leerstellen auf Al- oder N-Gitterplätzen (V_{Al} or V_N) können flache Donatoren in n-leitendem AlN kompensieren. Modellrechnungen zeigen, dass sich solche Leerstellen einfach bilden können [6]. Über ihre tatsächliche Konzentration in AlN-Kristallen ist nur wenig bekannt [7], das Vorhandensein von Stickstoffleerstellen V_N lässt sich in unseren Kristallen aber mittels Elektronen-Spinresonanz (EPR) eindeutig nachweisen. Andererseits könnten Aluminiumleerstellen V_{Al} leicht Komplexe mit benachbarten Sauerstoffatomen bilden. Solche Komplexe sind möglicherweise für die optische Absorption um 2,8 eV (440 nm) und damit für die Gelbtönung der AlN-Proben verantwortlich [8], der direkte Nachweis eines Zusammenhangs konnte aber bislang nicht erbracht werden.

Kohlenstoff baut sich vermutlich analog zum Sauerstoff auf N-Gitterplätzen ein. Collazo et al. [9] haben zum ersten Mal einen direkten Zusammenhang zwischen der chemischen Konzentration von Kohlenstoff und der starken UVC-Absorption bei 4,7 eV (265 nm) in ihren AlN-Kristallen gezeigt. Diese Absorption ist für einige wichtige Anwendungen kritisch, da z.B. die Desinfektion gerade bei Bestrahlung mit 265 nm am effektivsten ist. Die Absorptionsbande bei 4,7 eV ist auch in unseren Kristallen vorhanden, siehe Abb. 1b. Sie wird von Collazo et al. einem elektronischen Übergang von dem negativ geladenen Kohlenstoffatom C_N^- zu einem flachen Donator oder dem Leistungsband zugeordnet; dies haben die Autoren auch mit Modellrechnungen unterlegt [10]. Eine genauere Untersuchung der Form und der Polarisationsabhängigkeit dieser Absorptionsbande zeigt jedoch, dass mehrere Punktdefekte zur Bildung dieser Bande beitragen.

2013 haben wir gezeigt, dass das Auftreten der UVC-Absorption bei 4,7 eV immer auch zu einer Infrarotabsorption bei 1769 cm^{-1} (0.219 eV) führt. In einer AlN-Probe, die gezielt mit dem Kohlenstoffisotop ^{13}C dotiert wurde, ist die Infrarotabsorption zu einem Oktett aufgespalten. Die Position und Intensitätsverteilung der acht Banden lassen sich nur mit einer lokalen Schwingungsmode (LVM) erklären, deren harmonischen Oszillator aus exakt drei benachbarten Kohlenstoffatomen ^{12}C und/oder ^{13}C besteht [11]. Sowohl die UVC-Absorption bei 4,7 eV als auch die IR-Absorption bei 1769 cm^{-1} sind damit eindeutig dem Kohlenstoff zuzuordnen. Die "Drei-C-Anordnung" ist an der Entstehung beider Absorptionsbanden beteiligt, die Konzentration dieses Defekts sowie das Verhältnis des Anteils der Absorption zur Absorption isolierter einzelner Kohlenstoffatome C_N^- bleibt aber vorerst offen.

Vacancies on the aluminum or nitrogen site (V_{Al} or V_N) are expected to compensate shallow donors in *n*-type AlN. Well predicted to form by theory [6], not much is known about their actual concentration in PVT-grown bulk AlN [7], but at least the electron paramagnetic resonance (EPR) of V_N has been clearly evidenced in our samples. On the other hand, V_{Al} might easily form complexes with neighboring oxygen. It is assumed that such complexes contribute to the yellowish coloration of AlN by optical absorption at 2.8 eV (440 nm) [8], but direct evidence is still outstanding.

Carbon is presumably substituting for nitrogen in AlN, like oxygen. Collazo and coworkers [9] were the first to correlate the chemical concentration of carbon to a strong deep-UV absorption feature peaking at 4.7 eV (265 nm) in their AlN crystals. This absorption is most critical as major deep-UV applications such as disinfection work best with wavelengths in this range. We observe in our crystals the same absorption feature, see Fig. 1b. Collazo assigned the 4.7 eV absorption to an electron transition from negatively charged carbon atoms C_N^- to shallow donors or to the conduction band, which was later supported by theoretical calculations [10]. However, a closer inspection of the shape and polarization dependence shows that several different defects are contributing to this absorption.

In 2013, we showed that the presence of the 4.7 eV absorption is accompanied by an infrared absorption line at 1769 cm^{-1} (0.219 eV). In an AlN sample intentionally doped with ^{13}C, this absorption line splits into an octet, where the positions and intensity ratios evidence a local vibrational mode (LVM) harmonic oscillator involving exactly three carbon atoms of ^{12}C and/or ^{13}C [11]. Thus, the defect underlying absorptions at 4.7 eV as well as 1769 cm^{-1} is unambiguously related to carbon. The "tri-carbon" defect participates in both absorption features, but its concentration and effective contribution in respect to the single carbon impurity remains an open question.

Highlight

Wir haben herausgefunden, dass die Absorptionsbande bei 4,7 eV in AlN-Proben, die wesentlich mehr Sauerstoff als Kohlenstoff enthalten, nicht vorhanden ist (siehe Abb. 1b). Dasselbe Verhalten beobachten wir bei siliziumdotierten Proben, die wesentlich mehr Silizium als Kohlenstoff enthalten. Wie oben erwähnt wirken Sauerstoff und Silizium als Donatoren (selbst in einem DX-Zustand) mit Ionisierungsenergien von weniger als 1 eV bezogen auf die Leitungsbandkante. In sauerstoff- oder siliziumdominierten AlN-Proben befindet sich das Ferminiveau deshalb relativ nahe an der Leitungsbandkante. Besitzen die kohlenstoffhaltigen Punktdefekte wenigstens zwei Umladungsniveaus in der Bandlücke unterhalb dieses Ferminiveaus, dann verhindert die starke Besetzung des oberen Niveaus mit Elektronen die optische Absorption durch Elektronen aus dem unteren Niveau und damit auch die Ausbildung der UVC-Absorptionsbande bei 4,7 eV (siehe Abb. 2).

Eine entsprechende Anordnung der Umladungsniveaus wird zum Beispiel für den Defektkomplex zweier benachbarter Kohlenstoffatome (C_N-C_{Al}) vorhergesagt [9]. Dieses „Ferminiveau-Modell" haben wir auch für die „Drei-C-Anordnung" vorgeschlagen [11]. Das würde auch bedeuten, dass isolierte Kohlenstoffatome C_N- nicht wesentlich zur Absorption bei 4,7 eV beitragen, weil diese in Modellrechnungen nicht die erforderliche Abfolge der Umladungsniveaus zeigen [9, 10].

Gaddy et al. schlagen stattdessen vor, das die Bildung kompensierender Punktdefekte die kohlenstoffinduzierte Absorption aus dem UVC-Wellenlängenbereich hinausschiebt. Die Autoren geben aber auch an, dass sie Ihre Aussagen aus der Untersuchung hoch siliziumdotierter und kohlenstoffverunreinigter AlN-Proben ableiten, und dass diese Interpretation nicht unbedingt für AlN mit wesentlich geringeren Si- und C-Konzentrationen gültig sein muss, wie sie in unseren Kristallen vorliegen.

Abb. 2
Energiediagramm für AlN mit Umladungsniveaus von kohlenstoffhaltigen Defekten und den flachen Donatoren Sauerstoff und Silizium. Die Bereichsgrenzen bzw. die Lage des Ferminiveaus für kohlenstoffdominierte ([0]+[Si] < 3[C]) bzw. sauerstoff- oder siliziumdominierte ([0]+[Si] > 3[C]) AlN-Proben sind als gestrichelte Linien ausgeführt. Die kohlenstoffinduzierte UVC-Absorptionsbande bei 4,7 eV wird unterdrückt, wenn das Ferminiveau über dem oberen $(C_{related})^{x-1/x-2}$ Umladungsniveau liegt, in diesem Fall bei hoher Sauerstoff- oder Siliziumdotierung. Der Ladungszustand x für die geringste Elektronenbesetzung der kohlenstoffhaltigen Defektkomplexe wird als 0 oder +1 angenommen.

Furthermore we observed, that the absorption band at 4.7 eV is absent in samples containing much more oxygen than carbon (cf. Fig. 1b). This is also true for crystals intentionally doped with silicon to concentration levels far exceeding those of carbon. As mentioned above, both oxygen and silicon are donors in AlN and even if forming *DX* centers, their ionization energies are within 1 eV below the conduction band minimum. Consequently, in case of a dominating oxygen or silicon content of the samples, the Fermi level shifts upwards to near the conduction band edge. If the carbon-related defects possess at least two charge state transition levels in the mid-gap region, strong electron occupation of the upper level will inhibit the UV absorption starting from the lower level and thus the deep-UV absorption band is quenched, see Fig. 2.

Such a favorable order of the charge state transition levels is theoretically predicted for the nearest-neighbor carbon pair (C_N-C_{Al}) [9] and is also suggested for the tri-carbon defect in Ref. [11], where we first proposed the Fermi level model. But this would also mean that single C_N-point defects might not be the major cause of the 4.7 eV absorption, because they lack the necessary level order according to theory [9, 10].

Alternatively, Gaddy et al. argue that in highly Si-doped AlN, the formation of (compensating) defect complexes is shifting the carbon-related absorption to outside the UV range [14]. But they also admit that their explanation might be only valid for samples with high silicon and carbon concentrations, much beyond those found in our samples.

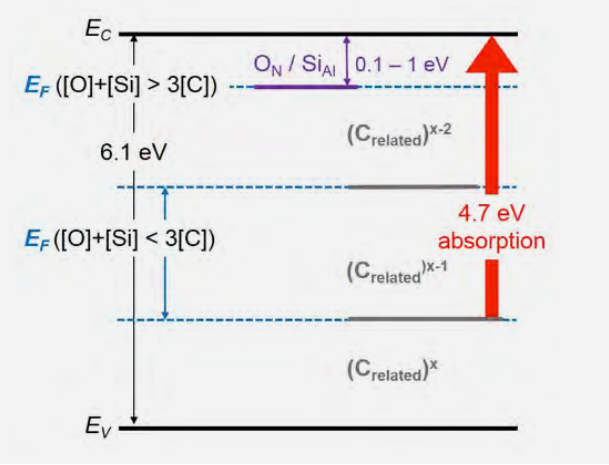

Fig. 2
Energy diagram of AlN with transition levels of carbon-related defects and shallow donors of oxygen and silicon. The Fermi level position ranges for "carbon dominated" ([0]+[Si] < 3[C]) and "oxygen/silicon dominated" ([0]+[Si] > 3[C]) AlN are drawn as blue dashed lines. The carbon-related 4.7 eV deep-UV absorption is quenched when the Fermi level is raised above the $(C_{related})^{x-1/x-2}$ transition level, in the present case by high oxygen or silicon doping. The charge state x of the least electron occupation is most probably 0 or +1 for the carbon related defects.

Highlight

Unser „Ferminiveau-Modell", also die Annahme, dass das Auftreten der UVC-Absorption vom stabilen Ladungszustand des kohlenstoffhaltigen Defektkomplexes abhängt, wird durch folgende Beobachtungen weiter gestützt: Die kohlenstoffinduzierte Absorption wird durch Röntgen- oder UVC-Strahlung deutlich verringert. Der Ausgangszustand wird nach dem Ende der Bestrahlung erst nach einigen Tagen bei Raumtemperatur (oder nach einer Stunde bei 150°C) wieder erreicht. Die relative Verringerung der Absorption ist bei Proben mit geringerem Sauerstoff- und Kohlenstoffgehalt höher, und sie ist wesentlich stärker, wenn zur Bestrahlung UVC-Licht verwendet wird, siehe Abb. 3.

Gleichzeitig bilden sich neue Absorptionsbanden bei 320 nm und 240 nm aus, und die AlN-Proben erhalten eine gelbliche Färbung aufgrund einer erhöhten Absorption im Wellenlängenbereich 400–500 nm. Es verblüfft, dass sogar die UVC-Emission von auf solchen AlN-Substraten aufgebrachten LED-Strukturen (bei 265 nm) zu einer Gelbfärbung in dem Substratbereich führt, der sich um die elektrischen Kontaktflächen herum befindet; aufgrund mangelnder Stromleitfähigkeit der AlN-Schichten wird dort die höchste Strahlungsleistung freigesetzt [12]. Dieser Effekt reicht jedoch nicht aus, um die UVC-Absorptionsbande vollständig zu unterdrücken.

Die Änderung der Absorptionseigenschaften durch Bestrahlung kann wie folgt erklärt werden: Die Photonen erzeugen Ladungsträger im Valenz- und Leistungsband durch Band-zu-Band-Anregung oder durch Photoionisation von Punktdefekten. Diese beweglichen Ladungsträger werden von tiefen Störstellen eingefangen. Dadurch entsteht eine Nichtgleichgewichts-Belegung der Defekt-Ladungszustände, die sich nach dem Ende der Bestrahlung nur langsam wieder dem Gleichgewicht nähert, da sich die Umladungsniveaus tief in der Bandlücke befinden (z.B. mehr als 1 eV von den Bandkanten entfernt). Bei Raumtemperatur dauert es entsprechend einige Tage, um diese Ladungsträger wieder thermisch zu aktivieren.

Abb. 3
Verringerung der UVC-Absorptionsbande einer AlN-Probe bei 4,7 eV (265 mm) bei Bestrahlung durch UVC-Licht der Wellenlängen 266 nm (frequenzvervierfachter Nd:YAG-Laser, rote Kurve) bzw. 254 nm (Quecksilberdampflampe, blaue Kurve). Die grüne Kurve zeigt den Absorptionsverlauf vor Bestrahlung, in etwa identisch zum Verlauf nach einer Stunde Tempern der Probe bei 150°C.

Strong support for the Fermi level model, i.e. that the respective stable defect charge state governs the absorption behavior, comes from the following observations. The carbon-related absorption features are partially decreased (quenched) upon X-ray or deep-UV irradiation. The relaxation to the initial state is rather slow: It takes some days at room temperature or one hour annealing at 150°C. The decrease is stronger in samples containing lower concentrations of oxygen and carbon, and it is significantly enhanced when deep-UV light is used as the irradiation source, see Fig. 3.

At the same time, new absorption features at around 320 nm and 240 nm appear, and the samples get a yellowish tint due to absorption in the 400–500 nm wavelength range. Strikingly, even the deep-UV emission of 265 nm LED structures lead to such yellowish coloration around the contact area where emission is strongest [12]. However, this effect is not sufficient to provide deep-UV transparent AlN.

The dependence of the UV-Vis absorption on the illumination history can be explained in the following way. Irradiation with photons transfers charge carriers to the valence and conduction band via band-to-band excitation or photoionization of defects. The mobile charge carriers can be trapped by different defects. The resulting nonequilibrium occupation of defect charge states decays after switching off the irradiation. The corresponding life time can be long at room temperature if the involved defect energy levels are deep enough (e.g., more than 1 eV away from the band edges).

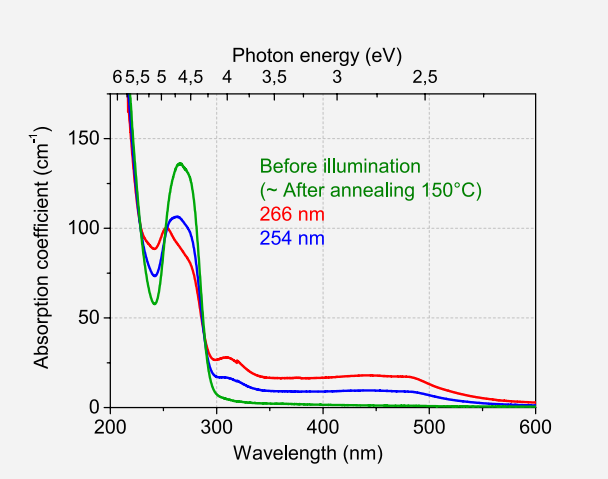

Fig. 3
Partial quenching of the 4.7 eV absorption feature under deep-UV irradiation at 266 nm (quadrupled Nd:YAG laser, red curve) or 254 nm (mercury lamp, blue curve). The green curve represents the coinciding spectra before illumination of the sample and after annealing at 150°C.

Highlight

Kontrolle des Einbaus von Verunreinigungen und Auswirkung auf die UV-Absorption

Die chemische Analyse der am IKZ gezüchteten AlN-Kristalle hat ergeben, dass die Sauerstoffkonzentration immer höher ist als die Kohlenstoffkonzentration ([O]/[C] > 1). Interessanterweise bleibt die kohlenstoffinduzierte UVC-Absorption für alle AlN-Proben mit [O]/[C] < 3 jedoch praktisch unverändert bestehen. Wir bezeichnen diese im UVC-Bereich intransparenten Proben deshalb als „kohlenstoffdominiert". AlN-Proben mit [O]/[C] > 3 zeigen dagegen keine kohlenstoffinduzierten Absorptionsbanden und werden als „sauerstoffdominiert" bezeichnet. Die Untersuchung siliziumdotierter AlN-Proben hat gezeigt, dass diese Zuordnung auch für Proben mit [Si] > [O] > [C] gilt („siliziumdominiert", siehe Abb. 1b). Die physikalischen Gründe für die Tatsache, dass eine in etwa dreifache Konzentration n-leitender Störstellen zu einer relativ abrupten Änderung der kohlenstoffinduzierten Absorptionsbanden führt, sind noch unklar.

In AlN-Proben, die die Bande bei 4,7 eV nicht zeigen, wird die UVC-Absorption durch Störstellen- sowie durch Donator-Akzeptor-Paarionisation dominiert. Die UVC-Absorption steigt dabei unterhalb der Bandkante mit abnehmender Wellenlänge immer mehr an. Liegt die Verunreinigungskonzentration in den Substraten im Bereich von einigen 10^{19} cm^{-3}, so führt bereits dieser Effekt zu Absorptionskoeffizienten um 50 cm^{-1} bei 265 nm, die für die Anwendung inakzeptabel sind. Eine Verringerung der Verunreinigungen in der PVT-Kristallzüchtung von AlN ist daher notwendig, aber schwierig zu realisieren, da das bei dem Gasphasentransport entstehende gasförmige Aluminium die Materialien des Züchtungsaufbaus angreift. Dabei entstehende flüchtige Verbindungen können die Wachstumsoberfläche erreichen und in den Kristall eingebaut werden. Sauerstoff ist als Restverunreingung sowohl in der Züchtungsatmosphäre als auch im AlN-Ausgangsmaterial (z.B. aufgrund einer Oxidation der Oberfläche) vorhanden.

Control of impurity incorporation during growth and impact on deep-UV transparency

A comprehensive chemical analysis of the AlN crystals grown at IKZ reveals the following details. The oxygen to carbon concentration ratio [O]/[C] is always exceeding unity. But interestingly, the carbon-related absorption features (and also the behavior of free-carrier absorption) as detailed above remain virtually unchanged in crystals with [O]/[C] < 3. This means that such crystals are still "carbon dominated" and not transparent in the deep-UV range. In contrast, the crystals or crystal parts with [O]/[C] > 3 do not show the carbon-related absorption features at all. They are thus called "oxygen dominated" hereafter. Experiments with silicon-doped AlN evidence that this also holds for [Si] > [O] > [C], see Fig. 1b. The physical meaning of the (roughly) threefold excess of *n*-type dopants required to quench the carbon-related absorption is not yet clear.

In AlN samples where the 4.7 eV feature is absent, deep-UV absorption is governed by the below band-gap tail which forms due to impurity-band as well as donor-acceptor pair transitions. For impurity concentrations in the low 10^{19} cm^{-3} range, this still leads to unacceptably high deep-UV absorption of around 50 cm^{-1} at 265 nm. This means that the overall impurity content must be significantly decreased. Mitigating impurity incorporation during PVT growth of AlN is extremely difficult, as the Al vapor easily attacks the set-up materials, and volatile impurity-containing compounds reach the growth interface. Oxygen is a residue in the growth atmosphere and a major contaminant of the AlN starting material's surface; during crystal growth, it is mainly transported via Al_2O gaseous species. We found that tantalum carbide (TaC) converts Al_2O into CO, which subsequently evades the crucible, thus lowering the oxygen concentration at the growing interface [3].

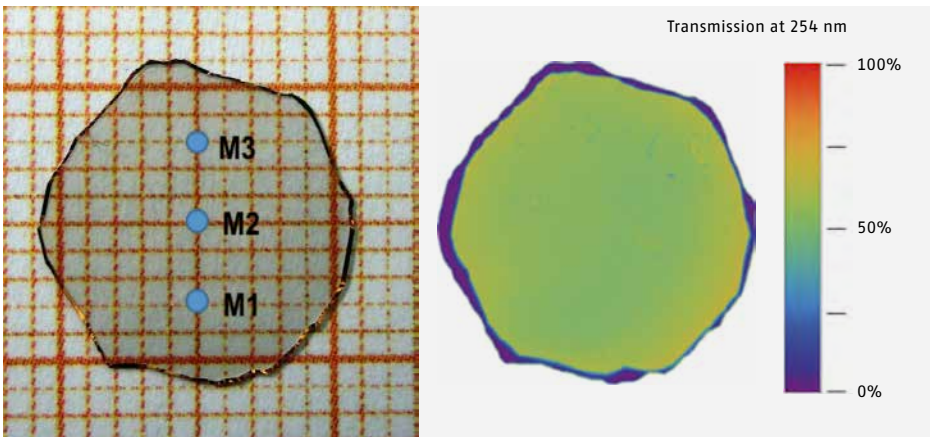

a) b)

Abb. 4
a) Fotographie eines (0001)-orientierten AlN-Substrates mit 11 mm Durchmesser und 140 µm Dicke auf Millimeterpapier mit eingezeichneten Messpunkten;
b) UVC-Transmission dieses Substrats bei einer Wellenlänge von 254 nm.

Fig. 4
a) Image of a (0001)-oriented AlN wafer, 11 mm in diameter and 140 µm thick, on millimetre grid with designated measuring locations;
b) transmittance of this wafer at 254 nm wavelength.

Highlight

Unter Züchtungsbedingungen befindet sich Sauerstoff überwiegend als gasförmiges Al_2O in der Züchtungsatmosphäre. Wir konnten zeigen, dass Al_2O an der Oberfläche von Tantalcarbid (TaC) zu CO umgesetzt wird. CO ist nur wenig reaktiv, kann somit den Tiegel leicht verlassen und führt in der Konsequenz zu einer Verringerung der Sauerstoffkonzentration an der Wachstumsoberfläche [3].

Andererseits werden gasförmige kohlenstoffhaltige Spezies auf Wolframoberflächen adsorbiert und umgesetzt. Wir nutzen dies, indem Wolframbleche in den Tiegelaufbau eingebracht werden. Durch die Kohlenstoffaufnahme wandelt sich Wolfram teilweise in die auch bei Züchtungsbedingungen stabile Verbindung W_2C um [3]. Der chemische Angriff der Al-Spezies, betroffen sind vor allem der TaC-Tiegel und die umgebende thermische Isolation aus Graphitfilz, kann weiter vermindert werden, in dem die Züchtungstemperatur von 2100°C auf 2030–2050°C abgesenkt wird. Durch den damit sinkenden CO-Gehalt steigt aber wiederum der Sauerstoffeinbau auf der Wachstumsoberfläche an [3]. Mittels Temperaturabsenkung und dem Einbringen der Wolframbleche in den Tiegelaufbau ist es gelungen, die Konzentration von Sauerstoff und Kohlenstoff auf der Haupt-Wachstumsfläche, der basalen (000-1)-Oberfläche, von 2×10^{19} cm^{-3} [13] auf $3{,}5\times10^{18}$ cm^{-3} [3] bzw. von 4×10^{18} cm^{-3} auf $1{,}8\times10^{18}$ cm^{-3} zu reduzieren.

Um das wichtige Verhältnis [O]/[C] > 3 einzuhalten wurden die Prozessparameter so justiert, dass die Verunreinigungskonzentrationen reproduzierbar und stabil bei 6×10^{18} cm^{-3} (Sauerstoff) und 2×10^{18} cm^{-3} (Kohlenstoff) im Kristallvolumen liegen [3]. AlN-Substrate, die aus diesen Kristallen hergestellt wurden, besitzen Absorptionskoeffizienten bei 265 nm im Bereich von 25 cm^{-1}, siehe Abb. 4c. Auch wenn damit immer noch die Hälfte des emittierten UVC-Lichts beim Durchgang durch ein 280 µm dickes AlN-Substrat absorbiert wird, haben wir damit die ersten weltweit AlN-Substrate hergestellt, bei denen die UVC-Emission direkt durch das AlN-Substrat gemessen werden konnte [15]. Die AlN-Substrate anderer Hersteller müssen mechanisch abgedünnt und auf ein Trägersubstrat transferiert werden [16], was erhebliche Zusatzkosten verursacht. Der niedrigste an einer AlN-Probe des IKZ bislang gemessene Absorptionskoeffizient bei 265 nm von 14cm^{-1} entspricht einer Transmission von 67% des UVC-Lichts durch ein 280 µm dickes Substrat. Zusätzliche Maßnahmen zur Erhöhung der Lichtauskopplung, z.B. der Einsatz reflektierender p-leitfähiger AlGaN-Kontaktschichten oder die Strukturierung der Substrat-Rückseite zur Verbesserung des Lichtaustritts, werden derzeit von vielen Forschergruppen intensiv untersucht.

On the other hand, volatile carbon species can be efficiently gettered by adding sheets of tungsten inside the crucible. With the uptake of carbon, these sheets partially convert into W_2C, which is solid and stable at growth temperature [3]. The chemical attack on the set-up materials (TaC crucible and carbon felt as thermal isolation) and thus also carbon incorporation can be further decreased by lowering the growth temperature from 2100°C to 2030–2050°C. However, at the same time the oxygen incorporation increases [3]. With these measures, the concentration of oxygen and carbon in the main (000-1) basal plane area have been reduced from 2×10^{19} cm^{-3} [13] to 3.5×10^{18} cm^{-3} [3] and from 4×10^{18} cm^{-3} to 1.8×10^{18} cm^{-3}, respectively.

In order to obey the [O]/[C] > 3 prerequisite, process conditions were carefully adjusted to reproducibly attain oxygen and carbon concentrations of 6×10^{18} cm^{-3} and 2×10^{18} cm^{-3}, respectively, in the main crystal volume [3]. Substrates cut from such crystals show absorption coefficients of about 25 cm^{-1}, see Fig. 4c. For light outcoupling through a 280 µm thick AlN substrate, this still means that 50% of the light is absorbed. This may sound much, but it allows for the first time to measure emitted light through the substrate directly [15] without mechanical thinning of the AlN substrate, which is costly and requires a submount transfer process [16]. Lowest absorption values in our crystals achieved for 265 nm are 14 cm^{-1}, corresponding to 67% transmission through the 280 µm thick wafer. Note that other means to improve light extraction, such as employing reflective *p*-type AlGaN contacts and substrate backside surface patterning, are also investigated by the device manufacturers.

Most important, the homogeneous UV transparent properties are observed on the whole wafer area, see Fig. 4. For this, we have built a calibrated set-up to map the local deep-UV transmission at 254 nm. It consists of a mercury lamp, tailored optical filters, and a UV-enhanced CCD camera for an easy inspection of AlN wafers. Note that in samples where the carbon-related absorption is fully quenched, the band-tail absorption leads to a monotonic increase of the absorption coefficient with decreasing wavelength. Thus, providing deep-UV transparent wafers for wavelengths below 240 nm is still an unsolved challenge, see Fig. 5.

Highlight

Für eine Anwendung ist besonders wichtig, dass die AlN-Substrate auf der gesamten Substratfläche homogene Eigenschaften aufweisen; dies gilt natürlich auch für die UVC-Absorption, siehe Abb. 4. Am IKZ wurde dazu ein kalibrierter Messaufbau auf einer Quecksilberdampflampe, optischen Filtern und einer UV-sensitiven CCD-Kamera entwickelt, der die UVC-Absorption bei 254 nm ortsaufgelöst misst und einfach zu bedienen ist. Damit kann man die Eignung der AlN-Substrate für Desinfektionsanwendungen gut dokumentieren. Aufgrund der steigenden UVC-Absorption mit sinkender Wellenlänge haben unsere AlN-Proben bei sehr kurzen Wellenlängen (unterhalb 240 nm) immer noch zu hohe Absorptionskoeffizienten, selbst wenn sie die kohlenstoffinduzierte Absorptionsbande nicht zeigen, siehe Abb. 5.

Das verbesserte Verständnis der Punktdefekte und der damit zusammenhängenden optischen Übergänge in AlN hat uns ermöglicht, Prozessbedingungen zu finden, mit denen AlN-Kristalle und Substrate reproduzierbar hergestellt werden können. Die AlN-Substrate des IKZ vereinen eine sehr hohe strukturelle Qualität mit einer sehr guten UVC-Transmission auf der gesamten Substratfläche. Diese AlN-Substrate werden nun standardmäßig in unserem Verbundvorhaben „AlN-Substrate" im Forschungs-Konsortium „Advanced UV for Life" eingesetzt. Wir arbeiten bereits an einer weiteren Verringerung des Einbaus an Verunreinigungen. Die größte Herausforderung ist derzeit jedoch die Vergrößerung des einkristallinen Kristall- und Substratdurchmessers, ohne dabei die strukturelle Qualität oder die UVC-Transparenz zu beeinträchtigen, denn beide Eigenschaften sind für die Anwendung im Bauelement von entscheidender Bedeutung.

In summary, the progress made in understanding the point defects and their optical transitions in PVT-grown bulk AlN crystals helped us to define process conditions where AlN crystals and substrates with unprecedented structural quality and deep-UV transparency in the whole volume can be fabricated reproducibly. Such substrates are now standard for research and development of deep-UV optoelectronic devices in our collaboration network "Advanced UV for Life". We are currently working on a further reduction of the impurity incorporation, but the main challenge will be to increase the single-crystalline diameter of the crystals without sacrificing the structural quality and deep-UV transparency which are both crucial for device application.

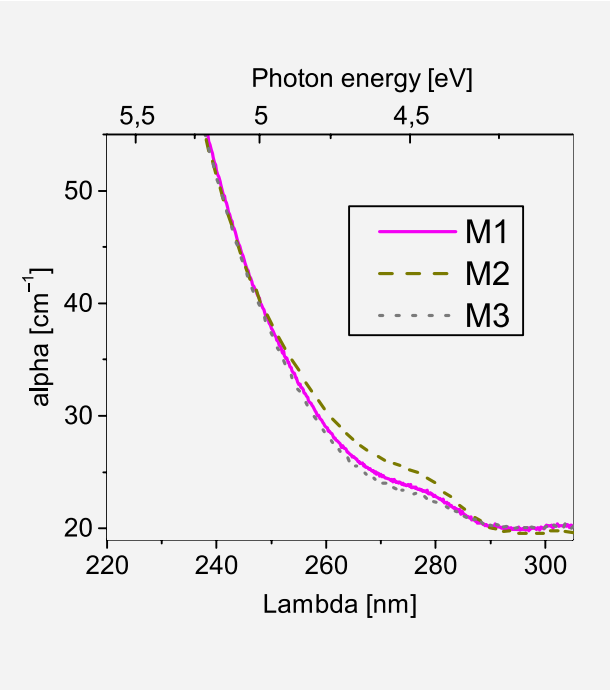

Abb. 5
UVC-Absorptionsspektren an den Messpunkten des AlN-Substrates aus Abb. 4.

Fig. 5
UV absorption spectra of the wafer from Fig. 4, measured at the designated locations.

References

[1] III-Nitride Ultraviolet Emitters – Technology and Applications, M. Kneissl and J. Rass (eds.); Springer Series in Materials Science 227, Springer Verlag 2016, ISBN: 978-3-319-24098-5

[2] M. Bickermann, Growth and Properties of Bulk AlN Substrates; in: III-Nitride Ultraviolet Emitters (see Ref. 1), chap. 2

[3] C. Hartmann, J. Wollweber, S. Sintonen, A. Dittmar, L. Kirste, S. Kollowa, K. Irmscher, and M. Bickermann; CrystEngComm 18 (2016) 3488

[4] L. Gordon; J.L. Lyons, A. Janotti, and C.G. Van de Walle; Phys. Rev. B 89 (2014) 085204

[5] L. Silvestri, K. Dunn, S. Prawer, and F. Ladouceur; EPL (Europhysics Lett.) 98 (2012) 36003

[6] B.E. Gaddy, Z. Bryan, I. Bryan, R. Kirste, J. Xie, R. Dalmau, B. Moody, Y. Kumagai, T. Nagashima, Y. Kubota, T. Kinoshita, A. Koukitu, Z. Sitar, R. Collazo, and D.L. Irving; Appl. Phys. Lett. 103 (2013) 161901

[7] F. Tuomisto, J.M. Mäki, T.Y. Chemekova, Y.N. Makarov, O. V. Avdeev, E.N. Mokhov, A.S. Segal, M.G. Ramm, S. Davis, G. Huminic, H. Helava, M. Bickermann, and B.M. Epelbaum; J. Cryst. Growth 310 (2008) 3998

[8] Q. Yan, A. Janotti, M. Scheffler, and C.G. Van De Walle; Appl. Phys. Lett. 105 (2014) 111104

[9] R. Collazo, J. Xie, B.E. Gaddy, Z. Bryan, R. Kirste, M. Hoffmann, R. Dalmau, B. Moody, Y. Kumagai, T. Nagashima, Y. Kubota, T. Kinoshita, A. Koukitu, D.L. Irving, and Z. Sitar; Appl. Phys. Lett. 100 (2012) 191914

[10] J.L. Lyons, A. Janotti, and C.G. Van de Walle; Phys. Rev. B 89 (2014) 035204

[11] K. Irmscher, C. Hartmann, C. Guguschev, M. Pietsch, J. Wollweber, and M. Bickermann; J. Appl. Phys. 114 (2013) 123505

[12] The LED structure was grown and investigated by C. Kuhn, AG Kneissl/Technische Universität Berlin, Germany

[13] C. Hartmann, A. Dittmar, J. Wollweber, and M. Bickermann; Semicond. Sci. Technol. 29 (2014) 084002

[14] B.E. Gaddy, Z. Bryan, I. Bryan, J. Xie, R. Dalmau, B. Moody, Y. Kumagai, T. Nagashima, Y. Kubota, T. Kinoshita, A. Koukitu, R. Kirste, Z. Sitar, R. Collazo, and D.L. Irving; Appl. Phys. Lett. 104 (2014) 202106

[15] C. Kuhn, T. Wernicke, M. Kneissl; Technische Universität Berlin, Germany, private communication

[16] J. Grandusky, J. Chen, S.R. Gibb, M.C. Mendrick, C.G. Moe, L. Rodak, G.A. Garrett, M. Wraback, and L.J. Schowalter; Appl. Phys. Express 6 (2013) 032101

Classical Semiconductors

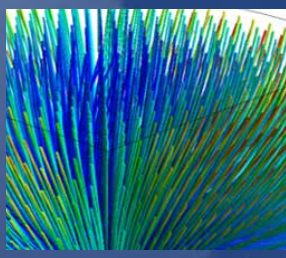

Classical Semiconductors

Acting head of department: Dr. Frank M. Kießling

Die Abteilung Klassische Halbleiter sieht sich in der Verantwortung, Grundlagenforschung und angewandte Forschung in enger Kooperation mit der Industrie auf dem Gebiet der Massivkristallzüchtung aus der Schmelze von Si, Ge, deren Mischkristalle und III-V-Halbleitern durchzuführen. Forschung und Entwicklung finden in den Themengruppen Silicium & Germanium, Multikristallines Silicium und Galliumarsenid statt. In der personell größten Gruppe Silicium & Germanium wird die Kristallzüchtung mit den Methoden Float-Zone (FZ) und Czochralski (Cz) betrieben. In den beiden anderen Themengruppen der Abteilung wurde in den letzten Jahren, und so auch in 2016, ausschließlich das Vertical Gradient Freeze (VGF) Verfahren unter Nutzung von geeigneten Magnetfeldern im Rahmen von industrienahen Projekten angewandt. Das in diesen Themengruppen entwickelte KRISTMAG®*-Prinzip findet dabei in vielfältiger Weise Anwendung, insbesondere bei der vorteilhaften Kontrolle der Konvektion in der Schmelze, der Reduzierung von Temperaturfluktuationen und der Steuerung der Form der Wachstumsfront.*

Die Reputation der Abteilung wurde durch erfolgreiche Projektbearbeitungen und -verteidigungen weiter erhöht. Da wäre z.B. das BMBF-geförderte Verbundprojekt „Toxikologische, physikalisch-chemische und gesellschaftliche Erforschung innovativer Materialien und Prozesse der Optoelektronik – TEMPO -, welches einen bedeutenden Beitrag zur toxikologischen Bewertung von Halbleitermaterialien leistet. Auch führte der erfolgreiche Abschluss des Projektes „Kilogramm-2" zu einer neuen, bis in das Jahr 2019 reichenden Projektfinanzierung. Das BMWi-geförderte Projekt ENOWA II – „Entwicklung hoch- und Kosteneffizienter PV-Si Wafer" - wurde Mitte des Jahres 2016 mit einer innovativen Technologieentwicklung erfolgreich abgeschlossen. Neue Projekte mit einer mehrjährigen Förderung, wie das „Silicium Granulat Eigentiegelverfahren" – SiGreT - oder ein DFG-Verbundprojekt zur modellbasierten Steuerung und Regelung unter Einbeziehung künstlicher neuronaler Netzwerke, konnten beispielhaft eingeworben werden. Damit setzt sich die Kontinuität der Drittmitteleinwerbung für alle bearbeiteten Materialien in der Abteilung fort und unterstreicht die Aktualität der Forschungstätigkeiten. Strukturell wurde für die Züchtung von hochreinen Germanium Einkristallen, welche zukünftig als Detektoren im GERDA-Projekt (GERmanium Detector Array) Anwendung finden sollen, nun sowohl die Cz-Züchtungs- als auch die Zonenreinigungsanlage in Betrieb genommen. Dagegen ist die Investition in die 8-Zoll FZ-Anlage (Sondertatbestand) in 2016 zurückgestellt worden.

Die WissenschaftlerInnen, IngenieurInnen und TechnikerInnen der Abteilung sind als kompetente Gesprächspartner gefragt, um Technologieaspekte zu beleuchten und definierte Materialqualitäten für spezielle Bauelemente herzustellen. Die Abteilung erfüllte auch in 2016 wichtige Servicefunktionen für Wissenschaft und industrielle Partner. Die Integration der ModelliererInnen als fester Bestandteil der Themengruppen hat sich bewährt. Die numerische Berechnung thermischer Felder in der Schmelze oder die Berechnung des Einflusses magnetischer Felder auf die Konvektion der Schmelze und den damit verbundenen Effekten an der Wachstumsfront werden innerhalb der Abteilung durchgeführt. Diese Ergebnisse sind unabdingbar für eine schnelle und zielorientierte Entwicklung von Kristallzüchtungsprozessen und des Züchtungsraums in den Anlagen. Die Betrachtung derartiger Zusammenhänge wird auch als Serviceleistung angefragt. Zur Entwicklung von Kristallzüchtungsprozesse ist die Materialcharakterisierung in enger Zusammenarbeit mit den Gruppen Kristallbearbeitung und Physikalische Charakterisierung bestens organisiert. Die Auswertung dieser Informationen zusammen mit den ModelliererInnen, KonstrukteurInnen und den KristallzüchterInnen erlaubt effektiv eine direkte Umsetzung in die Entwicklung der Züchtungsapparaturen und -prozesse.

The department Classical Semiconductors sees itself in the responsibility to carry out fundamental and applied research of bulk crystal growth from melts of Si, Ge, their solid solutions and III-V semiconductor materials in close cooperation with industry. Research and development take place in the groups Silicon & Germanium, Multicrystalline Silicon and Gallium Arsenide. In the biggest group Silicon & Germanium, crystal growth is pursued with the methods Float-Zone (FZ) and Czochralski (Cz). In the other two theme groups of the department, the Vertical Gradient Freeze (VGF) method has been applied in the last few years and thus also in 2016, using appropriate magnetic fields for industrial project needs. The KRIST*MAG*® principle developed in these groups has been used in a variety of ways, in particular to control advantageously melt convection, to reduce temperature fluctuations and to control the shape of the growth front.

Successful project processing and result defenses strengthened the reputation of the department. For example, there is the BMBF-funded joint research project "Toxicological, physico-chemical and social investigation of innovative materials and processes in optoelectronics" – "TEMPO" –, which makes a significant contribution to the toxicological assessment of semiconductor materials. Furthermore, the successful completion of the project "Kilogramm-2" also led to a new project financing that last until 2019. The BMWi-funded project – ENOWA II – „Development of high-efficient and cost-effective PV-Si wafer" was successfully completed with an innovative technology development in mid-2016. New projects with multi-years funding, such as „Silicon granulate crucible procedure" – SiGreT – or a joint research DFG project about model-based feedforward and feedback control design involving artificial neural networks, can be named exemplarily. In this way, there is a continuity of third-party funding for all processed materials in the department and it underscores the need of these research activities. Investment have been taken on a Cz-furnace and a zone refining machine, which were put into operation for the growth of high-pure Ge single crystals needed as detectors in the GERDA project (GERmanium Detector Array). On the other hand, the investment for the 8-inch FZ crystal growth equipment (special funding of science) has been on hold in 2016.

The scientists, engineers and technicians of the department are in demand as competent interlocutors in order to illuminate technology aspects and to grow defined material qualities for special device components. The department also fulfilled important service tasks for scientific and industrial partners in 2016. The group-related integration of the fellows doing simulations has proven itself. Modelers of the department carry out numerical modeling of thermal fields in the melt or the calculation of the influence of magnetic fields on the melt flow and the associated effects at the growth interface. These results are indispensable for a rapid and goal-oriented development of of crystal growth proces and hot zones in the furnaces. There is also a demand for those correlations as service tasks. For the development of crystal growth processes the material characterization is done in close cooperation with the theme groups Crystal Machining and Physical Characterization. A team of modelers, design engineers and crystal growers analyze all these information, which in this way allows effectively a direct implementation on the development of growth equipment and processes.

Classical Semiconductors:
Silicon & Germanium

Head Dr. Nikolay Abrosimov
Team M. Czupalla, Dr. K. Dadzis, J. Fischer, B. Faraji-Tajrishi, O. Gybin, B. Hallmann-Seifert, S. Kayser, L. Lehmann, Dr. A. Lüdke, Dr. R. Menzel, Dr. W. Miller, K. Reinhold, M. Renner, Dr. H. Riemann, Dr. H.-J. Rost, T. Turschner, S. Weiß

Überblick

Silizium (Si) und Germanium (Ge) sind Materialien mit einem breiten Anwendungsfeld in Industrie und Forschung. Obwohl es sich um weit etablierte Materialien handelt, gibt es weiterhin einen hohen Bedarf an Forschung zur Material- und Prozessentwicklung. Diese steht im Fokus der Aktivitäten der Gruppe Silizium & Germanium. Die Schwerpunkte der Gruppe liegen auf der Material- und Prozessentwicklung auf Basis der Float-Zone-(FZ)-Technik einschließlich der Züchtung von isotopen-angereichertem ^{28}Si-Einkristallen, sowie der Züchtung von Silizium- bzw. Silizium-Germanium (Si_xGe_{1-x})-Einkristallen mittels der Czochralski-(Cz)-Methode. Weitere wichtige Themen sind die Züchtung von hochreinen Ge-Kristallen für Detektoren im Rahmen des GERDA-Projekts, oder die Forschung zur Züchtung von speziell dotierten Ge- und Si-Kristallen, z.B. im BMBF-geförderten Projekt InTerFEL. Neben den Forschungsarbeiten leistet die Gruppe auch Service. Dazu zählt die Züchtung von Kristallen für Kunden mit genauer Spezifizierung, aber auch die Züchtung von kleinen Kristallen zur Materialcharakterisierung aus Material von Kooperationspartnern wie der Firma KEPP EU, Lettland. Die Verfügbarkeit unterschiedlicher Züchtungsmethoden zur Herstellung von Si- und Ge-Kristallen aus der Schmelze als auch die Expertise in der Züchtung eines breiten Spektrums von Si- und Ge-basierten Einkristallen erlaubt uns weltweit einzigartige Forschungsarbeiten.

Im Rahmen des Kilogramm-Projekts unter Leitung der Physikalisch-technischen Bundesanstalt (PTB) wurde 2016 der dritte ^{28}Si Einkristall gezüchtet. Das Ziel des Projekts ist die präzisere Bestimmung der Avogadro-Konstante, d.h. der Anzahl der Atome in einem Mol. Zum Erreichen der erforderlichen Kristallqualität, insbesondere in Hinblick auf die Kohlenstoff-Konzentration im finalen Kristall, werden einige Reinigungsdurchgänge durchgeführt. Erst danach kann ein versetzungsfreier ^{28}Si-Kristall mit 4 Zoll Durchmesser gezüchtet werden. Aus einem solchen Kristall können zwei Silziumkugeln präpariert werden. Nach Messung des Volumens, der Masse und des Gitterparameters kann eine Beziehung zwischen Volumen und Anzahl der Atome abgeleitet werden.

Das Projekt „Silizium Granulat Eigentiegel-Verfahren“ (SIGRET), das sich im Wettbewerbsverfahren der Leibniz-Gemeinschaft durchsetzen konnte, wurde Mitte 2016 begonnen. Ziel ist die Entwicklung eines stabilen Züchtungsprozesses für Si-Einkristalle in Industrie-relevanter Größe, z. B. für photovoltaische Anwendungen. Die Silizium-Kristallzüchtung aus der Schmelze im Eigentiegel ist ein neues Konzept, um Kristalle mit ähnlicher Qualität wie beim FZ-Prozess zu erhalten, aber bei deutlich geringeren Kosten des Ausgangsmaterials [1]. Dabei wird der Kristall aus einem induktiv geheizten Schmelzpool, der sich in einem Eigentiegel befindet, gezogen. Der Tiegel wird kontinuierlich mit Si Granulat befüllt. Aufgrund der fehlenden Kontamination durch das Tiegelmaterial kann eine geringe Sauerstoffkonzentration (< $1{\cdot}10^{16}$ atoms/cm^3) in den gezüchteten Kristallen erreicht werden.

Im GERDA-Projekt (GERmanium Detector Array) sind nun sowohl die Cz-Züchtungsanlage als auch die Zonen-Reinigungsmaschine zum Herstellen des hochreinen Ausgangsmaterials für die Kristallzüchtung in Betrieb. Bei beiden ist der Betrieb mit Wasserstoff oder Argon möglich. Die Modifikation der Hot Zone und der Züchtungsparameter bei der Cz-Züchtung ermöglicht Kristalle mit einer Versetzungsdichte im geforderten Bereich von 10^2 – 10^4 cm^{-2}. Als nächstes werden alle technologischen Schritte auf dem Weg zum Ge-Einkristall im Hinblick auf die Reinheit optimiert, um die für den Detektoren-Bau geforderte Netto-Ladungsdichte von ca. 10^{10} cm^{-3} im Kristall zu erreichen.

Die Aufgabe des IKZ im Rahmen des BMBF-Projktes InTerFEL (Zeitaufgelöste Infrarot- und Terahertz-Spektroskopie der Ladungsdynamik in Halbleitern mit Freien Elektronen Lasern) ist die Kristallzüchtung und Probenpräparation für die zeitaufgelöste und Raman-Spektroskopie von flachen Donatoren und Akzeptoren in Silizium und Germanium. Erste Experimente mit Mg-dotiertem Si, wobei das Mg nachträglich im nach dem Standard-FZ-Verfahren gezüchteten Si-Kristall eindiffundiert wurde, zeigten die Präsenz von Mg-O-Komplexen [2]. Dieses beruht auf der hohen Affinität von Mg zu Sauerstoff. Durch die Züchtung im Vakuum war es uns möglich, die Sauerstoffkonzentration in Si unter 10^{15} cm^{-3} zu senken. Erste Ergebnisse werden gerade veröffentlicht.

Im SEMITHERM-Projekt wurden den Partnern von der Universität Göttingen Ge-reiche und hoch Bor-dotierte $Si_{1-x}Ge_x$ Proben (x=0,75 und 0,9) zur Verfügung gestellt, um Untersuchungen zu thermo-physikalischen Eigenschaften der Halbleiterschmelzen unter Mikrogravitationsbedingungen während eines Parabelfluges durchzuführen [3]. Die Proben wurden aus nach dem Cz-Verfahren gezüchteten Polykristallen gewonnen. Eine Weiterführung der Experimente bei elektromagnetischen Levitation (EML) ist an Bord der ISS Raumstation für den September 2017 geplant.

Das Lateral Photovoltage Scanning (LPS) and die Scanning-Photoluminescence (SPL) werden für die Bestimmung der fest-flüssig Phasengrenze und von Defektstrukturen in Si-, Ge-, und SiGe-Kristallen eingesetzt [4, 5]. Ihre Weiterentwicklung wird im Rahmen einer Promotion durchgeführt. Simulationsrechnungen ermöglichen uns ein besseres Verständnis des Zusammenhangs zwischen Dotierstoffverteilung in der Probe und Messsignal. In 2016 konnten erste Ergebnisse zum Einfluss der Probengeometrie und -größe auf das Signal erhalten werden.

Ferner hielt sich die Promotionsstudentin Xiaofang Qi von der Xi'an Universität mit Beginn Oktober 2015 für ein Jahr in der Gruppe auf. Der Aufenthalt wurde durch ein Stipendium des Chinese Scholarship Council finanziert. Sie beschäftigte sich mit der Berechnung der Kornentwicklung während der Erstarrung von Silizium auf makroskopischer Skala. Die Ergebnisse wurden auf der 18th International Conference on Crystal Growth, Nagoya, Japan, im August 2016 präsentiert.

Overview

Silicon (Si) and Germanium (Ge) are materials with a wide application in industry and research. There is still a strong request for research on material and process development, which is in the focus of the activities of the Silicon & Germanium group. The main interest of the group is the material and process development based on the Float Zone (FZ) technique including the growth of isotopically enriched ^{28}Si crystals but also the growth of Si and silicon-germanium (Si_xGe_{1-x}) single crystals by the Czochralski (Cz) technique. Other important topics are the growth of high purity Ge single crystals for detectors in the frame of project GERDA or the research on the growth of specifically doped Ge and Si crystals for basic research as in the BMBF-funded project InTerFEL. A part of the group´s work comprises also service tasks.

This includes the growth of crystals according to customer's specifications but also the growth of small crystals for material characterisation from material produced by cooperation partners such as the company KEPP EU, Riga, Latvia. The availability of different techniques used for Si and Ge crystal growth from the melt as well as our expertise in Si and Ge based single crystals allows the Silicon & Germanium group to perform research activities, which are unique in the world.

In 2016, the third ^{28}Si single crystal was grown in frame of the "Kilogram" project led by the the German national metrology institute Physikalisch-Technische Bundesanstalt (PTB). The aim of the project is a more precise determination of the Avogadro constant, i.e. the number of atoms in one mole. To fulfil the requirements on crystal quality especially with respect to carbon concentration in the final crystal, many purification runs have to be made using the FZ technique before a dislocation free ^{28}Si crystals of 4" in diameter can be grown. One such crystal gives the possibility for the preparation of two silicon spheres and after measurement their volume, mass, and lattice parameter one can get a connection between the volume and the number of atoms.

We started the project "Silicon Crystal Growth from a Granulate Crucible" (SiGRET), which succeeded in the frame of the Leibniz Competition, in the middle of 2016. The aim of SIGRET is the development of a stable growth process for crystals with industry-relevant size, e.g. for photovoltaic applications. Silicon crystal growth from melt in a granulate crucible is a novel concept to obtain crystals with a quality similar to Float Zone (FZ) Si but at much lower feedstock costs [1]. The crystal is pulled from an inductively heated melt pool in a solid Si "self-crucible", which is continuously replenished with Si fluidized bed granules. Since there is no contamination from a crucible material, we achieved a low oxygen content (< $1 \cdot 10^{16}$ atoms/cm^3) in the grown crystals.

In the project GerDA (GERmanium Detector Array) both the Cz growth furnace operating with hydrogen atmosphere and the zone refining plant to produce the highly pure starting material for the single crystal growth are now in use. The modification of the hot zone and process parameters partly based on the global computer simulation of the growth process gives the possibility for control of the dislocation density (EPD) to be in the required range of $10^2 - 10^4$ cm^{-2}. Next, all technological steps towards the final crystal beginning from the material preparation will be optimized with respect to purity to achieve the net concentration of charge carriers of about 10^{10} cm^{-3} needed for production of radiation detectors.

Classical Semiconductors: **Silicon & Germanium**

The task of IKZ in the frame of BMBF-Project InTerFEL (*Time-resolved infrared and terahertz spectroscopy of carrier dynamics in semiconductors with free electron lasers*) is the crystal growth and sample preparation for time-resolved spectroscopy and Raman spectroscopy of shallow donors and acceptors in silicon and germanium. First experiments on Mg doped Si after Mg diffusion doping in standard FZ grown Si showed the presence of Mg-O complexes [2]. This is due to the high affinity of Mg to oxygen. By growth in vacuum, we were able to obtain an oxygen concentration below 10^{15} cm^{-3}. First results are under publication.

Ge-rich and highly boron doped $Si_{1-x}Ge_x$ samples with x=0.75 and 0.9 were provided to the SEMITHERM project partner from Göttingen University for investigating thermophysical properties of the semiconductor melt under microgravity conditions during parabola flights [3]. The samples were made from $Si_{1-x}Ge_x$ polycrystals grown in IKZ by Cz technique. The continuation of experiments using electromagnetic levitation technique (EML) is planned on the board of the ISS space station in September 2017.

Both Lateral-Photovoltage-Scanning- (LPS) and Scanning-Photoluminescence (SPL) are used for the detection of solid-liquid interfaces and defect structures in Si, Ge and SiGe crystals [4,5]. The further development of the methods is performed in the frame of a PhD thesis. Numerical simulation allow for a better understanding of the relation between dopant distribution and LPS signal. First results for the influence of sample shape and its size on the signal measured were obtained in 2016.

Finally, the PhD student Xiaofang Qi from Xi'an University was staying in the group for one year since October 2015 with a grant by the Chinese Scholarship Council. Her topic was the computation of the grain evolution during the solidification of silicon on a macroscopic scale. The results were presented on the 18th International Conference on Crystal Growth, Nagoya, Japan in August 2016.

Results

A ^{28}Si single crystal was grown using the crucible-free Floating Zone (FZ) technique in the frame of the "Kilogram"-project in Mai 2016. The peculiarity of this crystal is the extremely high enrichment of the starting material of 99,9995%. Such record-breaking enrichment is a challenge for all processes involved in crystal growth such as a mechanical preparation of the polycrystalline rod for the growth procedure including a cut of the contacts and making a cone on one side and a groove for the holder on the other side, etching of them and operation during the growth.

Fig. 1
Dislocation free ^{28}Si single crystal grown by FZ technique.

Furthermore, as in earlier experiments a big challenge is to avoid losses of the extremely expensive material in order to eventually have enough material for the final 4"crystal to be able to prepare two crystalline spheres from it.

Because more starting material was available than in previous cases and in addition, there were also residuals from the earlier experiments, it was decided to make eight FZ growth runs. Each growth run leads to a further purification of the starting material from residual impurities such as carbon. This is necessary, because their concentrations in the initial polycrystalline rod is far beyond the upper limit of the requested value [C]=2.0×10^{15} cm^{-3} for the final crystal.

Classical Semiconductors: **Silicon & Germanium**

Oxygen as a second unwanted impurity occurring in the starting material in concentration up to [O]=5 ×10^{17} cm^{-3} can be successfully avoided after some growth runs in vacuum. A more detailed description of the procedure developed for the growth of isotopically enriched ^{28}Si can be found in the institute's Annual Report 2015.

The final – dislocation free – crystal was 100.4 mm in diameter and had a mass of 5.76 kg (Fig. 1). This is 450 g more than in experiments a year before. Crystal growth was performed using an automatic diameter control system allowing precise control of the crystal shape including the tapered crystal end to protect the cylindrical part of the crystal from back-gliding dislocations. Similar to previous experiments <100> oriented ^{28}Si seed crystals were grown by the crucible-free pedestal technique. Two 2" Cz crystals of total mass 1.1 kg were grown from the fragments of polycrystalline silicon and rests from previous experiments. These were joined to the as-deposited material on the upper end of rod. Nearly all Cz grown material except 20 mm from the end of the FZ crystal was lost during the many purification runs (the upper part of so-called "fir" one can see in Fig. 1 above inductive coil). To avoid the isotope dilution during Cz growth, the quartz crucibles used were coated before the growth process with a $^{28}SiO_2$ layer of about 100 µm thickness.

All arrangements during the ^{28}Si processing led to a bigger mass of the crystal and to a 25 mm longer cylindrical part being 185 mm in this case. This means that additionally to two spheres that should be prepared from the beginning and the end of the cylindrical part, there will be enough material for the preparation of samples. These will be used for crystal homogeneity control like carbon distribution and other measurements that have to be determined with a relative uncertainty of better than 2 × 10^{-8} in order to define the value of the Avogadro constant.

New achievements can be reported in the field of the Czochralski growth of highly pure Ge crystals for elementary particle detectors as used in the project GERDA (the GERmanium Detector Array) that aims in the detection of the neutrinoless ββ-decay. ^{76}Ge crystals are used both as material for the decay and as the detector. In addition to the new Cz furnace, which was installed and approved in 2015 for growth in H_2 atmosphere, we developed a new horizontal furnace for zone refining of Ge, which has been installed and approved in 2016. It is dedicated for the purification of Ge both in Ar and H_2 atmosphere (Fig. 2). The furnace also allows the in-house preparation of highly pure material with a net charge carrier concentration less than 10^{10} cm^{-3} to be used for the Czochralski process. It will be also used for the operative recycling of the Ge residuals of crystal growth experiments and detector preparation.

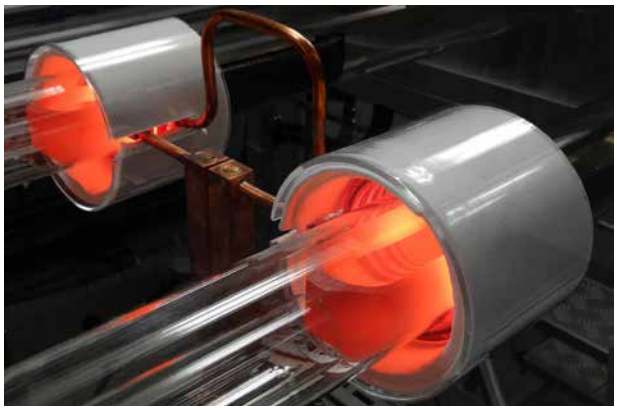

Fig. 2
Zone refining furnace for purification of Ge.

To reach the dislocation density < 10^4 cm^{-2} that is required for the detectors, we optimized the hot zone for better control of the dislocation density during the growth by axisymmetric yet fully transient calculations with the software CGsim. First growth experiments of 2"Ge crystals have been performed, but the results could be applied also for the planned 3" experiments.

The project SIGRET deals with the development of a growth process of silicon from granules. scheme of the process is presented in Fig.3. Prior to the growth experiments, a 2D numerical model for time-dependent calculation of the triple point and crystal shape during the Si-GC process has been implemented in the software COMSOL Multiphysics [6]. Suitable values for inductor power and pull rate (6 – 1.5 mm/min) for crystals with well-defined shape and larger diameter have been obtained. These results were applied to the construction of the hot zone of the standard FZ furnace used in this case. The use of the inductor power to control the diameter is limited, because the inductor power level must also ensure a sufficient extent of the melt pool as well as melting of the continuously replenished granules. On the other hand, control of the crystal diameter by the pull rate is difficult due to the highly nonlinear relationship.

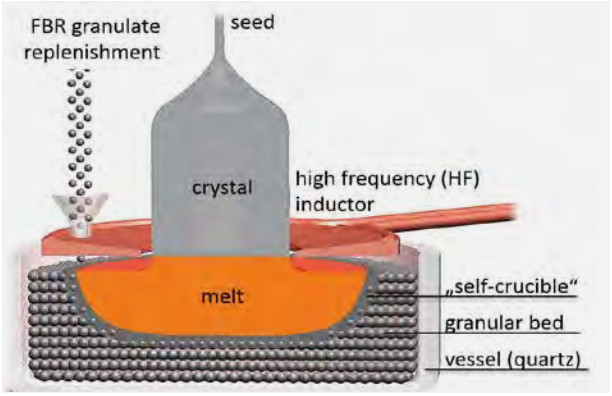

Fig. 3
Scheme of the Si-GC growth concept.

In first growth experiments strong fluctuations of the crystal diameter, as shown in 4a, were observed. Our process development led to crystals with improved cylindrical shape (see Fig. 4b), increased length up to 160 mm (Fig. 4c) and larger diameter up to 50 mm (Fig. 4d). Suitable values for pull rate (10–14 mm/min) and inductor power to perform the Dash seeding technique were identified and for the first time a thin neck was grown (see Fig. 4d).

A special setup for heating the Si granules in the beginning of the process has been installed. It reduced the time needed for the generation of the melt pool from several hours to about 50 min and allowed efficient melting of the Si granules in the center, where the heat induction by the high frequency coil is small.

The detection of doping inhomogeneities in grown semiconductors such as Si, Ge and Si_xGe_{1-x} is the main idea of the Lateral-Photovoltage-Scanning-Method (LPS). Due to the detection of these doping inhomogeneities, it is possible to determine the shape and deflection of the solid-liquid interface. As it is typically not possible to observe the interface during the growth process it is often the only way to get a "fingerprint" of the growth process. The LPS method works as follows: a modulated laser excites locally free charge carriers (electrons and holes), which will diffuse through the semiconductor. If there is a local gradient in the charge carrier density, a directed drift process of these charge carriers takes place, which will lead to a local dipole. The resulting electrical potential is detected with respect to the modulation frequency at the ohmic rim contacts. This process can be simulated using a three dimensional finite-volume calculation. Here the measuring signal can be analyzed for a known dopant distribution.

To determine whether the sample geometry influences the result and leads to a distortion of the measurement's amplitude, i.e. of the signal intensity, the dependency of the LPS-voltage on the sample width was measured and simulated for a rectangular silicon floating zone sample. For an enlarged sample width a decreasing LPS-voltage was detected, which is also described by an equivalent circuit diagram. It was still uncertain, whether the sample width effectively or directly (for every measured spot on the sample) influences the detected LPS-voltage. Clarification of this fact is essential, because a direct influence would distort the measured signal.

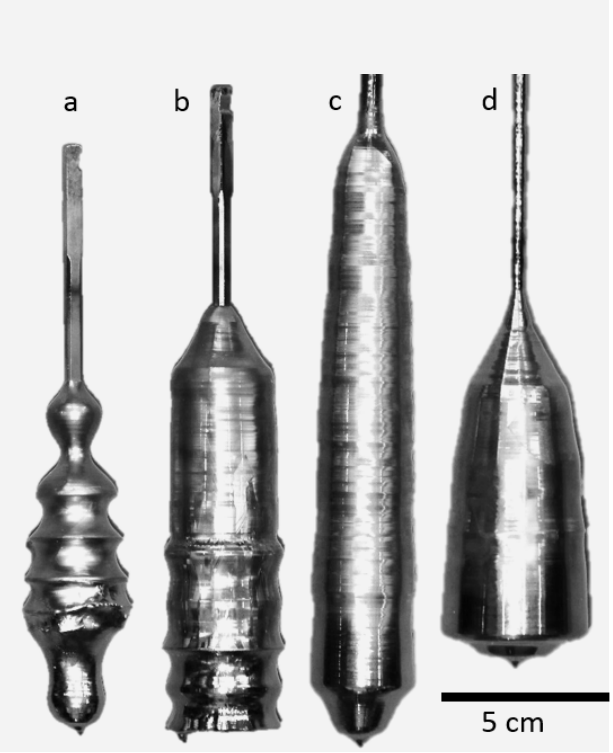

Fig. 4
(a–d) Evolution of Si-GC crystals towards well-defined cylindrical shape, increased length and diameter.

To answer this question, we designed a sample with the geometry shown in Fig. 5. A rectangular sample (blue) was measured with the LPS-setup. The data we are going to analyze are shown as a red line. After the LPS-measurement, the sample was shaped (dashed line) and measured again. For an effective influence of the sample width on the measured signal, every data point should be scaled the same compared to the original data. If there was a distortion, the measuring signal is influenced by the sample width.

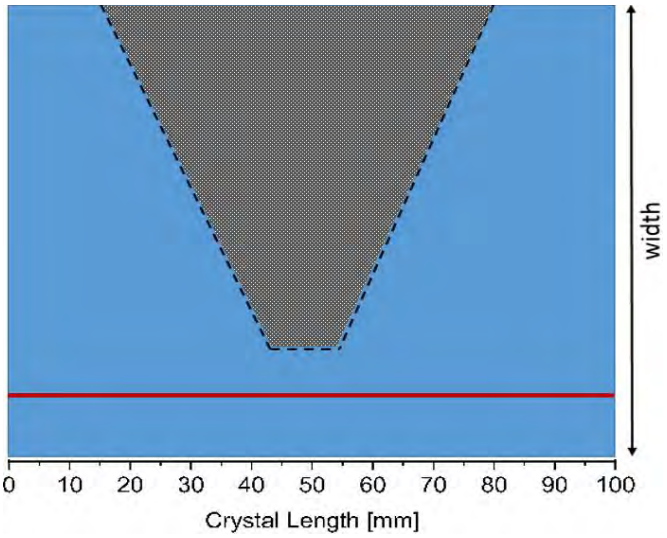

Fig. 5
Scheme of the rectangular sample (blue) with the line scan, which we used for the analysis (red). The dashed line corresponds to the cutting line, where the sample is shaped.

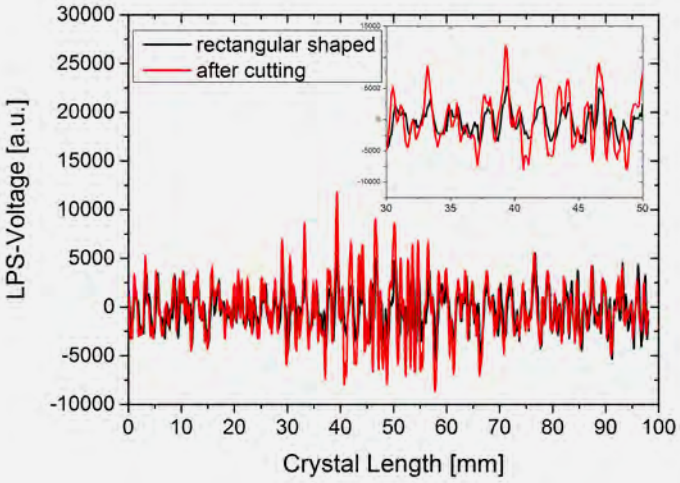

Fig. 6
Diagram of the LPS-voltage dependent on the crystal length for the two analyzed line scans. A distortion of the measurement is observable in the central region, where the sample width differs most.

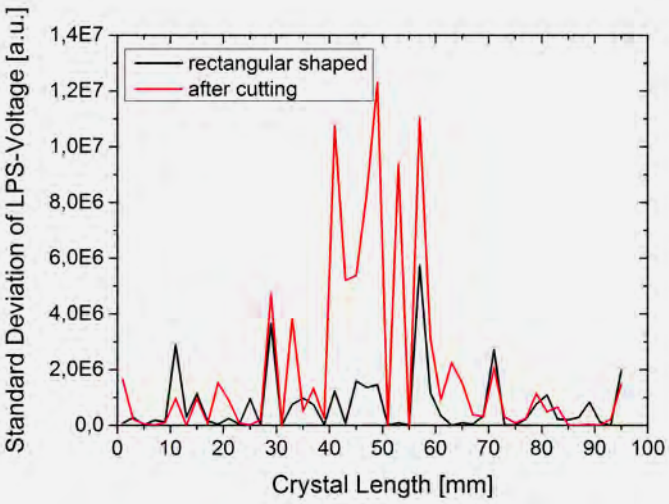

Fig. 7
Diagram of the standard deviation of the LPS-voltage dependent on the crystal length for the two analyzed line scans. For the calculation 20 sequent data points were combined.

The results of the line scans are shown in Fig. 6. Here, the red scan corresponds to the shaped sample and the black scan to the rectangular sample. Directly in the region of the constriction (40 mm ≤ x ≤ 60 mm) the height of the peaks differs between both scans, see Fig. 7, where the standard deviation of the shown LPS-voltage is shown dependent on the locations. Here, the red peaks are larger than the black ones. This difference in the peak height was not detectable in the edge regions (0 mm ≤ x ≤ 20 mm) and (70 mm ≤ x ≤ 100 mm), where the widths of the sample are equal. Consequently, a distortion of the measuring signal was proven due to the change of the sample geometry.

To conclude the results, a measurement of that shaped sample without a constant width is distorted, which indicates, that other geometries without a rectangular shape might also be affected (cone of a crystal, wafer, etc.). The shape of the detected doping inhomogeneities does not change, due to the fact, that the position of the peaks is independent of the sample width. But the height of the peak is distorted. Because of that, an analysis of the strength of the doping inhomogeneity of the increased LPS-voltage is wrong and has to be compensated by a geometry factor. Unclear remains the question, whether the distortion is an edge effect.

References

[1] H. Riemann, N. V. Abrosimov, J. Fischer, M. Renner; International Patent; W02011063795 A1

[2] S. G. Pavlov, N. Deßmann, A. Pohl, V. B. Shuman, L. M. Portsel, A. N. Lodygin, Yu. A. Astrov, S. Winnerl, H. Schneider, N. Stavrias, A. F. G. van der Meer, V. V. Tsyplenkov, K. A. Kovalevsky, R. Kh. Zhukavin, V. N. Shastin, N. V. Abrosimov, H.-W. Hübers; Phys. Rev. B 94 (2016) 075208

[3] Y. Luo, B. Damaschke, S. Schneider, G. Lohofer, N. Abrosimov, M. Czupalla, K. Samwer; npj Microgravity 2 (2016) 1

[4] A. Lüdge, H. Riemann; Inst. Phys. Conf. Ser. 160 (1997) 145

[5] N. V. Abrosimov, A. Lüdge, H. Riemann, W. Schröder; J. Cryst. Growth 237-239 (2002) 356

[6] R. Menzel, H. Riemann, N. Abrosimov; Conf. Proc.: Modelling for Electromagnetic Processing (2014) 465

Classical Semiconductors:
Multi-crystalline Silicon

Head Dr. Frank M. Kießling
Team I. Buchovska, Dr. N. Dropka, Dr. I. Herrmann-Geppert

Überblick

Auch in 2016 setze sich der Trend bei Solarpaneelen zu höheren Zelleffizienzen mit historisch niedrigsten Preisen fort. Industriell dominieren dabei weiterhin Zellkonzepte auf der Basis von p-dotierten multikristallinem (mc-Si) Material. Allerdings ist bekannt, dass n-dotiertes Silicium höhere Volumenlebensdauern und dementsprechend ein höheres Wirkungsgradpotential als p-dotiertes Silicium aufweist. Unter dem immerwährenden Kostendruck sind folglich Forschungs- und Entwicklungsarbeiten zu diesem Materialtyp hoch aktuell. Dabei liegt der Fokus auf der homogenen Verteilung von geeigneten Dotierstoffen bei gleichzeitiger Verringerung von rekombinationsaktiven Kristalldefekten. Auch erfordert die Entwicklung neuer Zellkonzepte für n-Typ mc-Si Material eine angepasste Materialqualität. So ist z.B. bekannt, dass metallische Verunreinigungen die Zelleffizienzen weniger stark beeinflussen. Damit könnte sich die Möglichkeit eröffnen, preiswertere Siliciummaterialqualitäten für diesen Typ von photovoltaischen Bauelementen einzusetzen.

Nachdem in der Arbeitsgruppe in den vergangenen Jahren Züchtungsprozesse für drei Qualitäten von p-Typ Silicium Material – multikristallines (mc), high-performance-mc (HPmc) und quasi-mono (QM) Silicium – mittels gerichteter Erstarrung unter dem speziellen Einsatz von Magnetfeldern entwickelt wurden, fokussierten sich 2016 die Forschungsaufgaben auf die Übertragbarkeit der Prozessparameter auf industrielle Volumina. Dazu wurden Modellrechnungen durchgeführt, um die Anwendbarkeit von Ähnlichkeitsprinzipien zu untersuchen. Erstmalig wurden Methoden der künstlichen neuronalen Netzwerktheorie auf die Prozessvorhersagen angewandt. Die experimentellen Möglichkeiten wurden auf die simultane Nutzung von bis zu 4 G0-großen Tiegeln (< 1kg Einwaage) erweitert, um schneller und kostengünstiger Ergebnisse zu Dotierstoffkonzentrationsverteilungen unter dem Einfluss von Wandermagnetfeldern zu erhalten. Der Einbau der Fremd- bzw. Dotierstoffe wird durch die Form und Morphologie der Wachstumsfront und den Konzentrationsverhältnissen bestimmt. Insbesondere der Transport von Phosphor zur n-Typ Dotierung in der Schmelze zur und weg von der fest-flüssigen Phasengrenze war Schwerpunkt der aktuellen Forschungsaktivitäten. Einige der Ergebnisse werden nachfolgend dargestellt.

Die Gruppe Multikristallines Silicium hat ihre Forschungs- und Entwicklungsaktivitäten auch in 2016 erfolgreich erweitert. Projektfinanziert wurden Untersuchungen des Einflusses von verschiedenen Heißzonenmaterialien auf das Verunreinigungsniveau bei gerichtet erstarrtem Silicium fortgeführt. Die Verfahrensentwicklungen für die G0- und G1-Prozesse wurden vollständig von numerischen Modellierungen begleitet, um die Einflüsse der KRISTMAG® Heizer-Magnet-Modul gesteuerten, magnetischen Kräfte auf das Temperaturprofil, die Schmelzströmungen und die Form der fest-flüssigen Grenzfläche zu untersuchen. Die Ergebnisse wurden in enger Zusammenarbeit mit den Gruppen Kristallbearbeitung und Physikalische Charakterisierung erhalten. Die Gruppe Multikristallines Silicium verfügt seit 2016 zudem über einen modernen Volumenlebensdauermessplatz (MDP-Methode).

Overview

In 2016, again, the trend for solar panels continued with higher cell efficiencies and historically lowest prices. In industrial terms, cell concepts based on p-type mc-Si material continued to dominate. N-doped silicon has higher life times and accordingly a higher efficiency potential than p-doped silicon. Consequently, under the constant cost pressure, research and development topics are highly relevant on this type of material for homogeneous distribution of suitable dopants with a simultaneous reduction of recombination-active crystal defects. Also, the development of new cell concepts for n-type mc-Si material requires an adapted material quality. For example, it is well known that metallic impurities have a deteriorated effect on the cell's efficiency. This could open up the possibility of using less expensive silicon materials for this type of photovoltaic device.

In the past, our group has developed processes for three grades of p-type silicon material – multi-crystalline (mc), high performance mc (HPmc) and quasi-mono (QM) silicon – by means of directional solidification under the special use of magnetic fields. In 2016, the research tasks focused on the transferability of the process parameters to industrial volumes. For this purpose, we carried out model calculations to examine the applicability of similarity principles. For the first time, methods of artificial neural network theory were applied to the process predictions.

We also developed an experimental setup for the simultaneous use of up to 4 G0-sized crucibles (< 1kg initial weight) in order to obtain faster and more cost-effective results on dopant concentration distributions under the influence of magnetic fields. The incorporation of the doping substance is determined by the shape and morphology of the growth front and its concentration ratios. In particular, transport of phosphorus for n-type doping in the melt towards and away from the solid-liquid phase boundary was the focus of the current research activities. Some of the results are presented below.

In 2016, the group Multi-crystalline Silicon has successfully expanded its research and development activities. Project-based investigations were carried out on the influence of different hot zone materials on the impurity level in directionally solidified silicon. The process developments for the G0 and G1 processes were completely accompanied by numerical modeling in order to investigate the influences of the KRIST*MAG*® heater magnet module-controlled magnetic forces on the temperature profile, the melt flows and the shape of the solid-liquid interface.

The results were obtained in close cooperation with the IKZ groups Crystal Processing and Physical Characterization. Since 2016, the group Multi-crystalline Silicon has also been equipped with a modern carrier lifetime measuring device (MDP method).

Results

Optimization of travelling magnetic fields in directional solidification of silicon using artificial intelligence

In directional solidification of silicon (DS-Si) the solid/liquid (s/l) interface shape is crucial for crystal quality and yield. One way to flatten the interface is to tailor the melt flow pattern by travelling magnetic fields (TMFs). Despite the first promising experimental results about the application of TMF in DS-Si on the industrial scale [1], it is still a very challenging task to derive optimal magnetic parameters, i.e., to find a suitable TMF and to adjust it to the continuously changing growth process dynamics. So far, no methodology for a fast identification of the optimal magnetic parameters, for various ingot scales and furnace geometries has been developed. In our numeric study the two statistical methods, artificial neural networks (ANN) [2] and Gaussian process models (GP) [3], have been used to represent the non-linear relationship between the crystal growth process parameters and the interface shape in order to optimize TMF for the interface flattening. ANNs are a family of models inspired by biological neural networks (brain) and are used to very quickly estimate outputs of unknown functions that can depend on a large number of inputs. The term: unknown function means that the physical relationship among inputs and outputs is not known. GPs (if imposed on ANN) provide additionally uncertainty information to the ANN predictions. Both methods can work in the stand-alone mode that enables numerous applications, particularly in the field of the automation and process control. Quick estimations of outputs for certain inputs are particularly attractive for DS-Si growth since outputs like temperature and velocity values in the silicon and the position/shape of the s/l interface are not available during the growth, neither experimentally due to the contamination risks by their measurements nor numerically due to the long time required to finish CFD simulations.

Fig. 1
Verification of ANN predictions of magnetic parameters for interface flattening, i.e. CFD results with corresponding interface deflection for buoyancy regime and TMF driven flow with optimized parameters: frequency 9.38 Hz, phase shift -90.12° and current 99.59 A.

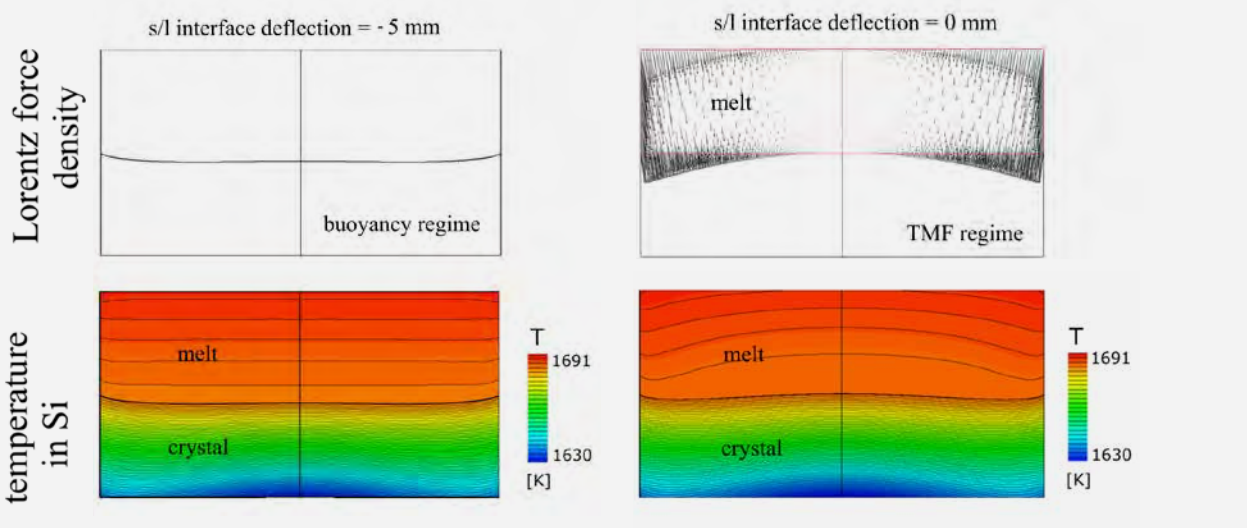

The basic concept of ANN can be explained as follows: ANN is characterized by a "net architecture" that comprises a set of so-called "artificial neurons" and connections between them structured into "hidden layers". Each neuron receives inputs and processes them, i.e. it multiplies them by "weights" and then uses the sum of such weighted inputs as the argument for some previously selected nonlinear function, which yields the final output of the neuron (so-called "activation"). The goal of network is to adjust the weights (process called "training") to minimize error between ANN predictions and targeted output values. Weights can be adjusted in a various ways e.g. using the method of gradient descendent with constant learning rate as used in this study. To derive a network, numerous input-output data sets are necessary that is in DS-Si nearly impossible to obtain experimentally. In this study, we used axisymmetric CFD modeling to generate data sets for ANN and GP. The CFD modeling was also used to verify the ANN predictions of the optimal magnetic parameters for interface flattening (Fig. 1). The CFD model described crystal growth in a G1- size furnace (G1 ingot size 22 x 22 x 13 cm^3) equipped with a side KRIST*MAG*® heater magnet module. For ANN and GP methods, the input parameters comprised: the common magnetic parameters (i.e. frequency, phase shift and current magnitude) and initial s/l interface deflection in a buoyancy mode. The output variable was the final interface deflection in TMF mode. Altogether, 437 such input-output data sets were used.

The best ANN with the lowest mean square error was obtained for the feedforward ANN architecture with three layers (i.e. input, hidden and output layers), 13 neurons in the hidden layer, a training algorithm Bayesian Regularization and the logistic sigmoid activation [2]. Using this ANN, an inverse derivation of magnetic parameters that assure flat interface was feasible for any initial deflection in a buoyancy regime. For example, for initial concave solid-liquid interface deflection of -5 mm, flat interface will be obtained using magnetic parameters frequency 9.38 Hz, phase shift -90.12° and current 99.59 A (Fig. 1). Applying GP method and training it on ANN residuals, probability distribution was calculated for flat interface as a function of frequency, phase shift, current and initial interface deflection (Fig. 2). The results showed that the higher initial interface concavity, the lower is the probability to flatten the interface. For very concave initial interface e.g. -21.89 mm, no combination of magnetic parameters can flatten the interface, i.e. the mean value of interface deflection remained close to the initial value and the probability was very close to 0. Detailed results of this study are given in [4].

The knowledge gained in this preliminary study was further used in a project "Model-based control and regulation of the VGF crystal growing process using distributed parametric methods" funded by the DFG and carried out in the group Galliumarsenide.

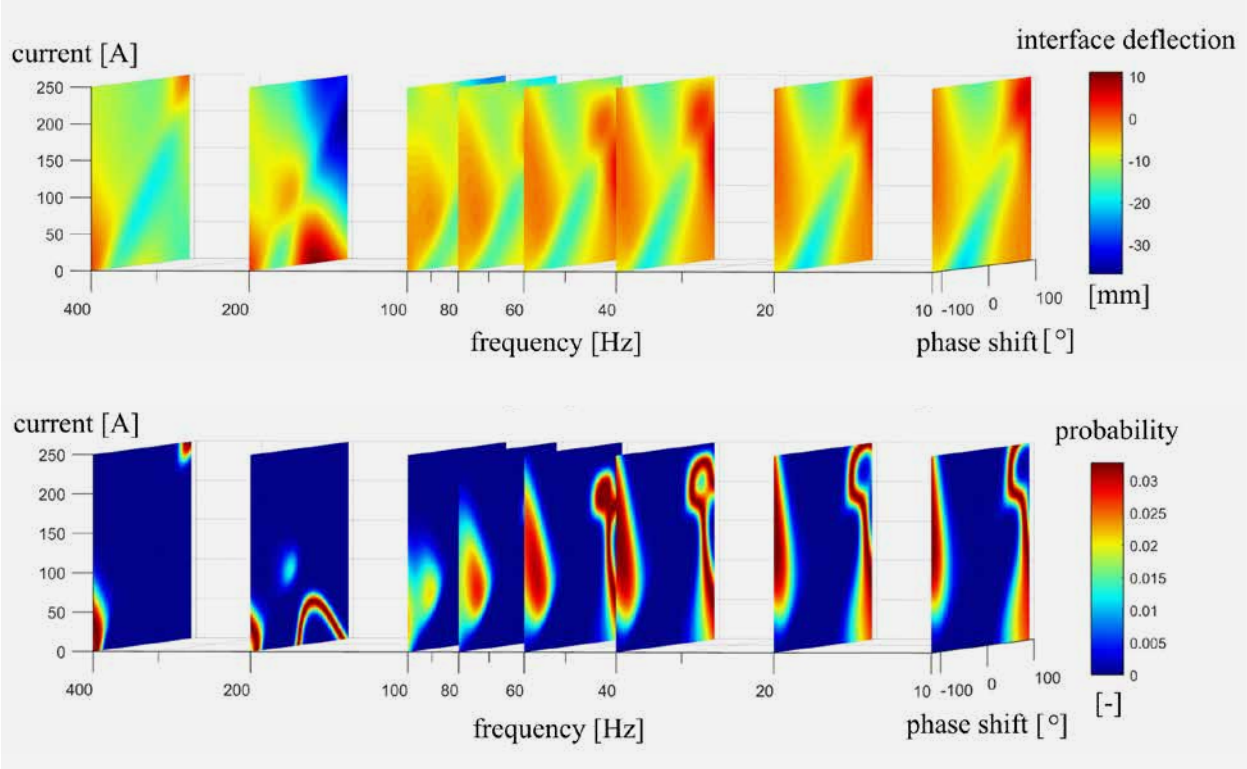

Fig. 2

Results for the superposition of the GP and ANN: mean value of interface deflection and probability distribution for flat interface as a function of frequency, phase shift and current magnitude. The initial interface deflection was – 7.45 mm.

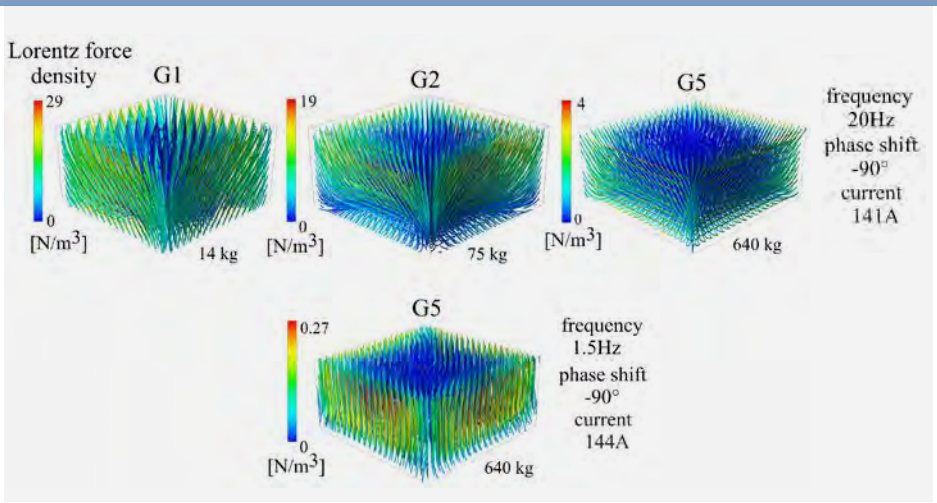

Fig. 3
Magnetic similitude in DS-Si melts during scale up. Lorentz force density streamlines: in G1-G5 sizes for the same magnetic parameters frequency 20 Hz, phase shift -90°, current 141 A, in G5 size for frequency 1.5 Hz, phase shift -90°, current 144 A.

Scale up aspects of directional solidification and Czochralski growth processes in travelling magnetic fields

A common approach to improve the economy of DS-Si and Cz-Si processes includes higher crystallization yields by upscale crystal sizes while preserving the material quality. Despite many research studies at the lab scale, transfer of technology between different scales is still empirical and limited to low scale up ratios, liquid metals experiments, low process temperatures and small cylindrical crucibles. Therefore, higher scale up ratios easily become speculative.

The fundamental scale up approach is achieved by applying a theory of similitude [5], which involves maintaining the characteristic dimensionless group constant during scale up. However, in magnetically driven DS-Si and Cz-Si growth processes, this is impossible to attain. For example, for preserving the magnetic forcing value F constant by upscaling from G1 to G5 size, magnitude of Lorentz force density F_L should decrease 50.6 times down to the negligible value of F_L = 0.57 N/m³ (Fig. 3). The same is valid for a shielding number S. To preserve S value by scale up from G1 to G5, the frequency has to decrease significantly. Consequently, the slope of Lorentz forces will also change and therewith the efficiency of TMF for interface shaping. Obviously, magnetic forcing F and shielding number S alone are not able to describe magnetic similarity.

Nevertheless, the similitude analysis, even incomplete, allows the most important phenomena and the impact of furnace size on the crystal growth process to identify.

The aim of our numerical study was to derive a set of similarity principles for 3D modeling of DS-Si and Cz-Si processes in TMF that assure safe scale up and to verify the obtained results with the available experimental data from the real furnaces (Fig. 4). Particularly, we studied DS-Si in real G1, G2 and G5 size furnaces and Cz Si growth in 6" and 24" crucibles (Fig. 4). TMF was adjusted to improve the s/l interface (DS growth) and melt stirring (Cz growth).

The results showed that the benefits of magnetic stirring and s/l interface shaping in crystal growth processes with more than one driving force (e.g. Lorentz force, rotational force, buoyancy force...) could be preserved by scale up, if the ratio of dimensionless numbers that include all variables relevant for the problem is kept constant. Particularly, during scale up of magnetic driven DS and Cz, it is important to preserve the ratios of Grashof, Forcing and Stefan numbers $F \cdot Gr^{-1} \cdot Ste^{-1}$ and $F \cdot Gr^{-1}$ constant, respectively. Details about this method are described in [6]. This result can be considered as an extension to the common scale up method that was derived for one driving force where each characteristic dimensionless number must remain constant by up scaling.

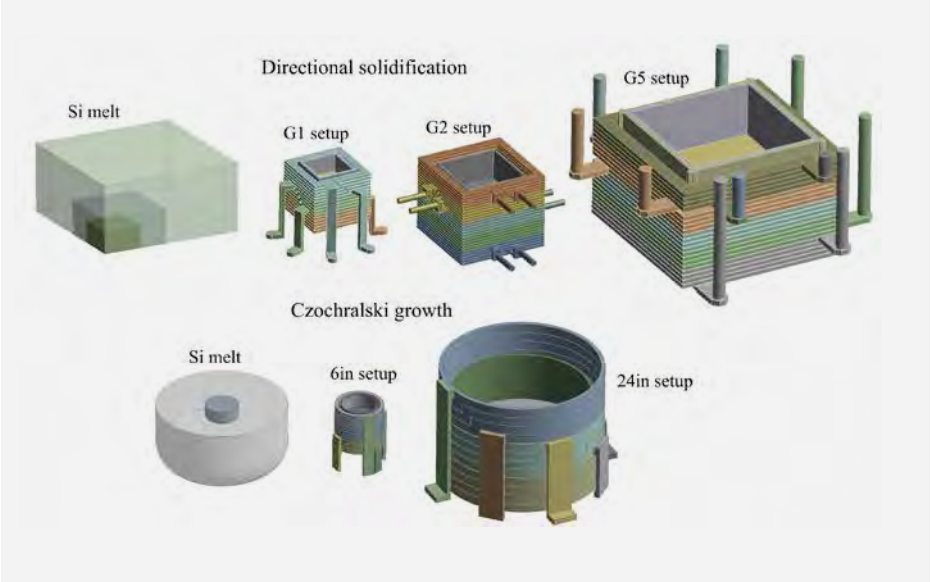

Fig. 4
Crucial parts of DS-Si and Cz-Si crystal growth furnaces equipped with KRISTMAG® heater magnet modules at various scales.

a)

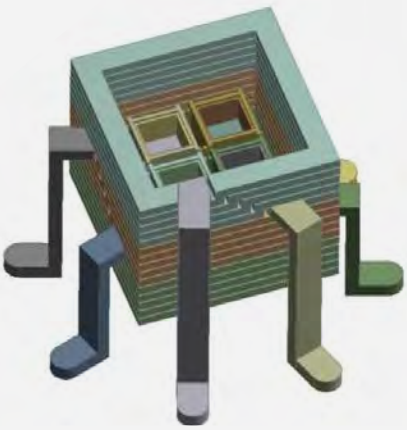

b)

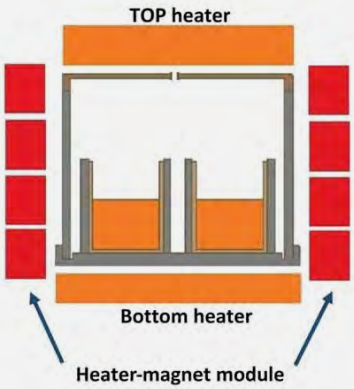

c)

d)

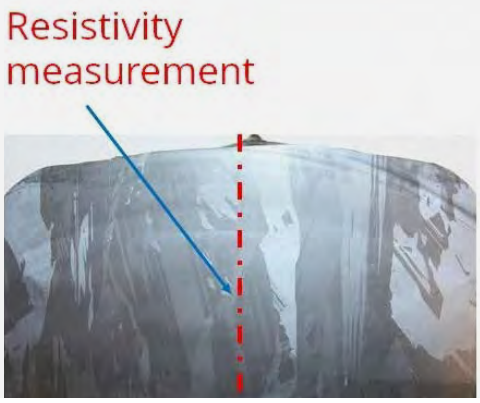

The influence of TMFs on phosphorus distribution in n-type multi-crystalline silicon

Since silicon material with n-type conductivity is the main candidate for utilization in novel high-efficiency solar cells, special attention was given to phosphorus-doped mc-Si. Directional solidification is a simple, relatively cheap and convenient process, but involves complex interaction between melt flow, growth conditions at the solid-liquid interface and impurity transport. Travelling magnetic fields (TMFs) give a contactless opportunity to influence directly the melt flow in direction and velocity. In consequence of enhanced melt stirring, heat and mass transport, the concentration of impurities and dopants along the solid-liquid interface and, hence, their distribution in the crystallized ingot [1, 7, 8] can be effectively controlled. In this research, it is used for two purposes: to decrease/avoid harmful inclusions in the crystallized material and to secure more homogeneous dopant distribution across the ingot.

A process for DS of mc-Si under the influence of different TMFs (no external stirring, weak external stirring, and strong external stirring) has been developed for rectangular G0-sized setups. Comparing resistivity profiles and impurity distributions, the influence of enhanced stirring by TMF on segregation effects has been investigated. All ingots grown within this research work had a non-deflected crystallization front and columnar grain structure (Fig. 5), proving that the developed 4xG0 setup can be successfully used for DS of 4 mc-Si ingots at a time. By keeping the quantity of dopant in each of 4 ingots the same for all sets enhanced melt stirring by TMF during DS significantly decreases phosphorus concentration in mc-Si ingots (Fig. 6). Since all other parameters such as charge composition, crucibles and their coating, temperature and heat profiles were identical, the results indicate that the main reason for dopant loss is not due to segregation effects but to evaporation from the melt surface during charge melting and melt homogenization. Experimental data show that phosphorus evaporation depends linearly from initial concentration in the charge, and increases with intensity of melt stirring by TMF (Fig. 7). Resistivity of G0 ingots were measured by 4-probe method and the values were compared to the target resistivity calculated from initial doping in accordance to Scheil segregation distribution [9]. We used resistivity measurements to derive the real distribution of phosphorus in experimental ingots and built a segregation model through curve fitting with ordinary least square (OLS) method by linear regression in log-log scale.

Fig. 5
a) 4xG0 setup for directional solidification of mc-Si;
b) Layout of DS furnace with 4xG0 setup and module for TMF;
c) 4 G0-sized mc-Si ingots grown in one set,
d) Columnar grain structure is seen on a vertical cut of a G0 ingot.

It can be concluded that an adopted DS recipe with variable strength of TMF on different stages of melting, homogenization and crystallization can be successfully used to enhance/reduce phosphorus evaporation during DS process and to control resistivity distribution along mc-Si ingots. Investigations are in progress to develop a suitable process for bigger ingots.

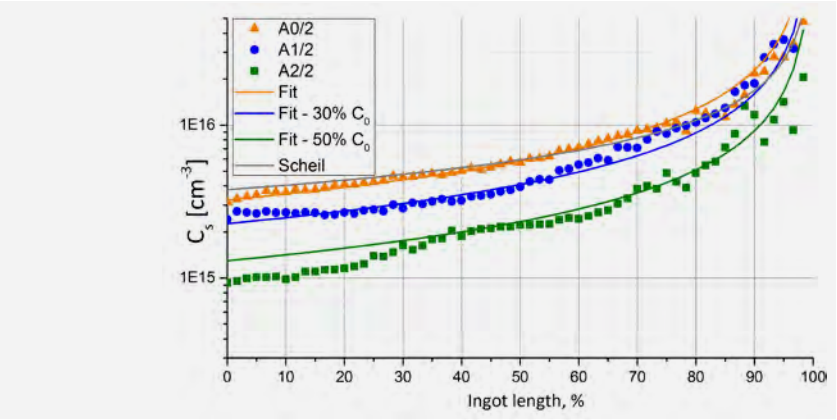

Fig. 6
Distribution of phosphorus along G0 mc-Si ingot length for different strength of TMF stirring (A0 – no magnetic stirring, A1 – weak magnetic stirring, A2 – strong magnetic stirring) and respective fitting curves. Initial concentration of phosphorus in the charge $C_0 = 2.2 \times 10^{16}$ cm^{-3}. Lorenz force for A2 experiment is 3 times higher than for A1. The same curve fitting coefficients suit phosphorus trends for all ingots. Variable fitting parameter is concentration at the beginning of crystallization.

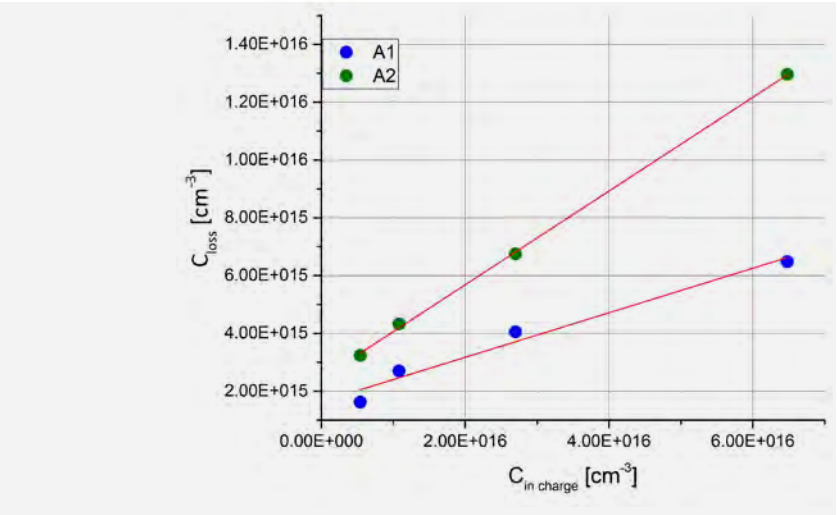

Fig. 7
Phosphorus evaporated from silicon melt surface during charge melting and melt homogenization vs initial phosphorus concentration in the charge depending on the strength of TMF (stirring A2 > A1).

References

[1] Ch. Kudla et al.; J. Cryst. Growth 365 (2013) 54

[2] R. Rojas; Neural Networks: A Systematic Introduction; Springer, Berlin (1996)

[3] E. Rasmussen, C. Williams; Gaussian Processes for Machine Learning; MIT Press, Cambridge (2006)

[4] N. Dropka, M. Holena; J. Cryst. Growth 471 (2017) 53

[5] G. Murphy; Similitude in engineering; The Ronald Press Company, New York (1950)

[6] N. Dropka, M. Czupalla, T. Ervik, F.-M. Kiessling; J. Cryst. Growth 451 (2016) 95

[7] M. Cablea, K. Zaidat, A. Gagnoud, A. Nouri, Y. Delannoy; J. Cryst. Growth 401 (2014) 883

[8] F. Santara, Y. Delannoy, A. Autruffe; J. Cryst. Growth 340 (2012) 41

[9] W. Thurber, R. Mattis, Y. Liu, J. Filliben; The relationship between resistivity and dopant density for phosphorus- and boron-doped silicon; National Bureau of Standards Special Publication 400-64 (May 1981)

Classical Semiconductors:
Gallium Arsenide

Head Dr. Christiane Frank-Rotsch
Team Dr. K. Giziewicz, Dr. R. Zwierz, O. Root, Dr. R. Bertram, Dr. N. Dropka

Überblick

Das III-V-Halbleitermaterial Galliumarsenid (GaAs) ist nach Silicium das häufigsten eingesetzte Halbleitermaterial. GaAs wird in der WLAN-Kommunikation, sowie in der Mikrowellen- und in der Hochfrequenztechnologie eingesetzt. In den letzten Jahren ist der GaAs-Markt durch den rasanten Anstieg der mobilen Kommunikation und des Leuchtdioden-Marktes stark gestiegen. Neben der stetigen Verbesserung der Kristallqualität stehen die Steigerung der Ausbeute der Kristallisationsprozesse sowie die Senkung der Prozesskosten im Fokus der Forschungsaktivitäten. Eine der Voraussetzungen für einen hochwertigen VGF-gewachsenen GaAs-Einkristall ist eine leicht konvexe Form der fest-flüssig-Phasengrenze (Kristallisationsfront). Die Verwendung von externen Feldern, insbesondere Wandermagnetfeldern (TMF) zeigt ein großes Potenzial, diese Anforderung zu erfüllen. Die von dem IKZ in enger Kooperation mit ihren akademischen und industriellen Partnern entwickelte KRISTMAG®*-Technologie [1], bietet ein einfaches und dennoch leistungsstarkes Werkzeug, um definierte Wandermagnetfelder in einem breiten Parameterbereich zu erzeugen. Die* KRISTMAG®*-Technologie wurde bei Züchtung verschiedener Halbleitermaterialien (z.B. Galliumarsenid,, Germanium, Silizium) erfolgreich eingesetzt.*

Derzeit sind zwei Vertical Gradient Freeze (VGF) Anlagen zur Züchtung von III-V-Verbindungshalbleitern mit einem KRISTMAG®*-Heizer-Magnet-Modul ausgestattet. Dieses ermöglicht eine gleichzeitige, aber entkoppelte Erzeugung von Wärme- und Wandermagnetfeldern. Die Forschungsaktivitäten der GaAs-Gruppe fokussieren sich vor allem auf eine weitere Verbesserung der Form der fest-flüssig-Phasengrenze bei der GaAs-Einkristallzüchtung sowie auf die Reduzierung von Temperaturfluktuationen während der Kristallzüchtung zur Stabilisierung des Einkristallwachstums. Um die Form der fest-flüssig-Phasengrenze bei längere Kristalle effektiver zu beeinflussen, wurde ein Decken-Heizermagnetmodul (THMM) [2] entwickelt, welches oberhalb des Tiegels positioniert wird.*

Die experimentellen Arbeiten wurden von numerischen Berechnungen der räumlichen Verteilung der mittels THMM erzeugbaren Lorentz-Kräfte begleitet.

Weiterhin ist in Zusammenarbeit mit der TU Dresden das DFG-Projekt „Modellbasierte Steuerung und Regelung des Vertical-Gradient-Freeze-Kristallisationsprozesses mit Hilfe verteilparametrischer Methoden" gestartet worden.

Hierzu werden in einer numerischen Studie künstliche neuronale Netze (ANN) angewandt, um nichtlineare Beziehungen zwischen den VGF-Prozessparametern zu bestimmen und die TMF-Parameter für die Verbesserung der fest-flüssig-Phasengrenze zu optimieren. Die Forschungsaktivitäten im BMBF-geförderten Verbundprojekt „Toxikologische, physikalisch-chemische und gesellschaftliche Erforschung innovativer Materialien und Prozesse der Optoelektronik – TEMPO" wurden im Oktober 2016 erfolgreich abgeschlossen. Die Projektergebnisse können bei der toxikologischen Evaluation von GaAs und weiterer bedeutender Halbleitermaterialien für die Mikroelektronik wie z. B. GaN im Zusammenhang mit REACh (Registrierung, Bewertung, Zulassung und Beschränkung chemischer Stoffe) und CLP (Klassifizierung, Kennzeichnung und Verpackung von Stoffen und Gemischen) der EU genutzt und berücksichtigt werden.

Overview

The III-V compound semiconductor gallium arsenide (GaAs) is, apart from silicon, the most widely deployed semiconductor material. GaAs is commonly used for wireless communication in microwave or high frequency technology. In the last years, strong growth of the GaAs market took place, mainly because of the rapid growth of the mobile telecommunication and the LED market. Besides the continuous improvement of the GaAs single crystal quality, the enhancement of the yield of the growth process and the reduction of process costs are our key research activities. One of the prerequisites for a high quality VGF-grown single crystal of GaAs is a slightly convex shape of the solid-liquid (s/l) interface. The use of external fields, especially traveling magnetic fields (TMF), shows great potential to fulfill this requirement.

The KRISTMAG® [1] technology developed at IKZ in close cooperation with academic and industrial partners provides a simple yet powerful tool to create traveling magnetic fields within a broad parameter range. It has been successfully applied to the growth of different crystalline materials, among them semiconductors like gallium arsenide, germanium or silicon.

Currently two of our Vertical Gradient Freeze (VGF) furnaces are equipped with a KRISTMAG® heater magnet module (HMM) allowing simultaneous, but decoupled generation of heat and travelling magnetic fields.

The research activities in the GaAs group are mainly focused on the further improvement of the s/l interface shape in the VGF growth of GaAs single crystals, as well as on the reduction of temperature fluctuations during the process to stabilize the single crystal growth. Additionally, to effectively influence the shape of the s/l interface by longer crystals, a top HMM (THMM) [2] has been developed and mounted above the crucible.

Our experimental work was accompanied by numerical calculations for the spatial distribution of the Lorentz forces generated by THMM.

Furthermore, in 2016 the DFG project "Model-based control and regulation of the VGF crystal growing process using distributed parametric methods" has been started in cooperation with the Dresden University of Technology. In the frame of this project artificial neural networks (ANN) are applied in a numeric study to determine the non-linear relationship among the VGF process parameters and to optimize the TMF parameters to improve the s/l interface shape.

The research activities in the BMBF-funded collaborative project "Toxicological, physico-chemical and social research on innovative materials and processes in optoelectronics – TEMPO" were successfully completed in October 2016. The project results can be considered in the toxicological evaluation process of GaAs in connection with REACh (Registration, Evaluation, Authorisation and Restriction of Chemicals) and CLP (Classification, Labelling and Packaging of substances and mixtures) regulations of the EU.

Results

The application of TMF to enhance the VGF growth of single GaAs crystals is one of the group's core activities. Continuous improvement of the KRIST*MAG*® technology, indicated by the subsequent achievements, has been partially covered in the annual reports since 2013. In particular, the following results are worth mentioning: the successful simultaneous growth of single crystals in a multi-crucible HMM with the help of special designed traveling magnetic fields (Annual Report 2013), the successful growth of 4 inch GaAs single crystals with a 2.5-fold increased growth velocity under adjusted TMF parameters without loss of crystal quality (Annual Report 2014) and the improved stability of facets in the conical segment of the crystal using TMF (Annual Report 2015). In 2016, flattening of the s/l interface through a precise and constant control of the melt flow during the growth has been the key aspect of our research. We could show that low thermal conductivity of GaAs hampers faster growth of high-quality crystals exceeding a certain length.

As shown in Fig. 1, increased deflection of the s/l interface has been observed in the upper part of crystals with more than 20 cm length. This could be solved with a top HMM for efficient heat removal during the growth of long GaAs crystals, which we already filed as patent [2]. Placed above the crucible and consisting of two spiral heaters, the THMM should enable generation of downward Lorentz forces, acting on the upper part of the melt. Favorable direction of the Lorentz force vector was confirmed in the first numerical simulations as shown in Fig 2. A further advantage of THMM is that its installation in the VGF equipment requires only minor changes in the hot zone, facilitating future transfer to the industry. The developed spiral shaped THMM has been already installed in an existing VGF furnace in IKZ (Fig. 3). Its applicability to GaAs single crystal growth will be experimentally proven in the framework of the joint project EneRed with Freiberger Compound Materials GmbH as industrial partner.

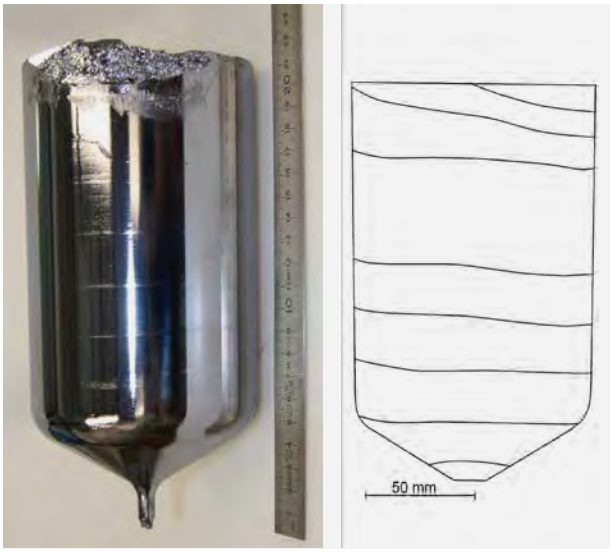

Fig. 1
4inch GaAs:Si single crystal (left) and its s/l interface shape (right). Weight: 9kg.

Within the frame of the DFG project "Model-based control and regulation of the VGF crystal growing process using distributed parametric methods" commenced in April 2016, artificial neural networks (ANN) and Gaussian process (GP) models have been applied to optimize the VGF parameter field. More details on the concept of ANN and our preliminary studies can be found in the chapter Multi-crystalline Silicon of the Annual Report 2016. In the initial project phase the focus was set on adjusting VGF and TMF parameters, in order to obtain a nearly flat s/l interface. Our goal was to derive ANN and use it as a standalone function that enables the experimenter to quickly select magnetic parameters for the next experiment without any knowledge of time-consuming and labour intensive Computational Fluid Dynamics (CFD) simulations. Such ANN function is the first step towards the advanced process control in the future cyber-physical systems, i.e., in smart factories.

Classical Semiconductors: **Gallium Arsenide**

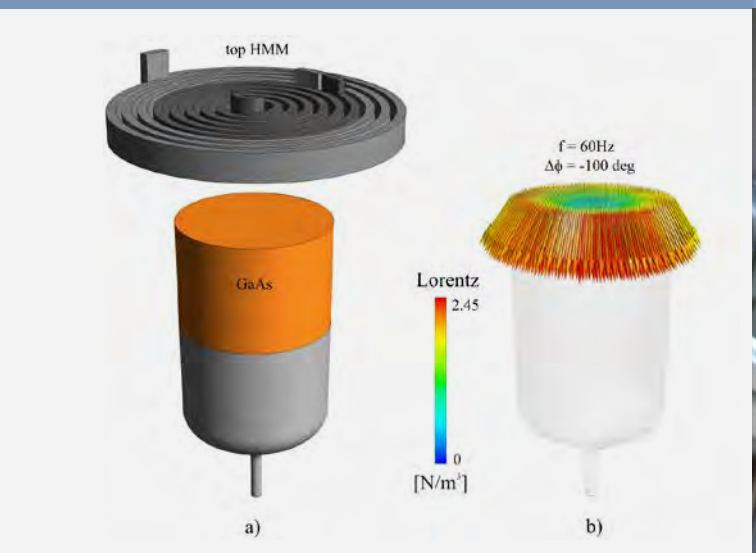

Fig. 2
THMM a) model, b) Lorentz force distribution calculated for f=60Hz, Δφ=-100° [2].

Fig. 3
Image of the newly developed spiral shaped THMM installed at IKZ.

The accuracy of ANN predictions depends on the availability of numerous input-output data sets to "train" the network. In VGF-GaAs crystal growth, the large number of diverse data is too costly to provide experimentally. Therefore, we generated data numerically by axisymmetric CFD simulations and verified them by available experimental data.

In our model, TMF was induced by a built-in side HMM, in a form of three coil stack. The set of input parameters for the quasi-steady state 2D simulations performed by the commercial software CrysMAS included: magnetic parameters (frequency f, phase shift Δφ and magnitude of the effective AC current I_{eff}) and crystal growth parameters (initial interface deflection Δ_{ini} and growth rate r_{growth}). The final interface deflection under TMF Δ was the derived output. From CFD simulations we obtained 135 input-output data sets necessary for ANN modeling. The best ANN predictions were obtained using ANN architecture shown in Fig. 4.

The success of the predictions of interface deflection by ANN in comparison to the "real values" provided by CFD simulations is shown in the parity plot in Fig. 5. In order to better understand the relationship among the magnetic and process parameters and the loci of optimal magnetic parameters, in cooperation with Leibniz Institute for Catalysis (M. Holena) the GP method was superimposed to the ANN basic function and the probability of flat interface |D| < 0.1 mm calculated, as a function of the set of growth and magnetic parameters f, Δφ, I_{eff}, Δ_{ini} and r_{growth}.

A higher probability for the flat interface can be obtained for various combinations of frequency, phase shift and current magnitude, if the initial interface is slightly concave (Fig. 6), while for very concave initial interface, no combination of magnetic parameters can flatten it, i.e. mean value of Δ remained close to the D_{ini} value and the probability was very close to 0. Further on, low frequencies and negative higher phase shifts benefited interface flattening (Fig. 6).

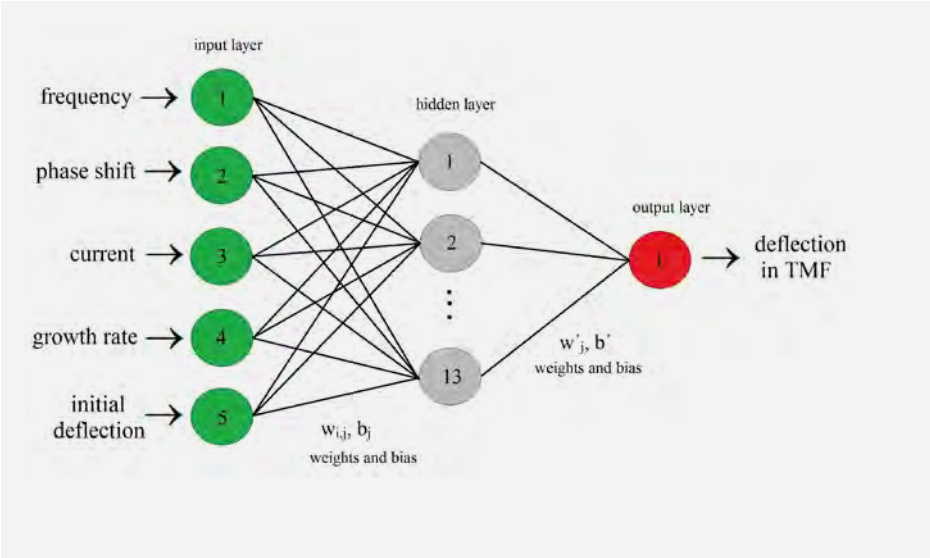

Fig. 4
Architecture of a neural network with five inputs, one output and one hidden layer with 13 neurons. Arrows and lines represent information flow.

Classical Semiconductors: **Gallium Arsenide**

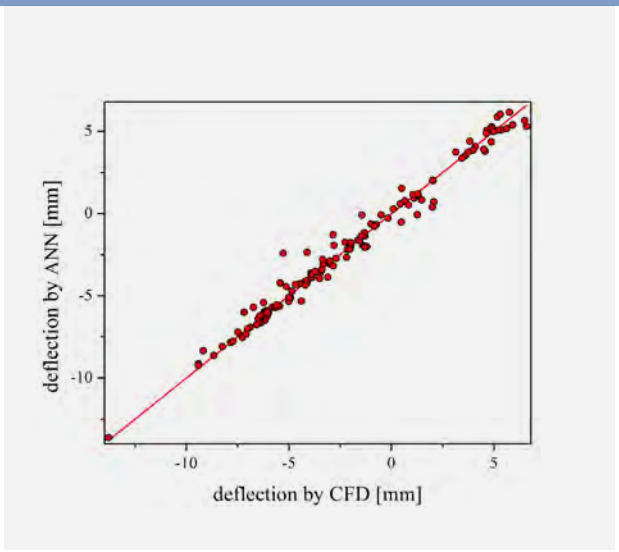

Fig. 5
Parity plots: interface deflections obtained by 2D CFD/magnetic modeling vs. deflections predicted by ANN.

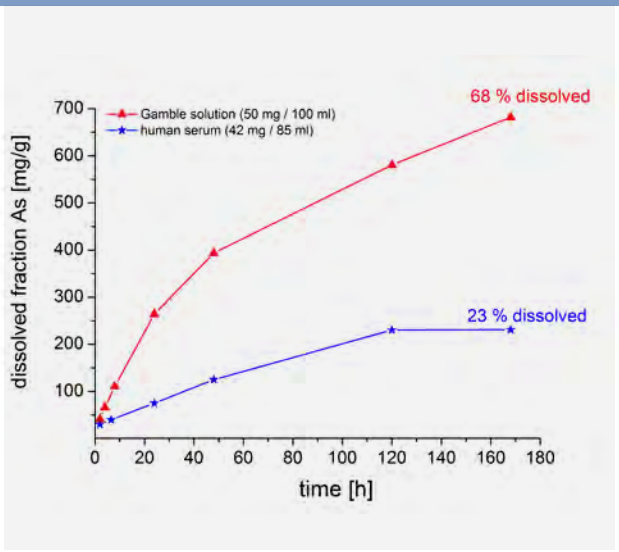

Fig. 7
Time dependence of dissolved fraction of the GaAs powder in human blood plasma compared to inorganic Gamble model solution.

Beside the enhancement of GaAs crystal growth and the process control development, a third major research point was focused on the systematic continuation of solubility experiments of semiconductors within the framework "TEMPO".

"TEMPO" stands for the German title of the BMBF funded project:"**T**oxikologische, physikalisch-chemische und gesellschaftliche **E**rforschung innovativer **M**aterialien und **P**rozesse der **O**ptoelektronik", which means "Toxicological, physical-chemical and social investigation of innovative materials and processes of the optoelectronics". In the previous annual report the results of GaAs solubility in inorganic simulated body fluids: lung fluid (Gamble, pH=7.4) and artificial lysosomal fluid (ALF, pH=4.5) were presented. It was shown that solubility of arsenic in the solution increases with the pH-value of the latter (Annual Report 2015).

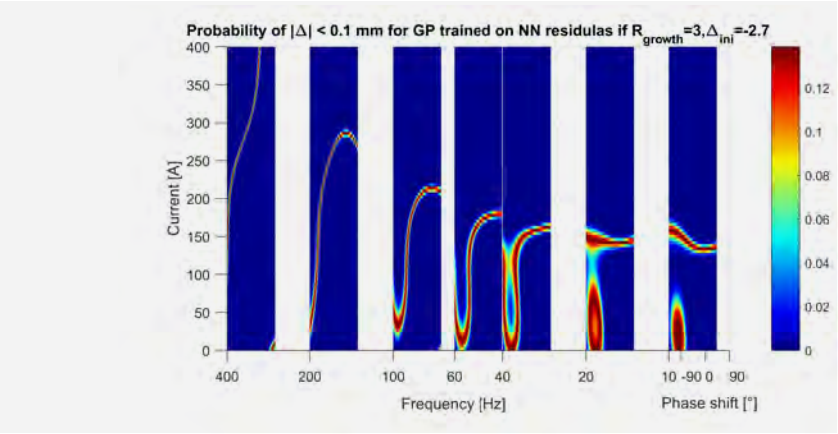

Fig. 6
Probability distribution for flat interface |Δ|<0.1 mm, as a function of f, Δφ, l_{eff} for fixed r_{growth} Δ_{ini}.

In the last year, series of experiments with human blood plasma were conducted to investigate the solubility behavior of GaAs powder in correlation to its toxicological evaluation process. Prior to these investigations, extensive preliminary tests were required to optimize the experiment execution, sampling and sample analysis. For instance, the finest, yet not dissolved solid particles could be separated from the solution in a centrifuge, but not by using a standard ultrafine filter. The results of the GaAs powder solubility behavior in the human blood plasma or diluted with Gamble solution are compared in Fig. 7. Under the same solution conditions, the dissolved fraction of the GaAs powder in the human blood plasma was lower by a factor of about 3, presumably due to colloid formation in the solution. Further detailed results of the solubility experiments will be communicated in a forthcoming publication.

The obtained results of the TEMPO project represent a scientifically reliable data base, which is available to all project partners in industry and research and can be used in future evaluations, in particular within the framework of the REACh process.

References

[1] P. Rudolph; J. Cryst. Growth 310 (2008) 1298

[2] N. Dropka, Ch. Frank-Rotsch, R.-P Lange, P. Krause; Crystallisation system and crystallisation method for crystallisation from electrically conductive melts, and ingots that can be obtained by means of the method; Patent description W02014/202284A1

Dielectric & Wide Bandgap Materials

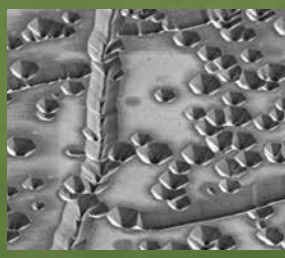

Dielectric & Wide Bandgap Materials

Head of department: Prof. Dr.-Ing. Matthias Bickermann

Die Abteilung Dielektrika und Wide-Bandgap-Materialien befasst sich mit der Volumenkristallzüchtung von Nitriden, Oxiden und Fluoriden. Unser Ziel ist die Herstellung einkristalliner Materialien mit maßgeschneiderten Eigenschaften und hoher Ausbeute, die als Substrate oder Massivkristalle für neuartige und energieeffiziente elektronische, optoelektronische und optische und piezoelektrische Bauelemente Verwendung finden. Unsere Aktivitäten zeichnen sich durch eine starke Zusammenarbeit IKZ-intern (Kristallbearbeitung, Epitaxie und Charakterisierung) sowie mit Industriepartnern und anderen Forschungseinrichtungen. Zur Abteilung gehören die Themengruppen Aluminiumnitrid (AlN), Galliumnitrid (GaN) und Oxide/Fluoride. Die Aktivitäten zu Galliumnitrid wurden zum Ende des Jahres eingestellt, die Mitarbeiter der Gruppe werden künftig die anderen Aktivitäten der Abteilung mit ihrer Expertise unterstützen.

Die Gruppe AlN erforscht und entwickelt Technologien der AlN-Kristallzüchtung aus der Gasphase. AlN-Substrate dienen der Herstellung von effizienten Leuchtdioden im tiefen Ultraviolett oder neuartigen Leistungsbauelementen. Die AlN-Züchtungstechnologie wird im Rahmen des Konsortiums „Advanced UV for Life“ zu einer industrietauglichen Methode weiter entwickelt, gleichzeitig werden den Partnern Substrate für die Bauelemententwicklung zur Verfügung gestellt. Die Entwicklung von UV-C-transparenten AlN-Substraten wird in diesem Jahresbericht als „Highlight“ vorgestellt. Zudem untersucht die Gruppe den Einsatz neuer Tiegel- und Isolationsmaterialien, die Kontrolle von Verunreinigungen, die gezielte Dotierung mit Sauerstoff, Kohlenstoff, Silizium und die Mischkristallbildung mit Scandium. In einem weiteren Projekt entwickelt die Gruppe zusammen mit mehreren Industriepartnern die plasma-gestützte Abscheidung von hochreinen dicken AlN-Schichten.

Die Aktivitäten der Gruppe Oxide/Fluoride gliedern sich in Substratkristalle für die Oxidelektronik, Kristalle für Hochtemperatur-Piezoelektrika, optische und Laser-Kristalle sowie Referenzkristalle für die Materialforschung. Der Fokus liegt auf der Czochralski-Züchtung bei hohen Temperaturen, bei Bedarf können auch andere Züchtungsverfahren zum Einsatz kommen. Die Vielfalt der Substratkristalle lässt sich weiter untergliedern in Kristalle mit Perowskit-Struktur (z.B. $SrTiO_3$, $BaSnO_3$) für ferroelektrische Schichten mit neuen Funktionalitäten und in transparente halbleitende Oxidkristalle (z.B. β-Ga_2O_3, In_2O_3, $MgGa_2O_4$). Beide sind Teil der umfangreichen, Epitaxie und Charakterisierung umfassenden IKZ-Aktivitäten im Leibniz WissenschaftsCampus „GraFOx“. Bei beiden Themen steigt das weltweite Interesse derzeit aufgrund der einzigartigen Materialeigenschaften stark an. Als neues Forschungsthema und DFG-Projekt wurde die Herstellung von Delafossit-Kristallen ($CuAlO_2$) aufgenommen. Im Bereich der Hochtemperatur-Piezoelektrika wurde zusätzlich zur Züchtung von Langasit-Kristallen mit der Erforschung von $LiNbO_3$-$LiTaO_3$-Mischkristallen begonnen.

Im September 2016 ist Dr. Reinhard Uecker, der langjährige Leiter und Vordenker der Gruppe Oxide/Fluoride in den Ruhestand getreten. Als Nachfolger wurde Dr. Steffen Ganschow eingesetzt, der die Oxidzüchtung seit der Institutsgründung 1992 begleitet und mitgeprägt hat.

The department Dielectric and Wide Bandgap Materials focuses on the bulk crystal growth of nitrides, oxides, and fluorides. Our research goal is to prepare single crystal materials with tailored properties and high yield for use as substrates or bulk material in novel and energy-efficient electronic, optoelectronic, optical/laser, and piezoelectric applications. Our activities are characterized by strong collaborations with companies and other research institutes as well as within the IKZ (wafering, epitaxy, characterization). In 2016, the department comprised the teams Aluminium Nitride (AlN), Gallium Nitride (GaN), and Oxides/Fluorides. At the end of the year, the Gallium Nitride activities will be discontinued, the team members will support the other groups with their expertise.

Aluminium Nitride focusses on research and development of the preparation of AlN bulk single crystals by physical vapour transport (PVT). These crystals are used as substrates for the preparation of efficient deep-UV optoelectronic and novel power electronic devices. AlN growth technology development towards industrial application as well as substrate supply for device development is performed within the "Advanced UV for Life" consortium. Our successful quest to provide deep-UV transparent AlN is described in the "Highlights" section. Additionally, we investigate utilization of advanced crucible and insulation materials, impurity control as well as doping and alloying with oxygen, carbon, silicon, and scandium during PVT growth. In a separate project, the team works with industrial partners to develop plasma-assisted deposition of thick, high-purity polycrystalline AlN films.

The activities of the group Oxides/Fluorides can be categorized into substrate crystals for oxide electronics, crystals for high-temperature piezoelectrics, optical and laser crystals, and unique crystals for material references and benchmarks. The focus lies on high temperature Czochralski melt growth techniques, although a variety of other methods are utilized as well. Substrate crystals for oxide electronics are further subdivided into perovskites for ferroelectrics and novel functionalities (e.g. $SrTiO_3$, $BaSnO_3$) and bulk transparent semiconducting oxides (e.g. β-Ga_2O_3, In_2O_3, $MgGa_2O_4$). Both are part of the broad IKZ activities within the Leibniz ScienceCampus "GraFOx", which also features epitaxy and dedicated characterization, and both see a steeply increasing worldwide interest because of their unique materials properties. In 2016, a new research topic has been opened up by DFG-funded crystal growth of delafossite ($CuAlO_2$) crystals. Regarding high-temperature piezoelectrics, research has started on $LiNbO_3$-$LiTaO_3$ mixed crystals to complement our activities on langasite-type crystals.

Dr. Reinhard Uecker, mastermind and long-term head of the Oxides/Fluorides team, retired in September 2016. Dr. Steffen Ganschow, senior expert in oxide crystal growth and IKZ member since 1992, was appointed as new team leader.

Dielectric & Wide Bandgap Materials:
Oxides/Fluorides

Head Dr. Reinhard Uecker , Dr. Steffen Ganschow
Team M. Brützam, Dr. Z. Galazka, Dr. S. Ganschow, Dr. C. Guguschev, D. Kok, M. Rabe, I. Schulze-Jonack, Dr. D. Schulz, A. Tauchert, E. Thiede

Überblick

Im Berichtszeitraum jährte sich Czochralskis Arbeit „Ein neues Verfahren zur Messung der Kristallisationsgeschwindigkeit der Metalle" zum einhundertsten Mal [1]. Dieser zwei Jahre nach der Einreichung des Manuskripts erschienene, dreiseitige Bericht gilt als Geburtsstunde des nach dem Autor benannten Verfahrens. Heute wird die Mehrheit technisch relevanter Einkristalle nach dem Czochralski-Verfahren hergestellt, allen voran Silizium. Aber auch für viele optische Komponenten, wie z.B. Laserkristalle, Faraday-Rotatoren oder nicht-linear optische Materialien ist es wegen der erreichbaren Kristallperfektion und -größe eines der meist angewandten Verfahren zur Einkristallzüchtung.

Unsere Arbeitsgruppe beschäftigt sich mit Fragestellungen, die im Zusammenhang mit dem Wachstum und der Züchtung von oxidischen und fluoridischen Einkristallen stehen. Methodisch steht hierbei die Schmelzzüchtung im Mittelpunkt, unter Anwendung des bereits erwähnten Czochralski-Verfahrens. Wegen der hohen Schmelztemperaturen der Oxide von nicht selten über 2000°C wird der meist aus Iridium oder Platin gefertigte Schmelztiegel induktiv geheizt. Dabei wird die zum Schmelzen benötigte Wärme nicht durch einen zusätzlichen Heizer erzeugt, sondern im Tiegel selbst. Dies hat zur Folge, dass das beheizte Volumen im Prinzip auf Tiegelgröße beschränkt werden kann, was zu einer kurzen Ansprechzeit und somit guten Regelbarkeit führt. Darüber hinaus wird durch diese Art des Wärmeeintrags die Wahl der Atmosphäre im Züchtungsrezipienten nicht eingeschränkt und kann von reduzierend bis oxidierend recht frei gewählt werden. Diesen Vorteil machen wir uns zu Nutze, um aus den verschiedenen möglichen Oxidationszuständen der den Kristall konstituierenden Metalle den „richtigen" zu stabilisieren. Unterstützung finden die experimentellen Arbeiten in der thermodynamischen Simulation der entsprechenden Systeme.

Seit Institutsgründung schon bilden Kristalle mit kubischer und pseudokubischer Perowskitstruktur einen Themenschwerpunkt der Arbeitsgruppe. In der Hauptanwendung dienen diese Kristalle als Substrate für die Abscheidung funktioneller Schichten. Durch gezielte Modifikation der Zusammensetzung und somit der Gitterparameter des Substrats lassen sich Gitterverspannungen der epitaktisch aufgewachsenen Schichten einstellen („strain engineering") und so die Eigenschaften der Schichten variieren. Insbesondere besteht derzeit ein hoher Bedarf an Substraten mit großen (pseudo)kubischer Gitterparametern. Die Seltenerdscandate ($RESc0_3$) decken einen weiten Bereich zwischen etwa 3,946 und 4,021 Å ab, doch für viele neue Materialien werden Substrate mit noch größeren Gitterparametern benötigt. Hier sind unsere Aktivitäten auf $RE(Sc,Lu)0_3$ fokussiert. Eines der klassischen und immer noch wichtigsten Perowskitsubstrate ist das Strontiumtitanat ($SrTi0_3$) mit einem Gitterparameter von 3,905 Å. Dieses Material wurde bisher mit Methoden realisiert, die zu einer relativ geringen Kristallqualität führten. Insbesondere für die Steigerung der Performance von Bauelementen, bei denen zweidimensionale, hochbewegliche Elektronengase (2DELs) Verwendung finden, sowie für moderne Feldeffekt-Transistoren und Speicherelemente sind $SrTi0_3$-Einkristalle höherer Perfektion erforderlich. Unsere im Leibniz-Wettbewerb geförderten und im Berichtszeitraum zum Abschluss gebrachten Forschungsarbeiten haben gezeigt, dass es mit einer innovativen Technik möglich ist, hochqualitative $SrTi0_3$-Volumenkristalle zu züchten. Im Rahmen des Projektes konnte Dirk J. Kok seine Doktorarbeit zum Thema „Influence of the growth conditions on the optical properties of $SrTi0_3$" am Institut für Chemie der Humboldt-Universität erfolgreich verteidigen.

Piezoelektrische Kristalle für Messanwendungen bei hohen Temperaturen stellen einen weiteren Schwerpunkt der Arbeiten dar. Hier stehen Materialien im Mittelpunkt, die eine hohe piezoelektrische Empfindlichkeit mit geringer Temperaturabhängigkeit der Eigenschaften kombinieren. Zu diesen gehören Materialien aus der Gruppe der Langasite, für die die Verbindung $La_3Ga_5Si0_{14}$ namensgebend ist. Es handelt sich ausnahmslos um synthetische Verbindungen, die ursprünglich als Laserwirtsmaterial, im Laufe der Zeit jedoch zunehmend als Material piezoelektrische Wandler und Resonatoren eingesetzt wurden.

In einer Zusammenarbeit mit Partnern an der TU Clausthal und dem IFW Dresden konnte gezeigt werden, dass auf der Grundlage von $Ca_3TaGa_3Si_2O_{14}$ verlustarme BAW-Resonatoren gefertigt werden können, die bis nahe an den Schmelzpunkt des Materials (1390°C) einsetzbar sind [2]. Transparente halbleitende Oxide (TCO) stehen im Mittelpunkt des Leibniz-WissenschaftsCampus GraFOx („Growth and fundamentals of oxides for electronic applications"). In diesem forschen zwei Leibniz-Institute, ein Max-Planck-Institut und zwei Universitäten in Berlin an Oxiden für elektronische Anwendungen. Oxidkristalle aus unserer Arbeitsgruppe spielen hier die wichtige Rolle des Substrats, auf dem funktionale Schichten wachsen werden.

Weiter fortgeschritten ist ein DFG-Projekt zur Züchtung und Charakterisierung von Delafossit ($CuAlO_2$) Einkristallen. Diese Substanz gehört zur sehr kleinen Untergruppe von transparenten, leitenden Oxiden, die intrinsisch p-leitend sind und diente bereits zur Herstellung rein oxidischer p-n-Übergänge [3]. Auch wenn für elektronische und optoelektronische Anwendungen oft keramisches Material oder aufgedampfte Schichten genügen, werden Einkristalle benötigt um grundlegende Eigenschaften des Materials zu untersuchen. In eigenen Voruntersuchungen [4] konnte gezeigt werden, dass das experimentelle Fenster, in dem zum einen Oxidation des in $CuAlO_2$ vorhandenen Cu^+ zum Cu^{2+}, zum anderen aber auch Reduktion zu metallischem Cu (welches sich mit Pt-Tiegeln legiert und diese zerstört) unterdrückt wird, extrem klein ist. Trotzdem konnten wir inzwischen erste einkristalline Flitter von 1-2 mm Durchmesser durch Kristallisation aus der Schmelze erzeugen.

Neben diesen Schwerpunktthemen wurden auch 2016 wieder zahlreichen Forschungsinstituten oxidische und fluoridische Einkristalle für Untersuchungen zur Verfügung gestellt.

Overview

The year 2016 marks the 100th anniversary of Czochralski's work on „A new method for measuring the speed of crystallization of metals" [1]. This three pages short report published two years after submission is considered the birth of the crystal growth technique named after the author. Today, the majority of single crystals with significant technological or scientific impact are made by the Czochralski technique. Thanks to the achievable crystal size and quality this technique is most commonly used one not only for semiconducting but also for optical materials.

Our group deals with problems connected with the growth of oxide and fluoride single crystals. From the methodical point of view our work is focussed on growth from melts, mainly by the Czochralski technique. Due to the usually high melting point temperatures of oxide compounds, the metallic crucible is heated by contactless radio frequency induction heating. Here the heat necessary for melting is generated in the crucible which is usually made of platinum or iridium. The heated volume is not much larger than the crucible itself and therefore the response time remains short and the process is easily controllable. Moreover, the atmosphere inside the growth vessel is not additionally constricted by the heater material and can be adjusted from oxidizing to reducing. Thus, we are able to stabilize the required oxidation state of the metal in the grown crystal. Accompanying thermodynamic simulation of the constituting metal–oxygen systems is an extremely helpful tool supporting the experimental work.

For several years crystals with cubic or pseudocubic perovskite structure have been a core topic of our group. The main application of these materials is as substrates for the deposition of functional films. Modifying the composition and therewith the lattice parameters of the substrate crystals is a way to intentionally strain the on-growing film and influence its physical properties. For new emerging oxides like $BaSnO_3$ for electronic applications there is a demand for substrates with large lattice parameters, larger than rare earth scandates ($REScO_3$) and solid solutions thereof can cover. Here we focus our current activities on the development of a crystal growth process for $RE(Sc,Lu)O_3$.

An "old" but still one of the most widely used perovskite substrates material is strontium titanate $SrTiO_3$. This material requires specific growth conditions that are realized only in techniques that lead to rather low structural perfection. So far, $SrTiO_3$ is the only oxide material which can host a 2D electron gas at the interface with another oxide layer, an effect that possibly enables creation of minituarized electronic components requiring high electron mobility. These applications involve an extraordinary perfection of substrate and films. During the report period a project aiming at the development of growth techniques yielding high quality $SrTiO_3$ crystals supported by the Leibniz Association in the frame of Leibniz Competition could be concluded with remarkable success. Moreover, Dirk Kok could successfully finalize his thesis "Influence of the growth conditions on the optical properties of $SrTiO_3$" at the chemistry department of the Humboldt University.

Dielectric & Wide Bandgap Materials: **Oxides/Fluorides**

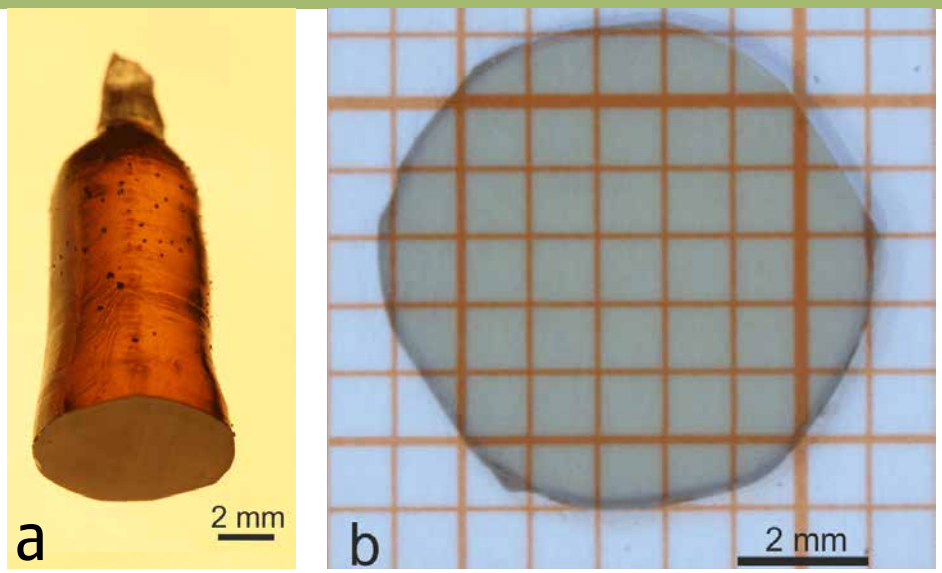

Fig. 1
(a) Mosaicity-free $SrTiO_3$ single crystal grown by top-seeded solution growth at temperatures below 1535°C [6].
(b) Chemo-mechanically polished wafer prepared from the crystal shown in (a) [6].

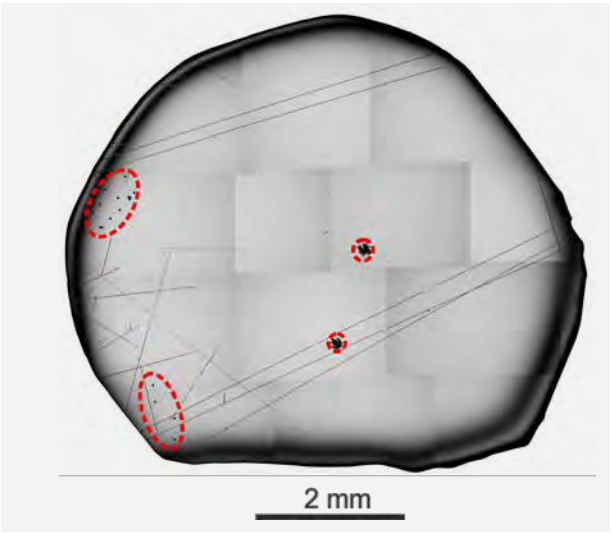

Fig. 2
Image of the defect selective etched wafer created from a series of micrographs across the sample [6]. The sample is almost dislocation-free, with the exception of the orange colored encircled regions. Dislocation positions are highlighted for visibility. Note: traces of wiping and few scratches are visible by smears and linear structures.

Piezoelectric crystals for sensing and measurement applications at high temperatures constitute a further field of work. Of special interest are materials combining high piezoelectric sensitivity and electric resistivity with weak temperature dependence of their properties. Among them the so-called langasites (named after the synthetic $La_3Ga_5SiO_{14}$) have attracted attention of numerous research groups. Initially expected to be of use as laser host materials, langasites have been used more and more in electro-mechanical transducers and resonators. In cooperation with our long-term partners at the Technical University in Clausthal and at the Leibniz-Institute for Solid-State Research in Dresden we could realize low-loss bulk acoustic wave resonators on the base of $Ca_3TaGa_3Si_2O_{14}$ single crystals that work up to temperatures less than 100 degrees the melting point of the material around 1350°C [2].

Transparent semiconducting oxides (TSO's) are in the focus of the Leibniz ScienceCampus GraFOx („Growth and fundamentals of oxides for electronic applications"). In the frame of this campus five research teams in Berlin explore novel oxides for electronic applications. Bulk crystals grown in our group serve as substrates for growth of functional films.

Our work on growth and characterization of delafossite ($CuAlO_2$) single crystals supported by the DFG has made remarkable progress. This material belongs to a small subgroup of TSO's that show intrinsic p-type conductivity and has already been used for the fabrication of p-n junctions exclusively on oxides [3]. Single crystals are required for fundamental exploration of physical properties of the material. Our preliminary studies [4] show that the experimental window for the exclusive stabilization of Cu^+ is extremely narrow. Nevertheless, we succeeded in preparing still tiny (linear dimensions around 1 mm) but after all single crystalline flakes by crystallization from the melt.

In addition to these activities we delivered crystal samples to numerous research institutes and groups around the world.

Results

Top-seeded solution growth of $SrTiO_3$ single crystals with improved structural quality

The unique properties of $SrTiO_3$ (STO) along with the phase stability allow a very broad application in the field of thin film growth. STO has been used as a substrate for high temperature superconducting, thermoelectric and multiferroic applications, including sensors, transducers, ferroelectric field effect transistors, memory devices and data storage. It can be considered as a key model material for oxide electronics based on an interfacial two-dimensional electron gas (2DEL) and for metal-oxide-semiconductor field-effect transistors. So far most of these devices are fabricated on commercially available substrate crystals grown by the Verneuil method, but the available crystal quality hinders progress for several applications in these fields.

Consequently, the development of devices outperforming today's limitations requires STO substrates of high perfection. In the frame of a project funded by the Leibniz Association, we applied several bulk crystal growth techniques to fill that gap. One of the most successful growth techniques we applied is called the edge-defined film-fed growth (EFG) method. Cylindrical high quality $SrTiO_3$ bulk single crystals with diameters between 15 and 16 mm and lengths between 13 to 50 mm were grown from stoichiometric melts by using this technique [5] (details can be also found in the annual report of 2015). For melt growth (at temperatures of about 2080°C), one of the factors that may lead to a further improvement of the structural quality is the use of nearly dislocation-free seeds. Therefore, a part of the work was focused on the growth and preparation of such "seed" crystals by application of an additional technique: the top-seeded solution growth (TSSG) method using TiO_2-rich self-fluxes (non-stoichiometric melts) and growth temperatures below 1535°C [6]. This was mainly done by optimization of the thermal conditions to achieve stress-free long-term cylindrical growth. Fig. 1 shows an example of a TSSG-grown $SrTiO_3$ single crystal with a diameter of about 7 mm and a length of 20 mm grown under these conditions. The crystal was grown from a dislocation free seed prepared from a heterogeneously nucleated crystal. As can be seen from the image of the defect selective etched wafer in Fig. 2, no subgrains were found, proving mosaicity-free material. Dislocations were mainly found in two minor areas close to the periphery of the crystal, marked with two ellipses. In these areas dislocation densities of 5×10^2 cm^{-2} and 2.3×10^3 cm^{-2} were determined, respectively. Additionally, near the central part of the samples two well-defined regions were identified as dislocation bundles, which can be described as traces of moscaicity.

The results clearly show that the TSSG method is indeed suitable to grow mosaicity-free and nearly dislocation-free $SrTiO_3$ single crystals. Sufficiently low infrared absorption of the material at temperatures below 1535°C helps to achieve stable cylindrical growth and excellent control of the growth process. Additionally, low temperature gradients along the growth front and moderate axial temperature gradients along the growing crystal allow a defect minimized broadening of the crystal and a negligible stress component during growth. It almost allows to preserve the superior quality of the dislocation-free seed crystal. The achieved crystal quality for the presented crystal geometry is important in scaling up, since such high quality crystals now can directly serve as seed crystals for bulk crystal growth experiments using the edge-defined film-fed growth (EFG) method.

Non-destructive detection of subgrains in calcium scandate bulk single crystals using the energy dispersive Laue mapping technique

In addition to bulk crystal growth a new, non-destructive characterization method, named energy dispersive Laue mapping (EDLM), has been introduced for checking the presence of low angle grain boundaries in bulk crystals, the details of which are shown in ref. [7]. This methodology was developed in cooperation with the Bruker Nano GmbH (Berlin, Germany) using $SrTiO_3$ single crystals and multicrystalline silicon as model systems and was also applied to other materials like Wüstite ($Fe_{1-x}O$) [8] or $NdGaO_3$ [9] to identify high and low angle grain boundaries as well as twin boundaries. In this chapter we demonstrate the practicability of this method for the subgrain detection in bulk $CaSc_2O_4$ crystals [10].

$CaSc_2O_4$:Ce is not only interesting as light phosphor for light emitting diodes [11], but it is also discussed as candidate for green solid-state lasers [12,13]. Calcium scandate crystallizes in a calciumferrate(II) ($CaFe_2O_4$) type (Pnam space group) structure [14] and has a high melting point of 2110°C [15,16]. It is known from the literature that this material usually shows growth instabilities during Czochralski growth, which led to small crystal sizes (10 mm in diameter and of 5 mm in length) [12]. We solved this issue by growing under modified conditions using N_2 as growth atmosphere, an iridium crucible and an actively-heated afterheater. We achieved a crystal diameter of 20 mm and a total crystal length of 70 mm (Fig. 3).

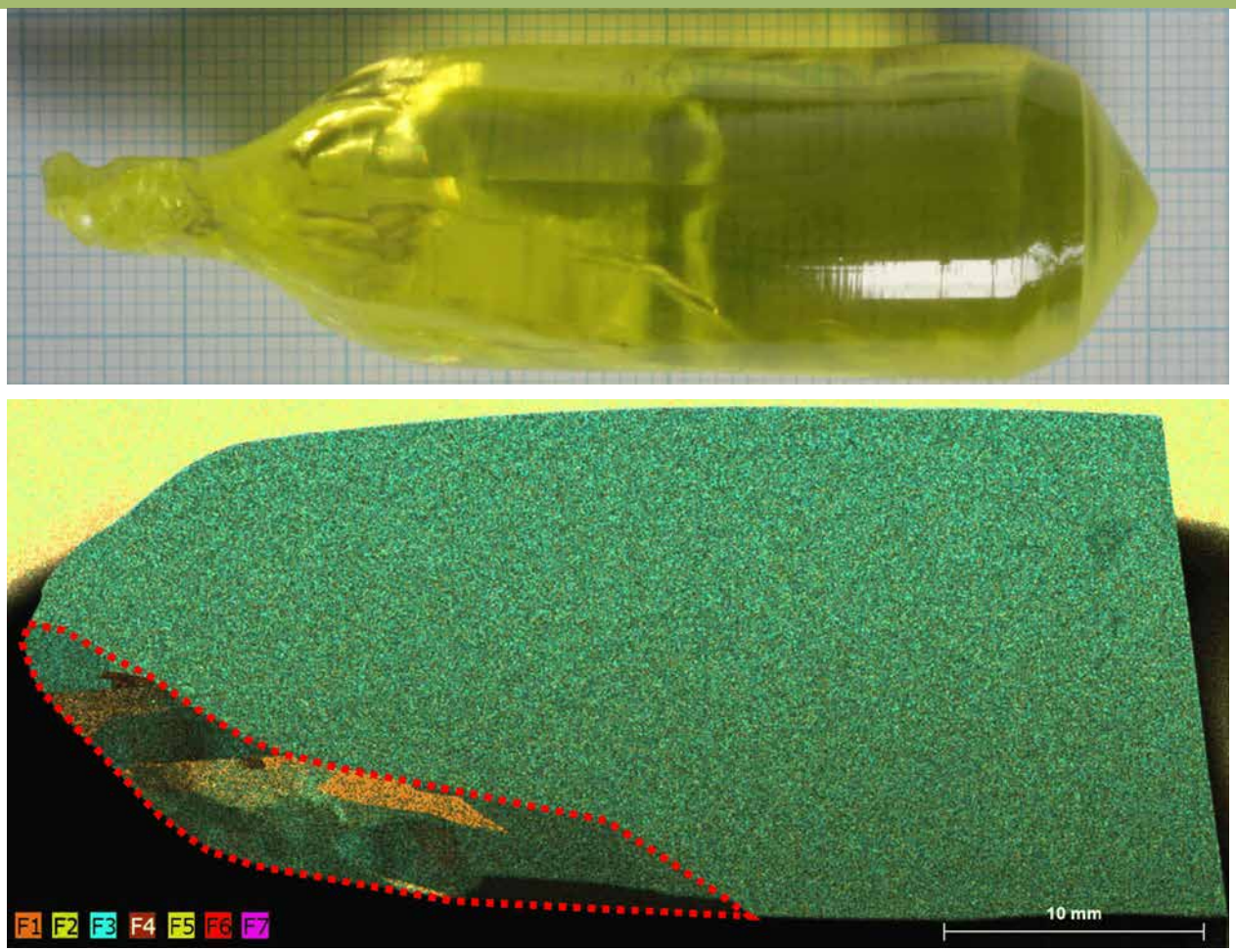

Fig. 3
Czochralski grown $CaSc_2O_4$ single crystal (grid size: 1 mm). The figure is reproduced from Ref. [10] with permission from the Royal Society of Chemistry.

Fig. 4
Competitive growth and grain-selection process visualized by application of the new EDLM technique on a longitudinally cut section of the grown cerium doped $CaSc_2O_4$ crystal. The left part of the sample is located close to the seed. The labels denote color-coded two-dimensional diffraction intensity maps of several Bragg reflexes (F1 to F7), which were superimposed to create this image. Subgrains are exclusively visible in the marked (red colored) region. Due to local cutting damages at the right side of the sample, local intensity variations are visible by topographic effects. The figure is reproduced from Ref. [10] with permission from the Royal Society of Chemistry.

Although, the grown crystal was nucleated on an Ir-rod, the main part of the crystal shows high crystalline quality since due to competitive growth and grain selection, initial subgrains grew out during cylindrical growth. The resulting microstructure of this process is visualized in Fig. 4 by application of that EDLM technique on a longitudinally cut section of the grown crystal. The subgrain distribution, size and position can be distinguished by different colorations and contrast values in the pattern. The EDLM mappings were performed using a commercial µ-XRF spectrometer (Bruker M4 Tornado). Within the main volume of the crystal, where no subgrains were found by EDLM, high crystalline quality was additionally verified by X-ray rocking curve measurements for the main crystallographic directions. As can be seen in Fig. 5, single peaks without appearance of secondary reflexes indicate the absence of a significant mosaicity. FWHM values of 24, 28 and 34 arcsec were determined for the 200, 020 and 002 reflexes, respectively.

Transparent semiconducting oxides

Bulk single crystals of transparent semiconducting oxides (TSOs) are being continuously researched and developed in response to an increased interest from scientific and industrial communities. Bulk TSOs single crystals constitute an important part within the multi-institutional Leibniz ScienceCampus GraFOx that has been granted in 2016.

At scientific and technological level, β-Ga_2O_3, that attracts the most attention, has been successfully scaled-up by the Czochralski method to 2 inch in diameter. This novel approach has been filed as international patent application [17]. Bulk β-Ga_2O_3 crystals are used as substrates for homoepitaxy by the group Semiconducting Oxide Layers, and the homoepitaxial structures are used for power transistor development in collaboration with Air Force Laboratory, USA. [18,19].

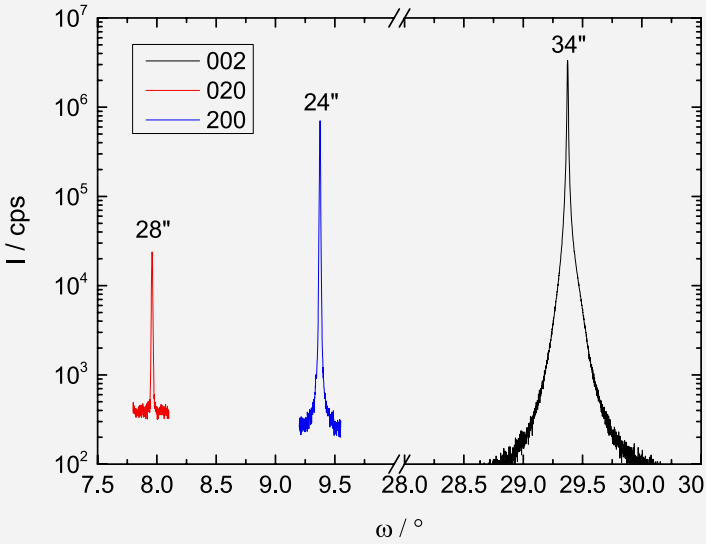

Fig. 5
X-ray rocking curves of 020, 200 and 002 peaks investigated for an oriented and polished cube prepared from the high quality (subgrain-free) volume of the grown crystal. The corresponding FWHM values are shown above the peak maxima. The figure is reproduced from Ref. [10] with permission from the Royal Society of Chemistry.

LED devices, GaN-on-Ga_2O_3, have been demonstrated in collaboration with Ferdinand-Braun-Institut, Leibniz-Institut für Hoechstfrequenztechnik (FBH). Long lasting and fruitful cooperation with Humboldt University has brought further results on thermal properties, surface properties and electronic structure of bulk β-Ga_2O_3 [20,21]. We demonstrated further possible extension of β-Ga_2O_3 applications in the field of detection of nuclear radiation, i.e. neutron and gamma radiation in cooperation with Karlsruhe Institute of Technology and Nicolaus Copernicus University (Poland), respectively. The capability of neutron detection by insulating bulk β-Ga_2O_3 crystals was demonstrated for the first time [22]. We found β-Ga_2O_3 as a first oxide binary compound that scintillates under gamma irradiation by doping with Ce. Although semiconducting β-Ga_2O_3 scintillates by its own, Ce enhances its scintillation performance. This topic will be studied in detail in near future.

Melt-grown bulk In_2O_3 single crystals were recently a subject of an intensive scientific study together with Humboldt University, Magdeburg University, National Institute for Materials Science (NIMS – Japan) and Technische Universität Berlin. In particular, the controversy on the presence of the surface electron accumulation layer (SEAL) in In_2O_3 has been finally explained, i.e. it is present when the crystal surface is exposed to the ambient environment, while it is not present when the crystals are cleaved in ultra-high vacuum [23,24]. Further, contacting an as-cleaved bulk In_2O_3 crystal surface with In revealed the presence of 2D electron gas at the In-In_2O_3 interface [25]. Also a dielectric function of In_2O_3 in the spectral region from mid infrared to ultraviolet has been measured and discussed in detail [26].

Bulk SnO_2 single crystals were used for the first time at University of Wyoming for photosensitisation study with dyes and quantum dots [27].

Bulk $MgGa_2O_4$ and $CoGa_2O_4$ single crystals have been proved, in collaboration with Alabama University, to be great materials as substrates for epitaxial spinel ferrites ($NiFe_2O_4$) with enhanced magnetic properties due to a very good lattice match and elimination of anti-phase boundaries present when other substrates are used.

The portfolio of bulk TSO crystals has further been extended by $InGaZnO_4$. We demonstrated for the first time the capability of obtaining bulk $InGaZnO_4$ samples directly from the melt. The very preliminary study of this material revealed a high electron mobility (about 100 $cm^2V^{-1}s^{-1}$) at very high free electron concentration at the level of 10^{20} cm^{-3}.

Thermodynamic studies of $CuAlO_2$ – a potential transparent p-type oxidic semiconductor

Established TSOs, such as CdO, Ga_2O_3, In_2O_3, SnO_2 and ZnO [28] are n-type semiconductors in which electrons act as main charge carriers. However, in semiconductor-electronics, p-n-junctions are of major importance where hole conduction is required in the p-type parts [29]. $CuAlO_2$–Delafossite (ABO_2) shows n- and p-type behaviour and a high mobility of holes due to hybridization of oxygen p-orbital with Cu^{1+} d-orbital [30]. It has Rm symmetry, the lattice constants a = b = 2.857 Å, c = 16.939 Å, an indirect bandgap of 2.22 eV and a direct one of 3.4 eV [31]. So far $CuAlO_2$ has only been grown as polycrystalline thin layers. However, active devices based on single crystalline layers of high structural quality require single crystalline native substrates. For their applications in transparent p-type semiconductors, the single crystals should have high transparency and conductivity.

For the top-seed solution growth (TSSG) technique with a Czochralski-setup, a suitable crucible material has to be found that does not react with either copper or its oxides in the melt. As alternative, for a crucible-free growth, the optical floating zone (OFZ) technique is preferred.

Dielectric & Wide Bandgap Materials: **Oxides/Fluorides**

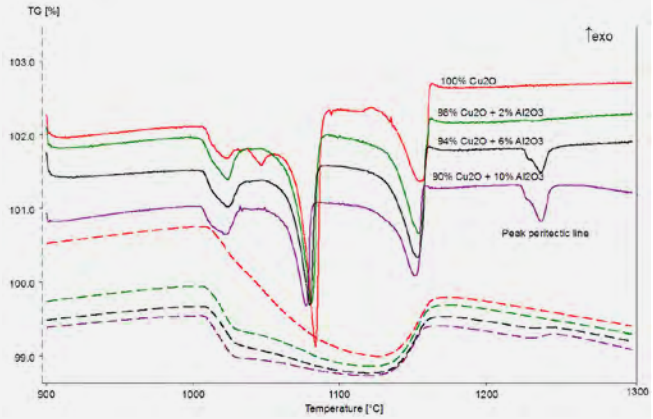

Fig. 6
TG (dashed)/DTA (solid)-curves of $CuAlO_2$-mixtures compared with pure Cu_2O measured in oxygen enriched atmosphere (15% O_2, 85% Ar). Growth is possible between the peritectic line and the eutectic point (1-2% Al_2O_3).

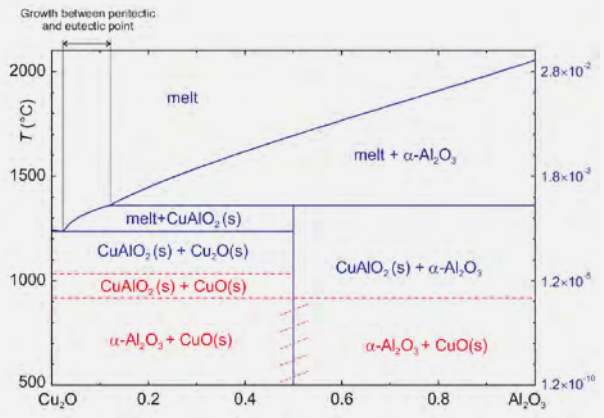

Fig. 7
Preliminary theoretical phase diagram of Cu_2O-Al_2O_3 calculated with FactSage (blue: pure CO_2, red: air).

For an understanding of the crystallization of $CuAlO_2$, the existing Cu_2O-Al_2O_3 phase diagram proved to be insufficient. First, under sufficiently oxidizing atmospheres, most melting and crystallization processes are accompanied by chemical redox reactions between Cu_2O and CuO. This is demonstrated by significant mass changes between 1000°C and 1150 °C in Fig. 6. On the other hand, if the oxygen activity in the growth atmosphere is too low, metallic copper can be formed in platinum crucibles, due to the entropic stabilization of Cu by alloying with Pt. These findings are in contrast to initial calculations (Fig. 7) where only Cu^+ and Cu^{2+} were expected. Solution growth should be carried out with 1-2 mol% Al_2O_3 in Cu_2O. The peritectic line was found at 1240°C (Fig. 6). The eutectic point has to be calculated theoretically. The conducted TG-DTA measurements indicate it to be between 0 and 1 mol% Al_2O_3, which results in an extremely small temperature growth window probably between 1240 and 1230°C.

A suitable growth atmosphere was determined to be 15-21% oxygen in argon. Elementary copper is formed under reducing conditions which reacts with basically every crucible material. Oxidizing atmospheres on the other hand favor the formation of $CuAl_2O_4$, a spinel without p-type character.

First crystals were grown spontaneously in Cu_2O-solutions with 1-2 % Al_2O_3 using Pt-crucibles (Fig. 8) X-ray flourescence analysis shows a $CuAlO_2$-composition of the crystals. The aluminium oxide is concentrated in the crystals whereas the matrix consists of almost pure copper oxide. An X-ray powder diffraction analysis of the sample shows the coexistence of $CuAlO_2$, Cu_2O and CuO. All of the Al_2O_3 is incorporated in the crystals.

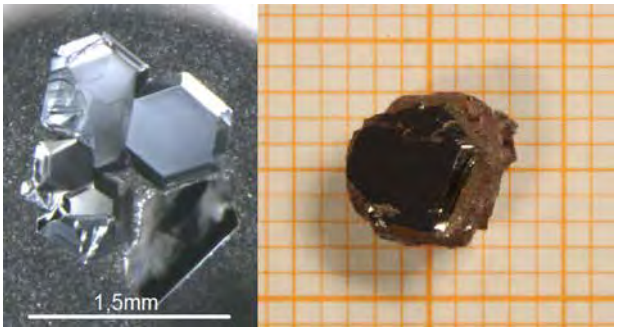

Fig. 8
$CuAlO_2$ crystals grown from a copper oxide rich melt solution. Left photo: hexagonal and trigonal shaped crystals grown in DTA-crucible under the microscope, right photo: crystal with trigonal structure grown in larger Pt-crucible.

References

[1] J. Czochralski; Zeitschr. Phys. Chemie 92 (1918) 219

[2] Y. Suhak, M. Schulz, H. Wulfmeier, W. L. Johnson, A. Sotnikov, H. Schmidt, S. Ganschow, D. Klimm, H. Fritze; MRS Advances 1 (2016) 1513

[3] A. N. Banerjee, S. Nandy, C. K. Ghosh, K. K. Chattopadhyay; Thin Solid Films 515 (2007) 7324

[4] O. Reetz; Masterarbeit, BTU Cottbus-Senftenberg (2017)

[5] C. Guguschev, Z. Galazka, D.J. Kok, U. Juda, A. Kwasniewski, R. Uecker; CrystEngComm 17 (2015) 4662

[6] C. Guguschev, D.J. Kok, U. Juda, R. Uecker, S. Sintonen, Z. Galazka, M. Bickermann; J. Cryst Growth, DOI: 10.1016/j.jcrysgro.2016.10.048, in press

[7] C. Guguschev, R. Tagle, U. Juda, A. Kwasniewski; J. Appl. Cryst. 48 (2015) 1883

[8] S. Ganschow, A. Kwasniewski, D. Klimm; J. Cryst. Growth 450 (2016) 203

[9] R. Tagle, C. Guguschev; Bruker lab report XRF 463, https://www.bruker.com/ (2016) 1 – 4

[10] C. Guguschev, J. T. Philippen, D. Kok, T. Markurt, D. Klimm, K. Hinrichs, R. Uecker, R. Bertram, M. Bickermann; CrystEngComm, DOI: 10.1039/C7CE00445A, in press

[11] Y. Chen, K. Wai Cheah, M. Gong; J. Lumin; J. Lumin. 131 (2011) 1770

[12] M. Fechner; doctoral thesis, Universität Hamburg (2011)

[13] M. Fechner, F. Reichert, K. Petermann, G. Huber; Advances in Optical Materials, Talk AIThC4 (2011)

[14] J. R. Carter, R. S. Feigelson; J. Am. Ceram. Soc. 47 (1964) 141

[15] O. Get'man, V. Panichkina; Powder Metall. Met. Ceram. 39 (2000) 584

[16] J. Philippen, C. Guguschev, R. Bertram, D. Klimm; J. Cryst. Growth 363 (2013) 270

[17] Z. Galazka, R. Uecker, D. Klimm, M. Bickermann; Method for growing beta phase of gallium oxide (β-Ga_2O_3) single crystals from the melt contained within a metal crucible, WO 2016110385

[18] A. J. Green, K. D. Chabak, E. R. Heller, R. C. Fitch, M. Baldini, A. Fiedler, K. Irmscher, G. Wagner, Z. Galazka, S. E. Tetlak, A. Crespo, K. Leedy, G. H. Jessen; IEEE Electr. Device Lett. 37 (2016) 902

[19] K. D. Chabak, N. Moser, A. J. Green, D. E. Walker Jr., S. E. Tetlak, E. Heller, A. Crespo, R. Fitch, J. P. McCandless, K. Leedy, M. Baldini, G. Wagner, Z. Galazka, X. Li, G. Jessen; Appl. Phys. Lett. 109 (2016) 213501

[20] M. Handwerg, R. Mitdank, Z. Galazka, S. F. Fischer; Semicond. Sci. Technol. 31 (2016) 125006

[21] C. Cocchi, H. Zschiesche, D. Nabok, A. Mogilatenko, M. Albrecht, Z. Galazka, H. Kirmse, C. Draxl, C. T. Koch; Phys. Rev. B 94 (2016) 075147

[22] D. Szalkai, Z. Galazka, K. Irmscher, P. Tüttő, A. Klix, D. Gehre ; IEEE Trans. Nucl. Sci. (2017), DOI 10.1109/TNS.2017.2698831

[23] T. Nagata, O. Bierwagen, Z. Galazka, M. Imura, S. Ueda, H. Yoshikawa, Y. Yamashita, T. Chikyow; Appl. Phys. Express 10 (2017) 011102

[24] V. Scherer, C. Janowitz, Z. Galazka, M. Nazarzadehmoafi, R. Manzke; Europhys. Lett. 113 (2016) 26003

[25] M. Nazarzahdemoafi, F. Titze, S. Machulik, C. Janowitz, Z. Galazka, R. Manzke, M. Mulazzi; Phys. Rev. B Condens. Matter Mater. Phys. 93 (2016) 081303

[26] M. Feneberg, J. Nixdorf, C. Lidig, R. Goldhahn, Z. Galazka, O. Bierwagen, J. S. Speck; Phys. Rev. B Condens. Matter Mater. Phys. 93 (2016) 045203

[27] L. A. King, Q. Yang, M. L. Grossett, Z. Galazka, R. Uecker, B. A. Parkinson; J. Phys. Chem. C 120 (2016) 15735

[28] Z. Galazka; Handbook of Crystal Growth (2015) 209 – 210

[29] C. Schulz, Dissertation, Technische Universität Carolo-Wilhelmina zu Braunschweig (2014)

[30] G. Hautier, A. Miglio, G. Ceder, G.-M. Rignanese, X. Gonze; Nat. Commun. 4 (2013) 2292

[31] J. S. Yoon, Y. S. Nam, K. S. Baek, C. W. Park, H. L. Ju, S. K. Chang; J. Cryst. Growth 366 (2013) 31

Dielectric & Wide Bandgap Materials:

Gallium Nitride

Head apl. Prof. Dr. Dietmar Siche
Team Dr. R. Zwierz, R. Nitschke

Überblick

Galliumnitrid (GaN) ist ein Basishalbleiter für optoelektronische und Hochfrequenz leistungselektronische Bauelemente. Ursprünglich suchten wir nach einer zur etablierten haliden Gasphasenepitaxie (HVPE) alternativen Züchtungsmethode, die deren Nachteile, wie die Bildung von NH_4Cl als Nebenprodukt, vermeidet. In diesem Zusammenhang wurde ein Cyano-Transportprozess etabliert, bei dem an Stelle des Cl^- – Ions das pseudo-halide CN^- – Ion genutzt wird.

Im Berichtszeitraum fokussierten wir uns hauptsächlich auf das DFG-Projekt QuartzGaN, das in Zusammenarbeit mit dem Institut für Festkörperphysik der Technischen Universität Berlin, Prof. A. Hoffmann, durchgeführt wird. Das Projektziel war die Präparation und Untersuchung einkristalliner, Kohlenstoff-dotierter Galliumnitrid (GaN) -Schichten aus der Gasphase. Um semiisolierendes (SI) Material für die Leistungselektronik zu erhalten, wurde mit Kohlenstoff aus dem HCN-Trägergas dotiert [1]. Die n-typ-Leitfähigkeit der gewachsenen GaN-Kristalle ist auf das allgegenwärtige Silizium und den Sauerstoff zurückzuführen. Die freien Ladungsträgerkonzentrationen können bei Raumtemperatur 10^{18} cm^{-3} überschreiten [2]. Lyons et al. [3] haben kürzlich aus hybriden Dichtefunktional-Rechnungen gefunden, dass C_N als ein tiefer Akzeptor mit einer Ionisationsenergie von ca. 0.9 eV wirkt. Daher sollte der kontrollierte, homogene Kohlenstoffeinbau effektiv die Hintergrund-Donatoren in GaN kompensieren und somit unsere weiteren Studien motivieren.

Overview

Gallium nitride (GaN) is a basic semiconductor for opto- and high frequency power electronics. Originally, we searched for a growth method, alternative to the more or less established Halide Vapour Phase Epitaxy (HVPE) on sapphire to overcome its disadvantages as NH_4Cl by-product formation. In this context a cyano transport process was established, where the pseudo halide ion CN^- is used instead of the Cl^- – ion.

In the reporting period, we mainly focused on the DFG project QuartzGaN, conducted in collaboration with the Institute of Solid State Physics at the Technische Universität Berlin, Prof. A. Hoffmann. The project target is to prepare and study single crystalline, carbon doped gallium nitride (GaN) layers from the gas phase. To achieve semi-isolating (SI) material for power electronics, carbon was doped from the HCN carrier gas [1]. The n-type conductivity of as grown GaN crystals is due to ubiquitous silicon and oxygen. Free carrier concentrations may exceed 10^{18} cm^{-3} at room temperature [2]. Lyons et al. [3] recently found from hybrid functional density calculations C_N as a deep acceptor level with about 0.9 eV ionization energy. Therefore, controlled homogeneous carbon incorporation should effectively compensate residual donors in GaN, motivating our further studies.

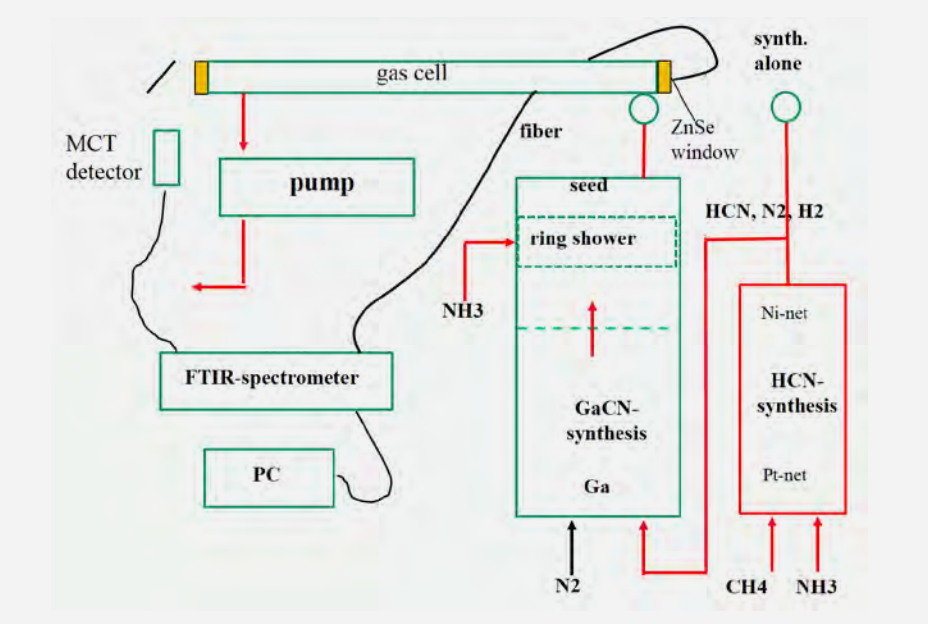

Fig. 1
Scheme of the home-made growth setup (with permission of Cryst. Res. Technol.).

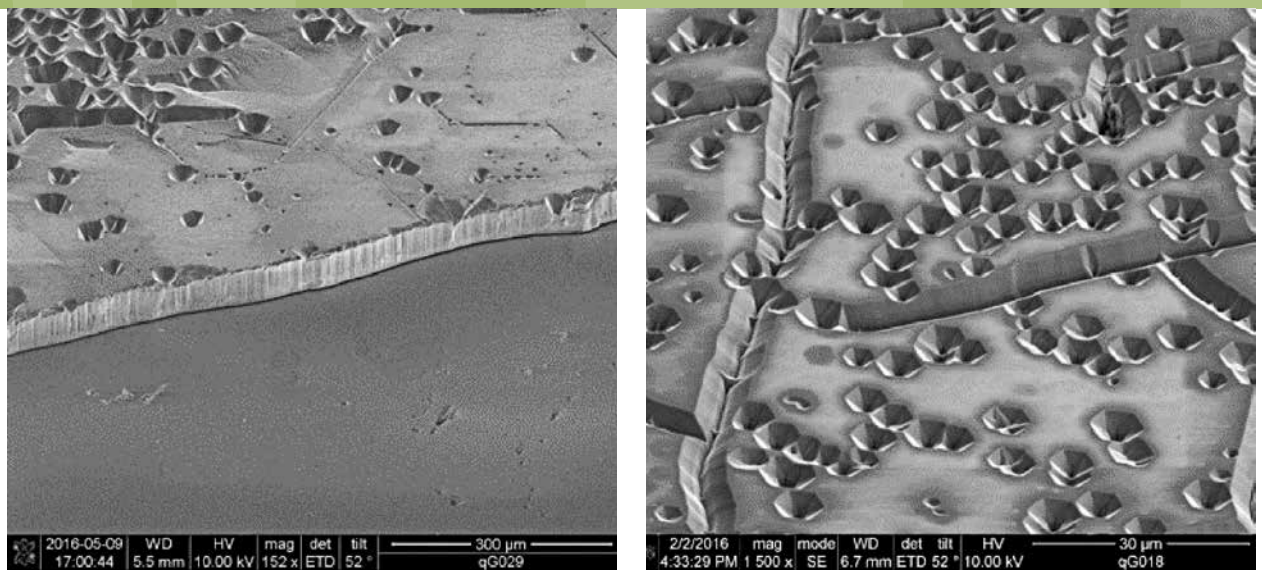

Fig. 2
GaN layers on standard MOVPE GaN on sapphire templates, left layer with crack surface, visible due to flaking of the front part, and right V-Pit arrangement at cracks (REM).

Results

Fig. 1 shows the scheme of the utilized home-made growth set-up. In the resistively heated tubular oven at the right side, the HCN gas was synthesized on Pt catalyst from CH_4 and NH_3. This is comparable with a Degussa process in the lab scale [4]. On the following nickel net unreacted ammonia is decomposed to prevent GaN crust formation on the liquid Ga surface in the higher temperature source zone at the bottom of the growth cell. There GaCN is formed from Ga and HCN. Transported by nitrogen carrier gas through a Ni-diaphragm to the seed, the GaCN reacts with ammonia from the ring shower to GaN.

$$GaCN(g) + 2NH_3(g) \rightarrow GaN(s) + C(s) + N_2(g) + 3H_2(g) \quad (1)$$

The gas cell in the exhaust gas line served to analyse the waste gas composition by in-situ Fourier Transform Infrared (FTIR) spectroscopy to optimize the process [5].

In the last year GaN:C layers were grown on standard Ga polar MOCVD-GaN on sapphire templates. All of these layers had cracks and V-pits (see Fig. 2). For the first time one structured template from Ulm University was employed in a single dual-seed experiment. Within its layer stack a SiN sub-monolayer causes an epitaxial lateral overgrowth (ELO) to decrease the dislocation density. The density of nucleated islands was higher in comparison to the standard templates, but stresses causing the V-pit formation have not been essentially reduced. Instead, homo-epitaxy on freestanding HVPE substrates, which have a lower stress level, could have had a better effect, but was not used.

The main reason was that we focused mainly on growth control, not on layer quality. This was challenging, because the transport HCN-gas synthesis in the pre-reactor was dependent on the optimal NH_3 to CH_4 ratio to avoid C_2H_2 formation, which results in a carbon film build up on the Pt catalysts. Thus, the average growth rates R_{av} of GaN were estimated by measuring the thicknesses of the grown layers divided by the growth time. R_{av} was in the range of 2 – 20 µm/h and declines with the growth time.

By SIMS measurements the layers purity was found to be low. Metallic impurities Zn, Mg, Mn were in the low $10^{16}cm^{-3}$ range. Ni and Pt from catalysts, hydrogen from decomposition of ammonia, methane and HCN, and Si from the quartz reactor have been found at a medium $10^{17}cm^{-3}$ level. The main unintentional impurity was oxygen from the sapphire seed, reactor leakage, and the Ga source and partly exceeded the 10^{20} cm^{-3} level. The intentional in-situ carbon doping concentration was in the range $10^{17}cm^{-3}$ to $10^{19}cm^{-3}$. In most samples, the carbon acceptor level was lower than the oxygen donor level, which was especially high on facets of V-pits. These stress induced negative growth pyramids are the main reason for inhomogeneous doping. Their facets grow slower than the c-plane and they are filled only slowly. On the facets the impurity incorporation is increased, the PL intensity is higher due to the increased yellow band (YL) intensity around 2.2 eV and the E_{2high} mode intensity vs. Raman shift in Micro-Raman spectra decreases from outside to inside a V-pit and shifts in comparison to unstrained material by ~ 2 cm^{-1} to higher wave numbers. From this shift, a biaxial compressive pressure of ~ 0.7 GPa was estimated. EDX images also revealed the macroscopically homogeneous but microscopically inhomogeneous carbon incorporation.

Dielectric & Wide Bandgap Materials: **Gallium Nitride**

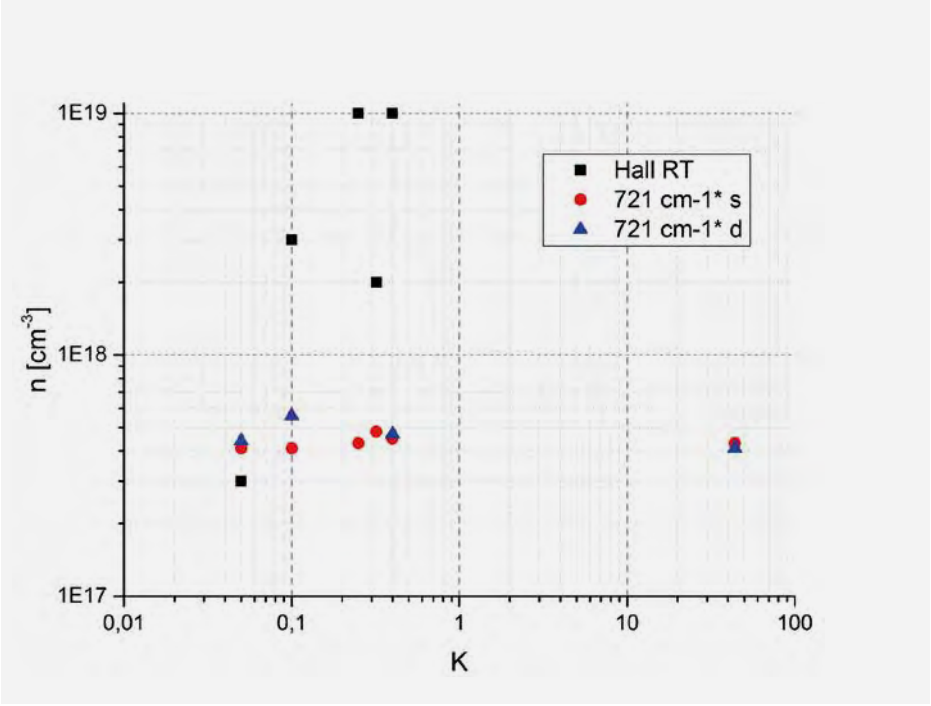

Fig. 3
Free carrier concentration n from RT-Hall effect measurements and estimated from A_1(LO) Raman mode position vs. K = [C] / ([O] + [Si]), depending strongly on the position of unstrained material (- values taken from [7]), s – surface, d – dark spot (V-pit) (with permission of Cryst. Res. Technol.).*

The density of screw and mixed dislocations could be estimated from HR-XRD rocking curves around the 0002 reflex with separated influence of wafer bow (lattice misfit to sapphire) and mosaicity (columnar growth) on the FWHM value from that of dislocation density ρ [6]. For the poorest quality layer we got the highest dislocation density ρ ~ 3 x 10^{10} cm^{-2} (FWHM = 3848 arcsec). Better layers with smaller FWHM of ~ 800 arcsec had ρ ~ 1.3 x 10^{9} cm^{-2}. With growing layer thickness the peak intensity increases, the FWHM of ~ 610 arcsec was lower and the dislocation density ρ ~ 7.2 x 10^{8} cm^{-2} slightly decreased.

The missing charging of samples by the electron beam in SEM was inconsistent with SI material. To confirm the poor compensation of our samples, the free carrier concentration n was estimated locally from the A_1(LO) Raman mode position and measured integrally by room temperature Hall effect (Fig. 3). In Fig. 3 the free carrier concentration is shown versus the concentration ratio K of carbon acceptor to the sum of the main donor impurities, i.e. a compensation ratio deduced from chemical analysis, neglecting self-compensation and electrical activity. Both measurements revealed n-type conductivity of the as grown carbon doped GaN layers. The free carrier concentration n from Hall effect was more than one order of magnitude higher, probably due to contributions from the surface and the sub-grain boundaries.

On the other hand the results from the phonon-plasmon coupled A_1(LO) Raman mode position depend strongly on the position of unstrained material. We choose the 721 cm^{-1} value, published for HVPE grown layers on sapphire [7] and n was in the range of 10^{17} cm^{-3} to 10^{18} cm^{-3}. Fig. 3 also shows, that n at the surface s is usually lower than at V-pits, marked as dark spots d. The free carrier concentration depends not on [C], because background oxygen is not compensated. Only for the layer with K = 44 no Hall measurement was possible, due to inhomogeneity of low resistance, not to semi-insulating behaviour. Therefore, we assume the chemical compensation was so high, that carbon was segregated, forming conductive particles.

In summary we adjusted the HCN formation in the HCN synthesis reactor by optimizing the NH_3 to CH_4 ratio to control the growth rate. A high carbon concentration [C] could be achieved, but the average growth rate R_{av} was dependent on [C], since the HCN gas is Ga and C precursor at the same time. Unfortunately, all samples showed high n-type conductivity, especially at V-pits. Increased YL band intensity in PL, μRaman measurements as well as SIMS results confirmed this behaviour. This hinders a real homogeneous dopant incorporation, as long as V-pit formation cannot be prevented. The latter could be achieved using homo-epitaxial low strain substrates [8]. It is also essential to lower the oxygen and silicon background levels to homogenize and decrease the necessary compensating carbon doping.

References

[1] K. Jacobs, D. Siche, D. Klimm, H.-J. Rost, D. Gogova; J. Cryst. Growth 312 (2010) 750

[2] D. Ehrentraut, E. Meissner, M. Bockowski (Eds.); Technology of Gallium Nitride Crystal Growth, Springer Verlag, Heidelberg (2010)

[3] J. L. Lyons, A. Janotti, C. G. Van de Walle; Appl. Phys. Lett. 97 (2010) 152108

[4] J. Gomez-Diaz and N. Lopez; J. Phys. Chem. C 115 (2011) 5667

[5] K. Kachel, D. Siche, S. Golka, P. Sennikov, M. Bickermann; Mater. Chem. Phys. 177 (2016) 12

[6] D. Siche, R. Zwierz, K. Kachel, N. Jankowski, C. Nenstiel, G. Callsen, M. Bickermann, A. Hoffmann; Cryst. Res. Technol. (2017) 1600364, DOI: 10.1002/crat.201600364

[7] E. V. Konenkova, Yu. V. Zhilyaev, V. A. Fedirko, D. R. T. Zahn; Appl. Phys. Lett. 83 (2003) 629

[8] M. Iwinska, R. Piotrzkowski, E. Litwin-Staszewska, T. Sochacki, M. Amilusik, M. Fijalkowski, B. Lucznik, M. Bockowski; Appl. Phys. Express 10 (2017) 011003

Dielectric & Wide Bandgap Materials:

Aluminium Nitride

Head Dr. Jürgen Wollweber
Team Prof. M. Bickermann, Dr. A. Dittmar, Dr. C. Dufloux, Dr. C. Hartmann, S. Kollowa, F. Langhans, R. Nitschke, H. Oppermann, A. Wagner

Überblick

UV-C-Licht ist wegen seiner Fähigkeit die DNS praktisch aller pathogenen Mikroorganismen in Wasser, Luft und auf kontaminierten Oberflächen zu zerstören sehr bedeutsam. Besonders gut durchdringt vor allem das 265 nm-Licht die Zellwände von Bakterien und Viren und erreicht dort tief im Innern der winzigen Partikel sein Ziel. Noch kürzere Wellenlängen bis zu 230 nm könnten für NO_x-Detektoren, zum Nukleinsäure-Nachweis und für medizinische Anwendungen eingesetzt werden.

Der Weg zu dieser Erkenntnis war lang. Er begann mit der ersten phänomenologischen Beschreibung der Wirkung von UV-Licht durch den dänischen Arzt *Niels Ryberg Finsen im Jahr 1903. Gegenwärtig werden für gewöhnlich Gasentladungslampen für die Generation von UV-Licht verwendet, wobei die aktuelle Entwicklung in Wissenschaft und Technik auf den Einsatz von modernen Leuchtdioden (LED) abzielt. Ein Beispiel dafür ist die weltweit erste 280 nm LED mit 70 mW optischer Leistung, die von der koreanischen Firma LG Innotek vorgestellt wurde. Andere Unternehmen wie Crystal IS und Hexatech sind dabei, vergleichbare Produkte zu entwickeln. Die wirtschaftlichen Erwartungen bezüglich der zu Grunde liegenden AlGaN-Technologie sind dabei ausgezeichnet. Allein für das UV-LED-Geschäft wird ein Wachstum von 90 Mill. $ im Jahr 2014 auf 520 Mill. $ im Jahr 2019 erwartet [1].*

Obwohl der größte Anteil dieser LEDs auf Saphirsubstraten hergestellt wird, sind Quasi-Eigensubstrate für Hochleistungsbauelemente und LEDs mit sehr kurzen Wellenlängen notwendig. Der Grund dafür liegt in der Reduzierung von Ausbeute und Leistungsfähigkeit der Bauelemente durch Strukturdefekte. Für hohe Al-Konzentrationen in den AlGaN-Schichten sind daher AlN-Wafer als Substrate zwingend erforderlich. Diese Substrate ergeben in den kompressiv verspannten Schichten die geringste Gitterfehlpassung, was mit relativ geringen Versetzungsdichten verbunden ist. Die Aktivitäten der Gruppe AlN resultieren aus diesem Kontext in Verbindung mit dem unzureichenden Entwicklungsstand der AlN-Züchtungstechnologien, der die Marktverfügbarkeit von AlN-Substraten gegenwärtig limitiert. Während wir in den vergangenen Jahren zunächst Probleme aus dem Bereich der technischen Infrastruktur (Züchtungsanlage, Quellmaterialreinigung, Keimpräparation und Tiegelfertigung) gelöst haben, liegt der Fokus jetzt auf spezifischen Anforderungen. So führt die Nachfrage nach hoch-effizienten Lichtemittern zu der Forderung nach noch höherer Reinheit und besserer kristalliner Perfektion bei stetig vergrößertem Kristalldurchmesser.

Das erreichte Niveau der Technologieentwicklung im IKZ gestattet es momentan, AlN-Kristalle bis zu 14 mm Durchmesser zu züchten. Diese Kristalle sind frei von Kleinwinkelkorngrenzen und haben Versetzungsdichten von im Bereich von null im Zentrum bis zu zirka 10^4 cm^{-3} in einzelnen Clustern und im Randbereich. Ein Teil dieser Wafer wurde durch CMP oberflächenbehandelt und Partnern für die Bauelementeentwicklung zur Verfügung gestellt (Projekt "Advanced UV for Life" im Rahmen der BMBF Programm „Unternehmen Region"). Mit Blick auf die Forderung nach AlN-Quellmaterial mit Verunreinigungskonzentrationen unter 100 ppm C, O sind wir gegenwärtig dabei, einen völlig neuen Ansatz für den Reinigungsprozess zu entwickeln. Dieser beruht auf der plasmagestützten Abscheidung von AlN (BMWi Verbundprojekt im ZIM-Programm; „Entwicklung einer Plasmafackel für die Abscheidung von halbleiterreinem AlN zur Herstellung von Sputtertargets"). Die aufgebaute Anlage kann nun für die Prozess-Entwicklung zur Herstellung von besonders reinem AlN-Quellmaterial eingesetzt werden.

Neben der Nutzung von AlN-Substraten für LEDs mit Wellenlängen unter 260 nm ist auch eine Verwendung für 300 nm LEDs denkbar, wenn es gelingt, den Gitterparameter um einige Hundertstel Angström zu höheren Werten zu verschieben. Mit Material dieser Art ist die Erwartung verbunden, die bestehende Lücke beim Wirkungsgrad von LEDs bei 300 nm Wellenlänge schließen zu können. Diese gewünschte Änderung der Gitterparameter kann durch Zugabe von Sc zum AlN erreicht werden, wobei bereits Konzentrationen von 2-5 at.-% den Anforderungen genügen würde. Allerdings ist das Züchten dieser Mischkristalle wegen des unterschiedlichen Dampfdruckverhaltens von AlN und ScN schwierig. ScN sublimiert bei rund 200 K über dem AlN. Um dieses Problem zu lösen, haben wir einen PVT-Aufbau mit unterschiedlichen Temperaturniveaus für beide Quellmaterialien und einer eingebauten Diffusionssperre für das AlN realisiert. Dieser Aufbau gestattet gegenwärtig das Wachstum von hochperfekten ScAlN-Kristallen (rocking curve FWHM ~ 21 arcsec) mit bis zu 0,55 at.-% Sc [7]. Zusätzlich zu der beschriebenen Arbeit setzt die Gruppe AlN die Untersuchung der Materialeigenschaften von AlN fort (DFG Projekt; „Elektromechanische Eigenschaften von AlN").

Dielectric & Wide Bandgap Materials: **Aluminium Nitride**

Zu den Hauptzielen unserer zukünftigen Arbeit werden die Optimierung der optischen Eigenschaften von AlN (UV-C-Transparenz) sowie vor allem die Vergrößerung der Waferdurchmesser auf 1 Zoll und darüber zählen. Abschließend möchten wir den Mitarbeitern der Abteilung Simulation und Charakterisierung des IKZ, der Gruppe Halbleiterphysik/Institut für Physik der TU Chemnitz, der Gruppe für Angewandte Physik an der TU Bergakademie Freiberg und der Gruppe „Sensoren für Hochtemperaturprozesse" am Institut für Energieforschung und Physikalische Technologien, Goslar für die Zusammenarbeit bei der Präparation und der Charakterisierung unseres Materials danken.

Overview

UV-C light is a very attractive means because of its capability to destroy the DNA of pathogenic microorganisms in water, air, and on contaminated surfaces of all types. Above all, the 265 nm wavelength can penetrate the membranes of bacteria and viruses and achieve its target of destruction deep insight these tiny particles. Shorter wavelength up to 230 nm could beneficially used for NO_x sensing devices, nucleic acid detection and medical applications.

The road to this realization was long and began with the first phenomenological description of the UV light effect published by the Danish physician Niels Ryberg Finsen in 1903. Currently, gas discharge lamps are commonly used for UV light generation. The present state of research and development is marked by the use of modern light-emitting diodes. As an example, LG Innotek from South Korea unveiled the world's first 280 nm-LED with 70 mW optical power for sterilization applications. Other companies, such as Crystal IS Inc. and Hexatech Inc., are developing comparable products. The mercantile expectations for the underlying AlGaN technology are outstanding. Only the UV LED business is expected to grow from $ 90m in 2014 to about $ 520m in 2019 [1]. Although the majority of these light-emitting diodes are fabricated on sapphire substrates, quasi-native substrates are needed for higher powers and even shorter wavelengths. The reason are structural defects that reduce the yield and performance of the devices. For high aluminum concentrations in the AlGaN layers, AlN wafers are required as substrates since they have the smallest lattice mismatch, resulting in compressively strained layers with relatively low dislocation densities.

The activities of the AlN group result from this context and the insufficient development level of AlN growth related technologies what still limits the market availability of AlN substrates today. While we have initially solved problems of the technical infrastructure (growth equipment, purification of source material, seed preparation, and crucible fabrication) in recent years, the focus is now on specific requirements.

The desire for high-efficiency emitters results in the demand for even better purity and crystalline perfection at steadily increased crystal diameter. The level of development of our technology allows us now to grow AlN crystals with a maximum diameter of 14 mm. These crystals have no small angle grain boundaries and threading dislocation densities in the range of zero in the center and about 10^4 cm^{-3} in individual clusters and at the edge region, respectively. Some of the wafers from these technology were finished by CMP and provided to partners for device development (in the frame of a project within the "Advanced UV for Life" consortium; BMBF Innovation Initiative "Entrepreneurial Regions").

Looking at the demand on AlN source material with impurity concentrations below 100 ppm C, O we are developing a fundamental new approach based on the plasma-assisted deposition of AlN (joint BMWi project "Plasma-assisted Deposition of High Purity III-Nitride Targets", ZIM program). In the following step, the built facility can now be used for the development of particularly pure AlN source material.

Beside the use of AlN substrates for LEDs with wavelength below 260 nm an application for 300 nm LEDs is conceivable when it succeeds to shift the lattice parameter a few hundredths of an angstrom to higher values. There is the expectation that such material could close the existing efficiency gap at 300 nm. Such a material can be created by mixing AlN with Sc. Already concentrations of only 2-5 at.% would meet the requirements. Growth of such mixed crystals suffers from the different vapor pressure behavior of AlN and ScN. ScN sublimes about 200 K above AlN. To resolve this problem we have realized a PVT setup with different temperature levels for both source materials and a built-in diffusion barrier for AlN. At the moment, this setup allows to grow crystals with an excellent crystalline perfection (rocking curve FWHM of ~ 21 arcsec) up to 0.55 at% Sc [7]. In addition to the described work we continue to working on fundamental questions (DFG project on electromechanical properties of AlN).

The main objectives of our future work are the optimization of the optical properties of the AlN (deep UV transparency) and, in particular, an increase in the wafer diameter to one inch and beyond.

Finally, we thank the staff from IKZ department Simulation & Characterization, the group Semiconductor Physics, Institute of Physics, TU Chemnitz, the group of Applied Physics, TU Bergakademie Freiberg, and the Group Sensors for High Temperature Processes, Institute of Energy Research and Physical Technologies, Goslar, for cooperation regarding the preparation and physical characterization of our material.

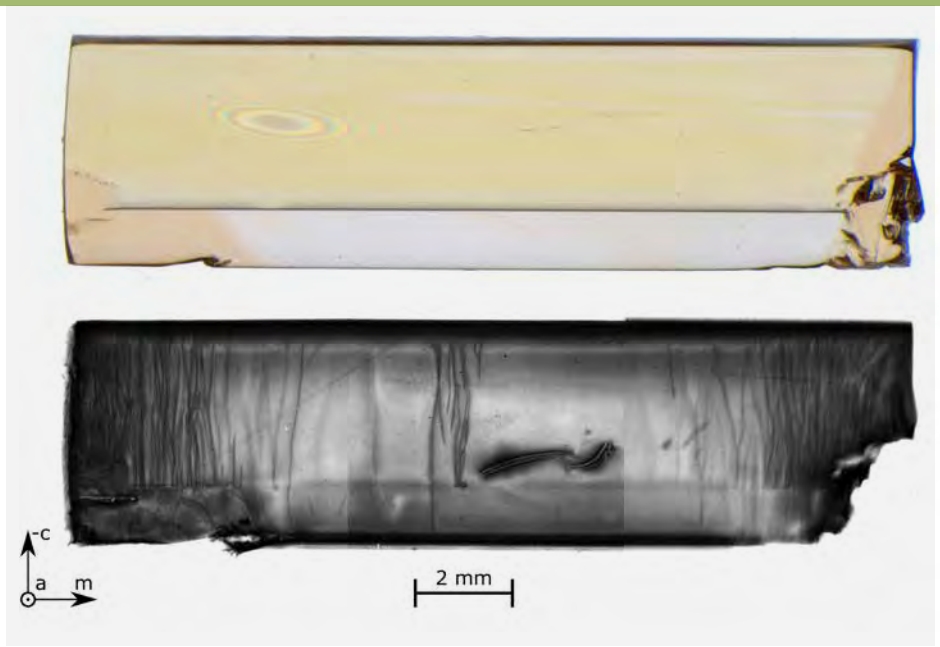

Fig. 1
Transmitted light image (above) and 0008 back reflection topograph (below) of a cross-sectional a-plane AlN wafer (thickness = 1.1 mm), showing dislocation generation at the regrowth interface at the crystal edges.

Results

I. AlN – a structural characterization

The state of development of the growth technology allows us to grow crystals with a diameter of 14 mm, without any grain boundaries, and threading dislocation densities (TDDs) between almost zero in the center of the crystals and about 10^4 cm^{-3} in individual clusters and at the edge region. However, the need to increase the diameter steadily involves quality problems.

To study how the structural quality of AlN evolves during seeded PVT growth, cross-sectional a-plane slices were cut from a larger AlN boule and measured with laser scattering tomography (LST) and synchrotron x-ray topography (SR-XRT). Fig. 1 shows a transmitted light image and the corresponding (0008) SR-XRT image recorded in back reflection geometry. The growth direction in Fig. 1 is upwards and the seed-layer interface is seen as a dark horizontal line in both images. The approximately vertical dark lines in the topograph are a-type threading dislocations (TDs) with Burgers vectors of type 1/3<1120>, determined by applying the invisibility criterion on topographs recorded from several reflexes. Almost all of the TDs are concentrated near the crystal edges. Apart from a few TDs originating in the substrate, virtually all TDs appear to be generated at the regrowth interface. The regions with higher threading dislocation densities (TDD ~ 10^3 cm^{-2}) correlate closely with the coloration seen in the optical image, which is in turn caused by differences in impurity incorporation between different growth zones, as determined in previous studies [2] and in the highlight article in this annual report. The pale-yellow and transparent regions were grown vertically in the [000-1]-direction and are oxygen dominated. The orange regions were grown horizontally on the six prismatic m-facets and are carbon dominated.

Fig. 2
Sublimation grown AlN crystal (diameter 14 mm) with tungsten aperture.

A few alternative mechanisms for the generation of TDs are currently under closer investigation. The temperature gradient during the heating at the beginning of the regrowth is reversed to avoid growth at too low temperatures, but it also leads to sublimation of material from all sides of the substrate. This could play a role in the generation of TDs in different ways which are now subject of intensive investigations. In the first model, the non-planar features on the sublimation-roughened surface yield a variety of growth centers resulting in local shear stresses, which may be sufficiently large to generate dislocations. Profilometry and AFM measurements show that heating up to growth temperature roughens the substrate surface at both macroscopic and microscopic scales. In the second mechanism, sufficiently large stresses could be caused by contact between the growing crystal, parasitic sub-grains and the aperture.

Initially, the seed crystal is at rest on top of the aperture, but it will slide through the aperture due to shrinkage caused by the sublimation. After passing the aperture, the shrunken crystal will then expand horizontally during regrowth and it may come into contact with the aperture. This theory is supported by the shape of the bottom right corner in the optical image Fig. 1, which has conformed to the shape of the aperture. This shape is not observed on the left side, because the left edge was cut to facilitate LST measurements. However, the aperture shape was observed on both sides of another a-plane slice. The bottom corner contains also a sub-grain, which is seen in the optical image as a darker region and in the topograph as no empty space due to diffraction orientation contrast. In the third mechanism, large stresses could be caused by impurity induced lattice mismatch at the growth zone interfaces. This is supported by the strong correlation between the coloring and the regions where dislocations are generated. This mechanism can be investigated by precise, local measurements of lattice constants. Even though further investigation on these mechanisms have to be carried out, we are able to grow AlN crystals with TDDs < $2x10^4$ cm^{-3} at present. Diameter expansion maintaining the structural quality is still a challenge.

II. $Al_{1-x}Sc_xN$ mixed crystals

AlGaN based ultraviolet (UV) light emitting diodes (LEDs) with an emission wavelength of 300 nm still suffer from relatively low external quantum efficiency (EQE) of around 1 % caused by a lack of lattice-matched substrates [3]. This fact results in dislocation densities of more than 10^8 cm^{-2} in the epitaxially grown AlGaN layer. Low concentrations of scandium in AlN (2–5 at.%) should lead to better lattice matching and could close this efficiency gap (Fig. 3). The use of such AlScN substrates should allow to provide low-defect pseudomorphic strained AlGaN layers even with aluminium contents less than 60%.

As a method of choice, physical vapour transport (PVT) of AlN/ScN mixed crystals is the most promising technique, since both compounds have a comparable sublimation behavior. However, chemical equilibrium calculations show that the Sc vapor pressure is much lower compared to the Al vapor pressure (Fig. 4). As indicated, comparable values for scandium are only reached at around 200 K higher temperatures than those of aluminium. Still, investigations on preparation of ScN nanocrystals confirmed the basic suitability of this method [6]. On this basis, we have developed a PVT process for the preparation of bulk $Al_{1-x}Sc_xN$ mixed crystals [7]. Typical $Al_{1-x}Sc_xN$ single crystals from these investigations are almost stress-free as well as of high crystalline quality, shown by the rocking curve FWHM of ~ 21 arcsec in Fig. 5. A comparatively high growth temperature was chosen to activate the ScN. Therefore, $Al_{1-x}Sc_xN$ single crystals grew mostly with rates between 200 µm/h and 300 µm/h. XRF and SIMS measurements over the whole N-polar (000-1)-facet of the crystal reveal a homogenous Sc incorporation measured by XRF and SIMS (Fig. 6).

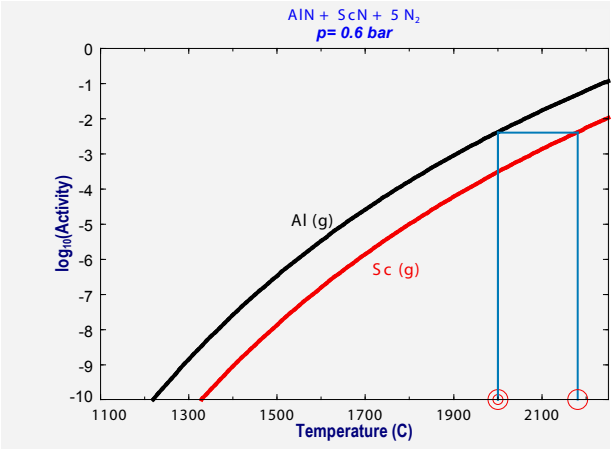

Fig. 4
Equilibrium partial pressures of aluminium and scandium gas phase species calculated with FactSage.

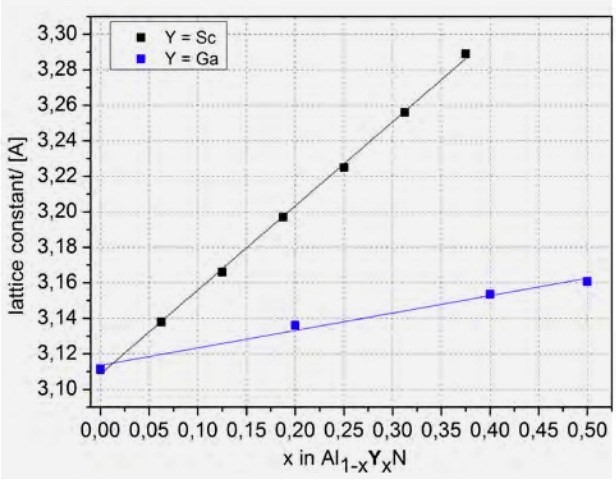

Fig. 3
Lattice constants of a-plane $Al_{1-x}Sc_xN$ and $Al_{1-x}Ga_xN$ in dependence on degree of alloying determined by HRXRD measurements (after [4,5]).

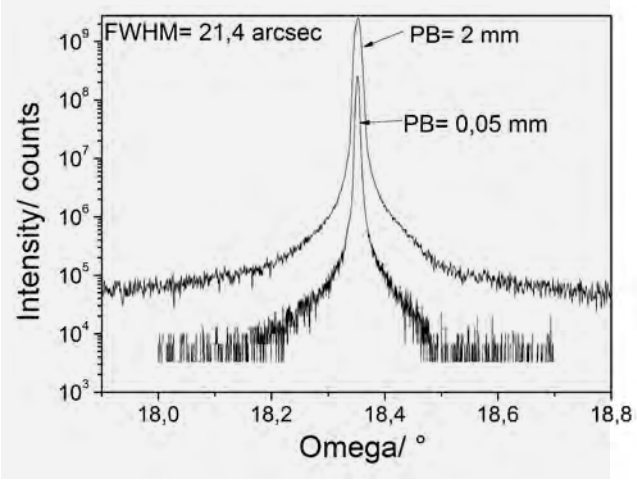

Fig. 5
Rocking curve measurement over the full as-grown (000-1) facet areas of an $Al_{1-x}Sc_xN$ single crystal.

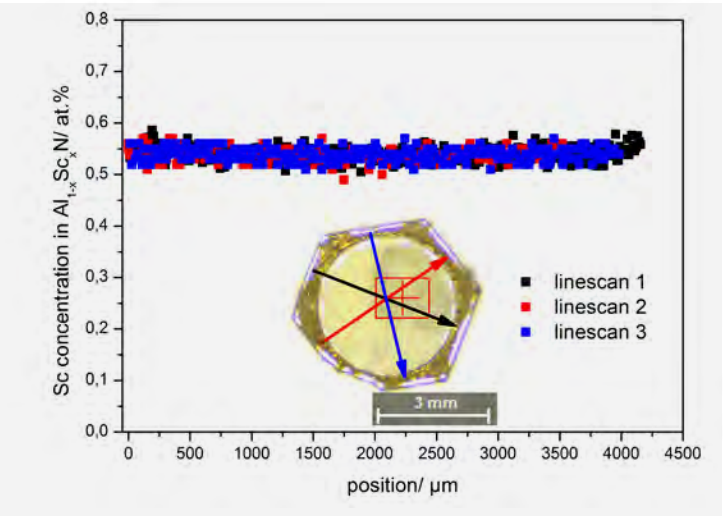

Fig. 6
Radial Sc concentration along the N-polar cap of $Al_{1-x}Sc_xN$ crystal, XRF line scans.

The results demonstrate the basic feasibility to grow $Al_{1-x}Sc_xN$ single crystals using the PVT method. In order to increase the degree of alloying of AlN with Sc requires a specific setup providing different temperature levels for both source components. This work will be supplemented by investigations to consider the resulting different Al and Sc supersaturations, respectively. Furthermore, the mixed crystals have to be characterized with regard to the Sc incorporation behavior (substitution, precipitation, and decoration of defects).

III. AlN deposition by a microwave stimulated nitrogen plasma torch

Besides the applications in optoelectronics, AlN is also a potential material for sensors and piezo devices. In chemical industry coatings made of AlN are produced by sputtering. For all these cases single crystalline AlN with high crystalline perfection is not required. Self-oriented AlN grains grown in a columnar structure with preference for the c-direction are often sufficient. If there were high purity cost-effective AlN targets, these products could be realized easily by sputtering.

To respond to this demand, we have developed an innovative technology based on reactive plasma spraying. The goal is to produce coarse grained AlN boules with high purity. In this process, an Al wire is injected into a microwave stimulated nitrogen plasma. AlN, as the product of the reaction between aluminum and the plasma activated N_2, is deposited onto a wolfram target. The technology, the device and the process were developed in close cooperation with our partners from a research institute and from the industry (Leibniz-Institut für Plasmaforschung und Technologie, AUTEAM Industrie-Elektronik GmbH, HTM Reetz GmbH, Sindlhauser Materials GmbH, Uwe Steingross Feinmechanik GmbH & Co. KG) (Fig. 7).

We used an aluminum wire as the initial material with low oxygen contamination in comparison to Al powder during the process. The material was guided through the nitrogen plasma. To avoid any impurity contamination by an erosion of the electrodes, an electrodeless microwave discharge was used for the plasma ignition. The pressure was maintained at 200–300 mbar, thus the plasma reached a temperature about 2000°C, high enough to vaporize aluminum, which was subsequently reacting with the surrounding nitrogen species in the plasma.

Fig. 7
Drawing of the deposition device (c) consisting of the Vessel, the waveguide based microwave discharge and the wire handling device (top to bottom); insets show the target in the afterglow (a) and the active plasma discharge with the Al-wire and the nozzle (b).

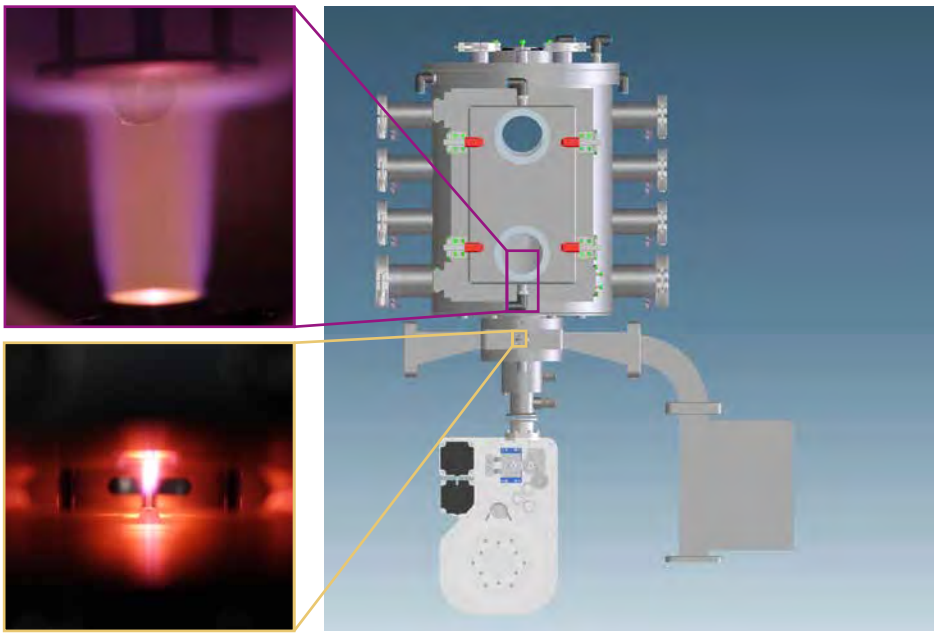

Dielectric & Wide Bandgap Materials: **Aluminium Nitride**

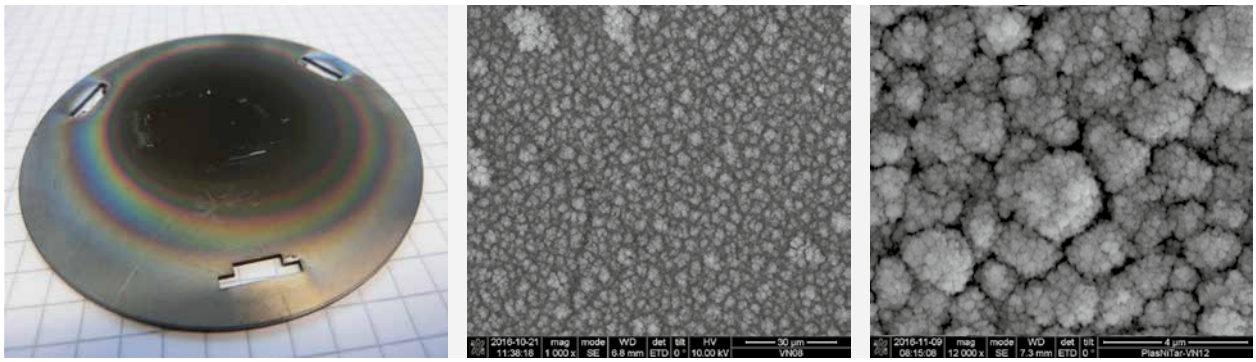

Fig. 8
Typical as-deposited AlN layer (SEM pictures, left); coated W target, right.

After approximately 60 min deposition time, the target was coated with a dark layer with a diameter of 2–3 cm. The crystallinity was determined by X-ray crystallography and the grain structure was investigated by optical and scanning electron microscopy (SEM). We found that the deposited material was built up of fine-grained polycrystalline AlN layers consisting of agglomerates with a diameter in the range of micrometers that in turn consisted of small particles with a diameter in the range of 100 nm (Fig. 8).

The x-ray crystallographic analysis of the layers confirms the crystallinity of the product. By means of a DTA/TG analysis in a temperature range of 25°C – 800°C the absence of free Al in the layer could be proved.

In order to control of the stability of the plasma torch with regard to temperature and species concentration optical emission spectroscopy was applied for the determination of the species in the active plasma torch. The spectrum showed strong emissions of nitrogen molecules, i.e. the Second Positive System (SPS) at 290–430 nm and the First Positive System (FPS) at 500–890 nm as well as emissions of the nitrogen ion, i.e. the First Negative System (FNS) at 350–520 nm. In the presence of aluminum in the plasma, the nitrogen signal decreases in intensity and an intense Al peak appears at 400 nm. With the help of this control parameter, the aluminum wire was injected into the plasma in such a manner that both nitrogen and aluminum were always present in the vapor phase.

Our partner from the Leibniz institute for Plasma Science and Technology applied optical emission spectroscopy for the determination of the gas temperature of the active discharge and for rough estimation of the densities of aluminum and nitrogen atoms in the afterglow. The rotational temperature of the SPS (0, 0) band of N_2 at about 337 nm was used as an approximation of the gas temperature in the active discharge region.

In the presence of aluminum, the rotational temperature was estimated to be between 1500 and 2000 °C without dependence on the pressure. The density of nitrogen atoms in the afterglow was estimated to be between 10^{13}–10^{14} atoms/cm^3. The density of aluminum atoms was estimated to 10^{12} atoms/cm^3. The first step towards the development of an alternative deposition technology for special applications of the AlN, the construction of AlN deposition facility based on a microwave stimulated nitrogen plasma was thus successfully completed.

References

[1] http://www.semiconductor-today.com/features/PDF/semiconductor-today_february2015-UV-LED.pdf

[2] C. Hartmann, J. Wollweber, S. Sintonen, A. Dittmar, L. Kirste, S. Kollowa, K. Irmscher, M. Bickermann; CrystEngComm 18 (2016) 3488

[3] M. Kneissl; A Brief Review of III-Nitride UV Emitter Technologies and Their Applications, in: III-Nitride Ultraviolet Emitters – Technology and Applications, M. Kneissl and J. Rass (eds.), Springer Series in Materials Science 227, chapter 1 (2016)

[4] R. Deng; AlN, ScN, and Al-Sc-N Ternary Alloys: Structural, Optical, and Electrical Properties; Dissertation, Rensselaer Polytechnic Institute (2013)

[5] M. R. Laskar, T. Ganguli, A. A. Rahman, A. Mukherjee, N. Hatui, M. R. Gokhale, A. Bhattacharya; J. Appl. Phys. 109 (2011) 013107

[6] G. Zhen, J. H. Edgar, J. Pomeroy, M. Kuball, D. W. Coffey; J. Mater. Sci.: Mater. Electr. 15 (2004) 555

[7] A. Dittmar, C. Hartmann, J. Wollweber, M. Bickermann; (Sc, Y): AlN single crystals for lattice-adapted AlGaN systems; patent filed WO 2017/050532 A1

Layers & Nanostructures

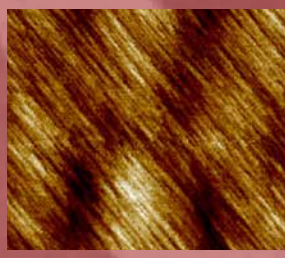

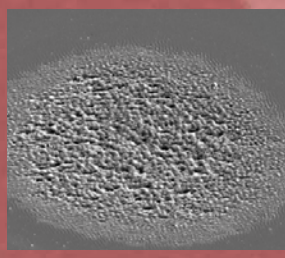

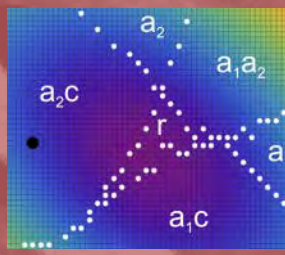

Layers & Nanostructures

Acting head of department: Dr. Günter Wagner

In der Abteilung Schichten und Nanostrukturen werden folgende Fragestellungen bearbeitet:

- *Grundlegende Untersuchungen zur Keimbildung und zu Wachstumsmechanismen*
- *Weiterentwicklung von Beschichtungstechnologien*
- *Entwicklung, Herstellung und Charakterisierung von Schichten und Mikrostrukturen für Anwendungen in der Sensorik, Mikro- und Leistungselektronik, Energiewandlung und für Speicher.*

Im Zentrum der Aktivitäten steht der Anspruch, die physikalischen Eigenschaften verschiedener kristalliner Substanzen durch maßgeschneiderte Größe, Form, chemische Zusammensetzung und Verspannungszustand gezielt einzustellen, um neue Anwendungsgebiete zu erschließen.

Folgende Forschungsschwerpunkte wurden in 2016 in den drei Gruppen der Abteilung bearbeitet:

1. *Homoepitaktisches Wachstum von transparenten halbleitenden Oxidschichten: Dies beinhaltet die Entwicklung und Herstellung von β-Ga_2O_3 Schichten auf arteigenen einkristallinen Substraten mit zielgerichteter Abweichung von der (100)-Orientierung und mit (010) Orientierung sowie Untersuchungen zur kristallinen Perfektion und den elektrischen Eigenschaften in Abhängigkeit von der Substratorientierung. Durch den Einbau von Silicium oder Zinn werden Schichten mit definierter n-Typ Leitfähigkeit und einer maximalen Beweglichkeit der Ladungsträger abgeschieden.*
2. *Abscheidung von ferro-/piezoelektrischen bleifreien Oxidschichten: Hierzu zählen ferro-/piezoelektrische $K_xNa_{1-x}NbO_3$ Schichten und Übergitterstrukturen mit variabler Zusammensetzung (x=0-1), $SrTiO_3$ Schichten, sowie leitfähiges $SrRuO_3$ als Elektrodenschicht. Durch die Dotierung der $K_xNa_{1-x}NbO_3$ Schichten mit Cu und Mn konnte der Leckstrom in den Schichten reduziert und der piezoelektrische Koeffizient erhöht werden. Zudem erfolgt die Abscheidung auf gitterfehlangepassten Oxidsubstraten (Heteroepitaxie) zum gezielten Einbau von anisotropen Gitterverspannungen. Das Ziel dabei ist es ihren Einfluss auf die ferroelektrische Domänenbildung und das Relaxorverhalten zu untersuchen und den piezoelektrischen Koeffizienten zu manipulieren.*
3. *(1) Wachstum von polykristallinen Siliciumschichten auf Fremdsubstraten, insbesondere auf Glas, mittels selbst entwickelter Züchtungsmethoden zur Kostenreduktion in der Photovoltaik, (2) Wachstum von $Cu(In_xGa_{1-x})Se_2$ (CIGSe) Inseln für Mikrokonzentrator-Solarzellen und (3) Züchtung von Si, Ge und $Si_{1-x}Ge_x$ Nanodrähten durch Molekularstrahlepitaxie (MBE). Diese Arbeiten sind in nationale und europäische Verbundprojekte eingebunden. Schwerpunkte der EU-Förderung sind die Entwicklung neuer Konzepte von Solarzellen mit hohem Wirkungsgrad bei gleichzeitiger Einsparung kostenintensiver Materialien.*

Die Abteilung verfügt über eine sehr moderne, hochwertige Ausstattung: Metallorganische Gasphasenepitaxie (MOVPE) sowohl für flüssige als auch für gasförmige Precursoren, Molekularstahlepitaxie (MBE), gepulste Laserabscheidung (PLD) und eine selbst entworfene Epitaxieapparatur für die Temperatur-Differenz-Methode (TDM). Zur sofortigen Charakterisierung der Schichten und Mikrostrukturen stehen u.a. folgende Methoden zur Verfügung: Atomkraftmikroskopie (AFM) mit diversen Messoptionen (u.a. Piezoresponse Force Microscopy PFM), taktile Profilometrie und spektrale Ellipsometrie.

The activities at the department „Layers and Nanostructures“ focuse on:

- fundamental investigations on nucleation and growth mechanisms
- development of deposition technologies
- development, growth and characterization of layers and microstructures for applications as sensors and memories, in microelectronics or photovoltaics.

By controlling chemical composition and strain of epitaxial layers as well as size, shape and position of nanostructures, it is possible to tailor the physical characteristics to open up novel applications.

The department consists of three groups, which performed the following research activities in 2016:

1. Epitaxy of transparent semiconducting oxides:
   This includes deposition of β-Ga_2O_3 layers on mature single crystalline substrates with an exact misorientation from (100) lattice direction and on (010) oriented substrates and the dependence of structural and electrical properties of the layers on the lattice orientation. By doping with silicon or tin, the tuning of n-type conductivity and free carrier mobility is a main task.
2. Deposition of ferro-/piezoelectric lead free oxide layers:
   The research tasks focus on ferro-/piezoelectric $Na_xK_{1-x}NbO_3$ layers and superlattice structures with variable composition (x=0-1), deposition of $SrTiO_3$ layers and conductive $SrRuO_3$ as electrode layer. Another topic is the deposition on lattice mismatched oxide substrates (heteroepitaxy) for targeted adjustment of lattice strain and investigation of the influence of the layers' functional properties as well as engineering of the piezoelectric coeffcients.
3. In the third group three topics are under investigation:
   (1) The growth of polycrystalline silicon layers on low cost substrates preferentially on glass by an in-house developed growth technique, (2) the deposition of indium droplets as precursors for the development of $Cu(In_xGa_{1-x})Se_2$ (CIGS) micro-concentrator solar cells, and (3) the MBE growth of Si, Ge and $Si_{1-x}Ge_x$ compound nanowires. Joint projects funded by the European Commission promote these activities largely. These projects aim for the development of advanced photovoltaic technologies enabling higher efficiency of solar cells and a cost reduction by minimising the consumption of expensive raw materials.

The department has an excellent infrastructure for the deposition and characterization of epitaxial layers and nanostructures:
Metal-Organic Vapour Phase Epitaxy systems for both, liquid and gaseous precursors, Molecular Beam Epitaxy, Physical Vapour Deposition, Pulse Laser Deposition and in-house designed Temperature Difference Method Epitaxy. A variety of methods for the immediately characterization of the layer properties are available: Atomic Force Microscopy at two state-of-the-art AFM devices enabling a variety of measuring options (e.g. Piezoresponse Force Microscopy PFM), Contact Stylus Profilometry and spectral Ellipsometry.

Layers & Nanostructures:

Semiconducting Oxide Layers

Head Dr. Günter Wagner
Team Dr. M. Baldini, R. Grüneberg

Überblick

Effizient schaltende mikroelektronische Leistungsbauelemente leisten einen bedeutenden Beitrag zur Entwicklung von innovativen Technologien. Sie ermöglichen eine höhere Effizienz bei der Produktion und Wandlung von Energie, was insbesondere auf den Gebieten der regenerativen Energien wie bei Windgeneratoren und Photovoltaikanlagen eine Rolle spielt. Auf diese Weise können sie wesentlich dazu beitragen, dass die mit der Energiewende angestrebten Klimaziele verwirklicht werden können.

β-Ga_2O_3 ist ein transparentes, halbleitendes Oxid mit einer aussichtsreichen Perspektive auf dem Gebiet der Leistungselektronik, wo es die gegenwärtig verwendeten Bauelementetechnologien auf der Basis von SiC und GaN überflügeln kann. Wegen des erheblich größeren Bandabstandes von 4.8 eV, der hohen theoretisch bestimmten Feldstärke von 8 MV/cm und der hohen Leistungskennzahl, bezogen auf Leistungsbauelemente, erscheint die Entwicklung von Bauelementen mit einer höheren Durchbruchfeldstärke (V_{br}) als bei SiC- und GaN-basierten Bauelementen möglich.

Der große Vorteil der Produktion von β-Ga_2O_3-basierten Bauelementen besteht darin, dass entsprechende Einkristalle mit hoher kristalliner Perfektion aus der Schmelze gezüchtet werden können. Züchtungsmethoden wie das Czochralski-Verfahren (CZ), das Floating Zone Verfahren (FZ) und das Edge-Defined Film Growth-Verfahren (EFG) sind in der Halbleiterindustrie etablierte Technologien. Dies ist ein Garant für die Verfügbarkeit von arteigenen Substraten für die Abscheidung von homoepitaktischen Schichten mit hoher struktureller Perfektion, die eine Voraussetzung für die Herstellung von Leistungsbauelementen einer neuen Generation sind.

In den vergangenen Jahren hat sich das IKZ eine ausgezeichnete Expertise bei der Züchtung von β-Ga_2O_3 Einkristallen erarbeitet. So wurde eine Technologie zur Züchtung von Kristallen mit isolierenden und n-typ halbleitenden Eigenschaften mit bis zu 51 mm Durchmesser und einem Gewicht von 1 kg mit einer Versetzungsdichte kleiner als $5x10^3$ cm^2 entwickelt. Aus diesen Kristallen wurden Substrate für die Abscheidung von dünnen epitaktischen Schichten präpariert. β-Ga_2O_3-Substrate mit verschieden orientierten Oberflächen wurden für die Homoepitaxie mittels Metallorganischer Gasphasenepitaxie (MOVPE) eingesetzt.

International werden für die Homoepitaxie von Ga_2O_3 erfolgreich ozon- oder plasmaunterstützte Molekularstrahlepitaxie-Verfahren (MBE) eingesetzt. Die MBE ist eine sehr ausgereifte Methode, mit der in der Grundlagenforschung hochqualitative und hoch reine Schichten hergestellt werden können. In der Industrie wird diese Technologie jedoch nur für sehr ausgewählten Anwendungen benutzt. Die MOVPE hat sich als eine Schlüsseltechnologie für die Massenproduktion von Schichten und Schichtstrukturen in Mikro-, Leistungs- und Optoelektronik durchgesetzt. Mit diesem Verfahren lassen sich simultan große Flächen unter moderaten technologischen Parametern beschichten. Die Schichten haben eine strukturell hohe Perfektion und ihre elektrischen Eigenschaften können zielgerichtet eingestellt werden.

In 2015 demonstrierten wir die erfolgreiche Abscheidung von halbleitenden homoepitaktischen Schichten aus (100)-orientierten Substraten, dotiert mit Si oder Sn. Im 4. Quartal 2015 wurden erste Abscheidungen auf (010) und definiert fehlorientierten (100) β-Ga_2O_3 Substraten durchgeführt. Das Ziel bestand in der Untersuchung des Einflusses der Substratorientierung auf die Entstehung von Planardefekten während des epitaktischen Wachstums. Die ersten experimentellen Ergebnisse waren sehr vielversprechend, so dass die intensive Untersuchung dieser Wechselwirkung die Hauptaufgabe für das Jahr 2016 darstellte. Die Schichten, gewachsen auf (001) orientierten Substraten, waren durch eine sehr hohe strukturelle Perfektion gekennzeichnet. Die Konzentration freier Ladungsträger konnte im Bereich von $1x10^{17}$ cm^{-3} bis zu $8x10^{19}$ cm^{-3}, bei einer maximalen Ladungsträgerbeweglichkeit von bis zu 130 cm^{-2}/Vs, eingestellt werden. Schichten, gewachsen auf (100) Substraten mit einer Fehlorientierung von 6 Grad, zeigten vergleichbare strukturelle und elektrische Eigenschaften. Der Vorteil bei der Verwendung von (100) fehlorientierten Substarten liegt in der einfacheren Präparation aus dem Ga_2O_3-Einkristall.

Parallel zu den Untersuchungen zur Epitaxie von Ga_2O_3-Schichten entwickelte sich eine sehr effektive Kooperation zum Air Force Research Laboratory in den USA, Arbeitsgruppe Dr. Gregg Jessen. Auf der Basis unserer ersten, nicht optimierten (100) β-Ga_2O_3 Schichten wurden von der Arbeitsgruppe MOS-FET Bauelemente prozessiert. Die ausgemessenen sehr guten Transistorkenndaten demonstrierten das große Potential von β-Ga_2O_3-Schichten als Basismaterial für Anwendungen in der Leistungselektronik.

Overview

High efficiency power switching devices play a major role in the reduction of greenhouse gas emissions and for global energy conservation and so also for one of the challenges of modern society. Monoclinic β-Ga_2O_3 is a transparent semiconducting oxide with very promising perspectives in this field, where it is predicted to outperform the leading technology based on SiC and GaN. Due to an ultra-wide band gap of 4.8 eV, an extremely high calculated field strength (8 MV/cm) and then large figures of merit for power devices are expected, enabling the fabrication of semiconductor structures with higher breakdown voltage (V_{br}) than their SiC and GaN counterparts. Moreover, especially in view of large-scale production, a key advantage of β-Ga_2O_3 is that large bulk crystals can be grown from the melt by standard cost-effective techniques like floating zone (FZ), the edge-defined film fed growth (EFG) and the Czochralski method (CZ). This will ensure the availability of reasonably priced native substrates for the growth of high quality homoepitaxial layers, which is essential for the production of high performance power devices.

In the last years, IKZ has developed an excellent expertise in the growth of bulk and epitaxial β-Ga_2O_3. Semi-insulating and n-type bulk crystals are grown by the Czochralski method with a diameter up to 2″ (1 kg in weight) and a dislocation density below 5×10^3 cm^{-2}. From these crystals β-Ga_2O_3 substrates were prepared suitable for epitaxial growth, performed in our laboratories by metal organic vapor phase epitaxy (MOVPE). In general the growth of homoepitaxial β-Ga_2O_3 is mainly investigated by ozone or plasma-assisted (PA) molecular beam epitaxy (MBE) and only rarely by MOVPE. However, while MBE is a very useful tool for scientific research, able to deliver extremely high-quality and high-purity epitaxial films, it has a quite limited productivity on an industrial scale. MOVPE, on the other hand, is highly suitable for mass production, thanks to large deposition areas and more flexible deposition systems working at moderate pressures, and also capable of producing high perfection layers with finely tuned doping and a thickness control below 1 nm.

In 2015 we demonstrated the growth of semiconducting homoepitaxial layers doped by Si or Sn on (100)-oriented substrates. In the last part of this year, we performed two brief sets of growth experiments on (010) and misoriented (100) β-Ga_2O_3 substrates to optimize the crystalline perfection of the layers, obtaining very promising preliminary results.

In 2016, we studied in detail the growth of β-Ga_2O_3 layers on these alternative substrate orientations through a comprehensive structural and electrical characterization. (010)-oriented layers showed very high crystalline perfection with free carrier density tunable in a wide range (1×10^{17}–8×10^{19} cm^{-3}) and record high mobility up to ~130 cm^2/Vs. Growths on misoriented (100) substrates led to comparable results, with the main advantage that their substrate fabrication is technologically much easier.

In parallel to this work, we started a very fruitful collaboration with Gregg Jessen's group at the Air Force Research Laboratories (AFRL), USA. Starting from our (100) β-Ga_2O_3 layers, AFRL fabricated metal-oxide-semiconductor field-effect transistors (MOSFETs) with excellent device characteristics, demonstrating the enormous potential of β-Ga_2O_3 for power electronics applications.

Homoepitaxial β-Ga_2O_3 layers grown on (010)-oriented substrates

For these experiments [1], we used commercial semi-insulating (Fe-doped) (010) β-Ga_2O_3 substrates grown by the EFG method. This substrate orientation has the advantage that the thermal conductivity (λ) perpendicular to the substrate surface is almost three times higher than in the case of (100)-oriented crystals. λ is, indeed, markedly anisotropic in β-Ga_2O_3, with the highest value along the [010] direction (λ = 27.0 W/mK at RT) and the lowest value along the [100] direction (λ = 10.9 W/mK at RT) [2]. Heat dissipation in devices fabricated on (010)-oriented substrates is then predicted to be much more efficient, mitigating the main disadvantage of β-Ga_2O_3 compared to SiC and GaN that both have much higher thermal conductivity. On the other hand, (010) β-Ga_2O_3 substrates are not ideal for large-scale production, since their wafering is very challenging. Contrary to the (100) and the (001) planes, the (010) is not a cleavage plane and the wafers have to be cut out from the bulk, leading to a higher risk of material loss by undesired cleavage along alternative crystallographic directions.

Growth on (010)-oriented substrates has been mainly performed by using the same experimental parameters optimized for the growth on (100)-oriented crystals [3], i.e. a susceptor temperature of 850 °C, a reactor pressure of 5 mbar, and triethylgallium (TEGa) and O_2 molar flows of 6.0×10^{-6} and 2.2×10^{-2} mol/min, respectively. Tetraethylorthosilicate (TEOS) and tetraethyltin (TESn) were used for the doping with Sn or Si and their flow rates were systematically varied in the range ~1×10^{-11}–1×10^{-8} mol/min.

Structural properties

At basic growth conditions, the layers showed surfaces with a mean roughness (RMS) of ~600 pm, dominated by elongated islands oriented along the [001] direction (Figure 1a). The growth rate, estimated from the resulting layer thickness obtained by spectroscopic ellipsometry and the growth time, was limited to 2 nm/min. To increase the growth speed we performed experiments with higher TEGa flows of 1.21×10^{-5} and 1.67×10^{-5} mol/min, adjusting the O_2 flux to keep the Ga/O ratio constant. The growth rate increased to 3.4 and 5.5 nm/min, respectively, but the roughness of the layers increased as well, with RMS values of 1.25 and 11.4 nm. For a given TEGa flow rate, different O_2 flow rate in the range 5×10^{-3}–3×10^{-2} mol/min had no measurable influence on the layer growth.

Doping generally did not affect the surface morphology of the layers. Only the highest Sn-doped sample, grown with a TESn flow rate of 6.4×10^{-9} mol/min, showed a surface morphology characterized by elongated blocks ascribable to step bunching and an increased RMS roughness of 3.09 nm (Figure 1b). In another series of experiments, the growth temperature was decreased from 850°C to 700°C, while keeping the other parameters unchanged, resulting in a slight increase of the growth speed with decreasing susceptor temperatures. Since different flow rates of O_2 did not alter this trend, the growth at high temperatures is probably limited by desorption of GaO from the growing surface.

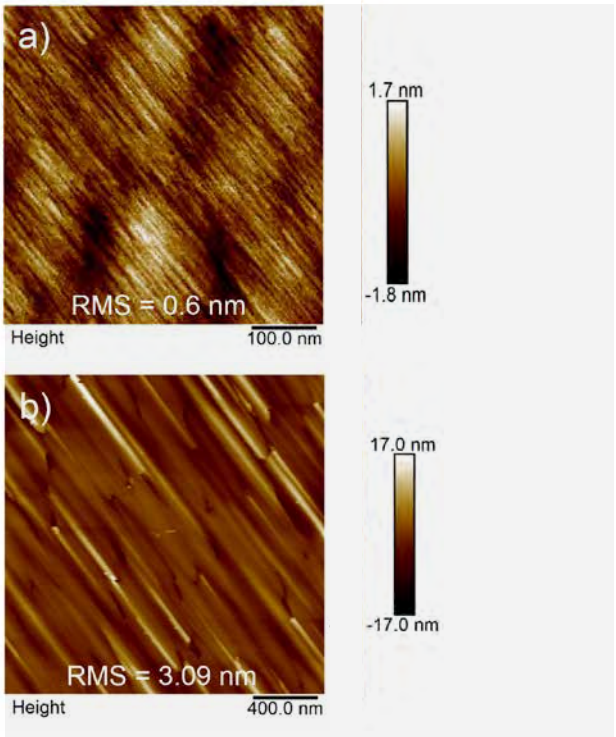

Fig. 1
AFM images of (010) β-Ga_2O_3 layers grown with (a) standard TEOS or TESn doping fluxes and (b) a high TESn flow rate of 6.4×10^{-9} mol/min.

By transmission electron microscopy investigation no extended defects such as planar defects or dislocations were observed in layers grown at standard conditions. More important, the interface between layer and substrate showed no measurable contrast, while in (100) β-Ga_2O_3 layers it was always decorated by defects. The very high crystalline perfection of the layers indicates that double positioning growth, previously observed for all layers grown on (100)-oriented β-Ga_2O_3 substrates [4], does not occur on the (010) surface.

Electrical properties

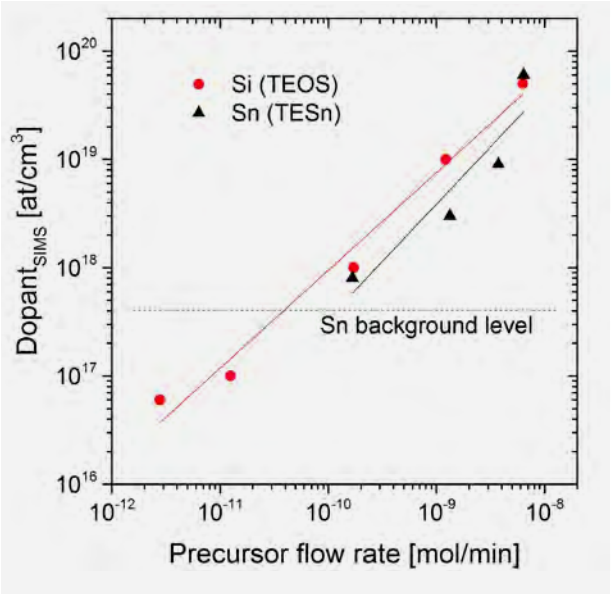

Fig. 2
SIMS concentration of Si and Sn versus TEOS and TESn flux in (010) β-Ga_2O_3 layers. The horizontal dashed line indicates the Sn background level due to memory effect.

The incorporation efficiency of Si from TEOS and of Sn from TESn is very similar, as can be deduced from the double-logarithmic plots of Figure 2. By increasing the amount of TEOS injected into the reactor from 2×10^{-12} to 7×10^{-9} mol/min, the chemical concentration of Si in the layers increases nearly proportionally from 6×10^{16} to 6×10^{19} cm^{-3}. In the case of Sn, the doping range is significantly reduced by a high Sn background level of ~4×10^{17} cm^{-3} due to Sn memory effect in the reactor after high doping experiments.

Figure 3 shows the free electron concentration *n* vs. the incorporation of Si and Sn as measured by SIMS. For both dopant species, the free carrier density increases linearly with the dopant concentration, pointing to negligible compensation as well as effective incorporation of the dopants in electrically active sites. The only exception to this trend is the layer doped with the highest Sn concentration that shows a carrier density of 3×10^{18} cm^{-3} despite a Sn incorporation of 6×10^{19} cm^{-3}.

This result can be explained by the altered growth mechanism, observed through the AFM measurements in Figure 1b, which leads to the formation of complexes and extended defects that can compensate the Sn donors and limit the electron transport properties of the material.

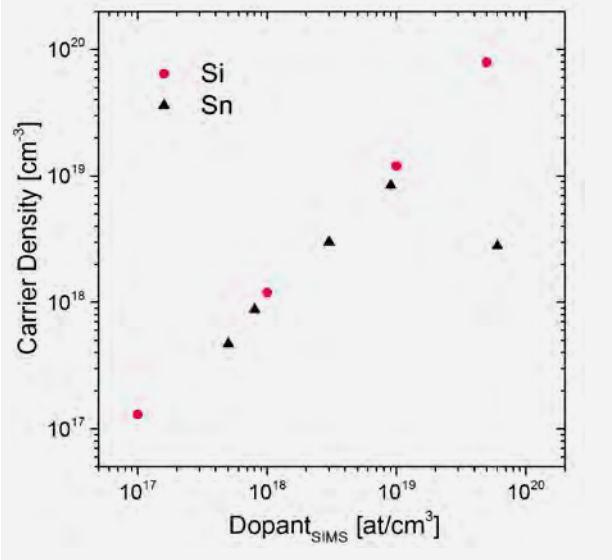

Fig. 3
Hall free carrier density versus the dopant (Si and Sn) concentration obtained by SIMS in (010) β-Ga_2O_3 layers.

Figure 4 shows the Hall mobility μ as a function of the free carrier concentration for Si- and Sn-doped layers. The electron mobility increases with decreasing free carrier density, spanning from ~50 cm²/Vs at n=8×10¹⁹ cm⁻³ to ~130 cm²/Vs at n=1×10¹⁷ cm⁻³. Such a mobility behavior indicates that scattering at ionized impurities dominates. The mobility values match the best literature data relative to β-Ga_2O_3 bulk crystals and layers grown by molecular beam epitaxy, setting a new standard for MOVPE-grown layers.

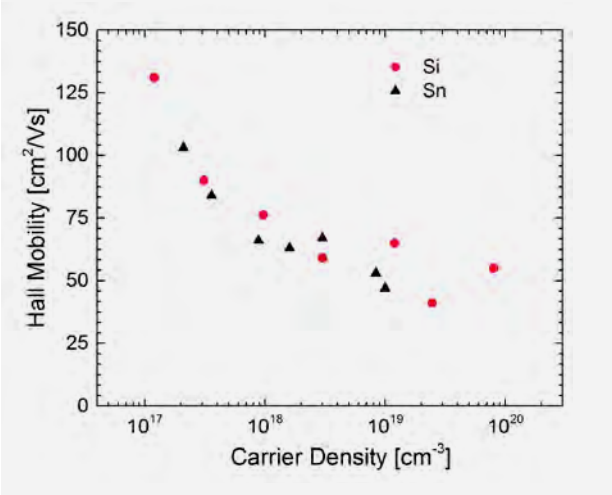

Fig. 4
Hall mobility as a function of carrier density for Si- and Sn-doped (010) layers.

Homoepitaxial β-Ga_2O_3 layers grown on misoriented (100) substrates

By increasing the miscut angle of (100)-oriented substrates, the width of the terraces on the substrate surface decreases so that the adatom diffusion length can be long enough to provide a step-flow mechanism and hence hinder the formation of 2D islands that lead to twin domains. Moreover, since the adatom diffusion length increases with temperature, high substrate miscuts potentially allow to grow layers with high crystalline perfection at lower temperatures. The growth rate of our layers, usually limited to ~2 nm/min, can then potentially increase due to a reduced desorption of Ga and Ga_2O species. With this aim, (100) β-Ga_2O_3 substrates with increasing miscut angles from 0° to 6° were produced by CrysTec GmbH starting from the bulk crystals grown by the Czochralski method at IKZ [5, 6]. The substrates had step-down direction along [001] in order to optimize the step-flow growth, since the adatom diffusion length on the β-Ga_2O_3 (100) surface is higher along the *b*-direction.

Structural properties

Figure 5 shows AFM images of β-Ga_2O_3 substrates with 2°, 4° and 6° miscut angles, along with AFM images of 200 nm-thick homoepitaxial layers grown thereon. The surface of the substrates is characterized by well-defined steps aligned along the [010] direction with a constant step height of ~600 pm, corresponding to half of the *a* lattice parameter, and decreasing terrace widths with increasing misorientation values. The surface of the samples with the lowest miscut angle shows the presence of stepped islands elongated in the [001] direction with the same height of the steps on the substrate surface. On their top, 2D islands are clearly visible, marked with arrows. At 4° miscut, the layers present surface steps parallel to [010] direction, with a mean terrace width of ~6 nm. On terraces with a width larger than 20 nm, 2D islands are still present, marked with arrows. At the highest miscut angle of the substrates, the grown layers show a regular array of steps with the same structure visible on the substrates prior to the growth, indicating a perfect step flow growth mode. No signs of step bunching are visible despite the significant miscut angle.

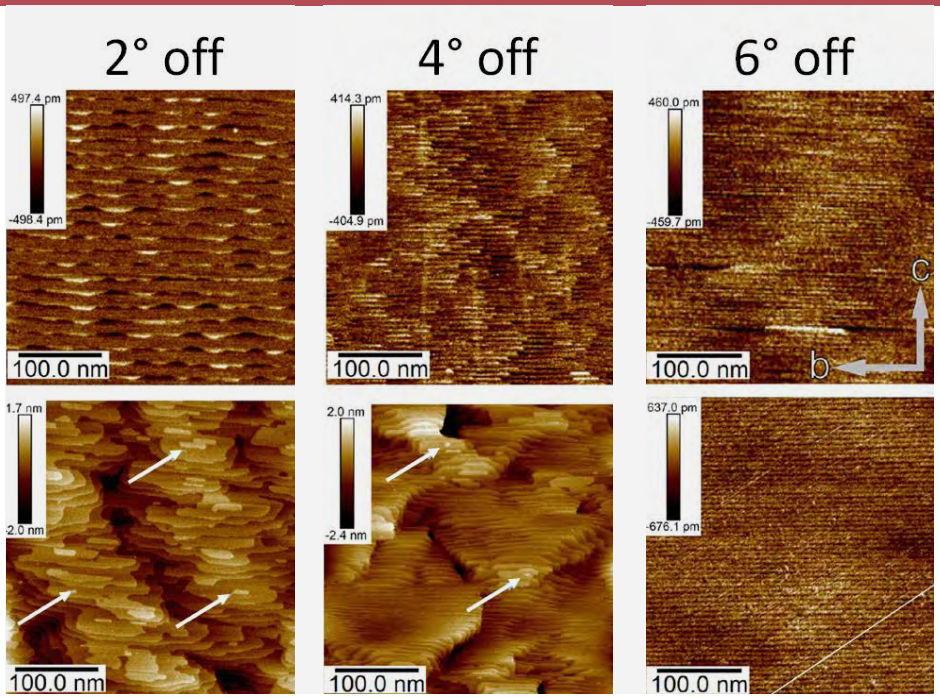

Fig. 5
AFM images of (100) substrates with miscut-angles of 2°, 4°, and 6° towards [001] direction (upper row) and epitaxial layers grown thereon (lower row). The white arrows indicate the presence of two-dimensional islands on the layer terraces.

For increasing miscut angles of the substrates, TEM investigation identified a decreasing density of stacking faults in form of twin lamellas, which are the main crystallographic defects previously observed in (100)-oriented β-Ga_2O_3 layers. Layers grown on substrates with a miscut-angle of 6° showed no defects at all within the field of view typical for TEM, confirming that the growth of homoepitaxial layers on misoriented (100) β-Ga_2O_3 substrates is an excellent approach to obtain high crystalline perfection layers. A comprehensive study of the evolution of planar defects in the growth of β-Ga_2O_3 layers on (100) substrates with different miscut angles is described in detail in the report of the group "Electron Microscopy".

Electrical properties

Twin lamellas have a detrimental effect on the electric properties of β-Ga_2O_3 layers, compensating and hampering the mobility of charge carriers. These defects are described by a *c*/2 glide reflection as twin relation. The coalescence of twinned and epitaxial 2D islands along the *c* plane results in the formation of incoherent twin boundaries that present dangling bonds. These form charged walls in the layers surrounded by cylindrical-shaped depletion regions with a radius R, which is inversely proportional to the square root of the net doping concentration. The effect of twin lamellas on the electrical properties of the layers is then stronger for low doping concentrations. Figure 6 shows the electron Hall mobility vs. carrier density for layers grown on the best quality 4° and 6° misoriented (100) substrates, compared to the results of (010) layers. Data relative to layers on 2°-miscut substrates are not reported since they do not differ significantly from those of (100) on-oriented layers.

For layers grown on higher miscut angles it is easy to observe that lower free carrier concentrations can be obtained, with resulting mobilities that match the reference values of (010)-oriented samples. More details on the electrical characterization of β-Ga_2O_3 layers grown on misoriented (100) substrates are reported by the "Physical Characterization" group.

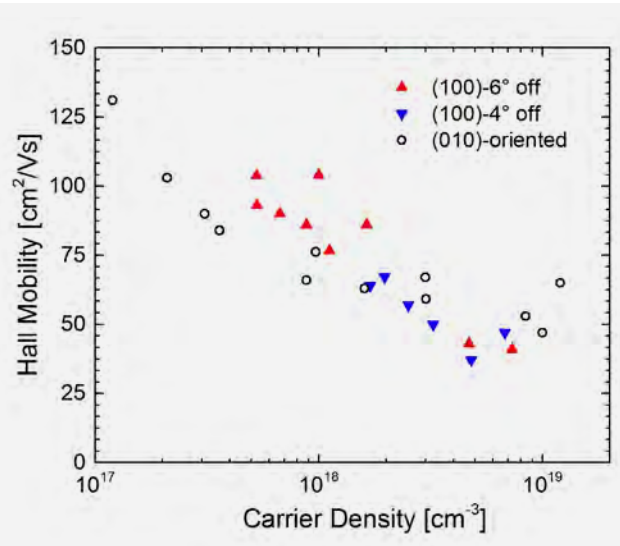

Fig. 6
Hall mobility versus carrier density for layers grown on (100) substrates with 4° and 6° miscut-angles compared to the reference values of (010) layers.

First MOSFETs based on homoepitaxial (100) β-Ga_2O_3 layers

The Air Force Research Laboratories (AFRL) fabricated two distinct MOSFET architectures on our β-Ga_2O_3 layers grown, at the end of 2015, on semi-insulating on-oriented (100) substrates (CZ). The layers were 200–300 nm thick, with free carrier density of 1×10^{18} cm^{-3} and mobility limited to ~20 cm^2/Vs due to compensation from dangling bonds at twin lamellas.

The first structure is a two-finger MOSFET with a 2-µm gate length, 3.4-µm source–drain spacing, and 0.6-µm gate–drain spacing [7]. Device isolation was performed by inductively coupled plasma etching, while source-drain electrodes were formed using evaporated Ti/Al/Ni/Au metals. A blanket 20-nm thick Al_2O_3 layer deposited by atomic layer deposition served as both the gate oxide and channel passivation. After removing Al_2O_3 in the ohmic regions, interconnect and gate metal were patterned and deposited using a Ti/Au metal stack. At a drain voltage of 10 V, the I_{ON}/I_{OFF} ratio was measured as high as 10^7 and the devices were observed to hold a gate-to-drain voltage of 230 V in the OFF-state at V_{GS}=–30 V without catastrophic breakdown. The gate-to-drain electric field corresponds to 3.8 MV/cm, which is the highest reported for any transistor and surpassing bulk GaN and SiC theoretical limits.

The second device architecture by AFRL is a wrap-gate fin-array FET fabricated from a 300-nm thick β-Ga_2O_3 layer [8]. Arrays of fin channels with a triangular cross-section, approximately 300 nm wide and 200 nm tall, were formed by electron beam lithography. Ohmic contacts consisted of a stack of Ti/Al/Ni/Au. A 20-nm Al_2O_3 gate dielectric was deposited by atomic layer deposition and patterned by reactive ion etching to allow for Ni/Au interconnects and ~2 µm long optical gate metal evaporation. The finFET has a centered two-finger gate layout with each gate finger wrapping along 48 fins. The total source to drain distance is ~4 µm and the fin-array spans approximately ~3 µm of this source-drain distance. FinFETs demonstrate normally-off operation with a threshold voltage between 0 and +1 V during high-voltage operation. The I_{ON}/I_{OFF} ratio is greater than 10^5 and is mainly limited by high on-resistance. At V_G=0, a finFET with 21 µm gate-drain spacing achieved a three-terminal breakdown voltage exceeding 600 V that represents the highest breakdown voltage measured without fieldplate for β-Ga_2O_3transistors, and the highest breakdown for any transistor technology utilizing non-planar device channels.

Based on these excellent device characteristics, which demonstrate the enormous potential of β-Ga_2O_3 for power electronics applications, we submitted a VIP+ proposal to the German Federal Ministry of Education and Research (BMBF), in collaboration with the Ferdinand Braun Institute (FBH Berlin) and the Technische Universität Berlin (TU Berlin) in autumn 2016. The aim of this project is to develop power devices based on β-Ga_2O_3 homoepitaxial layers within a Berlin-based research consortium that stands out for its excellent expertise and capabilities in bulk growth, epitaxy, device fabrication and high-power electrical characterization.

References

[1] M. Baldini, M. Albrecht, A. Fiedler, K. Irmscher, R. Schewski, G. Wagner; ECS J. Solid State Sci. Technol. 6 (2017) Q3040

[2] M. Handwerg, R. Mitdank, Z. Galazka, S. F. Fischer; Semicond. Sci. Technol. 31 (2016) 125006

[3] M. Baldini, M. Albrecht, A. Fiedler, K. Irmscher, D. Klimm, R. Schewski, G. Wagner; J. Mater. Sci. 51 (2016) 3650

[4] R. Schewski, M. Baldini, K. Irmscher, A. Fiedler, T. Markurt, B. Neuschulz, T. Remmele, T. Schulz, G. Wagner, Z. Galazka, M. Albrecht; J. Appl. Phys. 120 (2016) 225308

[5] Z. Galazka, K. Irmscher, R. Uecker, R. Bertram, M. Pietsch, A. Kwasniewski, M. Naumann, T. Schulz, R. Schewski, D. Klimm, M. Bickermann; J. Cryst. Growth 404 (2014) 184

[6] Z. Galazka, R. Uecker, D. Klimm, K. Irmscher, M. Naumann, M. Pietsch, A. Kwasniewski, R. Bertram, S. Ganschow, M. Bickermann; ECS J. Solid State Sci. Technol. 6 (2017) Q3007

[7] A. J. Green, K. D. Chabak, E. R. Heller, R. C. Fitch, M. Baldini, A. Fiedler, K. Irmscher, G. Wagner, Z. Galazka, S. E. Tetlak, A. Crespo, K. Leedy, G. H. Jessen; IEEE Electron Device Lett. 37 (2016) 902

[8] K. D. Chabak, N. Moser, A. J. Green, D. E. Walker, Jr., S. E. Tetlak, E. Heller, A. Crespo, R. Fitch, J. P. McCandless, K. Leedy, M. Baldini, G. Wagner, Z. Galazka, X. Li, G. Jessen; Appl. Phys. Lett. 109 (2016) 213501

Layers & Nanostructures:
Si/Ge Nanocrystals

Head Dr. Torsten Boeck
Team Dr. R. Bansen, Dr. K. Böttcher, C. Ehlers, O. Ernst, K. Eylers, Dr. F. Ringleb, S. Schaller, H.-P. Schramm, Dr. Th. Teubner, D. Uebel, A. Zimmermann

Überblick

Die Forschung der Gruppe ist fokussiert auf Themen zur Energiewandlung. Dabei steht die Entwicklung neuartiger kristalliner Strukturen und Kristallzüchtungsmethoden im Vordergrund. Die Arbeiten konzentrieren sich auf drei Themen:

(1) Züchtung von Siliziumschichten auf kostengünstigen Substraten, insbesondere auf Glas,
(2) Materialforschung zur Entwicklung von $CuIn_xGa_{1-x}Se_2$ (CIGSe) Mikrokonzentrator-Solarzellen,
(3) Züchtung von Si-, Ge- und Si_xGe_{1-x}-Nanodrähten für Thermoelektrika.

Zum überwiegenden Teil ist die Forschung zu allen Themen projektfinanziert und erfolgt in Zusammenarbeit mit einer Vielzahl von nationalen und internationalen. So fördert die EU mit jeweils einem Arbeitspaket des Photovoltaik-Projektes CHEETAH die ersten beiden Forschungsthemen. Das dritte Thema zur thermoelektrischen Energiewandlung ist in ein regionales Netzwerk eingebunden, bei dem acht Doktoranden aus verschiedenen Institutionen unter Federführung der Brandenburgischen Technischen Universität Cottbus–Senftenberg (BTU) im Rahmen der Graduiertenschule „Functional Materials and Film Systems for Efficient Energy Conversion" (FuSion) zusammenarbeiten.

Während beim EU-Projekt eher anwendungsorientierte Forschung im Vordergrund steht, zielen die begleitend auf dem Gebiet der Materialforschung für die Photovoltaik eingeworbenen DFG-Projekte auf die Aufklärung grundlegender Fragestellungen bei der Materialentwicklung und Charakterisierung und bilden einen guten Rahmen für Qualifizierungsarbeiten. Das DFG-Projekt „Lösungsmittelgenerierte Phasenumwandlung zur Erzeugung kristalliner Si-Schichten" konnte im Berichtszeitraum abgeschlossen werden. Das DFG-Projekt „Lokal gewachsene $Cu(In,Ga)Se_2$-Mikroinseln für Konzentratorsolarzellen" ermöglicht es, Forschungsergebnisse der Bundesanstalt für Materialforschung und -prüfung (BAM) auf dem Gebiet der Lasertechnik im IKZ zur ortsdefinierten Keimbildung beim Wachstum von CIGSe-Inseln anzuwenden, um dann am Helmholtz-Zentrum Berlin (HZB) Bauelemente-Eigenschaften zu messen und Solarzellen aufzubauen.

An den Forschungsarbeiten zu den genannten Themen waren im Berichtszeitraum insgesamt drei Doktorandinnen und Doktoranden, sowie vier Bachelor- bzw. Masterstudentinnen und -studenten beteiligt. Im Berichtszeitraum konnte Roman Bansen seine Dissertation „Solution growth of polycrystalline silicon on glass using tin and indium as solvents" mit dem Prädikat summa cum laude an der Humboldt-Universität zu Berlin abschließen [1].

Overview

The group is engaged in research on different topics in the field of energy conversion. The emphasis hereby lies on the development of novel crystalline structures and crystal growth methods. The work can be categorized into three topics:

(1) Growth of silicon layers on cost-efficient substrates, especially glass,
(2) Materials research for the development of $CuIn_xGa_{1-x}Se_2$ (CIGSe) microconcentrator solar cells,
(3) Growth of Si, Ge and Si_xGe_{1-x} nanowires for thermoelectric applications.

The research on all three topics is predominantly financed by third-party funds, and it is conducted in cooperation with numerous national and international partners. The first two research topics are funded by the EU, with one work package each, in the frame of the photovoltaics project CHEETAH. The third topic for thermoelectric energy conversion is embedded in a regional network, in which eight doctoral students from different institutions cooperate under the general leadership of the BTU Cottbus/Senftenberg within the framework of the graduate school "Functional Materials and Film Systems for Efficient Energy Conversion (FuSion)".

While the EU project is primarily focused on application-oriented research, the procured DFG projects on the field of materials research for photovoltaics aim at the solution of fundamental questions in materials development and characterization. They also create a more favorable environment for the qualification of young scientists.

The DFG project "Solution based phase change for the growth of crystalline Si layers" has been successfully completed during the report period. The DFG project "Locally grown Cu(In,Ga)Se_2 micro islands for concentrator solar cells" provides the opportunity to use research results on the field of laser technology achieved at the Bundesanstalt fuer Materialforschung und -pruefung BAM for the locally defined nucleation during growth of CIGSe islands at IKZ, which are then used at the Helmholtz-Zentrum Berlin (HZB) to build solar cells and measure their properties.

Within the report period, three doctoral students, as well as four bachelor and master students were involved with the research work on the above mentioned topics. Roman Bansen finished his dissertation on „Solution growth of polycrystalline silicon on glass using tin and indium as solvents" with *summa cum laude* at Humboldt-Universität zu Berlin [1].

Results

Growth of silicon layers on cost-efficient substrates

The motivation for the thin film approach is that a silicon solar cell only needs a few ten µm of silicon in order to absorb sunlight efficiently. Conventional silicon solar cells, however, have a thickness of about 140 to 200 µm, which is significantly more than required. In addition, further silicon is wasted during wafering due to kerf losses. Two different approaches are used in our group to tackle this challenge. Both of them are based on the deposition of silicon by steady-state liquid phase epitaxy (SSLPE) from a tin solution.

The first approach, which is part of the EU CHEETAH project, investigates the growth of silicon layers by SSLPE on reorganized porous silicon substrates. The main idea is to reuse a silicon wafer multiple times for a reorganization process and subsequent epitaxial growth. The grown layer can then be detached from the original wafer and processed into a thin film silicon solar cell, while the original wafer is reused for the next cycle of reorganization, growth and detachment.

The reorganized porous silicon substrates are fabricated by our project partner IMEC in Belgium. The substrates consist of a monocrystalline thin silicon layer attached by silicon pillars to a silicon substrate, and they are produced by forming cylindrical voids in a (100) or (111) silicon wafer by deep-UV lithography and subsequent SF_6/O_2 plasma etching. The resulting layer is then reorganized in a hydrogen atmosphere, thereby forming a thin layer, which is attached by pillars to the substrate as described in more detail in [2]. Epitaxial growth of a silicon layer by SSLPE was found to be possible on both (100) and (111) substrates as shown in Figure 1. While growth on (100) substrates leads to pyramidal growth due to kinetic restrictions, it is possible to grow flat layers on (111) substrates [3].

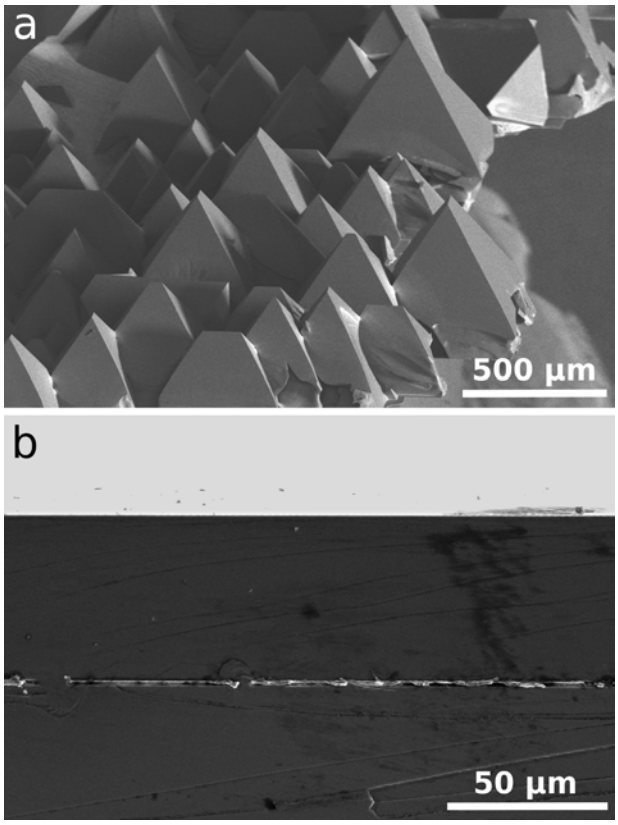

Fig. 1
Growth on Si (100) leads to formation of large pyramids (a), while deposition of flat layers is possible on Si (111) substrates (b).

Layers & Nanostructures: **Si/Ge Nanocrystals**

The second approach is the deposition of crystalline silicon on a seed layer on glass substrates. In the report period, this research was focused on experiments with a UV laser system to remove an oxide layer from the seed layer surface, as well as on simulations of the temperature distribution and convective flow in the melt. For the numerical simulations, the inner chamber of the solution growth setup has been modeled in 3D. To achieve a manageable simulation procedure, the gas flow and temperature distribution in the inner growth chamber was first simulated by steady-state calculations. Then, using the temperature data as boundary values of the metallic solution, the convective flow in the crucible, including Si species transport, was calculated in time-dependent simulations.

As can be seen in Figure 2, the simulations showed that the convective flow in the melt is characterized by the solvent rising up along the outer walls and then flowing along the surface toward the sample in the center, where the dissolved Si crystallizes on the seed layer. Underneath the sample, the solvent descends back to the bottom of the crucible, where it flows outward again, dissolving new Si from the solid Si source. Hereby, approximately four to six convective cells form [4].

Three different heater configurations for the growth mode have also been simulated: top and side heater, top and bottom heater, and a combination of all three. The configurations were based on previously experimentally determined heater powers in each case to achieve a preset temperature difference between two thermocouples in the crucible wall. The combined configuration of all three heaters was found to produce the most homogeneous temperature distributions.

A steady difference of 2 to 5 K between the hotter bottom and the colder top throughout the entire crucible has been found. An in-detail simulation of the bottom heater was then conducted to determine the tipping point, from which on higher heater powers lead to an inhomogeneous, chaotic convection structure without stable convection cells. As a result, the bottom heater power should not be increased beyond 15 % of its maximum power in the relevant growth scenarios.

Further results on the topic of crystalline silicon on glass have been published within the reporting period [5, 6].

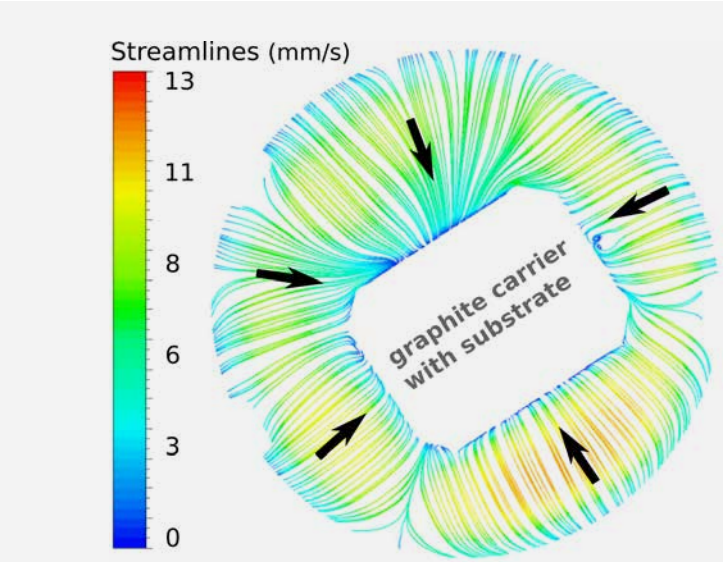

Fig. 2
3D simulation of the growth process with a tin solution at about 600°C. The convection in the crucible is shown by way of streamlines according to the velocity field of the melt at the surface. The flow direction is marked with arrows.

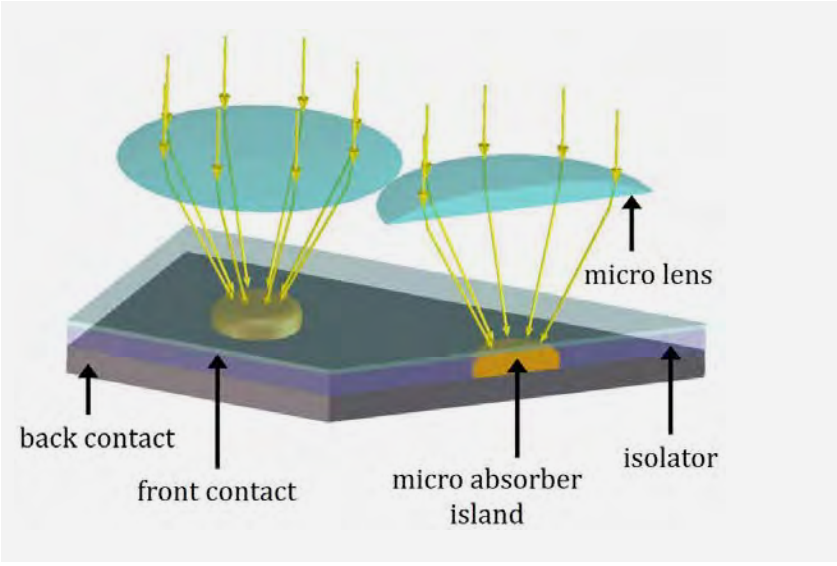

Fig. 3
Scheme of concentrator design including lenses and CIGSe absorbers.

Copper indium gallium selenide CIGSe for micro-concentrator solar cells

$CuIn_xGa_{(1-x)}Se_2$ (CIGSe) is a crystalline material, which is known as an efficient, direct absorber for thin-film solar cells of up to 22.6 % efficiency [7]. Nevertheless, these photovoltaic devices suffer from high costs, since indium is not only a rare element, but also used for a multitude of technical applications such as LCDs or LEDs. Therefore, it would be beneficial if the indium amount could be reduced. The concept of micro-concentrator CIGSe solar cells (Fig. 3) allows substantial material saving and an increase of solar cell efficiency. Proof-of-principle studies based on a top-down approach have already demonstrated the efficiency enhancement [8], but for material saving, however, a bottom-up approach is needed.

Our group is working on the local growth of CIGSe micro-absorbers, which are subsequently processed to functional solar cell devices by our project partner. Our approach is to use indium islands as precursors, which can be further processed to CIGSe micro-absorbers. The local arrangement of the islands, which is indispensable for the alignment of the absorber with the concentrator component, is realized by surface structuring using a femtosecond laser [9]. By adjusting the indium deposition rate and the substrate temperature we are able to control the island size, areal density and aspect ratio to achieve the desired array dimensions [10], details are shown in Figure 4.

The next steps, i.e. processing of such precursor structures into micro absorbers, require the controlled reaction between the indium islands, gallium, copper and selenium. Using the in-house made Se beam flux device, we have demonstrated the conversion of the indium islands into polycrystalline $CuInSe_2$ micro islands with promising material properties [11]. Recent research was mainly focused on the introduction of gallium into this system, i.e. the growth of $Cu(In,Ga)Se_2$ micro-absorbers. A thin film of copper selenides forms as a side product on the substrate. It can be successfully removed by chemical etching with a solution of potassium cyanide.

Furthermore we have been working on the insulation between front and back contact, which are connected in parallel. Insulation can be obtained by depositing a layer of the epoxy novolac SU-8 using a spin-coater. By choosing a suitable resist viscosity for spin coating, the insulating layer is thinner on top of the absorber islands than on the surrounding substrate and therefore the initially completely covered photovoltaic active absorber islands can be uncovered for front contacting by plasma etching.

A characterization of the resulting devices under a solar simulator yielded an efficiency of 2.3 % and thus provided evidence for their functionality.

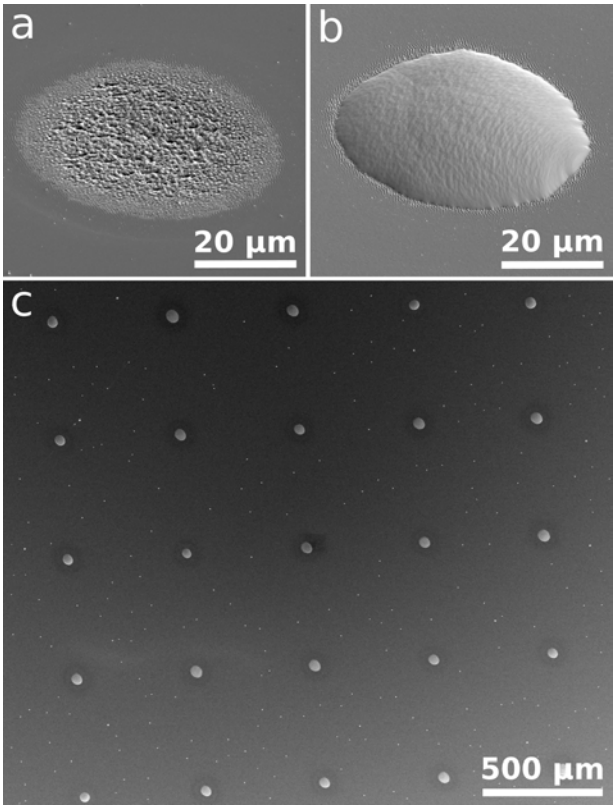

Fig. 4
SEM images of indium nucleation at fs laser spots.
a) Laser spot on glass,
b) laser spot after deposition of molybdenum and indium,
c) structured substrate with array of indium islands.

Layers & Nanostructures: **Si/Ge Nanocrystals**

SiGe nanowires for thermoelectric applications

Within the frame of the BTU graduate school FuSion, a doctoral scholarship was approved in 2016, which sets the focus of the established molecular beam epitaxy of either Si or Ge nanowires in our group to the growth of Si_xGe_{1-x} nanowires, their modelling and characterization. The goal of this work is the fabrication of high efficiency, high temperature thermoelectrics.

As can be seen from equation (1), it is possible to improve the efficiency of a thermoelectric material by either increasing its Seebeck coefficient S or the electrical conductivity σ, or by lowering the thermal conductivity κ. As these values are coupled by the electron transport in the material, however, it is difficult to achieve one without negatively affecting the others.

$$ZT = \frac{S^2\sigma}{\kappa}T \qquad (1)$$

Also, the Seebeck coefficient in Si_xGe_{1-x} depends on the material composition, and the highest values can be achieved for Ge contents in the region between 10 – 40 %. Unfortunately, the growth of single-crystalline, homogenous compositions such as $Si_{0.7}Ge_{0.3}$ is extremely difficult to realize for bulk crystals. A way to tackle this problem is to prepare the thermoelectric material out of nanowires. Caused by phonon scattering at the nanowire facets, it has been shown that κ can be reduced in nanowire materials, leading to significantly higher efficiencies compared to bulk materials.

Usually, two thermoelectric materials are combined. In the case of SiGe, these are made of p-type and n-type SiGe. In order to achieve the highest possible thermoelectric voltage, a serial connection of p- and n-type nanowires would be most desirable, just like the p- and n-type blocks or 'legs' in a conventional thermoelectric device. As the contacting of individual nanowires is not a viable option, however, we think the contacting of larger nanowire arrays, possibly embedded in polymer blocks with low thermal conductivity, would be a feasible approach, combining parallel and series connection of the nanowires (Fig. 5).

First research activities within the scope of the doctoral thesis were focussed on the chemical preparation of silicon substrates, on which the nanowires should be grown subsequently. It is mandatory for a reproducible growth process to remove the passivating oxide layer as well as structural defects and impurities from the silicon surface. For this purpose, the chemical cleaning and thermal annealing processes were monitored and optimized.

The cooperation with the Center for Nanoscience at Lund University in Sweden involved a medium-term stay of a visiting scientist from our group. This research on diffusion-controlled growth of nanowires has led to a joint publication in the report period [12].

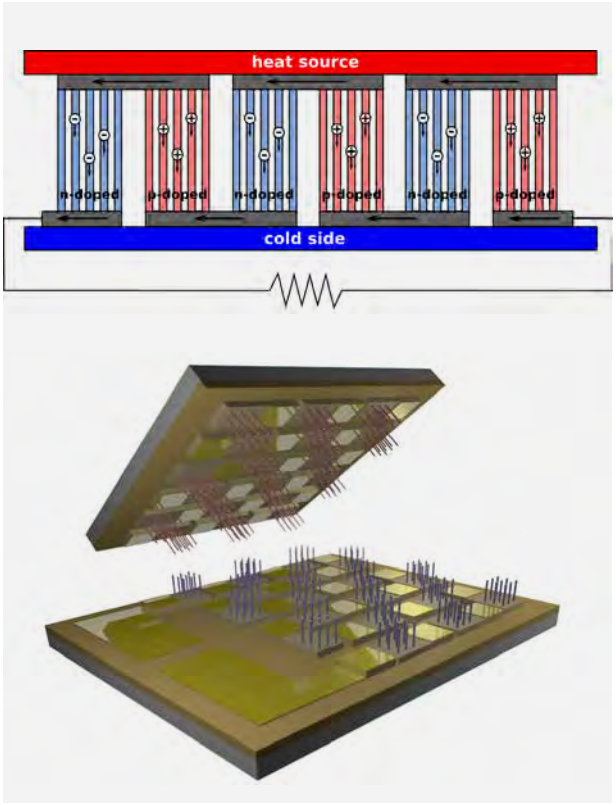

Fig. 5
(top) Thermoelectric generator, based on collectively contacted arrays of p- and n-doped NWs.
(bottom) 3D concept of thermoelectric module based on NW arrays.

References

[1] R. Bansen; Solution growth of polycrystalline silicon on glass using tin and indium as solvents, Dissertation, Humboldt-Universität zu Berlin (2016)

[2] V. Depauw, I. Gordon, G. Beaucarne, J. Poortmans, R. Mertens, J. P. Celis; J. Appl. Phys. 106 (2009) 33516

[3] C. Ehlers, R. Bansen, T. Markurt, D. Uebel, T. Teubner, T. Boeck; J. Cryst. Growth 468 (2017) 268

[4] R. Bansen, C. Ehlers, T. Teubner, K. Böttcher, K. Gambaryan, J. Schmidtbauer, T. Boeck; J. Photon. Energy 6 (2016) 25501

[5] R. Bansen, C. Ehlers, T. Teubner, T. Markurt, J. Schmidtbauer, T. Boeck; CrystEngComm 18 (2016) 1911

[6] R. Bansen, C. Ehlers, T. Teubner, T. Boeck; J. Semicond. 37 (2016) 93001

[7] P. Jackson, R. Wuerz, D. Hariskos, E. Lotter, W. Witte, M. Powalla; Phys. Status Solidi RRL 10 (2016) 583

[8] M. Paire, L. Lombez, N. Pere-Laperne, S. Collin, J.-L. Pelouard, D. Lincot, J.-F. Guillemoles; Appl. Phys. Lett. 98 (2011) 264102

[9] F. Ringleb, K. Eylers, Th. Teubner, T. Boeck, C. Symietz, J. Bonse, S. Andree, J. Krüger, B. Heidmann, M. Schmid, M. Lux-Steiner; Appl. Phys. Lett. 108 (2016) 111904

[10] F. Ringleb, K. Eylers, T. Teubner, H.-P. Schramm, C. Symietz, J. Bonse, S. Andree, B. Heidmann, M. Schmid, J. Krüger, T. Boeck; Appl. Surf. Sci. 418 (2017) 548

[11] T. Boeck, F. Ringleb, R. Bansen; Cryst. Res. Technol. 52 (2017) 1600239

[12] V. G. Dubrovskii, Y. Berdnikov, J. Schmidtbauer, M. Borg, K. Storm, K. Deppert, J. Johansson; Cryst. Growth Des. 16 (2016) 2167

Layers & Nanostructures:
Ferroelectric Oxide Layers

Head Dr. Jutta Schwarzkopf
Team D. Braun, C. Feldt, M. Klann, Dr. J. Sellmann

Überblick

Perowskitartige Oxidmaterialien mit ferro- und piezoelektrischen Eigenschaften werden für eine große Bandbreite von Speicher-, Aktuator-, Sensor- oder Hochfrequenzbauelementen eingesetzt. Bis heute basieren die für diese Zwecke verwendeten Materialien aufgrund ihrer exzellenten physikalischen Eigenschaften auf bleihaltigen Verbindungen. Wegen ihrer ökologischen und gesundheitlichen Problematik besteht ein dringender Bedarf sie durch umweltfreundlichere Materialien zu ersetzen. Ein vielversprechender Kandidat in dieser Hinsicht ist das Kalium-Natrium-Niobat ($K_xNa_{1-x}NbO_3$), welches in unserer Gruppe als kristalline Dünnschicht abschieden wird. Ein praktischer Ansatz, um äquivalente oder sogar bessere ferro- und piezoelektrische Eigenschaften im Vergleich zu den bleihaltigen Verbindungen zu erhalten, sind strukturelle Modifikationen [1]. Aufgrund der inhärenten Kopplung zwischen Struktur und Funktionalität ermöglicht dies eine gezielte Manipulation der physikalischen Eigenschaften dieser Schichten. Auf diese Weise wurde gezeigt, dass „riesige" piezoelektrische Antworten durch eine Modifizierung der kristallinen Symmetrie erreicht werden können [2]. Ein geeignetes Werkzeug für strukturelle Änderungen ist das epitaktische Wachstum von verspannten Dünnschichten auf Substraten mit maßgeschneiderter Gitterfehlanpassung. Für ein gezieltes Einstellen der funktionalen Eigenschaften von dünnen Schichten ist jedoch ein tiefergehendes Verständnis der Korrelation zwischen Gitterverspannung und ferroelektrischer Phasenbildung notwendig. Dies kann aus dem Verspannungs-Phase-Diagramm gewonnen werden, welches für $KNbO_3$ innerhalb der Landau-Ginzburg-Devonshire Theorie berechnet wurde und im ersten Teil des Berichtes vorgestellt wird.

Eine praktische Anwendung des Verspannungs-Phase-Diagramms wird im zweiten Teil diskutiert, wo die gezielte Abscheidung von $K_{0.7}Na_{0.3}NbO_3$ Schichten auf (110) $TbScO_3$ Substraten mit der metallorganischen Gasphasendeposition (MOCVD) und die resultierenden ferroelektrischen Eigenschaften beschrieben werden. Die Beobachtung von monoklin verzerrten Domänen, die entlang der pseudokubischen Achsen der Einheitszelle geschert sind, stimmt gut mit unseren Vorhersagen überein. Die Schichten wurden erfolgreich für erste akustische Oberflächenwellen (SAW) Experimente verwendet. Diese Ergebnisse wurden innerhalb eines DFG Projektes und der Kooperation mit der AG R. Wördenweber vom Forschungszentrum Jülich erzielt.

Neben dem sogenannten „Strain engineering" ist der Einsatz einer gezielten Stöchiometrieabweichung in dünnen Schichten eine weitere Möglichkeit, Schichteigenschaften selektiv zu ändern. Das ist der Fokus des dritten Themas. Dazu wurden kompressiv verspannte, dünne $NaNbO_3$ Schichten mit Na_2O Überschuss auf (110) $NdGaO_3$ Substraten mit gepulster Laserdeposition (PLD) abgeschieden. Wir untersuchten systematisch die Lage der Phasenübergangstemperatur und das ferroelektrische Umschaltverhalten mit Hilfe von temperaturabhängiger Röntgenbeugung (P.-E. Janolin an ECP), Raman Spektroskopie (M. Ramsteiner am PDI), dielektrischen Permittivitätsmessungen (R. Wördenweber am FZ Jülich) und spektroskopischer Ellipsometrie (R. Schmidt-Grund an der Universität Leipzig). Teile dieser Arbeiten wurden innerhalb der Masterarbeit von Christoph Feldt durchgeführt.

Weiterhin wurden Doppellagensysteme aus $K_{0.5}Na_{0.5}NbO_3$ und $NaNbO_3$ Dünnschichten mit PLD abgeschieden. Sie dienen als Vorarbeiten zur Abscheidung von verspannten Kalium-Natrium-Niobat-Übergittern. Fundamentale Untersuchungen intrinsischer Effekte in ferroelektrischen Übergitterstrukturen sind der Inhalt eines bei der DFG eingereichten Projektantrages.

Im Rahmen des Leibniz Wissenschaftscampus GraFOx wurden grundlegende Untersuchungen zum Wachstum und den Eigenschaften von $SrTiO_3$ Schichten begonnen, die ab 2017 im Rahmen einer Doktorarbeit weiter untersucht werden.

Overview

Perovskite-like oxide materials with ferro- and piezoelectric properties are used for a wide range of memory, actuator, sensor or RF devices. Until today, the materials commonly used for these purposes are based on lead-containing compounds due to their excellent physical properties. However, owing to ecological and health issues, there is an urgent need to replace them by environment-friendly materials. One promising candidate for this purpose is potassium-sodium-niobate ($K_xNa_{1-x}NbO_3$), which is grown in our group as thin crystalline layers. A practical approach to obtain equivalent or even better ferro- and piezoelectric properties than the lead-containing compounds are structural modifications of these layers [1]. Due to the inherent coupling between structure and functionality, this provides the opportunity for targeted engineering of the physical properties in these layers.

Thus, it has been shown that "giant" piezoelectric responses can be achieved due to a modification of the crystalline symmetry [2]. An adequate tool for structural adjustments is the epitaxial growth of strained thin films on substrates with tailored lattice mismatch. However, for a directive tuning of the functional properties of thin films, a detailed understanding of the correlation between lattice strain and ferroelectric phase formation is required. Such information can be obtained from strain-phase diagrams. For $KNbO_3$, this has been calculated within the framework of the Landau-Ginzburg-Devonshire theory and is presented in the first part of this report.

A practical application of the strain-phase diagram is discussed in the second part, where the selective deposition of $K_{0.7}Na_{0.3}NbO_3$ thin films on (110) $TbScO_3$ substrates by metal-organic chemical vapor deposition (MOCVD) and their ferroelectric properties are described. The observation of monoclinically distorted domains with shearing directions along the pseudocubic unit cell axes agrees well with our predictions. The films have been successfully applied for first surface acoustic wave (SAW) experiments. These results have been achieved within a DFG project and in cooperation with work group R. Wördenweber at Forschungszentrum Jülich.

Besides strain engineering, the use of intentional off-stoichiometries in thin films poses a further possibility to selectively change film properties in a targeted way, which is the focus of the third topic. For that purpose, compressively strained $NaNbO_3$ thin films with Na_2O excess were grown on (110) $NdGaO_3$ substrates by pulsed laser deposition (PLD). We investigated the position of the phase transition temperatures and the ferroelectric switching behavior systematically by temperature dependent x-ray diffraction (P.-E. Janolin at ECP), Raman spectroscopy (M. Ramsteiner at PDI), dielectric permittivity (R. Wördenweber at FZ Jülich) and spectroscopic ellipsometry (R. Schmidt-Grund at Uni Leipzig) measurements. Parts of these works were performed within the master thesis of Christoph Feldt.

Furthermore, double layer systems of $K_{0.5}Na_{0.5}NbO_3$ and $NaNbO_3$ thin films were grown by PLD as preliminary experiments for the deposition of strained potassium-sodium-niobate superlattices. Fundamental investigations of intrinsic effects in ferroelectric superlattice structures are the topic of a project proposal submitted to DFG.

Within the Leibniz Science Campus GraFOx fundamental investigations on growth and properties of $SrTiO_3$ films have been started and will be supported by a PhD student as of 2017.

Results

Strain-phase diagram calculations in $KNbO_3$ for targeted domain engineering

In a lattice mismatched film-substrate system, the correlation between lattice strain and ferroelectric phase formation is deduced from a strain-phase diagram. This can be calculated by means of the Landau-Ginzburg-Devonshire (LGD) theory, where the Gibbs free energy $G(T,\mathbf{P},\varepsilon_{xx},\varepsilon_{yy})$ as function of the temperature T, polarization vector **P** and misfit strain ε_{ij} is evolved in a Taylor expansion. For every strain configuration $\{\varepsilon_{xx},\varepsilon_{yy}\}$ the minimum for G has to be calculated in dependence of components of the electrical polarization vector P_1, P_2 and P_3. By comparing these minimum terms to ferroelectric equilibrium states, the stable ferroelectric film phase in dependence of the biaxal strain can be gained.

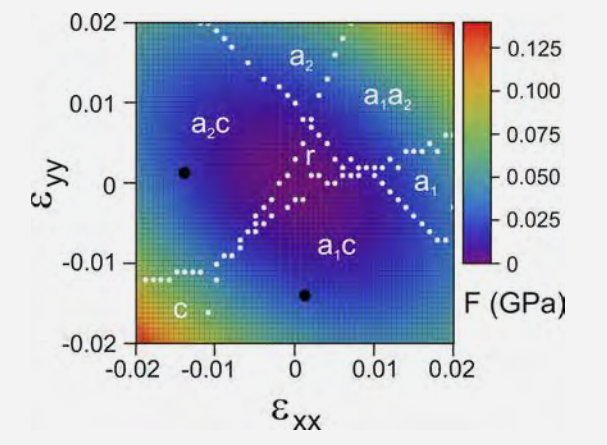

Fig. 1
Calculated strain-phase diagram for $KNbO_3$ using Landau-Ginzburg-Devonshire (LGD) theory. Black circles indicate the strain conditions for $(001)_{pc}$ oriented $K_{0.7}Na_{0.3}NbO_3$ on (110) $TbScO_3$, while white dots mark the stability transition points of the different phases.

Fig. 1 presents the calculated strain-phase diagram for $KNbO_3$. In contrast to existing calculations for this material system [3], the phase boundaries marked as white dots have been calculated on a finer grid, i.e., with remarkably higher accuracy. Consequently, the stable domain configuration can be predicted more precisely, which is indispensable for a targeted strain engineering. It has to be noted, that the elastic constants are reported for $KNbO_3$ only [3], while they are not available for $NaNbO_3$ or $K_xNa_{1-x}NbO_3$. But since we assume similar coefficients for $NaNbO_3$ or the $K_xNa_{1-x}NbO_3$ solid-solutions, we also refer for the phase predictions for these materials to the strain-phase diagram of $KNbO_3$. From Fig. 1, it is obvious that different monoclinic domains (like a_1c/a_2c (also named as M_C), r (sometimes denoted as M_A) and a_1a_2) can be realized in a wide range of strain conditions by an adequate application of lattice stress in $KNbO_3$ thin films. This confirms the choice of $KNbO_3$ (or more generally $K_xNa_{1-x}NbO_3$) as promising film material.

M_C domains in $K_{0.7}Na_{0.3}NbO_3$ on $TbScO_3$ and application for surface acoustic waves (SAW)

In order to investigate the influence of uniaxial and thus highly anisotropic strain, a film with x=0.7 was grown on $TbScO_3$ substrates by MOCVD. From linear elasticity considerations and the strain-phase diagram (see black circles in Fig. 1), ferroelectric M_C domains with $(001)_{pc}$ surface orientation are expected. In the M_C phase, the electrical polarization vector can continuously rotate within the pseudocubic (pc) $(100)_{pc}$ or $(010)_{pc}$ plane resulting in both a vertical and lateral polarization component.

On the basis of the combination of piezoresponse force microscopy (PFM), x-ray diffraction (XRD) and nanofocus XRD at the synchrotron source PETRA III (see also the report of the group Physical Characterization) we succeeded to prove the presence of M_C domains [4]. M_C domains can be described by a monoclinic shearing of the pseudocubic unit cell in $\pm[100]_{pc}$ or $\pm[010]_{pc}$ direction (schematically depicted for shearing in $[100]_{pc}$ in Fig. 2b). In lateral PFM periodically arranged lamellar domains with domain walls with oriented parallel to the $[-112]_{TSO}$ and $[1-12]_{TSO}$ directions can be observed (Fig. 2a). For charge neutrality reasons, the in-plane component of the polarization vector in adjacent domains alternates by 90°. Additionally, from XRD an inclination angle of the domain walls of about 22° with respect to the surface normal is obtained. The periodicity of the stripe domains scales with the thickness of the ferroelectric layer by $\sim t^{2/3}$.

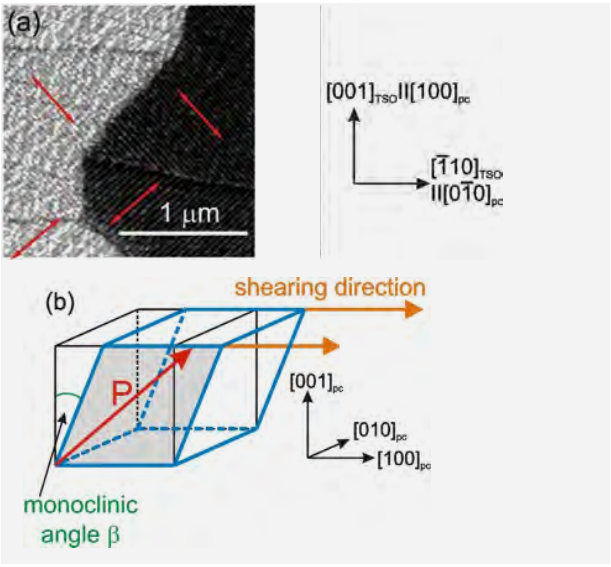

Fig. 2
(a) Lateral piezoresponse force microscopy amplitude image of a 35 nm thick $K_{0.7}Na_{0.3}NbO_3$ film on (110) $TbScO_3$. The red double arrows illustrate the orientation of the lamellar nanodomains. (b) Schematic presentation of the monoclinic unit cell of M_C domains by shearing (shearing direction is indicated by the orange arrows) the pseudocubic unit cell (black) unit cell along the $[100]_{pc}$ direction by the angle β. The electrical polarization vector P (red) can continuously rotate in the $(010)_{pc}$ plane (grey area).

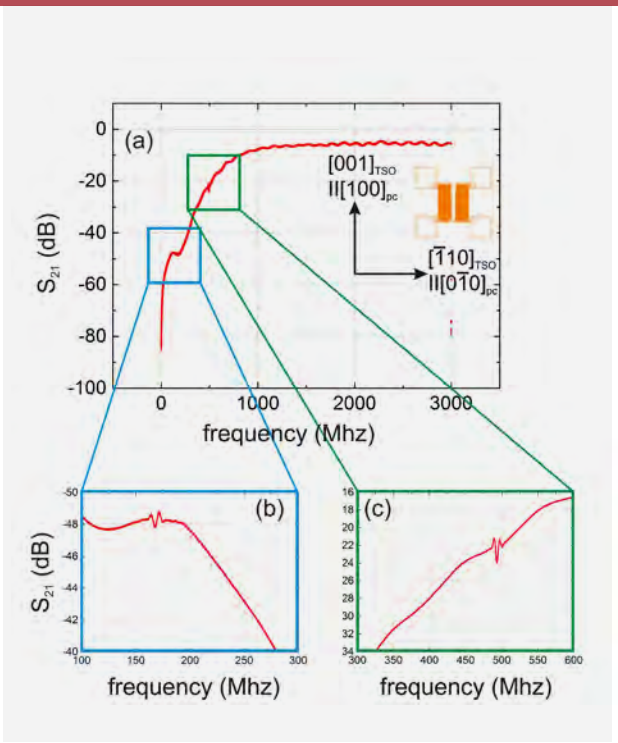

Fig. 3
(a) SAW transmission signal for 35 nm $K_{0.7}Na_{0.3}NbO_3$ thin film on (110) $TbScO_3$. The arrangement of the interdigital electrodes is depicted schematically (orange).
(b) and (c) Higher magnitude of the measurement in (a) in the range of 1st and 3rd harmonic.

Moreover, four orientations of the in-plane component of the polarization vector are possible running along $\pm[001]_{TSO}$ or $\pm[1-10]_{TSO}$. Since the in-plane component of the domains changes by 90° in adjacent domains, in total, four different variants of superdomains are formed containing two types of nanodomains each (Fig. 2a). In dependence on the film thickness, all variants of superdomains can be found within one ferroelectric film.

In collaboration with the group of R. Wördenweber (Forschungszentrum Jülich) surface acoustic wave (SAW) experiments have been performed. First SAW results clearly show the propagation of surface waves of 1st and 3rd order with sound velocities of about 3360 m/s (Fig. 3). A transmission coefficient of ΔS_{21} = 4 dB was measured which is a quite promising result, since the thickness was only 35 nm. In thin films, a higher energy density at the film surface compared to bulk-SAWs can provide a better signal-noise-ratio for optimized structures. Moreover, our measurements yield an exclusive propagation of surface waves parallel to the shearing directions of the monoclinic M_C unit cell, i.e. along $[100]_{pc}$ and $[010]_{pc}$, but not in any other direction. Further SAW experiments by using different (i) substrates ($DyScO_3$, $GdScO_3$, $SmScO_3$) and (ii) film thickness (20 – 80 nm) are in the focus of our ongoing research. On the basis of the presented results, a DFG project that combines SAW in strained $K_xNa_{1-x}NbO_3$ thin films with organic molecules for sensoring has been submitted to DFG.

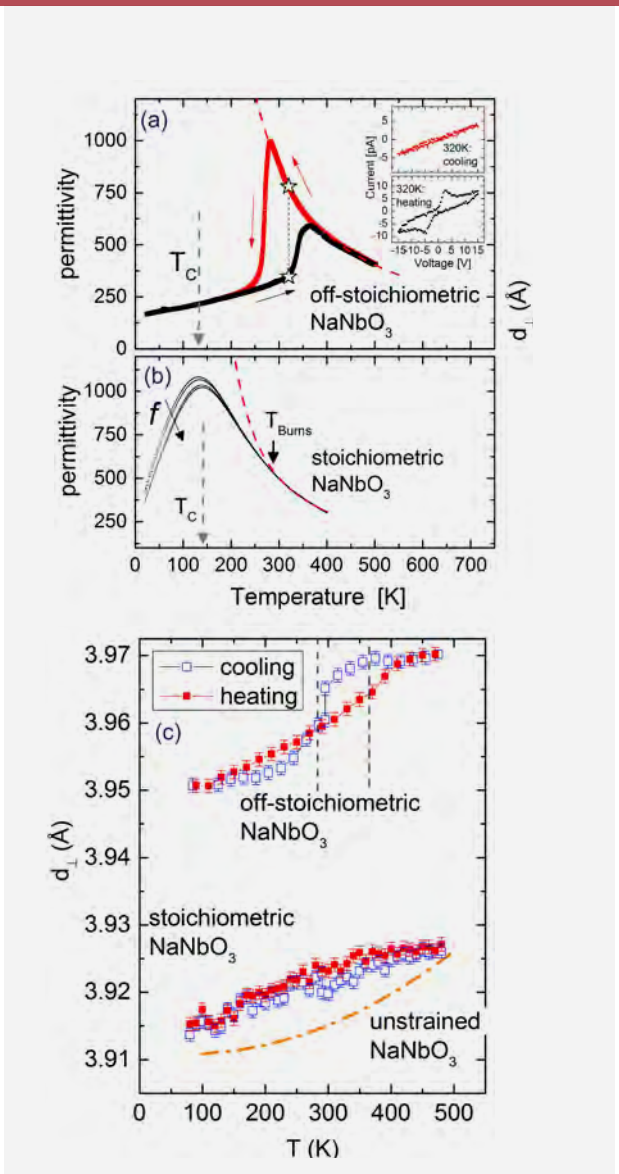

Fig. 4
Temperature dependence of the dielectric permittivity of $NaNbO_3$ thin films grown from (a) an off-stoichiometric (17% Na_2O excess) and (b) a stoichiometric $NaNbO_3$ target. Black and red arrows in (a) and (b) indicate heating and cooling cycles, respectively. (c) Evolution of the vertical lattice parameters of the same $NaNbO_3$ films like in (a) and (b) with temperature. Cooling and heating cycles are labeled by blue and red squares. The dashed, orange line depicts the pseudocubic lattice parameter of unstrained $NaNbO_3$.

Na_2O excess in $NaNbO_3$ thin films with hysteretic ferroelectric switching behavior

Compressively strained $NaNbO_3$ thin films were grown on (110) $NdGaO_3$ by PLD from targets which differ in their elemental composition. The composition varies from stoichiometric to a defined Na_2O excess (up to 20%). In cooperation with the group of R. Wördenweber (Forschungszentrum Jülich), we could show that the lattice strain in epitaxially films can be conserved beyond the critical thickness of plastic relaxation when the nominal Na_2O excess amounts to 17% or more.

Doing so we thus modify the ferroelectric properties of the film in a very controlled way. X-ray diffraction measurements at IKZ and by P.-E. Janolin at ECP as well as transmission electron microscopy analysis (in cooperation with IKZ's Electron Microscopy group) indicate a secondary phase in $NaNbO_3$ films grown from an off-stoichiometric target. In addition to the epitaxially grown $NaNbO_3$ majority phase, a foreign phase evolves shaped as vertically aligned pillars and crystalline precipitates with a dimension of a few nanometers. This secondary phase appears to suppress plastic lattice relaxation of the $NaNbO_3$ matrix. But not only the onset of plastic relaxation is effected/shifted with Na_2O excess from formerly a few nanometers for stoichiometric films and films with small Na excess. Moreover, the ferroelectric properties have changed significantly. The stoichiometric film shows relaxor-type ferroelectric behavior (Fig. 4c), whereas the Na_2O excess film exhibits the "classic" ferroelectric behavior (Fig. 4a) of unstrained $NaNbO_3$ (Fig. 4b) with a hysteretic structural and ferroelectric transition. However, the temperature of this hysteretic transition is shifted from 616 – 655 K for unstrained material to room temperature for the strained $NaNbO_3$ film grown from the off-stoichiometric target with 17% Na_2O excess. In the off-stoichiometric film, structural phase transitions are observed which proceed at the same transition temperatures like the permittivity (Fig. 4c). The hysteretic behavior is explained by a martensitic phase transition.

The presented results are published in Phys. Rev. B [5] and illustrate the potential of strain engineering and stoichiometry variation in ferroelectric thin films. This opens the way to interesting opportunities for basic research and understanding as well as possible applications of this type of ferroelectrics.

References

[1] D. G. Schlom, L.-Q. Chen, C.-B. Eom, K. R. Rabe, S. K. Streiffer, J.-M. Triscone; Annu. Rev. Mater. Res. 37 (2007) 589

[2] B. Noheda; Curr. Opin. Solid State Mater. Sci. 6 (2002) 27

[3] G. Bai and W. Ma; Physica B 405 (2010) 1901

[4] M. Schmidbauer, M. Hanke, A. Kwasniewski, D. Braun, L. von Helden, C. Feldt, S. J. Leake, J. Schwarzkopf; J. Appl. Cryst. 50 (2017) 519

[5] B. Cai, J. Schwarzkopf, C. Feldt, J. Sellmann, T. Markurt, R. Wördenweber; Phys. Rev. B 95 (2017) 184108

Simulation & Characterization

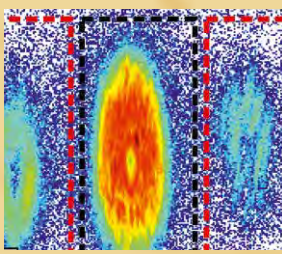

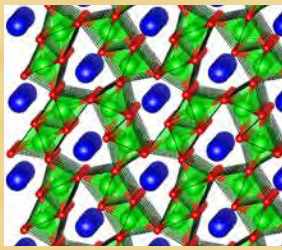

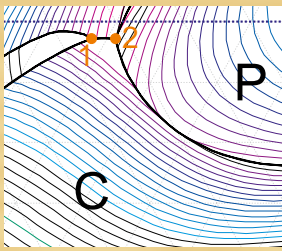

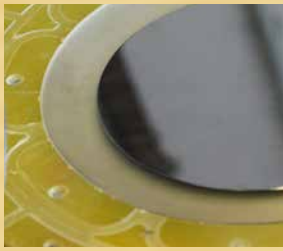

Simulation & Characterization

Head of the section: PD Dr. habil. Detlef Klimm

Die Abteilung Simulation und Charakterisierung befasst sich mit folgende Hauptaufgaben:

1. *wissenschaftlicher Service für das Institut und externe Partner*
2. *Fundamentale und angewandte Materialforschung auf dem Gebiet der kristallinen Materialien*
3. *Entwicklung und Anpassung wissenschaftlicher Methoden zur Charakterisierung von Materialien, die am Institut hergestellt werden*
4. *Bearbeitung von Kristallen und Oberflächen*

Ein wesentlicher Teil unserer Arbeiten dient der Unterstützung von Kristallwachstumsgruppen aus den anderen IKZ-Abteilungen. Dazu gehört die routinemäßige Charakterisierung von elektrischen, optischen und strukturellen Eigenschaften, die Herstellung von Impfkristallen, die kristallographische Orientierung durch Röntgenbeugung sowie das Schneiden und die Bearbeitung von Kristallen und Oberflächen für die Charakterisierung und Epitaxie. Das umfassende Ensemble von Charakterisierungstechniken und die Kompetenz der Forscher und Techniker in der Abteilung garantieren ein schnelles und wissenschaftlich fundiertes Feedback für die Züchter und damit einen schnellen Fortschritt bei den Kristallwachstumsaktivitäten. Ein ausgezeichnetes Beispiel für diese Aktivitäten ist die Etablierung der photothermischen Ionisationsspektroskopie zur Bestimmung der Restverunreinigungen in Germaniumkristallen, die als Detektoren für den ββ-Zerfall eingesetzt werden sollen (GERDA Projekt). Die wissenschaftliche Expertise wird auch von Industriepartnern wie OSRAM OS, Freiberger Compound Materials (FCM) und anderen nationalen und internationalen Partnern angefordert.

*Die vielfältigen Charakterisierungstechniken, die von der makroskopischen bis zur atomaren Skala reichen, sowie das profunde Wissen zu atomaren und ausgedehnten Defekten, in der Analyse von Wachstums- und Relaxationsprozessen sowie der Simulation bietet einzigartige Möglichkeiten, die im Institut hergestellten Materialien grundlegend zu erforschen. Im Bereich der Grundlagenforschung lag der Fokus in den letzten Jahren auf breitlückigen Halbleitern und Oxiden, z.B. von AlN- und Gruppe-III-Sesquioxiden. Diese Arbeiten werden kooperativ über die Abteilungen hinweg, in einigen Fällen auch im Rahmen gemeinsamer Projekte durchgeführt. Aktuelle Beispiele dieser gemeinsamen Arbeiten sind in diesem Bericht dokumentiert. Die Abteilung Simulation und Charakterisierung gehörte zu den treibenden Kräften, die den ScienceCampus GraFOx etablierten, und ist dort mit vier Doktorand*innen und einem PostDoc vertreten. Der ScienceCampus bietet neue Möglichkeiten für die Abteilung, vor allem den Zugang zu aktueller ab-initio-Theorie und zu Charakterisierungstechniken, die am Institut nicht zur Verfügung stehen. Die Abteilung initiierte und leitet ein Projekt zur adaptiven Elektronik im Rahmen des "Leibniz-Wettbewerbs", an dem drei Abteilungen des Instituts beteiligt sind.*

Die Bereitstellung von Substraten für das epitaktische Wachstum von im IKZ gewachsenen Kristallen ist ein wesentlicher Auftrag des IKZ. In den meisten Fällen erfordert die Oberflächenvorbereitung neuer Materialien eine wissenschaftlich fundierte Entwicklung. Die am IKZ vorhandenen Charakterisierungstechniken, die von der optischen Mikroskopie, die Rasterkraftmikroskopie, über die Röntgen-Topographie bis zur Elektronenmikroskopie im atomaren Maßstab reichen, liegen jenseits dessen was bei kommerziellen Anbietern verfügbar ist. Diese Möglichkeiten werden genutzt, um die gesamte Kette vom Volumenwachstum bis zum epitaktischen Wachstum am Institut zu schließen und für das Instituts und unsere Partner aus Forschung und Industrie Oberflächen so zu präparieren, dass sie für die Epitaxie geeignet sind. Jenseits von Service und Forschung leistet die Abteilung einen beträchtlichen Beitrag zur Ausbildung junger Wissenschaftler und Wissenschaftlerinnen am Institut. Dazu gehören die Unterweisung in grundlegenden Charakterisierungstechniken, Vorlesungen an der Humboldt-Universität, sowie die Betreuung von Bachelor-, Master- und Doktorarbeiten. Die Abteilung arbeitet in internationalen Projekten zur gemeinsamen Betreuung von Doktoranden und Doktorandinnen mit Partnern in Frankreich, Polen und China.

The department Simulation and Characterization has the following main tasks:

1. Scientific service for the institute and external partners
2. Fundamental and applied materials research in the field of crystalline materials
3. Development and adaption of scientific methods for characterization of materials grown at the institute
4. Development of surface preparation techniques

A substantial share of our efforts is devoted to support of crystal growth groups from the other IKZ departments. This includes routine characterization of electrical, optical and structural properties, the preparation of seed crystals, which requires typically crystallographic orientation by X-ray diffraction as well as cutting and surface preparation. The comprehensive ensemble of characterization techniques and the expertise of the researchers and technicians in the department guarantee quick and educated feedback for the growers and thus fast progress in crystal growth activities. An excellent example for these activities are the establishment of phothermal ionisation spectroscopy to measure the residual impurities in germanium cyrstals that are supposed to be used as detectors for the double β-decay (GERDA project). The scientific expertise is also requested from industrial partners like OSRAM OS, Freiberger Compound Materials (FCM), and other national and international partners.

The comprehensive characterization techniques ranging from macroscopic to the atomic scale, as well as the profound knowledge in atomic and extended defects, in the analysis of growth and relaxation processes and simulation techniques offers unique opportunities to perform fundamental research on the materials grown in the institute. In the last years the focus in the field of fundamental research was on wide band gap semiconductors and oxides, e.g. AlN and group III sesquioxides. This work is performed across the departments in some cases also in the framework of common projects. Some recent good examples of this collaborative work are documented in this report. The department Simulation and Characterization was among the driving forces that established the ScienceCampus GraFOx, were four of its PhD students and one of its PostDoc are working. The ScienceCampus offers new opportunities for the department, especially access to latest ab-initio theory and characterization techniques that are not available at the institute. The department initiated and leads a project on adaptive electronics in the framework of the "Leibniz-Wettbewerb" that joins activities in three departments across the institute.

Preparing substrates that are ready for epitaxial growth from the unqiue crystal grown at IKZ is at the heart of IKZs missions. In most cases surface preparation of novel matreilas requires a scientifically based development. The characterization techniques at IKZ that range from optical microscopy, AFM, over X-ray topography to electron microscopy at the atomic scale are far beyond that what is available in industry. These opportunities are used to close the gap between bulk crystal growth and epitaxial growth at the institute and to offer epiready surfaces within the institute and to our academic and industrial partners. Beyond service and research, the department contributes to a sizeable amount to the education of young researchers at the institute. This comprises introduction into basic characterization techniques, lectures at Humboldt-University, and the advising of Bachelor, Master and PhD theses. The department is engaged in international education projects with partners in France, Poland and China.

Simulation & Characterization:
Physical Characterization

Head Dr. Klaus Irmscher
Team K. Banse, A. Fiedler, A. Kwasniewski, M. Naumann, M. Pietsch, Dr. habil. M. Schmidbauer

Überblick

Die Gruppe Physikalische Charakterisierung beschäftigt sich hauptsächlich mit der Untersuchung der im IKZ gezüchteten Volumenkristalle und epitaktischen Schichten mittels Röntgenbeugung, optischer Spektroskopie und Bildgebung, elektrischer Messungen sowie verwandter Techniken. Einerseits liefern die Ergebnisse dieser Messungen die erforderliche Rückinformation an die Kristallzüchter, um die Züchtungsprozesse zu optimieren. Andererseits können interessante physikalische Effekte, die von grundlegendem oder anwenungsspezifischem Interesse sind, nachgewiesen werden.

Im Berichtszeitraum ist vor allem die elektrische Charakterisierung der β-Ga_2O_3 Schichten, die in der Gruppe Halbleitende Oxidschichten mittels metallorganischer Gasphasenepitaxie gewachsen werden, hervorzuheben. Die entsprechenden Messungen (Hall-Effekt, C-V, DLTS, Raman-Spektroskopie) sind Bestandteil einer laufenden Doktorarbeit und haben wesentlich zur Optimierung der Wachstumsbedingungen beigetragen. Seit Mitte 2016 werden diese Arbeiten auch im Rahmen des Leibniz-Wissenschaftscampus GraFOx durchgeführt. Eine weitere Schwerpunktaufgabe unserer Gruppe ist die Charakterisierung ferroelektrischer Oxidschichten mittels Röntgenbeugung in Zusammenarbeit mit der Gruppe Ferroelektrische Oxidschichten. Die Doktoranden und Masterstudenten dieser Gruppe erfahren eine intensive Betreuung bei der Durchführung und Auswertung der umfangreichen Röntgenbeugungsexperimente im Rahmen ihrer Qualifikationsarbeiten. Diese Arbeiten haben wesentlich zum Verständnis der Domänenstruktur in verspannten Oxidschichten beigetragen. In diesem Zusammenhang seien die Röntgenbeugungsexperimente an der European Synchrotron Radiation Facility (ESRF) erwähnt, die nur mit genehmigten Experimentanträgen möglich sind.

Viele wichtige Resultate werden in den Einzelberichten der jeweiligen Züchtungsgruppen beschrieben. Im vorliegenden Bericht konzentrieren wir uns auf zwei ausgewählte Themen unserer Arbeit. (i) Ferroelektrische Domänen in verspannten $K_{0.75}Na_{0.25}NbO_3$ Epitaxieschichten wurden mittels Nanofokus-Röntgenbeugung an einem entsprechenden Messplatz der European Synchrotron Radiation Facility (ESRF) untersucht. Diese hochentwickelte Röntgenmethode vereint hohe Empfindlichkeit bei der Messung der Gitterverzerrung mit hoher räumlicher Auflösung im Bereich von 100 nm. Dadurch konnten wir zwei im sub-Mikrometerbereich koexistierende Domänenvarianten unabhängig voneinander messen und deren unterschiedliche Verzerrungszustände verifizieren. (ii) Der Paramagnetismus und die Lumineszenz Chrom dotierter, elektrisch isolierender β-Ga_2O_3 Kristalle sind seit längerem bekannt. Die in unserem Institut betriebene Czochralski-Züchtung von β-Ga_2O_3 Einkristallen erlaubt neben der Dotierung mit Cr zusätzlich eine Dotierung mit Si oder Sn, so dass elektrisch leitfähige Kristalle gezüchtet werden können. Solche Kristalle könnten die Grundlage für elektronische Bauelemente sein, die die Steuerung von Magnetismus und Lumineszenz ermöglichen. Hier berichten wir über die an diesen Kristallen beobachtete Elektrolumineszenz.

Overview

The group Physical Characterization is mainly concerned with investigations of bulk crystals and epitaxial layers grown at IKZ using x-ray diffraction, optical spectroscopy and imaging, electrical measurements, and related techniques. On one hand, the results of these measurements provide necessary feedback to the crystal growers for optimizing the growth processes. On the other hand, interesting physical effects in these crystals may be revealed being of basic as well as application specific interest.

In the reporting period, the electrical characterization of the β-Ga_2O_3 layers, which are grown in the group Semiconducting Oxide Layers by means of organometallic vapor phase epitaxy, is particularly noteworthy. The corresponding measurements (Hall effect, C-V, DLTS, Raman spectroscopy) are part of an ongoing doctoral thesis and have contributed significantly to the optimization of the growth conditions. Since mid-2016, this work has also been carried out within the framework of the Leibniz Science Campus GraFOx. A further focus of our group is the characterization of ferroelectric oxide layers by means of x-ray diffraction in cooperation with the group Ferroelectric Oxide Layers. The doctoral students and master students of this group are given intensive supervision during the execution and evaluation of the extensive x-ray diffraction experiments as part of their qualification work. This work has contributed significantly to understanding the domain structure in strained oxide layers. In this context, the x-ray diffraction experiments at the European Synchrotron Radiation Facility (ESRF) are mentioned, which are only possible with approved experiment applications.

Many important results are communicated in the individual reports of the respective crystal growth groups. In the present report, we focus on two selected topics of our work. (i) Ferroelectric domains in strained $K_{0.75}Na_{0.25}NbO_3$ epitaxial layers were investigated by nanofocus x-ray diffraction at a customized experimental station of the European Synchrotron Radiation Facility (ESRF). This advanced x-ray method combines high strain sensitivity with high spatial resolution on the scale of 100 nm. Thus, we were able to measure independently two domain variants coexisting in the submicron range and to verify their different strain states. (ii) Paramagnetism and luminescence of chromium doped, electrically insulating β-Ga_2O_3 crystals have been known for quite some time. At our institute β-Ga_2O_3 single crystals are grown by the Czochralski method allowing besides the doping with Cr an additional doping with Si or Sn. Hence, electrically conductive, Cr doped crystals are available. Such crystals could be the basis for electronic devices making possible the control of magnetism and luminescence. Here we report on the observation of electroluminescence in these crystals.

Results

Scanning x-ray nanodiffraction from ferroelectric domains in strained $K_{0.75}Na_{0.25}NbO_3$ epitaxial layers

In a previous study [1] we could prove the emergence of an inclined monoclinic ferroelectric phase in $K_{0.75}Na_{0.25}NbO_3$ strained thin films which is associated with both a strong vertical and horizontal electrical polarization component (see annual report 2014). The phase formation is accompanied by the evolution of a one-dimensional periodic domain pattern which extends over several tens of micrometers. However, besides this prominent domain pattern which is aligned along the lateral $[-112]_{TS0}$ direction of the $TbScO_3$ (TS0) orthorhombic substrate – and which we refer to as the '0° variant' – a structural variant of a 90° rotated domain pattern is also observed. Here, the pseudocubic (pc) unit cells of the epitaxial layer are rotated in-plane by 90° leading to a corresponding rotation of the one-dimensional domain pattern, which is now aligned along $[1-12]_{TS0}$. Exemplarily, a lateral piezoresponse force micrograph (PFM) of a 23 nm $K_{0.75}Na_{0.25}NbO_3$ thin film grown on (110) $TbScO_3$ is shown in Fig.1a.

For the 90° configuration the elastic strain energy density is slightly enhanced compared to the 0° configuration leading to a remarkably reduced probability of appearance. The observed energy difference can be attributed to the elastic anisotropy of the epitaxial layer, which is also reflected in a different vertical lattice parameter for each domain variant: our calculations predict a slightly larger vertical lattice parameter for the 90° variant by about $(\Delta d/d)_z = 2.4\times10^{-4}$. Since macroscopic ferroelectric properties are strongly correlated to the incorporated lattice strain, the emergence of either one or two phases may change drastically the film ferroelectric properties on a nanoscale (e.g. temperature or broadness of a phase transition). With this regard as well as for a fundamental understanding, it is highly desirable to verify experimentally the different strain states of the two domain variants.

High-resolution x-ray diffraction is a powerful tool in order to investigate strain, surface orientation and monoclinic distortion on the nanoscopic length scale. However, in a conventional x-ray scattering experiment the footprint of the illuminating x-ray beam on the sample is typically in the regime of a few millimeters leading to incoherent averaging. Here, we report on an advanced x-ray diffraction experiment using a nano-sized x-ray beam where high strain sensitivity is combined with spatial resolution in the 100 nm regime. With such a small beam both domain variants could be independently identified and analyzed. In particular, the theoretical prediction of a different vertical lattice spacing could be verified and evaluated.

The nanofocus x-ray diffraction experiment was performed at the ID01 experimental station of the European Synchrotron Radiation Facility (ESRF). A 300 µm diameter gold Fresnel zone plate (FZP) with an outermost zone width of 70 nm was used to focus the x-ray beam (8 keV) to about 150 nm (h) × 90 nm (v) spot size at the sample position. The sample was mounted on an x-y-z scanning piezoelectric stage with a resolution of 2 nm in all three directions. The combined use of the FZP together with a fast area detector principally allows for (i) three-dimensional reciprocal space mapping at a selected fixed position in real space and (ii) scanning x-ray nanodiffraction at a selected fixed position in reciprocal space with a spatial resolution which is comparable to the focal size of the primary x-ray beam.

Simulation & Characterization: **Physical Characterization**

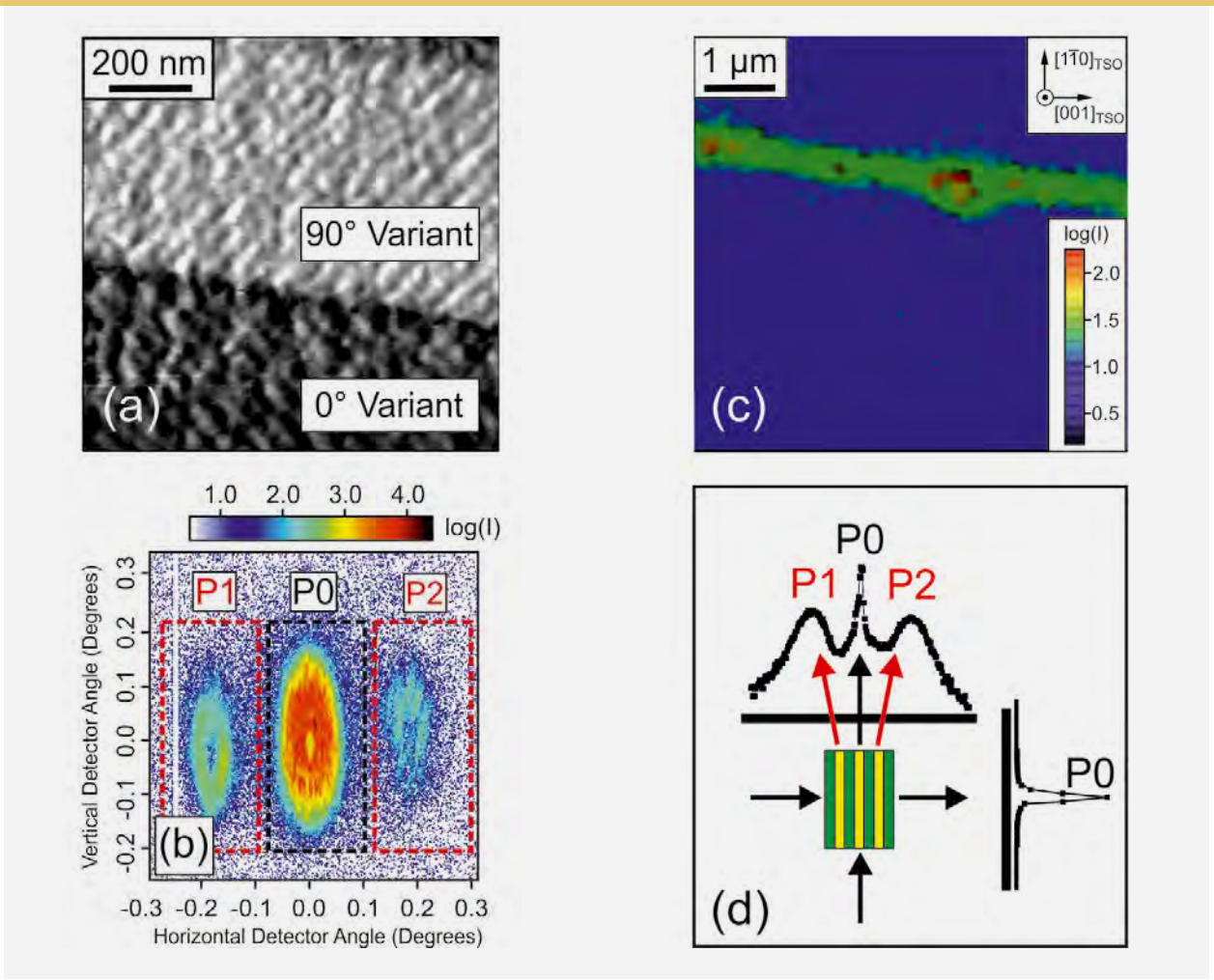

Fig. 1
(a) Lateral PFM image of a 23 nm $K_{0.75}Na_{0.25}NbO_3$ strained thin film grown on (110) $TbScO_3$ substrate,
(b) detector frame accumulated at $(113)_{pc}$ Bragg reflection,
(c) integrated intensity of P1 on different sample positions,
(d) scheme of scattering geometry.

Fig. 1b displays the diffracted intensity distribution in the vicinity of the $(113)_{pc}$ film Bragg reflection at a selected position on the sample. Nearby a strong central scattering feature P0, which we assign to the crystal truncation rod (CTR), two weak satellite peaks P1 and P2 are observed which are caused by the lateral domain periodicity. The integrated intensities of P1 and P2 were analyzed as a function of the position of the x-ray spot on the sample (exemplarily shown for P1 in Fig. 1c). Two different regions can be distinguished. Inside the needle-shaped region the intensities of P1 and P2 are strong whereas they vanish in the surrounding region. In the present scattering geometry the direction of the incident x-ray beam is chosen parallel to the domain walls of the 90° variant while it is perpendicular to the domain walls of the 0° variant (see scheme in Fig. 1d). Therefore, the needle-shaped region can be assigned to the 90° domain variant whereas the surrounding matrix consists of the 0° domain variant.

Also images recorded at the central CTR exhibit local differences in the contrast (Fig. 2a) although being substantially weaker than for the images taken at the satellite peaks. More interestingly, the CTR intensity maximum of the 90° domain variant appears at a slightly smaller Q_z-value than that of the 0° variant. This effect has been checked for a variety of different Bragg reflections and is exemplarily shown for the $(113)_{pc}$ and $(-113)_{pc}$ thin film Bragg reflections in Figs. 2b and 2c, respectively. The peak shift proves an enlarged vertical lattice parameter for the 90° domain variant as compared to the 0° domain variant in agreement with calculations based on linear elasticity theory. However, the experimental value $(\Delta d/d)_z = (6 \pm 1)\times10^{-4}$ is larger than the calculated value $(\Delta d/d)_z = 2.4\times10^{-4}$. The reason for this deviation is not understood in detail yet. It could be caused by local strain relaxation induced by the finite domain sizes and by defects, which both have not been taken into account in the elastic calculations. Nevertheless, our results demonstrate that linear elasticity theory is – at least – qualitatively suitable for a correct prediction of the surface unit cell orientation and consecutive strain field in the $K_{0.75}Na_{0.25}NbO_3$ epitaxial layers.

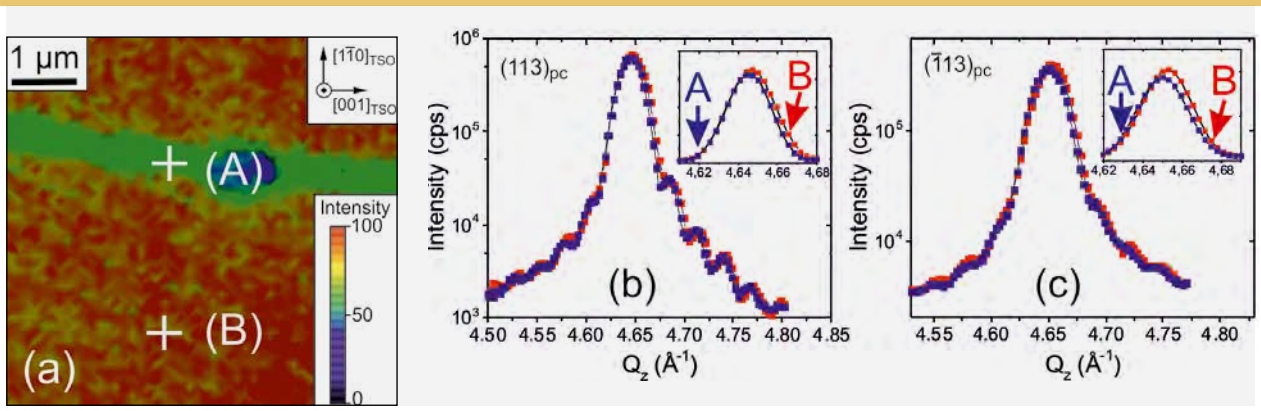

Fig. 2
(a) Integrated intensity map of the $(113)_{pc}$ CTR measured at Q_z = 4.65 Å^{-1} and
(b) corresponding integrated intensity as a function of Q_z measured at sample positions A (blue symbols) and B (red symbols)
(c) corresponding integrated intensity as a function of Q_z in the vicinity of $(-113)_{pc}$. The insets in (b) and (c) are zooms of the Bragg peaks on a linear intensity scale.

The enhanced vertical strain in the 90° variant may influence macroscopic ferroelectric properties. For example, in $SrTiO_3$ a lattice strain of about 6×10^{-4} would lead to an increase of the Curie temperature of about $\Delta T_C \approx 14$ K [2]. Based on this value a remarkable difference of T_C between the 0° and 90° domain variant could be expected. Corresponding temperature dependent investigation of ferroelectric phase transitions are planned for the future.

The present results have been achieved in close collaboration with the group Ferroelectric Oxide Layers and have been published [3]. We are grateful to S. Leake and T. Schülli, for assistance with the xray diffraction experiment at ESRF (MA-2851).

Photo- and electroluminescence of chromium doped β-Ga_2O_3 single crystals grown by the Czochralski method

Among the transparent semiconducting oxides, β-Ga_2O_3 is one of the most promising for optoelectronics and power electronics due to its large band gap of about 4.8 eV and the resultant high break down field of 8 MV/cm. The large band gap also suggests using β-Ga_2O_3 as a host material for optical active impurities in solid-state lasers. This diversity in applications is the reason that several groups worldwide have intensified research on this material. At our institute, we contribute to these studies by the growth of β-Ga_2O_3 bulk crystals using the Czochralski method in the group Oxides/Fluorides combined with electrical and optical investigations in the group Physical Characterization. Doping by foreign atoms usually plays a crucial role in obtaining certain functional properties. Here we report on the optical properties of Cr doped β-Ga_2O_3.

While undoped crystals are fully transparent to visible light, the chromium doping produces a greenish coloration of the crystal, which results from two broad absorption bands centered at wavelengths of about 424 nm and 597 nm, respectively. Similar absorption bands are well know from Al_2O_3:Cr (ruby) and assigned to Cr^{3+} on Al site, which is octahedrally coordinated. This suggests that Cr prefers the octahedral Ga site occupation in the Cr^{3+} oxidation state in β-Ga_2O_3:Cr crystals instead of occupying the other possible, tetrahedral Ga site. Since Ga is also in the +3 oxidation state, Cr^{3+} is electrically neutral with respect to the β-Ga_2O_3 crystal lattice. In analogy to ruby, we also see the characteristic red photoluminescence (PL) due to an intra-center transition of Cr^{3+} already reported in 1965 [4] and recently reinvestigated in more detail [5]. Figure 3 shows a term diagram that explains the origins of the PL. The crystal field (CF) in ruby and β-Ga_2O_3:Cr is predominantly octahedral which can be described by a strong cubic CF component. While in Al_2O_3:Cr a trigonal CF distortion has to be taken into account, in β-Ga_2O_3:Cr the CF distortion is monoclinic. However, this monoclinic distortion hardly deviates from a trigonal one and we may approximately apply the splitting scheme of Cr^{3+} in Al_2O_3. The cubic CF splits up the orbital states of the free ion in such a way that the orbital singlet $^4A_2$ is lowest in energy followed by a doublet ^2E. The trigonal CF distortion lifts the spin degeneracy of the $^4A_2$ term yielding two Kramers doublets of small separation (~ 50 µeV, not resolved in our luminescence spectra), while the combined action of the trigonal CF component and spin-orbit interaction splits the ^2E term into two Kramers doublets of larger separation (~ 5 meV). The excitation of the photoluminescence takes place via absorption transitions from the split $^4A_2$ ground state to the excited triplet manifolds $^4T_2$ (^4F), $^4T_1$ (^4F), and $^4T_1$ (^4P) (in Fig. 3: green, blue, and violet arrows, respectively). The Kramers doublets R_1 and R_2, which originate from the ^2E doublet, get populated due to partial thermalization and the transitions from them to the ground state are the origin of the zero-phonon lines of the red PL.

Simulation & Characterization: **Physical Characterization**

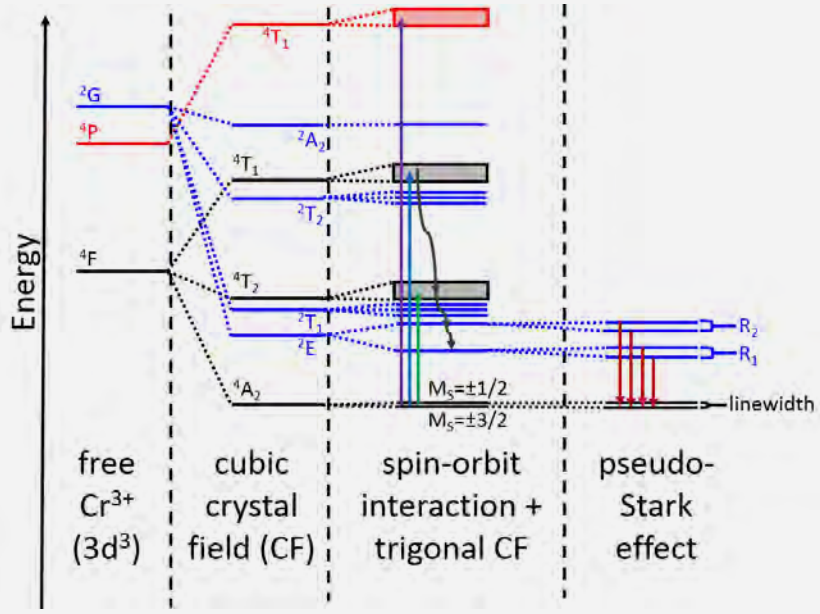

Fig. 3
Term diagram showing the energy level splitting of the Cr^{3+} ion under the successive action of a cubic (octahedral) crystal field, of a trigonal crystal field component combined with spin-orbit interaction, and of an external electric field leading to the pseudo-Stark effect.

The PL lines of ruby, R_1 at 694.3 nm and R_2 at 692.0 nm, are shifted in β-Ga_2O_3:Cr to 695.6 nm and 688.7 nm, respectively. Accordingly, the splitting due to the trigonal CF and spin-orbit interaction is larger in β-Ga_2O_3:Cr. For the lifetime of the R_1 luminescence we have measured 160 µs at room temperature. Although this is about an order of magnitude lower than in ruby, the lifetime should be long enough to generate a population inversion, which is necessary for laser applications.

In contrast to electrically insulating ruby, β-Ga_2O_3 crystals can be doped *n*-type. Without intentional doping the crystals grown at our institute are *n*-type conductive with donor concentrations in the 10^{17} cm^{-3} range due to Si impurities originating from the source powder. Intentional Cr doping of the crystals during growth to concentration levels not exceeding 10^{19} cm^{-3} preserves the *n*-type conductivity. Therefore, we have been able to prepare Schottky diodes by depositing Ni contacts on cleaved (100) surfaces of β-Ga_2O_3 samples.

Figure 4(a) displays a scheme of the test structure and the circuitry used in our experiments. Under reverse bias the Schottky diodes exhibit an intense red electroluminescence (EL) visible to the bare eye as shown in Fig. 4(b). To our knowledge, this is the first report of such an observation. In Figure 4(c) we compare PL with EL measured at low temperature (4 K) in the spectral range of the R_1 PL line. Although the EL consists of two lines which obviously are due to a splitting of the R_1 line, the origin of the red electroluminescence must be assigned to intra-center transitions of Cr^{3+} too. The most probable explanation for the EL excitation process is impact by electrons accelerated in the electric field of the Schottky diode's space charge layer. This view is corroborated by the correlation of the EL intensity with the reverse current. The R_1 and R_2 lines both split up by the same energy quantity, whereby the observation of the R_2 doublet has been restricted to temperatures below 150 K for intensity reasons.

Fig. 4
(a) Scheme of the circuit to generate electroluminescence. Nickel forms a Schottky diode on β-Ga_2O_3, which is reverse biased. (b) Photographic image of the electroluminescence at room temperature. (c) Spectrum of the photo- (PL) and electroluminescence (EL) at 4.2 K.

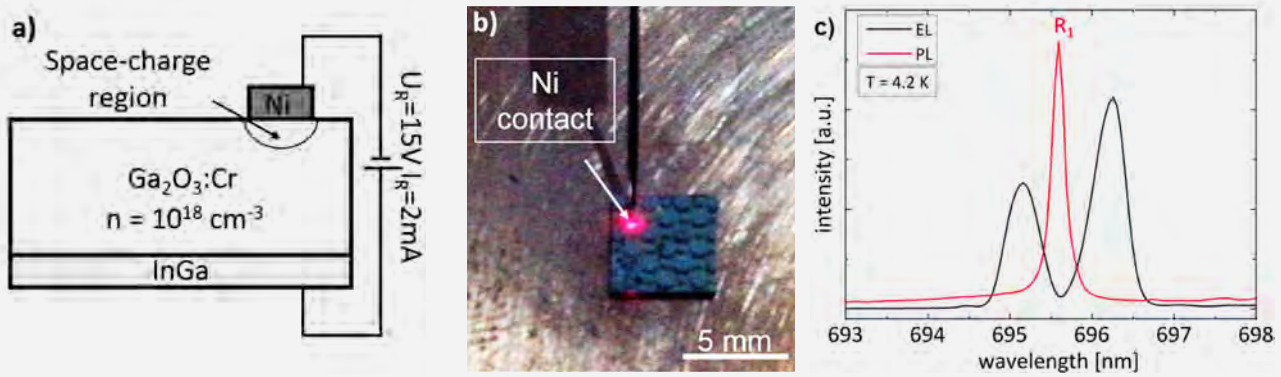

An explanation of the line splitting by the well-known Stark effect due to the diode's internal electric field is not possible, since an electric field cannot lift a Kramers degeneracy. Therefore, we need here a more sophisticated explanation by the so-called pseudo-Stark effect as developed in Ref. [6] for Al_2O_3:Cr. In β-Ga_2O_3:Cr the octahedral Cr sites are also of two kinds which can be transformed into each other only by including an inversion. Hence, the odd-parity crystal field at the site of the first kind differs by the sign from that at the site of the second kind, but energetically they are equivalent. With the superposition of an external electric field the energy equivalence is removed and the energy levels at sites of one kind shift in opposite direction to those at sites of the other kind. This is the pseudo-Stark effect we observe (Fig. 3, right hand side). The R_1 line at 695.6 nm splits into two lines at 695.2 nm and 696.3 nm, respectivly, under an electric field of approximately (1.5 – 2.5)×10^6 V/cm corresponding to the diode's electric field under the applied doping and biasing conditions. The beat frequency of these two transitions is 0.7 THz, which is in the so-called terahertz gap. This might be used for a liquid nitrogen cooled terahertz laser.

References

[1] J. Schwarzkopf, D. Braun, M. Hanke, A. Kwasniewski, J. Sellmann, M. Schmidbauer; J. Appl. Cryst. 49 (2016) 375

[2] J. H. Haeni et al.; Nature 430 (2004) 758

[3] M. Schmidbauer, M. Hanke, A. Kwasniewski, D. Braun, L. von Helden, C. Feldt, S. J. Leake, J. Schwarzkopf; J. Appl. Cryst. 50 (2017) 519

[4] H. H. Tippins; Phys Rev.137 (1965) 865

[5] Y. Tokida and S. Adachi; J. Appl. Phys. 112 (2012) 063522

[6] W. Kaiser, S. Sugano, D. L. Wood; Phys. Rev. Lett. 6 (1961) 605

Simulation & Characterization: Electron Microscopy

Head Dr. Martin Albrecht
Team M. Anikeeva, K. Banse, Dr. T. Markurt, St. Mohn, J. Moneta, T. Remmele, R. Schewski, Dr. T. Schulz, N. Stolyarchuk, C. Wouters

Überblick

Die Arbeitsgruppe Elektronenmikroskopie charakterisiert kristalline Materialien mit elektronenmikroskopischen Methoden sowohl im Rahmen des wissenschaftlichen Service als auch im Bereich der Grundlagenforschung. Thematischer Schwerpunkt ist der Zusammenhang zwischen physikalischen Eigenschaften und Struktur von Halbleitern. Die Methoden reichen von der Rasterelektronenmikroskopie (energie- und wellenlängendispersive Röntgenspektroskopie, Elektronenrückstreubeugung (EBSD), Kathodolumineszenz) über die Ionenstrahlbearbeitung bis zur Transmissionselektronenmikroskopie (aberrationskorrigierte Transmissionselektronen-mikroskopie und Rastertransmissionselektronenmikroskopie mit atomarer Auflösung). Die Gruppe arbeitet eng mit Gruppen des Kristallwachstums, der ab-initio Modellierung und der Simulation zusammen. Neben der Standardcharakterisierung von Oberflächen und Zusammensetzung, Phasenanalyse und Analyse von Einschlüssen werden insbesondere grundlegende Arbeiten zu Wachstums- und Relaxationsprozessen epitaktischer Schichten sowie zu Kristalldefekten durchgeführt. Um bildgebende Verfahren zu verbessern und sie auf die spezifischen Probleme und die laufenden Arbeiten am Institut anzupassen, werden eigenständige methodische Arbeiten durchgeführt. Die Gruppe arbeitet in nationalen und internationalen Forschungsprojekten und Forschungsverbünden und ist maßgeblich am Leibniz-ScienceCampus beteiligt, der im Abschnitt „Highlights“ genauer beschreiben wird. 2016 waren 5 Doktorandinnen und Doktoranden an den Forschungsaktivitäten der Arbeitsgruppe beteiligt. Das Projekt SPRInG, das von der Europäischen Unio im Rahmen des Marie-Curie-Sklodowska Programms „European Integrated Doctorate“ gefördert wird, hat zum Ziel Studierende zu gleichen Teilen in Industrie und akademischer Forschung auszubilden. Im Rahmen des französischen Exzellenz-Netzwerks GaNEX, wird Natalia Stolyarchuk ihre Promotion in einem gemeinsamen Verfahren der Humboldt-Universität zu Berlin und der Universität Nizza erhalten.

Da einige der Ergebnisse der Elektronenmikroskopie in den Berichten der Arbeitsgruppen der Kristallzüchtung vertreten sind, sollen im Folgenden einige ausgewählte Themen unserer derzeitigen Arbeit dargestellt werden, die zusammen mit der Arbeitsgruppe „Oxide und Fluoride“ und externen Partnern im Rahmen von gemeinsamen Forschungsprojekten. Es handelt sich dabei um Arbeiten (i) zur Analyse des Einbaus von Ce in $CaSc_2O_4$, (ii) der Kontrolle der N Polarität beim Wachstum von GaN auf Saphir, (iii) der Begrenzung des In-Einbaus beim Wachstum von InGaN, und (iv) der Struktur von GaN Schichten, die mit der gepulsten Sputterabscheidung hergestellt werden. Die Arbeiten in (i) wurden zusammen mit der Arbeitsgruppe „Oxide und Fluoride“ am IKZ, in (ii) miit CHREA-CNRS in Valbonne, im Rahmen von GaNEX, in (iii) zusammen mit dem Max-Planck-Institut für Eisenforschung in Düsseldorf, der Universität Peking, dem Institut für Hochdruckphysik der polnischen Akademie der Wissenschaften, sowie dem Paul-Drude Institut in Berlin im Rahmen des EU-Projket SPRInG und in (iv) in Kooperation mit der TU Braunschweig, der Universität Magdeburg und OSRAM OS in Regensburg im Rahmen des BMBF-Projketes PlaNB durchgeführt.

Overview

The electron microscopy group performs scientific service and basic research in the field of characterization of crystalline material by means of electron microscopy. Main focus is the relation between physical properties and structure. The methods cover the whole field ranging from scanning electron microscopy, i.e. energy and wavelength dispersive spectroscopy, electron backscatter diffraction, cathodoluminescence through transmission electron microscopy, i.e. aberration corrected transmission electron microscopy and scanning transmission electron microscopy with atomic resolution. The team works in close collaboration with groups performing crystal growth, as well as ab-initio modelling and simulation. Standard characterization of surfaces and composition, phase analysis and analysis of inclusions are performed as well as basic analyses of growth and relaxation mechanisms and of defects. Besides this, methodological work is done to improve electron optical imaging techniques and to adopt them to the specific problems at the institute. The group works in collaborative national and international research projects and is significantly involved in the Leibniz ScienceCampus, whose activities are described in more detail in the Highlight section of this report.

Simulation & Characterization: **Electron Microscopy**

In 2016, five PhD students have been involved in our research activities. Especially the project SPRInG, funded by EU as Marie Curie Innovative Training Network, aims at a joint training of students in research and industry. In addition, in the frame of the French GaNEX network, Natalia Stolyarchuk will be jointly promoted by Humboldt-Universität zu Berlin and University of Nizza, France.

Since some of the results are described in the individual reports of the groups working in crystal growth, the following chapter will highlight some selected topics of our current work, which have been performed with the group "Oxides and Fluorides" and external partners in the framework of joint projects. We will present results on: (i) a site specific analysis of Ce incorporation into $CaSc_2O_4$ by transmission electron microscopy; (ii) the control of N-polarity in the growth of GaN on sapphire; (iii) limitations in In incorporation into InGaN and (iv) the structure of GaN deposited by pulsed sputter deposition. The work in (i) is an internal cooperation with the group Oxides and Fluoridies, (ii) has been performed with CRHEA-CNRS in France within the GaNEX-project, (iii) in cooperation with the Max-Planck-Institut für Eisenforschung (MPIE) in Düsseldorf, Germany, Peking University in China, the institute of High-Pressure Physics (UNIPRESS) in Warsaw Poland, and the Pauls-Drude-Institut in Berlin, in the framework of the EU project SPRInG and (vi) in cooperation with TU Braunschweig, University of Magdeburg and OSRAM Optical Semicondcutors in Regensburg in the framework of the project PlaNB, funded by the Federal Ministry of Education and Research.

Results

Site specific analysis of Ce incorporation into $CaSc_2O_4$ by transmission electron microscopy

Cerium doped wide bandgap crystals like Ce:$CaSc_2O_4$ and their applications such as e.g. solid state lasers and phosphors for light conversion e.g. in LEDs have attracted much attention in the past decade [1-6]. Next to the tunability of the optical properties [1,2,4] and the broad range of possible emission wavelength [7], a major advantage of Ce doped crystals is the direct emission in the UV – green spectral range without the need of second harmonic generation [6]. Absorption and emission of wide band gap crystals doped with Ce originates from transitions of loosely bound electron between the 4f- and 5d-levels of Ce. While the energetical position of the Ce 4f-level (ground state of the optical transition) is rather unaffected by the crystallographic surrounding of the Ce dopants, the larger radial extension of the Ce 5d-orbital, the energetical position as well as the width of the Ce 5d-level – the excited state of the optical transition – strongly depend on the host crystal lattice structure and the actual lattice site occupied by Ce dopants. In this context $CaSc_2O_4$ is an interesting materials system. Ce dopants can, according to theory, be incorporated either into the eight-fold coordinated Ca^{2+} or the six-fold coordinated Sc^{3+} lattice site (see Fig. 1b) depending on the oxygen partial pressure during growth [8]. In order to verify this assumption we performed TEM investigations of Ce doped $CaSc_2O_4$ crystals grown in different atmospheres by the Czochralski and laser heated pedestal growth (LHPG) method in the IKZ. The Ce dopant concentration was in the range between 0.04-0.08 at%.

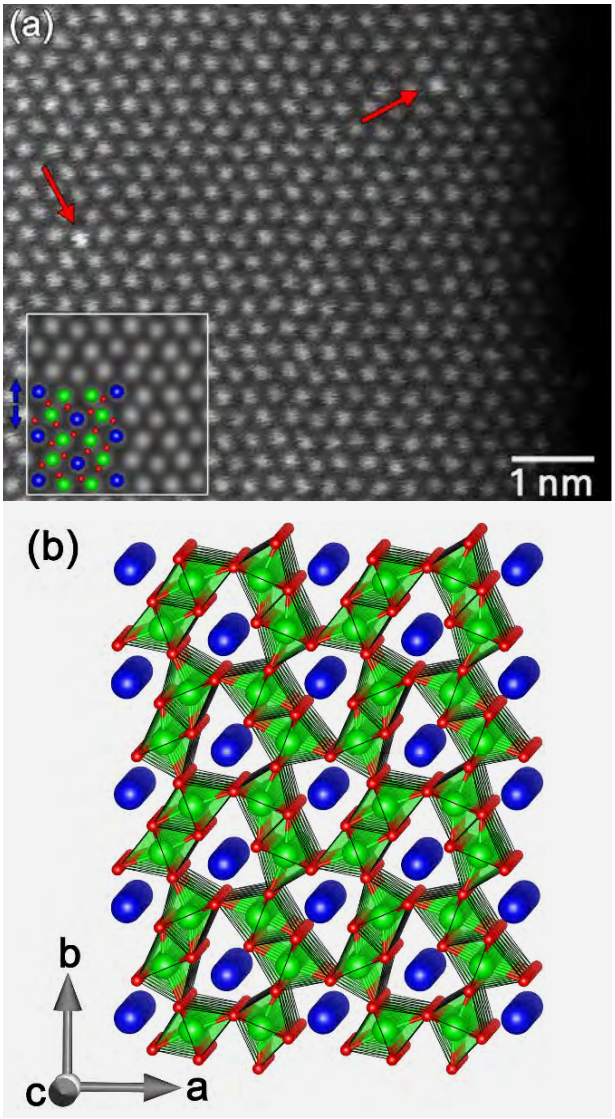

Fig. 1
High resolution STEM Z-contrast image of a cerium doped $CaSc_2O_4$ sample where atomic columns appear bright. Columns with increased intensity contain single Ce atoms and are indictaed by red arrows. The inset shows a STEM image simulation together with a model of the $CaSc_2O_4$ unit cell seen along the [001] direction where blue, green and red balls denote Ca, Sc and O atomic columns, respectively. Blue arrows indicate the displacement of Ca atomic columns from the average position of {010} lattice planes, which lie horizontally in the image. (b) Stick-and-ball model of the $CaSc_2O_4$ lattice structure built of ScO_6 octahedra and Ca ions in channels between them. Colors of the atoms as in (a).

Simulation & Characterization: **Electron Microscopy**

Fig. 1a shows a STEM Z-contrast image of a Ce doped $CaSc_2O_4$ crystal in [001] projection, which allows to observe Ca- and Sc-atomic columns separately (cf. Fig. 1b). Since the difference in the atomic numbers between Ca (Z=20) and Sc (Z=21) is small, the resulting contrast in the experimental image is negligible, making them indistinguishable by means of contrast analysis. Instead, we identified Ca lattice sites by their displacement of 0.5 Å from the average position of respective {010} lattice planes. A careful inspection of the STEM image intensity shows that approximately 2% of individual cation columns exhibit an intensity (marked by red arrows in Fig. 1a) which is significantly higher than the mean intensity of columns in the local vicinity. Since this increased intensity cannot be related to cationic host atoms, we conclude it must be related to incorporation of heavy Ce (Z=58) on cation sites. Comparing the experimental STEM image intensities on a quantitative scale with STEM frozen phonon simulations shows that the intensity increase in fact corresponds to that of an individual Ce dopant incorporated into a host cation column of an approximately 10 nm thick sample. This agreement justifies to use our experimental STEM Z-contrast images to count individual Ce dopants and to determine even their sub-lattice position in the $CaSc_2O_4$ host lattice. Performing a statistical analysis of in total more than 3000 cation columns (approximately 20 x 20 nm² field of view) reveals that more than 90% of the Ce dopants occupy Ca-lattice sites (see histogram in Fig. 2a).

In order to verify this result at the macroscopic scale, we performed ALCHEMI (*Atomic site* location by *channelling* enhanced *microanalysis)* measurements, probing approximately 10^8 cation columns in parallel. This EDX based technique uses the dependency of the generation of characteristic X-ray photons on the tilt of the incident electron beam relative to the sample, to determine the lattice site of dopants in the host matrix [9]. While the measured intensity ratio of Sc-Kα/Ca-Kα X-ray lines (blue circles in Fig. 2b) shows a strong dependency on the tilt angle, the intensity ratio of the Ce-Lα/Ca-Kα characteristic X-ray lines (red squares in Fig. 2b) stays constant within the measurement error. This behavior follows very well the calculated curves (dashed lines in Fig. 2b) which are expected for Ce doped $CaSc_2O_4$ where Ce occupies Ca-lattice sites. This confirms independently the findings of ours STEM HAADF analysis.

Interestingly our result that Ce is incorporated mainly in the Ca-lattice site was found irrespectively whether the $CaSc_2O_4$ crystal was grown in a pure nitrogen atmosphere or in an oxygen/argon mixture, i.e. under nominally either reducing or oxidizing conditions. This result, while in contradiction to the expected dependence of the Ce site occupation on the oxygen partial pressure [8,10], agrees with the outcome of optical measurements of these crystals, which do not show a shift of Ce related luminescence peak [8].

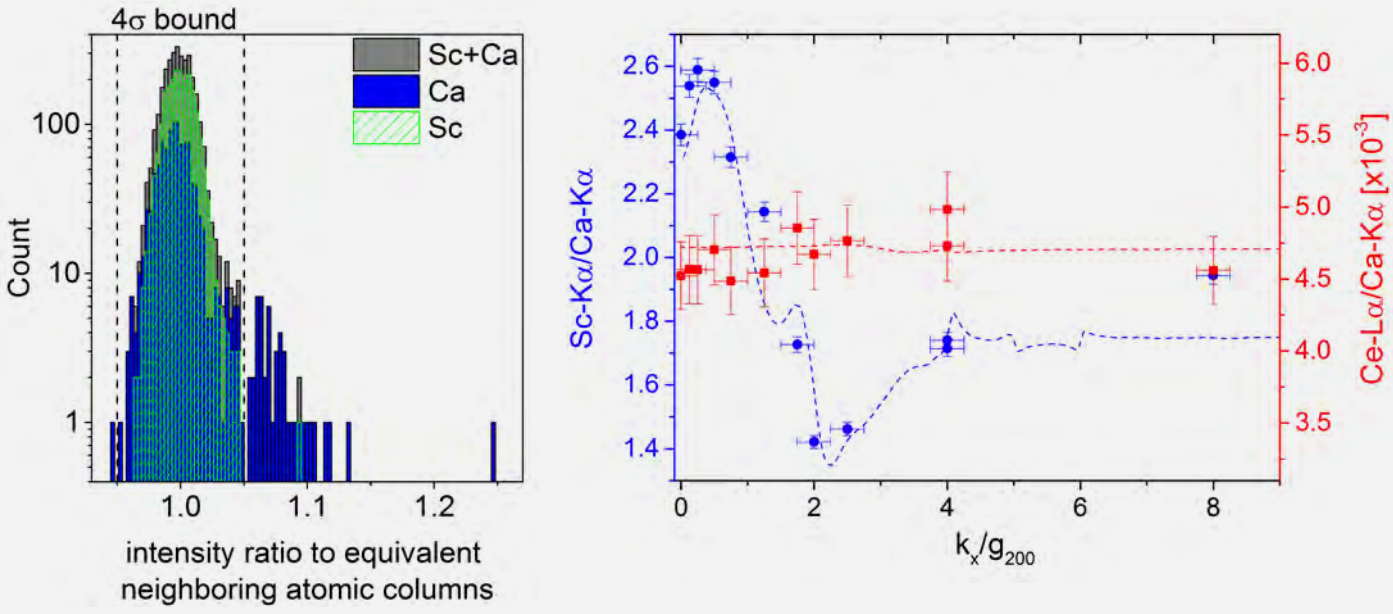

Fig. 2

(a) Histogram of the normalized STEM Z-contrast intensity of atomic columns of the Ca- and Sc-sub-lattice. Events outside of the 4σ bound are considered to be Ce containing columns. (b) ALCHEMI measurement showing the intensity ratio of Sc-Kα/Ca-Kα (blue circles) and Ce/Ca-Kα (red squares) characteristic X-ray lines versus the tilt of the incident electron beam with respect to the (200) planes of the $CaSc_2O_4$ lattice (k_x/g_{200}). Dashed curves denote calculated intensity ratios for the $CaSc_2O_4$ matrix (blue curve) and for Ce dopants incorporated at Ca-lattice sites.

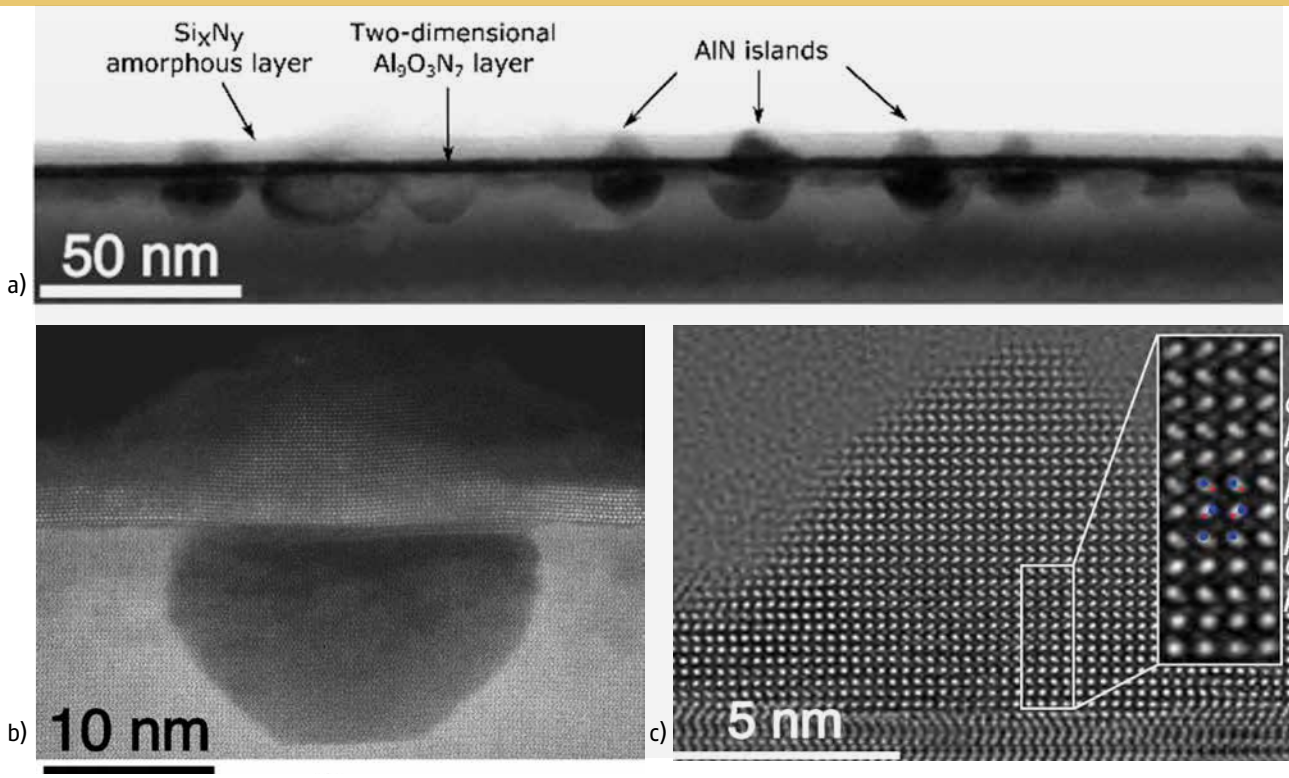

Fig. 3
a) Cross-sectional bright field TEM image [11-20] multibeam condition) of the sapphire surface, nitridated for 30 minutes at 1080 °C. Pyramidal islands are visible on the surface along with the two-dimensional thin layer. Each island is associated with a hexagonally-shaped void in sapphire.
b) Cross-sectional STEM-HAADF image in AlN [11-20] projection of the sample, nitridated for 30 minutes at 1080 °C. A two-dimensional continuous nitridation layer is visible on top of the sapphire surface along with a three-dimensional island of 10 nm in height. The island is situated over a hexagonal shaped void in sapphire, which is characterized by reduced HAADF intensity;
c) High-resolution TEM image of the island along the AlN[11-20] projection. The island has Al-polarity, as it can be seen on the magnified area on the inset (the bright and greyish spots correspond to Al- and N-atomic columns, respectively).

Control of N-polarity in the growth of GaN on sapphire

Most of today's group-III nitride devices are based on metal-polar heteroepitaxial layers grown on nonpolar c-plane sapphire substrates. Compared to their N-polar counterparts, metal polar surfaces exhibit major advantages as lower incorporation of unwanted impurities (e.g. oxygen [11]) and higher surface diffusivity [12], which promotes step-flow growth and improves the structural perfection of the heterostructures [13]. Recently, however, N-polar AlN and GaN heterostructures gained renewed interest due to inherent advantages for device application such as high-frequency transistors [14,15,16] or even for light emitting diodes and laser applications [17].

While the growth of smooth and inversion domain free metal-polar films on sapphire is well established, N-polar films still suffer from a rough surface morphology and the presence of inversion domains with metal polarity (ID) [3,18-20]. Since inversion domains have a negative impact on the electrical properties of the resulting devices, growth recipes allowing to suppress their formation is of major importance.

In our work, performed within a common a project between CNRS-CRHEA and IKZ, in the framework of the French Network of Excellence GaNEx, we study the relation between the processes during nitridation of the sapphire substrate and the microstructure of N-polar AlN films grown by metal organic chemical vapor deposition (MOCVD). More specific, we study the morphology and atomic structure of the films as dependent on nitridation conditions, i.e. duration and temperature, by atomic force microscopy (AFM), high resolution transmission electron microscopy (HR-TEM) and high resolution high-angle annular dark field (HAADF) scanning TEM, which allows to resolve even light oxygen and nitrogen atomic columns and so the polarity of the layers.

Our experimental results show that above substrate temperatures of 850°C a smooth two-dimensional layer of $Al_9O_3N_7$ is formed. This layer promotes the inversion from N polarity at the interface with the sapphire substrate to Al polarity at the top monolayers, as it was discussed in detail in the previous work of our group [21]. However, beyond a critical temperature of 1000°C the surface roughens and in addition to an omnipresent two-dimensional aluminum-oxynitride layer, three-dimensional Al-polar AlN islands are forming. (Fig. 3)

Simulation & Characterization: **Electron Microscopy**

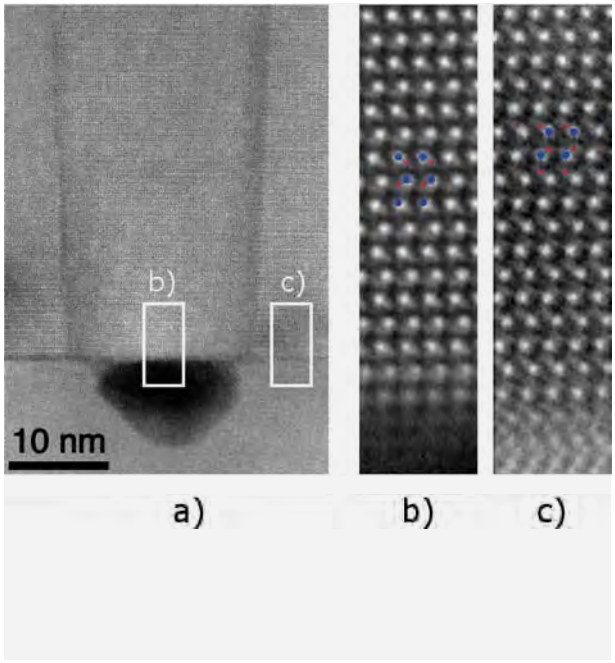

Fig. 4
HAADF-STEM images, along the [11-20] projection, of the AlN layer, grown at 1080°C on sapphire substrate, pre-nitridated for 30 minutes at 1080°C.
a) Columnar inversion domain, situated above the hexagonal void in sapphire.
b) High resolution HAADF-STEM image of the area over the void inside the inversion domain. The layer has Al-polarity, which starts from first monolayer at the interface.
c) High resolution HAADF-STEM image of the area inside the AlN matrix. The layer is N-polar.

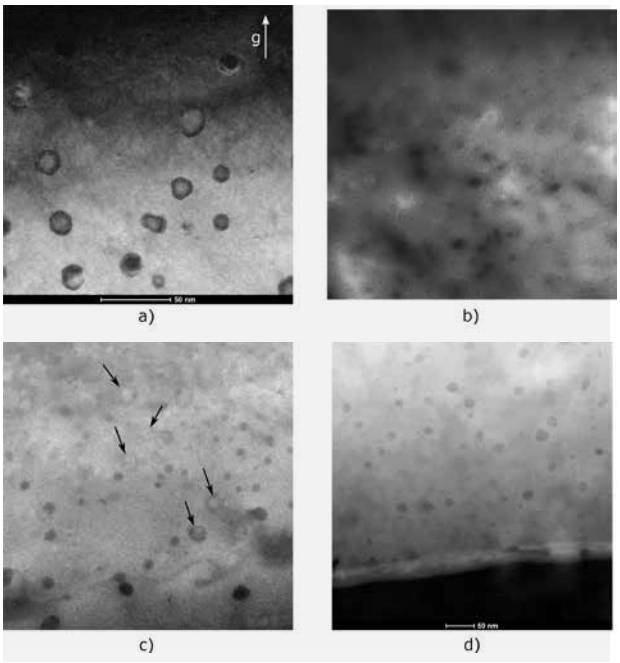

Fig. 5
a) Dark field plan-view TEM image of the sapphire surface nitridated at 1080°C for 30 minutes. The observed Moiré planes is the result of superposition of sapphire lattice and the lattice of nitridation layer;
b) dark field plan-view TEM image of the nitridated sapphire surface at the moment when annealing temperature T reaches 850°C. The Moiré fringes partially disappeared, indicating the degradation of nitridation layer;
c) dark field TEM plan-view after 2 minutes of annealing at 850°C. The Moiré fringes remain visible only above the regions of dark faceted voids (indicated by black arrows);
d) HAADF-STEM image of the surface when the annealing temperature reaches 1000°C. No Moiré fringes are visible, the nitridation layer has completely decomposed.

These Al-polar islands are observed exclusively on the sites above the hexagonal shaped voids in sapphire substrate. An epitaxial AlN layer grown at high temperature on top of this nitridation layer is mainly N-polar but exhibits a high density of Al-polar columnar inversion domains present at the sites, where Al-polar AlN islands are observed in the nitridation layer. (Fig. 4)

We use an in-situ TEM holder that allows to perform TEM measurements under controlled atmosphere up to atmospheric pressure and 1000°C (Protochips Atmosphere), to study the transformation of the heterogeneous nitridation layer during annealing in vacuum environment at the temperature range between 250°C and 1000°C. Our measurements show that the two-dimensional $Al_9O_3N_7$ layer, covering the sapphire surface in between hexagonal voids, starts to decompose as soon as T reaches 850°C and completely vanishes after 2 minutes of annealing at 850°C (cf. Fig. 5 (b), (c)). The AlN islands present above the hexagonal voids remain stable even at high temperatures, (Fig. 5 (c)). The AlN islands disappear at temperatures above 1000°C, (Fig. 5(d)).

These results confirm our hypothesis that the two-dimensional aluminum-oxynitride layer is unstable under high temperatures and the polarity-inverting monolayers of $Al_9O_3N_7$ decomposes, thereby promoting a dominant N-polar matrix (see the scheme on Fig. 6). The Al-polar AlN islands on the other hand are stable under high-temperature annealing conditions, generating Al-polar columnar inversion domains in the layer during the deposition of the N-polar AlN films at high temperatures.

In consequence, we suggest that the clue to achieve smooth homopolar N-polar AlN layers with low density of inversion domains is a proper adjustment of the nitridation conditions (approximately 10 minutes at T = 850°C – 950°C), as well as adjustment of growth parameters (reactor pressure, NH_3 flux, etc.). The goal is to avoid the formation of Al-polar AlN islands that cause the nucleation of Al polar domains in the layer.

Simulation & Characterization: **Electron Microscopy**

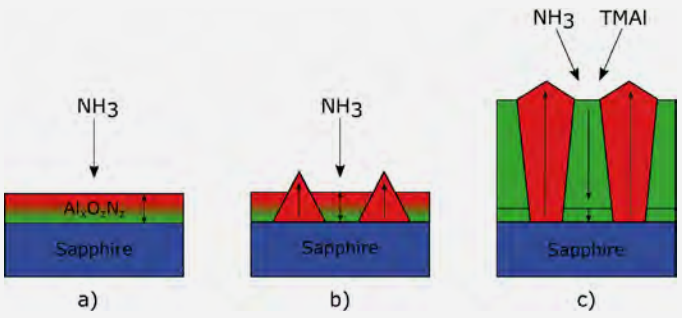

Fig.6
Schematic representation of the formation mechanism of Al-polar inversion domains in N-polar AlN. Arrows and color indicate the polarity of the layer: upwards arrow, red color – Al-polar layer; downwards arrow, green color – N-polar layer.
a) Initial sapphire annealing in NH_3 results in two-dimensional $Al_9O_3N_7$, which induces the inversion from N polarity at the interface with the sapphire substrate to Al polarity at the top monolayers;
b) excessive sapphire nitridation results in formation of stable Al-polar AlN islands in addition to $Al_9O_3N_7$ layer;
c) during the high temperature growth, the AlN islands promote Al polar domains in the layer, while the two-dimensional polarity-inverting $Al_9O_3N_7$ partially decomposes resulting in N-polarity. (The hexagonal voids in sapphire, observed in experimental images, are not shown on the sketch.)

Limitations in indium incorporation into InGaN

Within the framework of the European project "SPRInG", a collaborative project between the Leibniz Institute for Crystal Growth (IKZ), the Paul-Drude Institute (PDI) and TopGaN located in Warsaw, we tackled the growth of short period superlattices composed of coherently strained InN single monolayers separated by GaN barriers. Instead of changing the composition of the (In,Ga)N alloy, such structures allow to tune the bandgap by varying the periodicity of the superlattice, i.e. the thickness of the GaN barriers. This circumvents inevitable local bandgap fluctuations due to the alloying since only binary compounds are used. Our samples were grown by molecular beam epitaxy at the PDI and TopGaN, while the contribution of the IKZ was structural analysis by means of transmission electron microscopy (TEM) investigations. Despite exploring a wide range of growth parameters, all efforts in growing coherent InN single monolayers on GaN remained unsuccessful. Instead, TEM studies revealed that the indium content within the (In,Ga)N layer is limited to around 25%, i.e. forming an $In_{0.25}Ga_{0.75}N$ monolayer. Moreover, the indium distribution within the (In,Ga)N monolayer is not random but exhibits an intra-plane ordering. Fig. 7(a) displays a typical TEM image of an $In_{0.25}Ga_{0.75}N$ monolayer, recorded in the <1-100> zone axis. The monolayer becomes easily identifiable by means of a periodic intensity variation, whereby every 3rd atomic column appears darker compared to the surrounding GaN matrix.

For such imaging conditions, the darker spots indicate atomic columns with an increased indium content, while the bright spots refer to atomic columns which are mostly composed of GaN. This chemical ordering is not preserved within the entire layer but rather occurs in patches, laterally extending over a few nanometers. In the <11-20> zone axis, no periodic pattern are found implying that all atomic columns exhibit a very similar chemical composition. By crystallographic considerations, we can infer that the indium atoms in (In,Ga)N monolayers are distributed in patches which exhibit a $(n\sqrt{3} \times m\sqrt{3})R\ 30°$ atomic configuration. Given that the Indium content within the monolayer is 25 %, we conclude that n=m=2. Fig. 7 (b) displays a TEM image simulation for the $(2\sqrt{3} \times 2\sqrt{3})R\ 30°$ revealing a very similar contrast pattern. A stick and ball model of this configuration is shown in Fig. 7(c) in the <1-100> zone axis, corresponding to the experiment. In order to clarify, why a compositional limitation of 25 % indium cannot be overcome and how the chemical ordering occurs, we initiated a collaboration with the Max-Planck Institute for Eisenforschung in Düsseldorf. Density functional theory calculations were performed within the local density approximation (LDA) on (0001) (In,Ga)N surfaces. Starting point of our calculations was a 2x2 N-adatom terminated GaN surface, which coincides with reflection high energy electron diffraction (RHEED) experiments performed in-situ before adding indium to the MBE chamber.

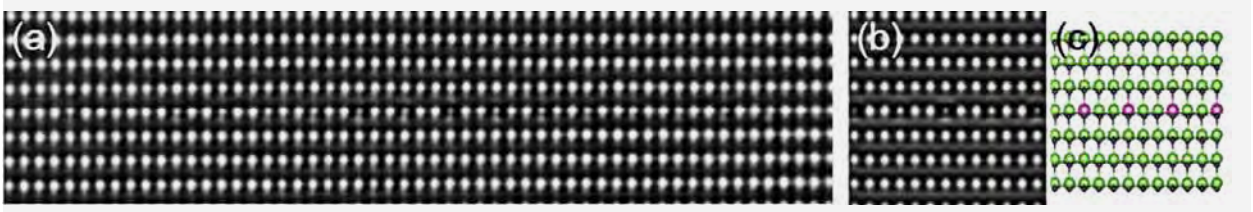

Fig. 7
(a) Experimental images of the $In_{0.25}Ga_{0.75}N$ monolayer region using negative Cs imaging conditions in the <1-100> zone axis.
(b) TEM image simulations of a $(2\sqrt{3} \times 2\sqrt{3})R\ 30°$ $In_{0.25}Ga_{0.75}N$ monolayer and
(c) the corresponding stick and ball model.

For this surface termination, two different lattice sites are available to be substituted with indium: (a) a 3-fold coordinated site and (b) a 4 fold coordinated site involving the N-adatom. Our calculations have revealed that the indium atoms strongly prefer the 4 fold coordination (like in the bulk state) over of 3 fold one. Such a configuration is against the well-established mechanism that Ga/In coordination tends to maximize the number of Ga-N bonds at the expense of In-N bonds, because the latter ones have a significantly lower bond energy. The physical origin for this surprising outcome is due to the fact that for the 3 fold coordinated indium configuration rehybridization from the bulk-like sp^3 to a planar sp^2 configuration is hindered due to the larger size of the indium atom preventing its downward relaxation. This inhibited relaxation makes an incorporation of indium on the 3 fold coordinated site highly unfavorable compared to the 4 fold coordination.

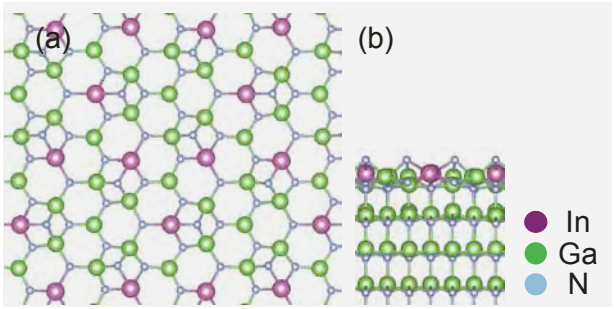

Fig. 8
Stick and ball model of the (2√3 x 2√3)R 30°configuration as it occurs during the growth of the (In,Ga)N monolayer seen in the (a) <0001> and (b) <1-100> zone axis.

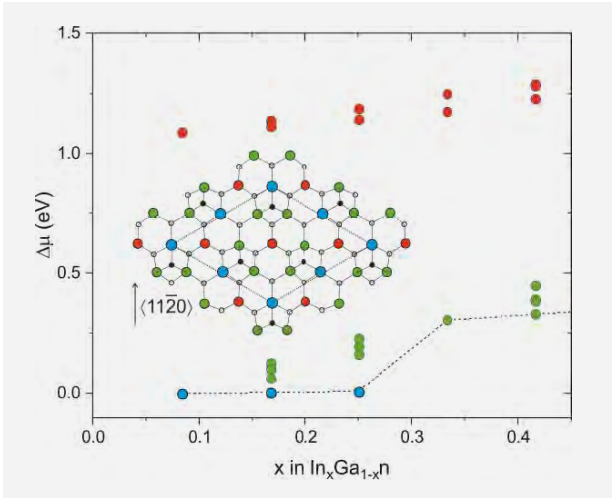

Fig. 9
Chemical potential Δμ as a function of composition x. Green/blue and red dots correspond to the lowest and higher energy configuration/s for different lattice sites as indicated in the stick and ball model (see inset).

As a second process, we identified that the repulsive strain interaction between indium atoms at the surface plays a major role for the chemical ordering, as well as for the limitation of indium incorporation. Essentially, the strain repulsion hampers incorporation of indium on spatially close lattice sites, promoting the formation of a (2√3 x 2√3)R 30° configuration.

A stick and ball model of this configuration is displayed in Fig. 8 in the <0001> (left) and <1-100> (right) orientation. The effect of both factors on the incorporation of indium, i.e. prevented rehybridization and strain repulsion, can be seen by plotting the chemical potential over the indium content in an (In,Ga)N monolayer at the surface, as displayed in Fig. 9. Incorporation on 3 fold coordinated lattice sites (red balls) is practically excluded due to a huge energy barrier. In contrast, the four-fold configuration is strongly preferred, particularly in the (2√3 x 2√3)R 30°configuration (blue), which is energetically most favorable. Increasing the indium concentration above 25 %, requires additional incorporation of indium atoms of fourfold coordinated lattice sites spatially close to already occupied ones (green). For x>0.25, this results in an increase of the chemical potential by ≈0.3 eV, limiting the incorporation of more Indium. To overcome this barrier, one would require raising the indium flux by a factor of ≈5. Such a huge increase in the In flux in an MBE process would eventually flood the surface with In, resulting in In droplets and poor growth morphology. Thus, using standard growth technologies, achievement of coherently grown InN on GaN is not possible. We believe that the incorporation barrier also plays an essential role for the growth of (In,Ga)N quantum wells.

Pulsed Sputter Deposition of GaN

For the epitaxial growth of group-III nitrides, plasma sputter deposition (PSD) is a promising growth method which is suitable for upscaling to production lines. In the framework of the joint project PlaN B project (**Pl**asma**a**bscheidung von Ga**N**-**B**auelementen) between OSRAM OS, Technical University of Braunschweig, University Magdeburg and the company CREAVAC in Dresden we explore the feasibility of the PSD method for realizing GaN devices. At IKZ PSD grown layers on different templates are structurally characterized by transmission electron microscopy. A homoepitaxial GaN layer grown by PSD on MOCVD-GaN/sapphire templates shows a pseudomorphic PSD GaN layer (Figure 10 left). Although the threading dislocation density is moderate the PSD layer is electrically isolating. In TEM investigations the PSD layer exhibits a speckled contrast compared to the MOCVD-GaN (Figure 10 right).

Simulation & Characterization: **Electron Microscopy**

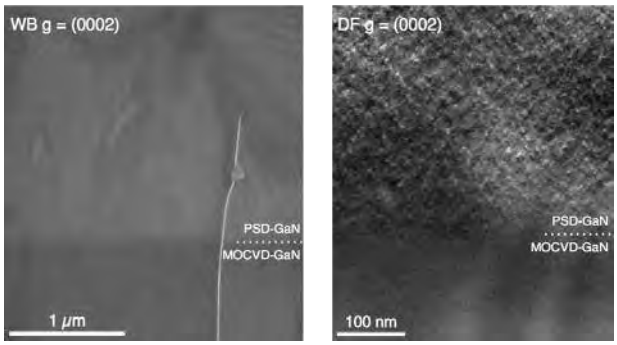

Fig. 10
The pseudomorphic PSD-GaN exhibits a brighter contrast compared to the MOCVD-GaN substrate in weak beam imaging with g =(0002). In dark field images with higher magnification the speckle contrast in the PSD-GaN layer indicates small isolateds strain sources.

With high-resolution TEM, the spreckles were identified as very small isolated basal stacking faults (ISF, see Fig. 11). A similar observation was reported for plasma assisted molecular beam epitaxy of GaN where N-ions were intentionally accelerated by a bias voltage towards the growth target. The energetic ion bombardment leads eventually to the generation of the isolated basal stacking faults [22]. From the density and size of the ISF we can approximate the dangling bond density to 5 × 10^{19} cm^{-3} for the investigated PSD-GaN sample. This value corresponds to a threading dislocation density of 10^{12} cm^{-2} which easily explains the observed isolating electrical characteristic of this layer. As such types of isolated stacking faults are formed by agglomeration of interstitials the hypotheses is that high energetic plasma ions (E_{kin} > 20 eV) impinging at the growth target cause a high density of interstitials which eventually form the ISF. Thus, to prevent isolated stacking faults, the high energetic ions have to be suppressed e.g. by increase of the background pressure in the growth chamber. In first experiments with a higher pressure during growth cathodoluminescence of the PSD-GaN were achieved.

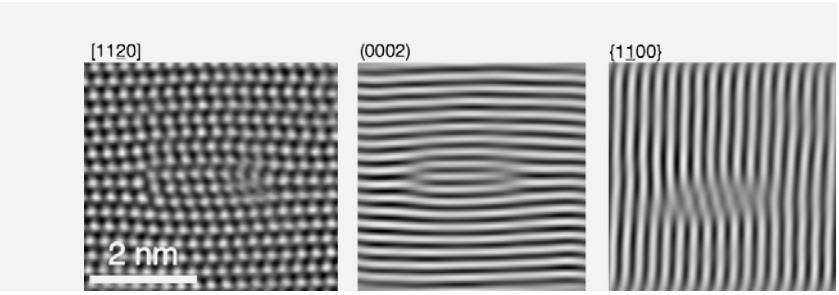

Fig. 11
HRTEM Image in [11$\bar{2}$0]-projection of an isolated basal stacking fault responsible for the speckle contrast shown in Figure 1. Bragg filtering the (0002) lattice planes shows clearly the inserted (0002) half plane and Bragg filtering the {1$\bar{1}$00} lattice planes reveals the ⅓ ⟨1$\bar{1}$00⟩ shift of the inserted half plane expected for low energy type I_2 stacking faults.

References

[1] Y. Shimomura et al.; J. Electrochem. Soc. 154 (2007) J234

[2] W. Lü et al.; Inorg. Chem. 52 (2013) 3007

[3] X. Zhang et al.; J. Phys. Chem. C 118 (2014) 7591

[4] Y. C. Wu et al.; ACS Appl. Mater. Interfaces 3 (2011) 3195

[5] Y. Chen et al.; J. Lumin. 131 (2011) 1770

[6] Y. Kaneda et al.; Opt. Lett. 20 (1995) 2204

[7] P. Dorenbos: J.Lumin. 91 (2000) 155

[8] J. Philippen et al.; J. Cryst. Growth 363 (2013) 270

[9] J. C. H. Spence and J. Taftø; J. Microsc. 130 (1983) 147

[10] R. D. Shannon; Acta Cryst. A32 (1976) 751

[11] N. A. Fichtenbaum et al.; J. Cryst. Growth 310 (2008) 1124

[12] J. Neugebauer et al.; Phys. Rev. Lett. 90 (2003) 056101

[13] J. L. Rouviere et al.; MRS Internet Journal of Nitride Semiconductor Research 1 (1996)

[14] O. Ambacher et al.; J. Appl. Phys. 85 (1999) 3222

[15] S. Rajan et al.; Jpn. J. Appl. Phys. 44 (2005) L1478

[16] M. H. Wong et al.; Semicond. Sci. Technol. 28 (2013) 074009

[17] J. Verma et al.; Appl. Phys. Lett. 99 (2011) 171104

[18] J. Jasinski et al.; Appl. Phys. Lett. 83 (2003) 2811

[19] R. Miyagawa et al.; Appl. Phys. Express 5 (2012) 025501

[20] V. Kueller et al.; Phys. Status Solidi C 9 (2012) 496

[21] S. Mohn, N. Stolyarchuk, T. Markurt, R. Kirste, M. P. Hoffmann, R. Collazo, A. Courville, R. Di Felice, Z. Sitar, P. Vennéguès, M. Albrecht; Phys. Rev. Appl. 5 (2016) 054004

[22] V. Kirchner et al.; Phys. Rev. B 58 (1998) 15749

Simulation & Characterization:
Chemical & Thermodynamic Analysis

Head PD Dr. habil. Detlef Klimm
Team Team: Dr. R. Bertram, O. Reetz, L. Schmack, L. Schwarz

Überblick

Wie schon in den vergangenen Jahren stellten Service-Messungen für andere Arbeitsgruppen (besonders für die Gruppe Oxide/Fluoride) den überwiegenden Teil der von der Gruppe geleisteten Arbeit dar. Drei Themen, die alle im Rahmen von Qualifizierungsarbeiten junger Wissenschaftler bearbeitet wurden, sollen an dieser Stelle hervorgehoben werden:

Bereits im vorigen Bericht erfolgte die Vorstellung experimenteller und theoretischer Arbeiten zum System Al_2O_3 – Cu_2O – CuO, und inzwischen verteidigte O. Reetz erfolgreich seine Masterarbeit an der Brandenburgischen Technischen Universität Cottbus-Senftenberg. Seit 2016 erfolgt die Weiterführung dieser Arbeiten durch eine im Rahmen eines DFG-Projektes angestellte Doktorandin mit dem Ziel der Züchtung von Delafossit ($CuAlO_2$) Substratkristallen. Der Stand der Arbeiten wird in diesem Jahresbericht durch die Gruppe Oxide/Fluoride vorgestellt.

Eine weitere Doktorandin (L. Schmack) führt die Neubestimmung des pseudobinären Systems $LiNbO_3$–$LiTaO_3$ durch. Beide Endglieder sind auch kommerziell wichtige piezoelektrische und ferroelektrische Kristallmaterialien. Mischkristalle könnten möglicherweise eine genaue Einstellung relevanter physikalischer Eigenschaften ermöglichen; jedoch stehen solche Mischkristalle bisher nicht zur Verfügung und die wenigen Literaturdaten zum pseudobinären System sind widersprüchlich. Für dieses System erfolgten verschiedene thermoanalytische Messungen (DTA, spezifische Wärmekapazität), und erste Züchtungsexperimente wurden in Zusammenarbeit mit der Gruppe Oxide/Fluoride durchgeführt.

Die Züchtung von Substratkristallen zur Epitaxie von elastisch verspannten Perowskit-Schichten beispielsweise aus $BaTiO_3$ oder $SrTiO_3$ („strain engeneering") stellt seit vielen Jahren eines der wichtigsten Arbeitsfelder der Gruppe Oxide/Fluoride dar. Die Suche nach weiteren neuen Substraten dauert an, und im Rahmen dieser Suche werden oft neue mehrkomponentige Phasendiagramme untersucht – in der Regel mit sehr hohen liquidus-Temperaturen jenseits 2000°C. Im Bericht des vergangenen Jahres beschrieben wir, dass Mischkristalle zwischen $LaLuO_3$ und $LaScO_3$ mit dem Czochralski-Verfahren hergestellt werden können; diese besitzen pseudokubische Gitterkonstanten 4,12 Å. Im Rahmen der 2016 erfolgreich abgeschlossenen Masterarbeit von T. Hirsch [1] erfolgten ähnliche Untersuchungen zum System $NdLuO_3$ – $NdScO_3$.

Overview

As usual, service measurements for other IKZ groups, but especially for the Oxides/Fluorides group, make the largest work share of our group. Three topics should be mentioned here separately, however. All of them are connected with the graduation of young scientists.

Already in the previous annual report experimental and theoretical work on the Al_2O_3 – Cu_2O – CuO system was mentioned, and meanwhile O. Reetz defended his master thesis on this topic successfully at Brandenburgische Technische Universität Cottbus-Senftenberg. Since 2016 these works are continued by a PhD student as a DFG project that is aimed on the growth of delafossite ($CuAlO_2$) substrate crystals. The status will be reported by the Oxide/Fluoride group in this annual report.

Another PhD student (L. Schmack) reevaluates the pseudobinary system $LiNbO_3$– $LiTaO_3$. Both end members are important piezoelectric and ferroelectric materials and single crystals are commercially available. Mixed crystals are currently not available but would potentially allow a fine tuning of the relevant physical properties. However, the few reports on the pseudobinary system found in literature are contradictory. For this system different thermoanalytic measurements (DTA, specific heat capacity) and (in collaboration with the Oxides/Fluorides group) first growth experiments were performed. Since many years the growth of substrate crystals allowing the deposition of "strain engineered" perovskite layers such as $BaTiO_3$ or $SrTiO_3$ is an important field of work for the Oxide/Fluoride group. The quest for new substrates continues, and this requires often the evaluation of new multi-component phase diagrams – typically with very high liquidus temperatures beyond 2000°C. In the previous report we described that solid solutions between $LaLuO_3$ and $LaScO_3$ can be grown by the Czochralski method, making pseudocubic lattice constants >4.12 Å accessible. In the framework of the master thesis of T. Hirsch [1], which was successfully finished in 2016, similar investigations for the system $NdLuO_3$ – $NdScO_3$ were performed.

Results

The variety of crystal structures that are shown by sesquioxides R_2O_3 is large already for the 3rd main group metals R = Al (corundum, trigonal), Ga (β-gallia, monoclinic), In (bixbyite structure, cubic). For 3-valent rare earth oxides RE_2O_3 the variety of crystal structures is even larger, and at room temperature the polymorphs A (hexagonal, for RE = La, Ce, Pr, Nd); B (monoclinic, for RE = Sm, Eu, Gd), and C (cubic, sometimes also Sm, Eu, Gd, plus elements from Tb on) can be observed. At very high temperatures (>2250°C) oxides especially of the larger RE^{3+} show transformation to another hexagonal H-phase, or to another cubic X-phase [2]. Both high temperature modifications cannot be stabilized by quenching to room temperature, but transformations between A, B and C can partially be quenched. Besides this, transformations between polytypes are sometimes influenced by volatiles which makes phase equilibrium studies complicated and leads partially to insufficient reproducibility of experiments [3].

Mixtures of two rare earth sesquioxides can show different phenomena, depending on the size ratio of the RE^{3+} and RE'^{3+}. Especially pseudobinary systems Sc_2O_3–RE_2O_3 were elaborately studied by Badie [4], but the corresponding phenomena are not limited to systems containing scandium oxide.

1. Formation of solid solutions of type A, B, C; H, or X. The homogeneity range can be infinite for RE^{3+} radii slightly larger than scandium (Sc: 88.5 pm, Lu: 100.1 pm, both type C); or limited if the RE^{3+} radii are much larger (Nd: 112.3 pm, <<5% Nd_2O_3 can be incorporated in C-Sc_2O_3, 10–15% Sc_2O_3 can be incorporated in A-, H-, and X-Nd_2O_3, respectively).
2. Formation of orthorhombic perovskite (P-) type phases $RESCO_3$ for the larger RE^{3+}, down to Ho or Y, respectively. However, P-type holmium and yttrium scandate decompose above ca. 1800°C to a C-type $(RE,Sc)_2O_3$ solid solution (Ho^{3+}: 104.1 pm, Y^{3+}: 104.0 pm). Only for the larger rare earth ions from dysprosium on (Dy^{3+}: 105.2 pm), the $RESCO_3$ are in equilibrium with the melt, and melt congruently between 2100°C ($DyScO_3$) and 2390°C ($LaScO_3$). $RESCO_3$ bulk crystals are grown at IKZ meanwhile for RE = Dy, Tb, Gd, Eu, Sm, Nd, and Pr [5]. It is a big benefit of these materials, that they are not subject of phase transformations between their high melting points and room temperature, which allows not only the growth of high quality crystals, but also the deposition of stable epitaxial layers at almost every process temperature.
3. For a few systems, rhombohedral intermediate phases such as Dy_3ScO_6 can be formed that undergo at ca. 1700–1850°C peritectoid decomposition to P and C [2].

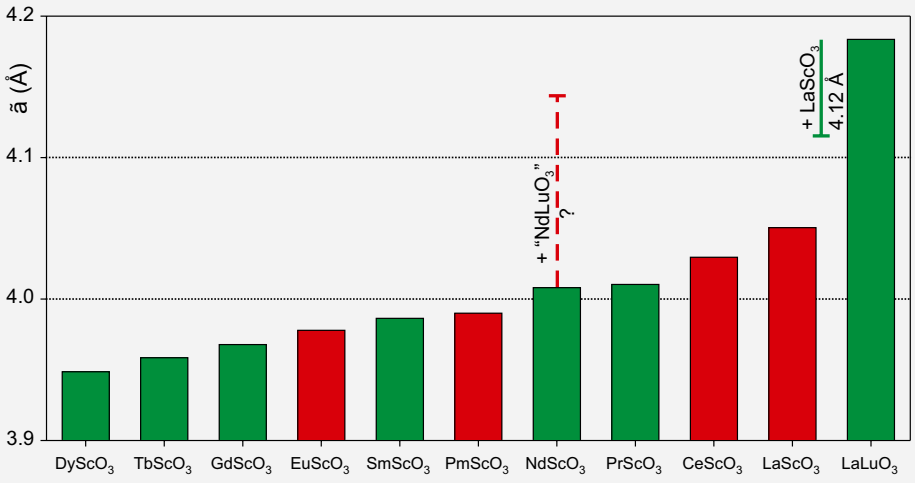

Fig. 1
Potential perovskite type mixed RE oxides for substrates and their pseudocubic lattice parameter ã. Substances marked in red are either partially not useful ($EuScO_3$ not stable against Si, $PmScO_3$ radioactive) or not (yet) available for bulk crystal growth ($LaScO_3$ melts at 2390°C [4]).

Simulation & Characterization: **Chemical & Thermodynamic Analysis**

The choice of $RESc0_3$ crystals is large but limited [5], which restricts the number of accessible pseudocubic lattice parameters to ca. 6–7 which are shown as green bars in Fig. 1. Meanwhile it could be shown that neighboring rare earth scandates mix almost ideally and the "2-phase-field" liquid & solid of the phase diagrams is very narrow. Consequently, mixed crystals of neighboring $RESc0_3$ can be grown without significant segregation [6], allowing fine-tuning of lattice parameters and bridging the gaps at $EuSc0_3$ and $PmSc0_3$. The next breakthrough was reported in the previous annual report, where complete miscibility of the P-type mixed oxides $LaLu0_3$ (which melts already at 2120°C [9]) and $LaSc0_3$ could be shown. Very large pseudocubic lattice parameters beyond 4.1 Å were measured for single crystals of their solid solutions [7]. The available range is indicated by the green marker in Fig. 1, adjacent to $LaLu0_3$.

The question remains, if other solid solutions could be created starting e.g. from $NdSc0_3$, raising its lattice parameter into the "empty" range between 4.0103 Å ($PrSc0_3$) and 4.1224 Å (solid solution of 43% $LaSc0_3$ in $LaLu0_3$ [7]). $NdLu0_3$ was considered as candidate for alloying $NdSc0_3$, because it was in some references prepared under high pressure as single phase P-type with ã=4.146 Å [10] (red dashed marker in Fig. 1).

A thorough reevaluation of the Lu_2O_3–Nd_2O_3 system [1,11] allowed the assessment of the pseudobinary phase diagram that is shown in Fig. 2. All phases A, B, C, H, and X exist with partially wide homogeneity ranges, but no indication for the formation of $NdLu0_3$ perovskite was found. This is a drawback, because obviously the upper limit of the red bar over $NdSc0_3$ in Fig. 1 cannot be reached.

In contrast, the intermediate P-phase exists in the Nd_2O_3–Sc_2O_3 system and melts congruently (Fig. 3). It should be noted that Sc_2O_3 as well as Lu_2O_3 are isomorphous C-type up to their melting points, which allows infinite miscibility as mentioned above. A small positive Gibbs excess energy leads to an azeotrope point almost in the middle of the system (not shown here), ca. 100 K below the melting points of both components.

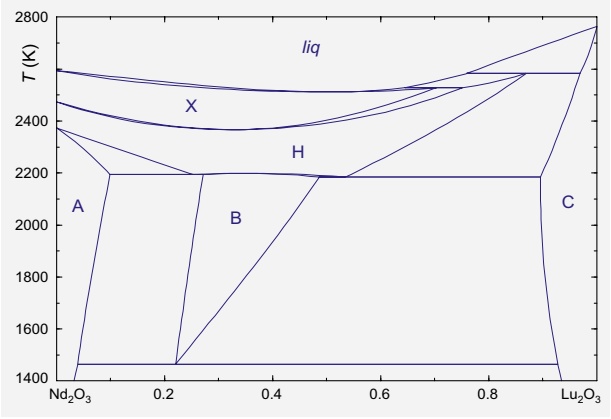

Fig. 2
The equilibrium phase diagram Lu_2O_3–Nd_2O_3 at 1 bar shows no perovskite phase (all single phase fields are labelled, assessment with FactSage [1]).

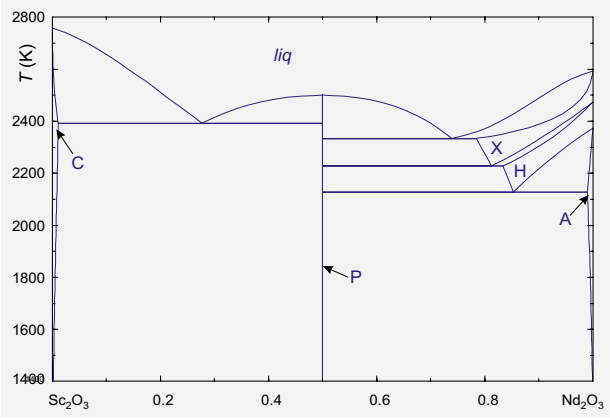

Fig. 3
The equilibrium phase diagram Nd_2O_3–Sc_2O_3 is dominated for intermediate compositions by the perovskite (P) phase $NdSc0_3$.

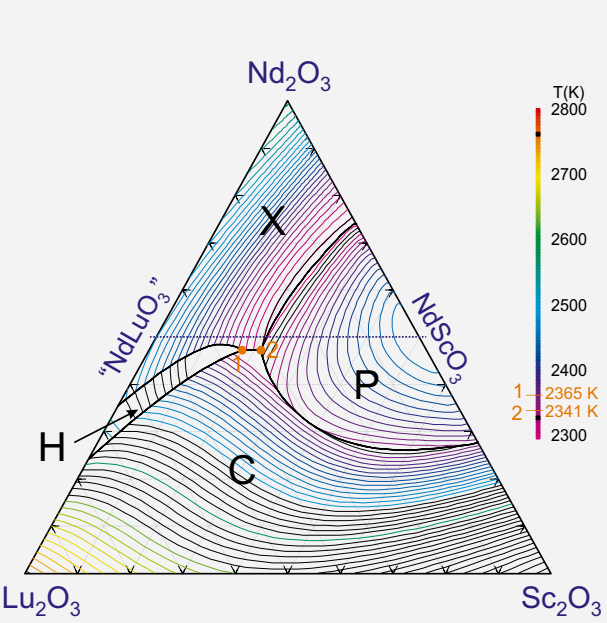

Fig. 4
The liquidus projection (10 K isotherms) of the ternary system Nd_2O_3–Sc_2O_3–Lu_2O_3 shows four primary crystallization fields. The left and right rim systems are depicted in Fig. 2 and 3, respectively.

Starting from the assessed three pseudobinary rim systems, the concentration triangle that is shown in Fig. 4 could be calculated. The fitting of ternary interaction parameters was performed, however, only on the basis of DTA measurements on the "$NdLuO_3$"–$NdScO_3$ join that is marked by a blue dotted line in the triangle. The primary crystallization field of the perovskite phase extends widely into the ternary: A more detailed concentration vs. temperature projection on this line [1] (not shown here) demonstrates that ca. 58% neodymium lutetate could be added to $NdScO_3$ before the P field is left. In the subsolidus P is probably stable even closer to the composition $NdLuO_3$, but without equilibrium to any liquid phase which prohibits crystal growth from the melt.

The highest $NdLuO_3$ concentrations can be obtained from compositions close to the eutectic valley X–P, and this are ca. 20% $NdLuO_3$ from the 58% melt mentioned above. A first Czochralski growth experiment with a melt composition in the P crystallization field was performed, however, further work is required to obtain single crystals that are useful for the preparation of substrates.

References

[1] T. Hirsch; Phasenbeziehungen im System $NdLuO_3$–$NdScO_3$, MSc thesis, TU Bergakademie Freiberg (2016)

[2] M. Zinkevich; Prog. Mater. Sci. 52 (2007) 597

[3] M. V. Fedorov, R. M. Nazarkin, R. M. Zakalyukin; Crystallogr. Reports. 47 (2002) 281

[4] J. M. Badie, Phases et transitions de phases à haute température dans les systèmes Sc_2O_3-Ln_2O_3 (Ln = lanthanide et yttrium), Rev. Int. Hautes Temp. Réfract., Fr. 15 (1978) 183

[5] R. Uecker, B. Velickov, D. Klimm, R. Bertram, M. Bernhagen, M. Rabe, M. Albrecht, R. Fornari, D. G. Schlom; J. Cryst. Growth 310 (2008) 2649

[6] R. Uecker, D. Klimm, R. Bertram, M. Bernhagen, I. Schulze-Jonack, M. Brützam, A. Kwasniewski, Th. M. Gesing, D. G. Schlom; Acta Phys. Pol. A. 124 (2013) 295

[7] R. Uecker, R. Bertram, M. Brützam, Z. Galazka, T.M. Gesing, C. Guguschev, D. Klimm, M. Klupsch, A. Kwasniewski, D. G. Schlom; J. Cryst. Growth. 457 (2017) 137

[8] J. E. Greedan, K. Seto; Mater. Res. Bull. 16 (1981) 1479

[9] K. Ovanesyan, A. Petrosyan, G. Shirinyan, C. Pedrini, L. Zhang; Opt. Mater. 10 (1998) 291

[10] S. Wenhui, W. Daiming, L. Xiaoyuan, M Xianfeng, Z. Jianshi, Q. Zhengnan, W. Yifeng, L. Weina, G. Zhongjiu; Phys. B+C 140B (1986) 658

[11] T. Hirsch, R. Uecker, D. Klimm; Cryst. Res. Technol. 52 (2017) 1600237

Simulation & Characterization:
Crystal Machining

Head Dr. Uta Juda
Team K. Berger, M. Imming-Friedland, V. Lange, Th. Wurche

Überblick

Die Arbeit der Gruppe Kristallbearbeitung konzentriert sich vorrangig auf folgende Aufgaben:

- *die Probenpräparation für die routinemäßige züchtungsbegleitende Diagnostik der im Haus gezüchteten Kristalle mit vielseitigen Anforderungen an, durch das breite Spektrum zu bearbeitender Materialien mit unterschiedlichen mechanischen Eigenschaften und Dimensionen bedingten, Probengeometrie und Oberflächenqualität*
- *Herstellung von kristallographisch genau orientierten Kristallkeimen und epi-ready-Substraten für den Einsatz in der Kristallzüchtung*
- *Entwicklung von Schneid- und Oberflächenpräparationstechnologien und -vorschriften, vor allem für neue am Institut gezüchtete Kristallmaterialien, um auch hierbei den Anforderungen der Züchtung und der Materialdiagnostik gerecht zu werden*
- *Service- und Forschungsaufträge für die Industrie, für Hochschulen und außeruniversitäre Forschungseinrichtungen, die von der Lieferung bearbeiteter Proben bis hin zur Entwicklung von Technologien und die Erarbeitung der damit verbundenen Dokumentationen reicht.*

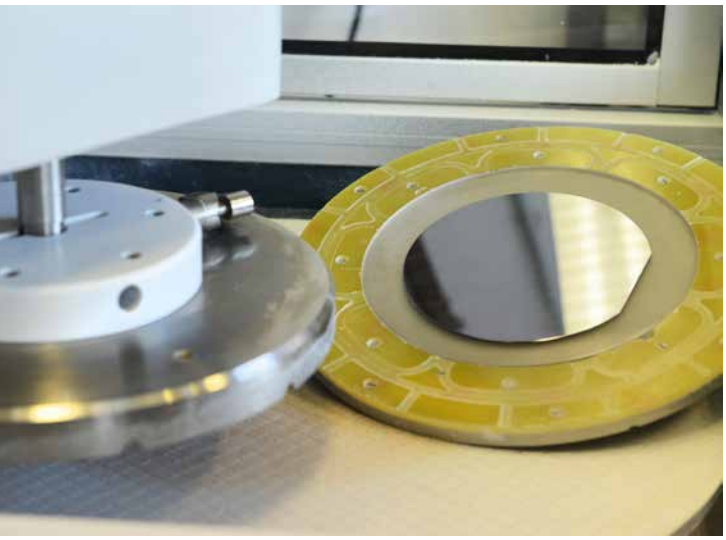

Die Präparation von Halbleitermaterialien oder von Kristallen für optische Anwendungen, für die Diagnostik oder für den Einsatz als Substrate für die Epitaxie erfordert meist eine hohe Präzision in der Bearbeitung. Unabhängig von Material oder Verwendungszweck durchläuft jede Probe bzw. jeder Wafer bis zur Fertigstellung verschiedene Arbeitsschritte wie Schneiden, Formatieren und Oberflächenpräparation mittels unterschiedlicher Schleif-, Läpp- und Polierprozesse. Die dazu in unserer Gruppe zur Verfügung stehenden Methoden umfassen:

- *röntgenografisches Orientieren von Kristallen*
- *Trennschleifen mit verschiedenen Verfahren (Diamantdraht- und Diamant-Innentrennsägen)*
- *Flachschleifen mit Diamantwerkzeugen*
- *Läppen mit verschiedenen Läppmitteln (Aluminiumoxid, Ceroxid, Siliciumcarbid, Borcarbid, Diamant) in verschiedener Korngrößen und Suspensionen*
- *mechanisches und chemo-mechanisches Polieren*
- *Oberflächencharakterisierung mittels Lichtmikroskopie, Atomkraftmikroskopie (AFM), Konfokalmikroskopie (CFM) und Rasterelektronenmikroskopie (REM)*
- *Bestimmung von Wafergeometrie und Oberflächenparametern wie Waferdicke, Ebenheit, Parallelität und Oberflächenrauigkeit*

Durch enge personelle und gerätetechnische Vernetzung der Gruppen Kristallbearbeitung und Charakterisierung können neben den täglichen Routineaufgaben mehr wissenschaftliche Aspekte der Präparation bearbeitet werden. Eine entsprechende anlagentechnische Ausstattung und fachliche Kompetenz aller Mitarbeiter machen es darüber hinaus auch möglich, kurzfristig und in hoher Qualität auf unterschiedliche Probenanforderungen zu reagieren.

Simulation & Characterization: **Crystal Machining**

Overview

The work of the group Crystal machining is focused on the following tasks:

- sample preparation for routine characterization and material diagnostics of the in-house grown crystals with special requirements on sample geometry and surface parameters such result from the wide spectrum of materials with a wide range of mechanical properties and sample sizes.
- preparation of crystallographically oriented seed crystals and epi-ready substrates for use in crystal growth.
- development of cutting and surface preparation technologies and instructions for new materials grown at the institute in order to meet the requirements for crystal growth and material diagnostics.
- service for and research orders from industry, universities and other research institutes from the supply of machined samples up to the development of technologies and related documentations.

The preparation of crystals for semiconductor and optical applications, for diagnostics or as substrates for epitaxial processes requires high-precision machining. Whatever the application or material, each sample or wafer undergoes several stages during manufacture, which include formatting, slicing the wafer from the crystal and preparing the surface using different grinding, lapping and polishing techniques. The methods used in our group include:

- crystal orientation using x-ray techniques
- crystal cutting and wafering by different methods (single and multi diamond wire and inner diameter diamond sawing)
- wafer grinding with diamond tools
- wafer lapping with various abrasives (aluminum oxide, cerium oxide, silicon carbide, boron carbide, diamond) in different particle sizes and suspensions
- mechanical and chemo-mechanical polishing
- surface characterization by light microscopy, atomic force microscopy (AFM) confocal microscopy (CFM) and scanning electron microscopy (REM)
- determination of standard wafer geometry and surface parameters like thickness, evenness, planarity and roughness.

The close co-operation with the group Characterization by a personal- and device-related network contributed to a more scientific approach to crystal machining. Appropriate equipment and also valuable experience and great proficiency of all staff members in the field of sample preparation and characterization enable us to supply custom-made products and to fulfil ambitious service in short time and high quality.

Results

An ambitious challenge in this year has been the development of preparation technologies for some oxides (Strontium Titanate, Gallium Oxide and Tin Oxide). The aim of this work is to prepare epi-ready surfaces for epitaxial growth using a suitable chemo-mechanical polishing (CMP) method including a high quality mechanical pre-polishing. CMP is a process of polishing and planarization of wafer surfaces with slurries containing abrasive particles and reactive chemicals. It represents the final step in wafer preparation. The important tasks of CMP are the removal of scratches, surface and subsurface damages caused by the precedent mechanical polishing as well as the reduction of residual roughness and unevenness of the surface without leaving disturbing residual surface layers. A basic requirement for successful CMP is also a high-quality mechanical prepolish because only few microns of the material should be removed by CMP, otherwise further geometric restraints cannot be maintained. Different experiments on polishing with colloidal silica slurries, aluminium oxide and cerium oxide were performed with varying process parameters like pressure, velocity of plate- and carrier rotation, polishing time, mixture of polishing fluid, flow rate of the slurry and the type of polishing pad.

In 2016 the experiments focused on the polishing of Al-polar AlN surfaces continued to develop the preparation technology. In order to proof whether the surface has epi-ready quality these samples were used as substrates for homo-epitaxial layer deposition. In the last time a good quality was obtained which suggests an excellent CMP. Based on these results and depending on the availability of samples, the mechanical and chemo-mechanical polishing of Al-polar surfaces will be optimized, especially focused on the reduction of polishing time, and also applied to other planes of AlN crystals.

Appendix

Appendix: **Publications**

Articles in books

D. Klimm; *Growth of Bulk ZnO*, in: S. Hashmi (editor-in-chief), Reference Module in Materials Science and Materials Engineering, Elsevier (2016), 1 – 18

D. Klimm; *Scintillator Crystals*, in: S. Hashmi (editor-in-chief), Reference Module in Materials Science and Materials Engineering, Elsevier (2016), 1 – 7

D. Klimm, S. Ganschow, Z. Galazka, R. Bertram, D. Schulz, R. Uecker; *Reactive Atmospheres for Oxide Crystal Growth;* in: N. P. Bansal, M. Kusnezoff, K. Shimamura (eds), Advances in Solid Oxide Fuel Cells and Electronic Ceramics: A Collection of Papers Presented at 39th International Conference on Advanced Ceramics and Composites – Ceramic Engineering and Science Proceedings, John Wiley & Sons, Inc., (2016), Chapter 16, 157 – 167

Articles in international peer reviewed journals and proceedings

L. Ahrem, G. Scholz, R. Bertram, E. Kemnitz; *Thermal evolution of 4- and 5-fold coordinated Al-sites in aluminum hydroxide fluorides with low fluorination degree;* J. Phys. Chem. C **120** (2016) 9236 – 9244

A. V. Andrianov, A. O. Zakhar'in, R. Kh. Zhukavin, V. N. Shastin, D. V. Shengurov, N. V. Abrosimov; *Terahertz emission at Impurity electrical breakdown in Si(Li);* Tech. Phys. Lett. **42** (2016) 1031 – 1033

N. Arutyunov, N. Bennett, N. Wight, R. Krause-Rehberg, V. Emtsev, N. Abrosimov, V. Kozlovski; *Positron probing of disordered regions in neutron-irradiated silicon;* Phys. Status Solidi B **253** (2016) 2175 – 2179

M. Baldini, M. Albrecht, A. Fiedler, K. Irmscher, D. Klimm, R. Schewski, G. Wagner; *Semiconducting Sn-doped β-Ga_2O_3 homoepitaxial layers grown by metal organic vapour-phase epitaxy;* J. Mater. Sci. **51** (2016) 3650 – 3656

M. Baldini, M. Albrecht, A. Fiedler, K. Irmscher, R. Schewski, G. Wagner; *Si- and Sn-doped Homoepitaxial β-Ga_2O_3 layers grown by MOVPE on (010)-oriented substrates;* ECS J. Solid State Sci. Technol. **6** (2016) Q1 – Q5

R. Bansen, C. Ehlers, Th. Teubner, T. Markurt, J. Schmidtbauer, T. Boeck; *Continuous polycrystalline silicon layers on glass grown from tin solutions;* CrystEngComm **18** (2016) 1911 – 1917

R. Bansen, C. Ehlers, Th. Teubner, K. Böttcher, K. Gambaryan, J. Schmidtbauer, T. Boeck; *Silicon on glass grown from indium and tin solutions;* J. Photon. Energy **6** (2016) 025501/1 – 025501/10

R. Bansen, C. Ehlers, Th. Teubner, T. Boeck; *Steady-state solution growth of microcrystalline silicon on nanocrystalline seed layers on glass;* J. Semicond. **37** (2016) 093001/1 – 093001/4

D. Borisova, N.V. Abrosimov, K. Shcherbachev, V. Klemm, G. Schreiber, D. Heger, U. Juda, V. Bublik, H. Oettel; *Evolution of real structure in Ge-Si mosaic crystals;* Cryst. Res. Technol. **51** (2016) 742 – 751

B. Burganov, C. Adamo, A. Mulder, M. Uchida, P. D. C. King, J. W. Harter, D. E. Shai, A. S. Gibbs, A. P. Mackenzie, R. Uecker, M. Bruetzam, M. R. Beasley, C. J. Fennie, D. G. Schlom, K. M. Shen; *Strain control of Fermiology and many-body interactions in two-dimensional ruthenates;* Phys. Rev. Lett. **116** (2016) 197003/1 – 197003/6

B. Cai, J. Schwarzkopf, E. Hollmann, D. Braun, M. Schmidbauer, T. Grellmann, R. Wördenweber; *Electronic characterization of polar nanoregions in relaxor-type ferroelectric $NaNbO_3$ films;* Phys. Rev. B **93** (2016) 224107/1 – 224107/8

G. Calvert, C. Guguschev, A. Burger, A. Groza, J.J. Derby, R.S. Feigelson; *High speed growth of SrI_2 scintillator crystals by the EFG process;* J. Cryst. Growth **455** (2016) 143 – 151

K. D. Chabak, N. Moser, A. J. Green, D. E. Walker Jr., S. E. Tetlak, E. Heller, A. Crespo, R. Fitch, J. P. McCandless, K. Leedy, M. Baldini, G. Wagner, Z. Galazka, X. Li, G. Jessen; *Enhancement-mode Ga_2O_3 wrap-gate fin field-effect transistors on native (100) β-Ga_2O_3 substrate with high breakdown voltage;* Appl. Phys. Lett. **109** (2016) 213501/1 – 213501/5

C. Chèze, M. Siekacz, F. Isa, B. Jenichen, F. Feix, J. Buller, T. Schulz, M. Albrecht, C. Skierbiszewski, R. Calarco, H. Riechert; *Investigation of interface abruptness and In content in (In,Ga)N/GaN superlattices*; J. Appl. Phys. **120** (2016) 125307/1 – 125307/7

Y. Cho, S. Sadofev, S. Fernández-Garrido, R. Calarco, H. Riechert, Z. Galazka, R. Uecker, O. Brandt; *Impact of substrate nitridation on the growth of InN on In_2O_3(111) by plasma-assisted molecular beam epitaxy;* Appl. Surf. Sci. **369** (2016) 159 – 162

Appendix: **Publications**

Y. Yu. Choporova, V. V. Gerasimov, B. A. Knyazev, S. M. Sergeev, O. A. Shevchenko, R. Kh. Zhukavin, N. V. Abrosimov, K. A. Kovalevsky, V. K. Ovchar, H.-W. Hübers, G. N. Kulipanov, V. N. Shastin, H. Schneider, N. A. Vinokurov; *First terahertz-range experiments on pump – probe setup at Novosibirsk free electron laser;* Physics Procedia **84** (2016) 152 – 156

C. Cocchi, H. Zschiesche, D. Nabok, A. Mogilatenko, M. Albrecht, Z. Galazka, H. Kirmse, C. Draxl, C. T. Koch; *Atomic signatures of local environment from core-level spectroscopy in β-Ga_2O_3;* Phys. Rev. B **94** (2016) 075147/1 – 075147/6

S. Dadgostar, J. Schmidtbauer, T. Boeck, A. Torres, O. Martínez, J. Jiménez, J. W. Tomm, A. Mogilatenko, W. T. Masselink, F. Hatami; *GaAs/GaP quantum dots: Ensemble of direct and indirect heterostructures with room temperature optical emission;* Appl. Phys. Lett. **108** (2016) 102103/1 – 102103/5

A. P. Detochenko, S. A. Denisov, M. N. Drozdov, A. I. Mashin, V. A. Gavva, A. D. Bulanov, A. V. Nezhdanov, A. A. Ezhevskii, M. V. Stepikhova, V. Yu. Chalkov, V. N. Trushin, D. V. Shengurov, V. G. Shengurov, N. V. Abrosimov, H. Riemann; *Epitaxially grown monoisotopic Si, Ge, and $Si_{1-x}Ge_x$ alloy layers: production and some properties;* Semicond. **50** (2016) 345 – 348

N. Dropka, Ch. Frank-Rotsch, P. Rudolph; *Influence of peripheral vibrations and traveling magnetic fields on VGF growth of Sb-doped Ge crystals*; J. Cryst. Growth **453** (2016) 27 – 33

N. Dropka, T. Ervik, M. Czupalla, F. M. Kiessling; *Scale up aspects of directional solidification and Czochralski silicon growth processes in traveling magnetic fields*; J. Cryst. Growth **451** (2016) 95 – 102

V.G. Dubrovskii, Y. Berdnikov, J. Schmidtbauer, M. Borg, K. Storm, K. Deppert, J. Johansson; *Length distributions of nanowires growing by surface diffusion;* Cryst. Growth Des. **16** (2016) 2167 – 2172

V. V. Emtsev, N. V. Abrosimov, V. V. Kozlovskii, G. A. Oganesyan; *Electrical properties of defects in Ga-doped Ge irradiated with fast electrons and protons;* Solid State Phenom. **242** (2016) 316 – 321

V. V. Emtsev, N. V. Abrosimov, V. V. Kozlovskii, G. A. Oganesyan, D. S. Poloskin; *Some Challenging Points in the Identification of Defects in Floating-Zone n-Type Silicon Irradiated with 8 and 15 MeV Protons;* Semicond. **50** (2016) 1291 – 1298

A. A. Ezhevskii, A. P. Detochenko, S. A. Popkov, A. A. Konakov, A. V. Soukhorukov, D. V. Guseinov, D. G. Zverev, G. V. Mamin, N. V. Abrosimov, H. Riemann; *Spin relaxation times of donor centers associated with lithium in monoisotopic ^{28}Si;* Solid State Phenom. **242** (2016) 322 – 326

M. Feneberg, J. Nixdorf, C. Lidig, R. Goldhahn, Z. Galazka, O. Bierwagen, J. S. Speck; *Many-electron effects on the dielectric function of cubic In_2O_3: Effective electron mass, band-nonparabolicity, band gap renormalization, and Burstein-Moss shift;* Phys. Rev. B **93** (2016) 045203/1 – 045203/11

S. Fernández-Garrido, J. Lähnemann, C. Hauswald, M. Korytov, Mr. Albrecht, C. Chèze, C. Skierbiszewski, O. Brandt; *Comparison of the luminous efficiency of Ga- and N-polar $In_x Ga_{1-x}N/In_yGa_{1-y}N$ quantum wells grown by plasma-assisted molecular beam epitaxy;* Phys. Rev. Appl. **6** (2016) 034017

D. P. Franke, M. Szech, F. M. Hrubesch, H. Riemann, N. V. Abrosimov, P. Becker, H.-J. Pohl, K. M. Itoh, M. L. W. Thewalt, M. S. Brandt; *Electron nuclear double resonance with donor-bound excitons in silicon;* Phys. Rev. B **94** (2016) 235201/1 – 235201/6

S. Ganschow, A. Kwasniewski, D. Klimm; *Conditions for the growth of $Fe_{1-x}O$ crystals using the micro-pulling-down technique;* J. Cryst. Growth **450** (2016) 203 – 206

A. J. Green, K. D. Chabak, E. R. Heller, R. C. Fitch, M. Baldini, A. Fiedler, K. Irmscher, G. Wagner, Z. Galazka, S. E. Tetlak, A. Crespo, K. Leedy, G. H. Jessen; *3.8-MV/cm breakdown strength of MOVPE-grown Sn-doped β-Ga_2O_3 MOSFETs;* IEEE Electr. Device Lett. **37** (2016) 902 – 905

J. Haeberle, S. Brizzi, D. Gaspar, P. Barquinha, Z. Galazka, D. Schulz, D. Schmeißer; *A spectroscopic comparison of IGZO thin films and the parent In_2O_3, Ga_2O_3, and ZnO single crystals;* Mater. Res. Express **3** (2016) 106302

M. Handwerg, R. Mitdank, Z. Galazka, S. F. Fischer; *Temperature-dependent thermal conductivity and diffusivity of a Mg-doped insulating β-Ga_2O_3 single crystal along [100], [010] and [001];* Semicond. Sci. Technol. **31** (2016) 125006

C. Hartmann, J. Wollweber, S. Sintonen, A. Dittmar, L. Kirste, S. Kollowa, K. Irmscher, M. Bickermann; *Preparation of deep UV transparent AlN substrates with high structural perfection for optoelectronic devices;* CrystEngComm **18** (2016) 3488 – 3497

Appendix: **Publications**

S. Höfer, R. Uecker, A. Kwasniewski, J. Popp, Th. G. Mayerhöfer ; *Complete dispersion analysis of single crystal yttrium orthosilicate;* Vib. Spectrosc. **83** (2016) 151 – 158

K. Kachel, D. Siche, S. Golka, P. Sennikov, M. Bickermann; *FTIR exhaust gas analysis of GaN pseudo-halide vapor phase growth;* Mater. Chem. Phys. **177** (2016) 12 – 18

F. Kamutzki, C. Guguschev, D. J. Kok, R. Bertram, U. Juda, R. Uecker; *The influence of oxygen partial pressure in the growth atmosphere on the coloration of $SrTiO_3$ single crystal fibers;* CrystEngComm **18** (2016) 5658 – 5666

L. Khirunenko, M. Sosnin, A. Duvanskii, N. Abrosimov, H. Riemann; *Boron-related defects in low temperature irradiated silicon*; Solid State Phenom. **242** (2016) 285 – 289

L. I. Khirunenko, M. G. Sosnin, A. V. Duvanskii, N. V. Abrosimov, H. Riemann; *Defects involving interstitial boron in low-temperature irradiated silicon;* Phys. Rev. B **94** (2016) 235210/1 – 235210/7

L. A. King, Q. Yang, M. L. Grossett, Z. Galazka, R. Uecker, B. A. Parkinson; *Photosensitization of Natural and synthetic SnO_2 single crystals with dyes and quantum dots;* J. Phys. Chem. C **120** (2016) 15735 – 15742

D. J. Kok, C. Guguschev, T. Markurt, M. Niu, R. Bertram, M. Albrecht, K. Irmscher; *Origin of brown coloration in top-seeded solution grown $SrTiO_3$ crystals;* CrystEngComm **18** (2016) 4580 – 4586

R. A. Kornev, P. G. Sennikov, D. A. Konychev, A. M. Potapov, D. Yu. Chuvilin, P. A. Yunin, S. A. Gusev, M. Naumann; *Hydrogen reduction of $^{98}MoF_6$ in RF discharge;* J. Radioanal. Nucl. Chem. **309** (2016) 833 – 840

K. A. Kovalevsky, R. Kh. Zhukavin, V. V. Tsyplenkov, S. G. Pavlov, H.-W. Hübers, N. V. Abrosimov, V. N. Shastin; *Polarization of the induced THz emission of donors in silicon;* Semicond. **50** (2016) 1673 – 1677

F. Langhans, S. Kiefer, C. Hartmann, T. Markurt, T. Schulz, C. Guguschev, M. Naumann, S. Kollowa, A. Dittmar, J. Wollweber, M. Bickermann; *Precipitates originating from tungsten crucible parts in AlN bulk crystals grown by the PVT method;* Cryst. Res. Technol. **51** (2016) 129 – 136

Y. Luo, B. Damaschke, S. Schneider, G. Lohöfer, N. Abrosimov, M. Czupalla, K. Samwer; *Contactless processing of SiGe-melts in EML under reduced gravity;* npj Microgravity **2** (1) (2016) 1

S. Mohn, N. Stolyarchuk, T. Markurt, R. Kirste, M. P. Hoffmann, R. Collazo, A. Courville, R. Di Felice, Z. Sitar, P. Vennéguès, M. Albrecht; *Polarity control in group-III nitrides beyond pragmatism;* Phys. Rev. Appl. **5** (2016) 054004/1 – 054004/9

K. J. Morse, R. J. S. Abraham, D. P. Franke, N. V. Abrosimov, M. L. W. Thewalt; *Even-parity excited states of the acceptor boron in silicon revisited;* Phys. Rev. B **93** (2016) 125207/1 – 125207/8

M. Nazarzahdemoafi, F. Titze, S. Machulik, C. Janowitz, Z. Galazka, R. Manzke, M. Mulazzi; *Comparative study of the electronic structures of the In and Sn/In_2O_3(111) interfaces*; Phys. Rev. B **93** (2016) 081303/1 – 081303/5

F. Nippert, A. Nirschl, T. Schulz, G. Callsen, I. Pietzonka, S. Westerkamp, T. Kure, C. Nenstiel, M. Strassburg, M. Albrecht, A. Hoffmann; *Polarization-induced confinement of continuous hole-states in highly pumped, industrial-grade, green InGaN quantum wells;* J. Appl. Phys. **119** (2016) 215707/1 – 215707/6

S. G. Pavlov, N. Deßmann, A. Pohl, V. B. Shuman, L. M. Portsel, A. N. Lodygin, Yu. A. Astrov, S. Winnerl, H. Schneider, N. Stavrias, A. F. G. van der Meer, V. V. Tsyplenkov, K. A. Kovalevsky, R. Kh. Zhukavin, V. N. Shastin, N. V. Abrosimov, H.-W. Hübers; *Dynamics of nonequilibrium electrons on neutral center states of interstitial magnesium donors in silicon;* Phys. Rev. B **94** (2016) 075208/1 – 075208/8

Yu. M. Pokotilo, A. N. Petukh, V. V. Litvinov, V. P. Markevich, N. V. Abrosimov, A. S. Kamyshan, A. V. Giro, K. A. Solyanikova; *Formation of donors in germanium–silicon alloys implanted with hydrogen ions with different energies; Semicond.* **50** (2016) 1122 – 1124

F. Ringleb, K. Eylers, Th. Teubner, T. Boeck, C. Symietz, J. Bonse, S. Andree, J. Krüger, B. Heidmann, M. Schmid, M. Lux-Steiner; *Regularly arranged indium islands on glass/molybdenum substrates upon femtosecond laser and physical vapor deposition processing;* Appl. Phys. Lett. **108** (2016) 111904/1 – 111904/4

X. Rong, X. Wang, S. V. Ivanov, X. Jiang, G. Chen, P. Wang, W. Wang, C. He, T. Wang, T. Schulz, M. Albrecht, V. N. Jmerik, A. A. Toropov, V. V. Ratnikov, V. I. Kozlovsky, V. P. Martovitsky, P. Jin, F. Xu, X. Yang, Z. Qin, W. Ge, J. Shi, B. Shen; *High-output-power ultraviolet light source from quasi-2D GaN quantum structure*; Adv. Mater. **28** (2016) 7978 – 7983

Appendix: **Publications**

B. Sadovyi, A. Nikolenko, J. L. Weyher, I. Grzegory, I. Dziecielewski, M. Sarzynski, V. Strelchuk, B. Tsykaniuk , O. Belyaev, I. Petrusha, V. Turkevich, V. Kapustianyk, M. Albrecht, S. Porowski; *Diffusion of oxygen in bulk GaN crystals at high temperature and at high pressure;* J. Cryst. Growth **449** (2016) 35 – 42

M. Sander, A. Koc, C. T. Kwamen, H. Michaels, A. v. Reppert, J. Pudell, F. Zamponi, M. Bargheer, J. Sellmann, J. Schwarzkopf, P. Gaal ; *Characterization of an ultrafast Bragg-Switch for shortening hard x-ray pulses;* J. Appl. Phys. **120** (2016) 193101/1 – 193101/7

V. Scherer, C. Janowitz, Z. Galazka, M. Nazarzadehmoafi, R. Manzke; *Polaron character of the near-E_F band of cleaved In_2O_3 (111) single crystals;* EPL Journal **113** (2016) 26003/1 – 26003/6

R. Schewski, M. Baldini, K. Irmscher, A. Fiedler, T. Markurt, B. Neuschulz, T. Remmele, T. Schulz, G. Wagner, Z. Galazka, M. Albrecht; *Evolution of planar defects during homoepitaxial growth of ß-Ga_2O_3 layers on (100) substrates – A quantitative model*; J. Appl. Phys. **120** (2016) 225308/1 – 225308/8

P. Schönherr, F. Zhang, D. Kojda, R. Mitdank, M. Albrecht, S. F. Fischer, T. Hesjedal; *Free-standing millimetre-long Bi_2Te_3 sub-micron belts catalyzed by TiO_2 nanoparticles;* Nanoscale Res. Lett. **11** (2016) 308

J. Schwarzkopf, D. Braun, M. Hanke, A. Kwasniewski, J. Sellmann, M. Schmidbauer; *Monoclinic M_A domains in anisotropically strained ferroelectric $K_{0.75}Na_{0.25}NbO_3$ films on (110) $TbScO_3$ grown by MOCVD;* J. Appl. Cryst. **49** (2016) 375 – 384

S. Sintonen, S. Wahl , S. Richter, S. Meyer, S. Suihkonen, T. Schulz, K. Irmscher, A. N. Danilewsky, T. O. Tuomi, R. Stankiewicz, M. Albrecht; *Evolution of impurity incorporation during ammonothermal growth of GaN;* J. Cryst. Growth **456** (2016) 51 – 57

S. Sintonen, P. Kivisaari, S. Pimputkar, S. Suihkonen, T. Schulz, J. S. Speck, S. Nakamura; *Incorporation and effects of impurities in different growth zones within basic ammonothermal GaN;* *J. Cryst. Growth* **456** (2016) 43 – 50

J. Smalc-Koziorowska, C. Bazioti, M. Albrecht, G. P. Dimitrakopulos; *Stacking fault domains as sources of a-type threading dislocations in III-nitride heterostructures;* Appl. Phys. Lett. **108** (2016) 051901/1 – 051901-5

A. V. Soukhorukov, D. V. Guseinov, A. V. Kudrin, S. A. Popkov, A. P. Detochenko, A. V. Koroleva, A. A. Ezhevskii, A. A. Konakov, N. V. Abrosimov, H. Riemann; *The impurity spin-dependent scattering effects in the transport and spin resonance of conduction electrons in bismuth doped silicon;* Solid State Phenom. **242** (2016) 327 – 331

J. A. Steele, R. A. Lewis, J. Horvat, M. J. B. Nancarrow, M. Henini, D. Fan, Y. I. Mazur, M. Schmidbauer, M. E. Ware, S.-Q. Yu, G. J. Salamo; *Surface effects of vapour-liquid-solid driven Bi surface droplets fromed during molecular-beam-epitaxy of GaAsBi;* Sci. Rep. **6** (2016) 28860/1 – 28860/17

R. Stübner, Vl. Kolkovsky, J. Weber, N. V. Abrosimov; *Carbon-hydrogen complexes in n- and p-type SiGe-alloys studied by Laplace deep level transient spectroscopy;* Solid State Phenom. **242** (2016) 184 – 189

Y. Suhak, M. Schulz, H. Wulfmeier, W. L. Johnson, A. Sotnikov, H. Schmidt, S. Ganschow, D. Klimm, H. Fritze; *Langasite-type resonant sensors for harsh environments;* MRS Advances **1** (2016) 1513 – 1518

B. Süss, F. Ringleb, J. Heberle; *New ultrarapid-scanning interferometer for FT-IR spectroscopy with microsecond time-resolution;* Rev. Sci. Instrum. **87** (2016) 063113/1 – 063113/7

B. K. Tanner, J. Garagorri, E. Gorostegui-Colinas, M. R. Elizalde, D. Allen, P. J. McNally, J. Wittge, C. Ehlers, A. N. Danilewsky; *X-ray asterism and the structure of cracks from indentations in silicon;* J. Appl. Cryst. **49** (2016) 250 – 259

D. Wiedemann, S. Indris, M. Meven, B. Pedersen, H. Boysen, R. Uecker, P. Heitjans, M. Lerch; *Single-crystal neutron diffraction on γ-$LiAlO_2$: structure determination and estimation of lithium diffusion pathway;* Z. Kristallogr. **231** (2016) 189 – 193

H. Wulfmeier, A. Omelcenko, D. Albrecht, D. Klimm, W. El Mofid, M. Strafela, S. Ulrich, A. Bund, H. Fritze; *Thermal stability of materials for thin-film electrochemical cells investigated by thin-film calorimetry;* MRS Advances **1** (2016) 1043 – 1049

Appendix: **Talks and Posters**

Invited talks at national and international conferences

M. Albrecht; *Stain relaxation processes in heteroepitaxial growth (in memory of late Horst Strunk);* Extended Defects in Semiconductors; Les Issambres, France; September 2016

M. Albrecht; *Miscibility and phase separation in the $(In_xGa_{1-x})_2O_3$ system;* R. Schewski, T. Markurt, T. Schulz, Th. Remmele, G. Wagner, M. Baldini, H. von Wenckstern, M. Grundmann, M. Albrecht; Focused Session DPG March Meeting; Regensburg, Germany; March 2016

M. Albrecht; *Structure and properties of dislocations in III-Nitrides;* M. Albrecht, L. Lymperakis, J. Neugebauer; 18th International Conference on Crystal Growth and Epitaxy (ICCGE-18); Nagoya, Japan; August 2016

M. Baldini; *Homoepitaxial growth of β-Ga_2O_3 layers by MOVPE for power electronics applications;* 2nd AFRL Workshop on beta-Ga_2O_3 at BRICC; Arlington, VA, USA; December 2016

M. Baldini; *Semiconducting β-Ga_2O_3 layers grown by metal organic vapor phase epitaxy;* M. Baldini, M. Albrecht, A. Fiedler, Z. Galazka, K. Irmscher, R. Schewski, M. Schmidbauer, G. Wagner; Electronic Materials and Applications 2016; Orlando, FL, USA; January 2016

R. Bansen; *Growth of polycrystalline silicon on glass from tin and indium as solutions;* Energy, Materials, and Nanotechnology (EMN) Photovoltaics Meeting 2016; Hong Kong, China; January 2016

Ch. Frank-Rotsch; *Improvement of GaAs VGF process by using travelling magnetic fields;* Ch. Frank-Rotsch, N. Dropka, K. Giziewicz, A. Glacki, U. Juda; 18th International Conference on Crystal Growth (ICCGE-18); Nagoya, Japan; August 2016

Z. Galazka; *Advances in bulk crystal growth of transparent semiconducting oxides;* 18th International Conference on Crystal Growth (ICCGE-18); Nagoya, Japan; August 2016

Z. Galazka; *Bulk single crystals and properties of transparent semiconducting oxides;* E-MRS Fall Meeting 2016; Warsaw, Poland; September 2016

S. Ganschow; *Controlled oxygen fugacity environment for melt growth of oxide single crystals;* 10th International Conference of Polish Society for Crystal Growth (ICPSCG 10); Zakopane, Poland; October 2016

C. Guguschev; *Growth of $SrTiO_3$ bulk crystals by the EFG and TSSG methods;* C. Guguschev, Z. Galazka, D. J. Kok, U. Juda, R. Uecker, M. Bickermann; 18th International Conference on Crystal Growth and Epitaxy (ICCGE-18); Nagoya, Japan; August 2016

D. Klimm; *Eutectic halide systems: from basic to tricky;* Directionally Solidified Eutectic Ceramics V conference (DSEC V); Warsaw, Poland; April 2016

Invited seminars at national and international institutions

M. Albrecht; *Homoepitaxial growth of β-Ga_2O_3 studied by transmission electron microscopy;* Seminar CHREA; Valbonne, France; September 2016

M. Albrecht; *Polarity control in the growth of III-Nitride heterostructures;* Gedenkkolloquium zu Ehren von H. Strunk; Universität Stuttgart, Germany; September 2016

M. Baldini; *Transparent semiconducting β-Ga_2O_3 layers grown by metal organic vapor phase epitaxy;* "Science & Coffee" seminar series, OSRAM Opto Semiconductors GmbH; Regensburg, Germany; April 2016

R. Bertram; *Kristallzüchtung und Analyse;* Anwendertreffen ICP OES 2016; Hannover, Germany; November 2016

M. Bickermann; *Atomic scale mechanisms and morphology evolution in crystal growth*; Vorlesung auf der „BaCaTec-Sommerschule über ammonothermale Kristallzüchtung" der DFG-Forschergruppe „AmmonoFOR"; Universität Erlangen, Germany; July 2016

M. Bickermann; *Perfekte Substrate für elektronische Bauelemente: Oxid- und Nitrid-Kristallzüchtung am IKZ*; Seminar der Arbeitsgruppe Prof. Grundmann, Halbleiterphysik Universität Leipzig, Germany; November 2016

M. Bickermann; *UVC-transparente Substrate aus Aluminiumnitrid (AlN) mit hoher struktureller Qualität für optoelektronische Bauelemente*; Vortrag im Seminar Festkörperphysik im Freiburger Materialforschungszentrum (FMF); Freiburg/Breisgau, Germany; January 2016

M. Bickermann; *UVC-transparente Substrate aus Aluminiumnitrid (AlN) mit hoher struktureller Qualität für optoelektronische Bauelemente*; Vortrag im Physikalischen Colloquium, TU Bergakademie Freiberg/Sachsen, Germany; July 2016

Appendix: **Talks and Posters**

M. Bickermann; *Züchtung von Volumenkristallen aus Halbleitern großer Bandlücke aus der Gasphase am Beispiel AlN – UVC-transparente Substrate aus Aluminiumnitrid (AlN) mit hoher struktureller Qualität für optoelektronische Bauelemente*; Vortrag im Materialforum Rhein-Main des Vereins Materials Valley e.V.; Hanau, Germany; January 2016

D. Braun; *Monoclinic domains in $K_xNa_{1-x}NbO_3$ on rare earth scandate substrates;* D. Braun, M. Schmidbauer, M. Hank, C. Feldt, L. v. Helden, J. Schwarzkopf; Kolloquium, Zernike Institute for Advanced Materials; University of Groningen, Netherlands; September 2016

D. Klimm; *Oxide crystal growth at IKZ Berlin;* Kolloquium Helmholtz-Zentrum Berlin, Germany; June 2016

D. Klimm; *Seltenerd-Scandiumoxid-Systeme: Phasendiagramme und Kristallzüchtung;* Praxistag Thermische Analyse für Hochtemperatur-Anwendungen; Dresden, Germany; June 2016

R. Zwierz; *Pseudo halide vapor phase epitaxy-growth of GaN layers*; R. Zwierz, K. Kachel, S. Golka, D. Siche, M. Bickermann; Technische Universität Berlin, Arbeitskreis Hoffmann; Berlin, Germany; February 2016

Oral contributions at national and internationals conferences and workshops

M. Albrecht; *Homoepitaxial growth of β-Ga_2O_3 studied by transmission electron microscopy*; R. Schewski, T. Markurt, T. Schulz, Th. Remmele, G. Wagner, M. Baldini, H. von Wenckstern, M. Grundmann, M. Albrecht; German-Japanese Gallium Oxide Technology Meeting; IKZ Berlin, Germany; September 2016

M. Baldini; *Si- and Sn-doped homoepitaxial β-Ga_2O_3 layers grown by MOVPE on different substrate orientations;* M. Baldini, M. Albrecht, A. Fiedler, Z. Galazka, K. Irmscher, R. Schewski, G. Wagner; German-Japanese Gallium Oxide Technology Meeting 2016; IKZ Berlin, Germany; September 2016

M. Baldini; *Semiconducting homoepitaxial β-Ga_2O_3 layers grown by MOVPE for power device applications;* M. Baldini, M. Albrecht, A. Fiedler, Z. Galazka, K. Irmscher, R. Schewski, G. Wagner; 18th International Conference on Metal Organic Vapor Phase Epitaxy (ICMOVPE-XVIII); San Diego, CA, USA; July 2016

R. Bansen; *SiGe-Nanodrähte für Thermoelektrika;* Naturwissenschaftstage Lausitz 2016; Senftenberg, Germany; May 2016

M. Bickermann; *Epitaxial growth and characterization of deep UV AlGaN devices on bulk AlN substrates;* M. Bickermann, C. Hartmann, A. Knauer, J. Wollweber, K. Irmscher, T. Schulz, S. Sintonen, A. Dittmar, J. Jeschke, C. Kuhn, M. Guttmann, M. Martens, L. Sulmoni, T. Wernicke, K. Peters, M. Weyers, M. Kneissl; International Workshop on Nitride Semiconductors (IWN 2016); Orlando, FL, USA; October 2016

D. Braun; *Coexistence of monoclinic domains in $K_xNa_{1-x}NbO_3$ on $NdScO_3$ grown with MOCVD;* D. Braun, M. Schmidbauer, M. Hanke, J. Schwarzkopf; 2016 Joint IEEE International Symposium on the Applications of Ferroelectrics, European Conference on Applications of Polar Dielectrics & Workshop on Piezoresponse Force Microscopy (ISAF/ECAPD/PFM); Darmstadt, Germany; August 2016

I. Buchovska; *The influence of travelling magnetic field on phosphorus distribution in n-type multicrystalline silicon;* I. Buchovska, N. Dropka, S. Kayser, F. M. Kiessling; DGKK Arbeitskreis „Massive Halbleiterkristalle"; Erlangen, Germany; October 2016

N. Dropka; *Optimization of TMF driven directional solidification of silicon by artificial intelligence;* N. Dropka and F. M. Kiessling; 18th International Conference on Crystal Growth and Epitaxy (ICCGE-18); Nagoya, Japan; August 2016

C. Ehlers; *Growth of silicon on porous silicon and glass substrates from Sn solution;* C. Ehlers, R. Bansen, D. Uebel, T. Markurt, Th. Teubner, T. Boeck; 26th International Photovoltaic Science and Engineering Conference (PVSEC-26); Singapore, Republic of Singapore; October 2016

C. Ehlers; *Properties of Crystalline Silicon Layers grown on Glass for Photovoltaic Applications;* C. Ehlers, R. Bansen, T. Teubner, T. Markurt, K. Irmscher, A. Fiedler, T. Boeck; 1st German Czechoslovak Conference on Crystal Growth (GCCCG-1 / DKT2016); Dresden, Germany; March 2016

A. Fielder; *Influence of incoherent twin boundaries on the electrical properties of β-Ga_2O_3 layers homoepitaxially grown by metal-organic vapor phase epitaxy;* A. Fiedler, R. Schewski, M. Baldini, Z. Galazka, G. Wagner, M. Albrecht, K. Irmscher; DPG Spring Meeting; Regensburg, Germany; March 2016

A. Fiedler; *Influence of incoherent twin boundaries on the electrical properties of β-Ga_2O_3 layers homoepitaxially grown by metal-organic vapor phase epitaxy;* A. Fiedler, R. Schewski, M. Baldini, Z. Galazka, G. Wagner, M. Albrecht, K. Irmscher; E-MRS Fall Meeting; Warsaw, Poland; September 2016

Appendix: **Talks and Posters**

Z. Galazka; *Growth of bulk β-Ga_2O_3 single crystals by the Czochralski method*; German-Japanese Gallium Oxide Technology Meeting 2016; IKZ Berlin, Germany; September 2016

C. Guguschev; *Microstructural investigations of $SrTiO_3$ single crystals and multicrystalline silicon using a powerful new X-ray diffraction surface mapping technique;* C. Guguschev, R. Tagle, U. Juda , A. Kwasniewski, T. Ervik, R. Uecker, S. Kayser, F. M. Kiessling, M. Bickermann; 18th International Conference on Crystal Growth and Epitaxy (ICCGE-18); Nagoya, Japan; August 2016

C. Guguschev; *Microstructural investigations of $SrTiO_3$ single crystals and multicrystalline silicon using a powerful new X-ray diffraction surface mapping technique;* C. Guguschev, R. Tagle, U. Juda , A. Kwasniewski, T. Ervik, R. Uecker, S. Kayser, F. M. Kiessling, M. Bickermann; 1st German Czechoslovak Conference on Crystal Growth (GCCCG-1/DKT2016); Dresden, Germany; March 2016

C. Hartmann; *Strongly improved UV transparency of bulk AlN crystals by impurity gettering during the PVT process;* C. Hartmann, J. Wollweber, A. Dittmar, S. Sintonen, S. Kollowa, K. Irmscher, M. Bickermann; E-MRS Fall Meeting; Warsaw, Poland; September 2016

L. v. Helden; *Domain evolution in compressively strained $K_{0.7}Na_{0.3}NbO_3$ epitaxial films on $TbScO_3$ substrates;* L. v. Helden, D. Braun, M. Schmidbauer, M. Hanke, C. Feldt, J. Schwarzkopf; E-MRS Fall Meeting; Warsaw, Poland; September 2016

K. Irmscher; *Electrical and optical characterization of β-Ga_2O_3 bulk crystals;* K. Irmscher, A. Fiedler, M. Naumann, R. Schewski, T. Schulz, M. Pietsch, Z. Galazka; German-Japanese Gallium Oxide Technology Meeting 2016; IKZ Berlin, Germany; September 2016

F. Kamutzki; *The influence of oxygen partial pressure in the growth atmosphere on the coloration of $SrTiO_3$ single crystal fibers;* F. Kamutzki, C. Guguschev, D. J. Kok, R. Bertram, U. Juda, R. Uecker; 1st German Czechoslovak Conference on Crystal Growth (GCCCG-1/DKT2016); Dresden, Germany; March 2016

F. M. Kiessling; *TMF assisted control of s/l interface during DS growth of G2-size quasi-mono Si;* F. M. Kiessling, N. Dropka, Ch. Frank-Rotsch, T. Ervik, D. Linke, R. Menzel, T. Richter, L. Sylla; 9th International Workshop on Crystalline Silicon for Solar Cells (CSSC-9); Phoenix, AZ, USA; October 2016

R. Menzel; *Experimental setup for new crucible-free growth concept for Si*; R. Menzel, N. V. Abrosimov, H. Riemann, F. M. Kiessling; 9th International Workshop on Crystalline Silicon for Solar Cells (CSSC-9); Phoenix, AZ, USA; October 2016

W. Miller; *Evolution of grains during solidification of silicon – attempts of numerical simulations for an understanding;* W. Miller, X. F. Qi, A. Popescu; 18th International Conference on Crystal Growth an Epitaxy (ICCGE-18); Nagoya, Japan; August 2016

W. Miller; *Temperature and stress distribution during growth of ß-Ga_2O_3 single crystals by the Czochralski method: numerical calculations*; W. Miller, K. Böttcher, Z. Galazka, J. Schreuer; 18th International Conference on Crystal Growth an Epitaxy (ICCGE-18); Nagoya, Japan; August 2016

W. Miller; *The relation between interface attachment kinetics, capillarity and heat transfer and evolving Czochralski grown oxide crystal shapes;* W. Miller, O. Weinstein, S. Brandon; 18th International Conference on Crystal Growth an Epitaxy (ICCGE-18); Nagoya, Japan; August 2016

W. Miller; *Convection related to crystal growth: Peculiarities and challenges;* W. Miller, K. Böttcher; 1st Leibniz "Mathematische Modellierung und Simulation (MMS)" Mini Workshop; Berlin, Germany; September 2016

X. Qi; *Numerical modeling of grain evolution in directional solidification of silicon;* X. Qi, W. Miller, L. Liu; 18th International Conference on Crystal Growth an Epitaxy (ICCGE-18); Nagoya, Japan; August 2016

T. Schulz*; Limitations for indium incorporation in coherently grown (In,Ga)N layers*; International Workshop on Nitride Semiconductors (IWN 2016); Orlando, FL, USA; October 2016

J. Schwarzkopf; *Variable arrangement of domain walls in monoclinic $K_{0.9}Na_{0.1}NbO_3$ epitaxial films on $NdScO_3$ substrates;* J. Schwarzkopf, D. Braun, T. Markurt, M. Hanke, M. Schmidbauer; DPG-Frühjahrstagung; Regensburg, Germany; March 2016

J. Sellmann; *Effect of doping in ferroelectric $K_{0.5}Na_{0.5}NbO_3$ thin films on $DyScO_3$ substrates grown by PLD;* J. Sellmann, P. Kehne, D. Braun, L. v. Helden, C. Feldt, A. Kwasniewski, M. Schmidbauer, J. Schwarzkopf; 2016 Joint IEEE International Symposium on the Applications of Ferroelectrics, European Conference on Applications of Polar Dielectrics & Workshop on Piezoresponse Force Microscopy (ISAF/ECAPD/PFM); Darmstadt, Germany; August 2016

Appendix: **Talks and Posters**

D. Siche; *GaN:C thick layers grown with the use of HCN precursor gas;* D. Siche, R. Zwierz, K. Kachel, K. Irmscher, N. Jankowski, G. Callsen, M. Bickermann, A. Hoffmann; 10th International Conference of Polish Society for Crystal Growth (ICPSCG 10); Zakopane, Poland; October 2016

S. Sintonen; *Dislocation generation during homoepitaxial growth of bulk AlN by physical vapour transport;* S. Sintonen, C. Hartmann, J. Wollweber, M. Naumann, M. Bickermann, M. Albrecht; International Workshop on Nitride Semiconductors (IWN 2016); Orlando, FL, USA; October 2016

S. Sintonen; *Generation of dislocations at the substrate interface during homoepitaxial growth of bulk AlN by physical vapour transport;* S. Sintonen, C. Hartmann, J. Wollweber, M. Naumann, M. Bickermann, M. Albrecht; E-MRS Fall Meeting; Warsaw, Poland; September 2016

G. Wagner; *Homoepitaxial growth of semiconducting β-Ga_2O_3 thin layers by metal organic vapor phase epitaxy;* G. Wagner, M. Baldini, A. Fiedler, K. Irmscher, R. Schewski, M. Albrecht, Z. Galazka; 58th Electronic Materials Conference (EMC), University of Delaware; Newark, USA; June 2016

N. Wolff; *Growth of delafossite substrate crystals;* N. Wolff, D. Siche, D. Schulz, D. Klimm; 5th French-German Workshop on Oxide, Dielectric and Laser Crystals 2016; IKZ Berlin, Germany; September 2016

Contribution as co-authors

S. Brandon; *Facets, capillarity and heat transfer during oxide growth from the melt;* S. Brandon, O. Weinstein, W. Miller; 1st German Czechoslovak Conference on Crystal Growth (GCCCG-1/DKT2016); Dresden, Germany; March 2016

B. Heidmann; *Locally grown CISe micro-absorbers;* B. Heidmann, F. Ringleb, K. Eylers, Ch. Symietz, S. Andree, J. Krüger, S. Levcenco, T. Unold, T. Boeck, M. Lux-Steiner, M. Schmid; 20th International Conference on Ternary and Multinary Compounds (ICTMC-20); Halle/Saale, Germany; September 2016

M. Pillaca; *Inclined Rotary Bridgman method for forced convection in growing $FeSb_2$ and $CoSb_3$ from Sb-rich solutions;* M. Pillaca, W. Miller, P. Gille; 18th International Conference on Crystal Growth and Epitaxy (ICCGE-18); Nagoya, Japan; August 2016

Poster presentations at national and international conferences

R. Bansen, Th. Teubner, T. Boeck; *Si, Ge, and SiGe nanowires for thermoelectrics;* German MBE workshop 2016; Garching, Germany; October 2016

D. Braun, M. Schmidbauer, M. Hanke, J. Schwarzkopf; *Poling of monoclinic domains in $K_{0.9}Na_{0.1}NbO_3$ thin films grown on $NdScO_3$;* 2016 Joint IEEE International Symposium on the Applications of Ferroelectrics, European Conference on Applications of Polar Dielectrics & Workshop on Piezoresponse Force Microscopy (ISAF/ECAPD/PFM); Darmstadt, Germany; August 2016

I. Buchovska, N. Dropka, S. Kayser, F. M. Kiessling; *Segregation effects during growth of n-Type multicrystalline silicon using travelling magnetic fields;* 18th International Conference on Crystal Growth and Epitaxy (ICCGE-18); Nagoya, Japan; August 2016

N. Dropka, F. M. Kiessling; *Optimization of magnetic parameters in magnetic driven directional solidification of silicon by artificial neural networks;* 10th PAMIR International Conference Fundamental and Applied MHD; Cagliari, Sardinia; Italy; June 2016

C. Ehlers, R. Bansen, T. Markurt, D. Uebel, Th. Teubner, T. Boeck; *Solution growth on reorganized porous Si foils and on glass substrates;* 18th International Conference on Crystal Growth and Epitaxy (ICCGE-18); Nagoya, Japan; August 2016

C. Ehlers, R. Bansen, Th. Teubner, T. Markurt, K. Irmscher, A. Fiedler, T. Boeck; *Properties of crystalline silicon layers grown on glass for photovoltaic applications;* 5th Seminar of the „Junge DGKK" on current research projects in crystal growth and epitaxy; Dresden, Germany; March 2016

K. Eylers, F. Ringleb, B. Heidmann, Ch. Symietz, J. Bonse, S. Andree, Th. Teubner, J. Krüger, M. Schmid, T. Boeck; *CISe micro-absorber islands for concentrator photovoltaic applications;* PhotoVoltaic Technical Conference (PVTC 2016); Marseille, France; May 2016

A. Fiedler, R. Schewski, M. Baldini, Z. Galazka, G. Wagner, M. Albrecht, K. Irmscher; *Influence of incoherent twin boundaries on the electrical properties of β-Ga_2O_3 layers homoepitaxially grown by metal-organic vapor phase epitaxy;* German-Japanese Gallium Oxide Technology Meeting 2016, Berlin; IKZ Berlin, Germany; September 2016

Appendix: **Talks and Posters**

C. Guguschev, Z. Galazka, D. J. Kok, U. Juda, R. Uecker, M. Bickermann; *Growth of $SrTiO_3$ bulk crystals by the EFG method;* 1st German Czechoslovak Conference on Crystal Growth (GCCCG-1); Dresden, Germany; March 2016

C. Hartmann, J. Wollweber, K. Irmscher, A. Dittmar, T. Schulz, S. Sintonen, S. Kollowa, M. Bickermann; *Strongly enhanced deep UV transparency of AlN bulk crystals grown by physical vapor transport;* International Workshop on Nitride Semiconductors (IWN 2016); Orlando, FL, USA; October 2016

B. Heidmann, F. Ringleb, K. Eylers, J. Bonse, S. Andree, J. Krüger, S. Levcenco, Th. Unold, T. Boeck, M. Lux-Steiner, M. Schmid; *Local Growth of $CuInSe_2$ Micro-Absorbers;* 20th International Conference on Ternary and Multinary Compounds (ICTMC-20); Halle/Saale, Germany; September 2016

M. Herms, M. Wagner, S. Kayser, F.M. Kießling, A. Poklad, M. Zhao, U. Kretzer; *Photo-elastic characterization of defect structures in mono and multi-crystalline semiconductor materials;* Extended Defects in Semiconductors; Les Issambres, France; September 2016

D. Klimm; *Substrates with tuned lattice parameters for ferroic oxides;* Materials Research Society Fall Meeting; Boston, MA, USA; November/December 2016

W. Miller, K. Böttcher, Z. Galazka, J. Schreuer; *Temperature and stress distribution during growth of ß-Ga_2O_3 single crystals by the Czochralski method: numerical calculations*; German-Japanese Gallium Oxide Technology Meeting 2016; IKZ Berlin, Germany; September 2016

M. Pillaca, W. Miller, P. Gille; *Inclined Rotary Bridgman method for growing Sb-based binary compounds*; 1st German Czechoslovak Conference on Crystal Growth (GCCCG-1/DKT2016), Dresden, Germany; March 2016

F. Ringleb, K. Eylers, Th. Teubner, H.-P. Schramm, T. Boeck, S. Andree, J. Bonse, J. Krüger, B. Heidmann, M. Schmid; *Indium island growth on molybdenum at micro-roughened spots created by femtosecond laser pulses;* E-MRS Spring Meeting; Lille, France; May 2016

F. Roca, D. Casaburi, F. Beone, K. Bittkau, A. Hoffmann, I. Lauermann, M. C. Lux-Steiner, M. Schmid, P. Malbranche, I. T. Theologitis, N. Taylor, J. M. Kroon, P. M. Sommeling, M. Drießen, I. Gordon, K. Van Nieuwenhuysen, S. A. Gevorgyan, S. Binetti, S. Buecheler, C. del Cañizo, A. di Carlo, M. Grossberg, G. Halambalakis, A. Joyce, E. Lotter, E.-J. Øvrelid, E. Román, F. Ringleb, G. Sánchez-Plaza, J. F. Trigo, R. Turan, N. Wyrsch, S. Zamini; *Innovation Brought by FP7-CHEETAH Project in Management of Knowledge Exchange for PV RTD;* 32nd European Photovoltaic Solar Energy Conference and Exhibition (EU PVSEC 2016); Munich, Germany; June 2016

J. Schwarzkopf, D. Braun, M. Hanke, C. Feldt, M. Schmidbauer; *Variation of domain wall angles and periodicity in monoclinic $K_{0.95}Na_{0.05}NbO_3$ epitaxial films on $NdScO_3$ substrates;* Kavli Royal Society Centre; Buckinghamshire, United Kingdom; February 2016

S. Sintonen, S. Wahl , S. Richter, S. Meyer, S. Suihkonen, T. Schulz, K. Irmscher, A. N. Danilewsky, T. O. Tuomi, R. Stankiewicz, M. Albrecht; *On the impurity incorporation evolution during growth of ammonothermal GaN;* 1st German Czechoslovak Conference on Crystal Growth (GCCCG-1); Dresden, Germany; March 2016

R. Zwierz, D. Siche, K. Kachel, S. Golka, M. Bickermann, N. Jankowski, A. Hoffmann; *Vapour phase epitaxy of thick GaN:C layers using HCN precursor gas;* E-MRS Fall Meeting; Warsaw, Poland; September 2016

Appendix: **Patents**

Granted

S. Ganschow, R. Bertram, D. Klimm, P. Reiche, R. Uecker
Verfahren und Anordnung zur Herstellung von ZnO-Einkristallen
DE 10 2004 003 596.2

Ch. Frank-Rotsch, P. Rudolph, R.-P. Lange, O. Klein, B. Nacke
Vorrichtung und Verfahren zur Herstellung von Kristallen aus elektrisch leitenden Schmelzen
DE 10 2007 028 548.7
08784553.3 (DK, ES, FR, NO)
KRIST*MAG*®

R.-P. Lange, M. Ziem, D. Jockel, P. Rudolph, F. Kießling, Ch. Frank-Rotsch, M. Czupalla, B. Nacke, H. Kasjanow
Vorrichtung zur Herstellung von Kristallen aus elektrisch leitenden Schmelzen
DE 10 2007 028 547.9
08784554.1 (DK, ES, FR, NO)
KRIST*MAG*®

Ch. Frank-Rotsch, P. Rudolph, R.-P. Lange, D. Jockel
Vorrichtung und Verfahren zur Herstellung von Kristallen aus elektrisch leitenden Schmelzen
DE 10 2007 046 409.8
KRIST*MAG*®

P. Rudolph, M. Ziem, R.-P. Lange
Vorrichtung zum Züchten von Einkristallen aus elektrisch leitfähigen Schmelzen
DE 10 2007 020 239.5
KRIST*MAG*®

R. Fornari, S. Ganschow, D. Klimm, M. Neubert, Schulz
Verfahren und Vorrichtung zur Herstellung von Zinkoxid-Einkristallen aus einer Schmelze
DE 10 2007 006 731.5

P. Rudolph, M. Ziem, R.-P. Lange, D. Jockel
Vorrichtung zur Herstellung von Kristallen aus elektrisch leitenden Schmelzen
DE 10 2008 035 439.2

F. Büllesfeld, U. Sahr, W. Miller, P. Rudolph, U. Rehse, N. Dropka
Verfahren zum Erstarren einer Nichtmetall-Schmelze
DE 10 2008 059 521.7
09 749 132.8 (DK, ES, IT, NO, R, GB)

R. Fornari
Vorrichtung und Verfahren zur Züchtung von III-Nitrid-Volumenkristallen
08 161 254.1 (DE, PL, FR, GB, SE)

P. Rudolph, R.-P. Lange, M. Ziem
Vorrichtung zur Herstellung von Sililziumblöcken
DE 10 2009 045 680.5

N. Dropka, P. Rudolph, U. Rehse
Verfahren und Anordnung zur Herstelllung von Kristallblöcken von hoher Reinheit und dazugehörige Kristallisationsanlage
DE 10 2010 028 173.5

H. Riemann, N. Abrosimov, J. Fischer, M. Renner
Verfahren und Vorrichtung zur Herstellung von Einkristallen aus Halbleitermaterial
EP 2 504 470 (NO, ES, NL, FR, DK, GB, BE, IT)

N. Dropka, Ch. Frank-Rotsch, M. Ziem, P. Lange
Verfahren und Vorrichtung zur gerichteten Kristallisation von Kristallen aus elektrisch leitenden Schmelzen
DE 10 2012 204 313.6

N. Dropka, Ch. Frank-Rotsch, P. Rudolph, R.-P. Lange, U. Rehse
Kristallisationsanlage und Kristallisationsverfahren zur Herstellung eines Blocks aus einem Material, dessen Schmelze elektrisch leitend ist
DE 10 2010 041 061.6

O. Klein, F. Kießling, M. Czupalla, P. Rudolph, R.-P. Lange, B. Lux, W. Miller, M. Ziem, F. Kirscht
Verfahren und Vorrichtung zur Züchtung von Kristallen aus elektrisch leitenden Schmelzen, die in der Diamant- oder Zinkblendestruktur kristallisieren
DE 10 2009 027 436.7

H. Riemann, N. Abrosimov, J. Fischer, M. Renner
Verfahren und Vorrichtung zur Herstellung von Einkristallen aus Halbleitermaterial
DE 10 2010 052 522.7
10801372.3 (EP), 13/511,751 (US), 2012-540285 (JP)

F. Kießling, Ch. Frank-Rotsch, N. Dropka, P. Rudolph
Verfahren zur gerichteten Kristallisation von Ingots
DE 10 2011 076 860.2

Appendix: **Patents**

Pending

U. Rehse, P. Rudolph, W. Miller, N. Dropka,
F. Büllesfeld, U. Sahr
Method for the solidification of a non-metal melt
W00020120608O2A3 (CN, US, TW)

R. Fornari, F. Kießling, P. Rudolph, V. Trautmann
Kristallisationsanlage und Kristallisationsverfahren
DE 10 2009 046 845.5

T. Boeck, R. Fornari, R. Heimburger, G. Schadow,
J. Schmidtbauer, H.-P. Schramm, T. Teubner
Kristallisationsverfahren zur Erzeugung kristalliner Halbleiterschichten
DE 10 2010 044 014.0

Z. Galazka, R. Uecker, R. Fornari
Method and apparatus for growing indium oxide (In203) single crystals and indium oxide (In203) single crystal
PCT/EP2012/057447

M .Wünscher, H. Riemann
Vorrichtung für das tiegelfreie Zonenziehen von Kristallstäben
DE 10 2012 022 958.8
PCT/DE2013/000627

N. Dropka, Ch. Frank-Rotsch, P. Lange, P. Krause
Kristallisationsanlage und Kristallisationsverfahren zur Kristallisation aus elektrisch leitenden Schmelzen sowie über das Verfahren erhältliche Ingots
DE 10 2013 211 769.8
PCT/EP2014/059684

A. Dittmar, C. Hartmann, J. Wollweber,
U. Degenhardt, F. Stegner
Keimhalter einer Einkristallzüchtungsvorrichtung, Einkristallzüchtungsvorrichtung und Kompositwerkstoff
DE 10 2014 017 021.7

Z. Galazka, R. Uecker, D. Klimm, M. Bickermann
Method for growing beta phase of gallium oxide (ß-Ga203) single crystals from the melt contained within a metal crucible
EP 15150582.3, PCT/EP2015/079938

A. Dittmar, C. Hartmann, J. Wollweber, M. Bickermann
(Sc, Y): Einkristalle für Gitter-angepasste AlGaN Systeme
DE 10 2015 116 068.4, PCT/EP2016/070539

Registered Trademark

KRIST*MAG*®

Appendix: **Teaching and Education**

Prof. Dr. Matthias Bickermann
- *Kristallzüchtung II: Methoden und Anwendungen*; Technische Universität Berlin, Institut für Chemie, WS 2015/16 und WS 2016/17
- *Kristallzüchtung I: Grundlagen und Methoden;* Technische Universität Berlin, Institut für Chemie, SS 2016
- Forschungspraktikum: Betreuung von Studienenden am IKZ Technische Universität Berlin, Institut für Chemie

PD Dr. habil. Detlef Klimm
- *Phasendiagramme*; Humboldt-Universität zu Berlin, Institut für Chemie, WS 2015/16 und WS 2016/17
- Versuch „*Phasendiagramme*" im Fortgeschrittenen-Praktikum Physik
- Humboldt-Universität zu Berlin, WS 2015/16, SS 2016 und WS 2016/17

Dr. habil. Martin Schmidbauer
- *Röntgenstreuung: Grundlagen und Anwendungen in der Materialwissenschaft*; Humboldt-Universität zu Berlin, Institut für Physik, WS 2015/16, SS 2016 und WS 2016/17

apl. Prof. Dr. Dietmar Siche
- *Kristallzüchtung*; Brandenburgische Technische Universität Cottbus-Senftenberg, Blockseminar SS 2016

Doctoral theses (ongoing)

Mariia Anikeeva
Transmission Electron Microscopy of Short Period Superlattices for Rational (In,Ga)N

Dorothee Braun
Ferro- und piezoelektrische Charaktersierungen von bleifreien Perowskitschichten

Christian Ehlers
Wachstum und Charakterisierung von Silizium aus Zinn Lösungen für die Photovoltaik

Katharina Eylers
Wachstum und Charakterisierung von Cu(In,Ga)Se_2 Absorbern für Mikrokonzentratorsolarzellen

Andreas Fiedler
Electrical and Optical Characterization of the Transparent Semiconducting Oxide beta-Ga_2O_3

Leonard von Helden
Characterization of Domain Structures in Strained Ferroelectric $Ka_{1-x}Na_xNbO_3$ Thin Films

Stefan Kayser
Charakterisierung mono- und multikristalliner Halbleiter wie SiGe, Si, Ge_{1-x} und GaAs mit LPS- und SPL-Methoden

Dirk Kok
Einfluss der Züchtungsbedingungen auf die Realstruktur von $SrTiO_3$

Sandro Kollowa
Dotierung und Kompensation bei der Sublimations-züchtung von AlN-Volumenkristallen

Stefan Mohn
Elektronenmikroskopische Charakterisierung von hetero-polaren Nitrid-Nitrid und Nitrid-Oxid Grenzflächen

Joanna Moneta
Transmission Electron Microscopy of Short Period Superlattices for Rational (In, Ga)N

Lena Schmack
New Ferroelectric Single Crystals:
A Study of the $LiNb_{1-x}{\cdot}Ta_x\ O_3$ Solid Solution

Appendix: **Teaching and Education**

Robert Schewski
Wachstum und Relaxation von Gruppe III Sesquioxiden

Natalia Stolyarchuk
Investigation of III-Nitride/Oxide Interfaces of Atomic Scale

Nora Wolff
Züchtung von Delafossit-Substratkristallen

Charlotte Wouters
Transmission Electron Microscopy Studies on Phase Formation in Group III-Sesquioxides

Doctoral theses (completed)

Roman Bansen
Solution Growth of Polycrystalline Silicon on Glass using Tin and Indium as Solvents
Humboldt-Universität zu Berlin, Institut für Physik

Frank Langhans
Extended defects in PVT-grown AlN
Technische Universität Berlin, Fakultät II, Mathematik und Naturwissenschaften

Diploma, Master and bachelor theses (completed)

Igor Erdle, Bachelor
Aluminiumnitrid-Züchtung nach dem Vapour-Liquid-Solid-Mechanismus
Technische Universität Berlin,
Fachbereich Werkstoffwissenschaften

Christoph Feldt, Master
Impact of Sodium Excess on Electric and Structural Properties of Compressively Strained $NaNbO_3$ Thin Films
Technische Universität Berlin, Institut für Chemie

Tamino Hirsch, Master
Phasenbeziehungen im System $NdLuO_3$-$NdScO_3$
Technische Universität Bergakademie Freiberg

Frederike Lehmann, Master
Dotieren von Aluminiumnitrid mit Scandium bei der Gasphasenzüchtung
Universität Potsdam, Institut für Chemie

Linda Schwarz, Bachelor
Thermoanalytische Untersuchungen zum Inversionsgrad von Spinellen
Humboldt-Universität zu Berlin

Stefan Spitzer, Master
Aufbau eines UV-Transmissionsmessplatzes zur Analyse von AlN-Wafern
Beuth Hochschule Berlin

Oliver Reetz, Master
Untersuchungen zur Thermodynamik und Kristallzüchtung des Delafossits $CuAlO_2$
Brandenburgische Technische Universität Cottbus-Senftenberg

Professional Education at IKZ (completed)

Jacques-Willi Boerner
Elektroniker für Betriebstechnik
Electronics technician

Alexander Naumann
Fachinformatiker für Systemintegration
IT systems integration specialist

Sarah Sefrin
Kauffrau für Bürokommunikation
Office administrator

Appendix: **Membership in Committees**

Committees

Dr. Rainer Bertram
- DIN – Deutsches Institut für Normung e.V. – NA 062 – Normenausschuss Materialprüfung (NMP), member

Prof. Dr. Matthias Bickermann
- IGAFA e.V. – Initiativgemeinschaft Außeruniversitärer Forschungseinrichtungen in Adlershof e.V., member of the board

Dr. Natascha Dropka
- European Commission 2016, evaluator/external expert

Dr. Christiane Frank-Rotsch
- Deutsche Gesellschaft für Kristallzüchtung und Kristallwachstum (DGKK), secretary
- International Organization for Crystal Growth (IOCG), member of the council
- European Network of Crystal Growth (ENCG), member of the council

PD Dr. habil. Detlef Klimm
- Commission on Crystal Growth and Characterization of Materials (IUCr), member

Dr. Wolfram Miller
- Deutsche Gesellschaft für Kristallzüchtung und Kristallwachstum (DGKK), chairman
- European Network of Crystal Growth (ENCG), coordinator

Editorial committees

Prof. Dr. Matthias Bickermann
- Progress in Crystal Growth and Characterization of Materials, Elsevier, associate editor
- Physica Status Solidi A, Proceeding E-MRS Fall Meeting – Symposium F, Warsaw, Poland, September 2016, guest editor
- Journal of Crystal Growth, Proceeding Conference ICCGE-18, Nagoya, Japan, August 2016, guest editor

apl. Prof. Dr. Dietmar Siche
- Crystal Research & Technology, editorial board

Conference committees

Prof. Dr. Matthias Bickermann
- International Workshop on Nitride Semiconductors (IWN), Orlando, FL, USA, October 2016, member of program committee and topical committee for bulk growth
- E-MRS Fall Meeting, Warsaw, Poland, September 2016, Symposium organizer: AlN and AlGaN Materials and Devices (Symposium F)
- French-German Workshop on Oxide Dielectric, and Laser Crystals (DGKK Arbeitskreis Kristalle für Laser und Nichtlineare Optik); IKZ Berlin, Germany, September 2016, conference organizer
- German-Japanese Gallium Oxide Technology Meeting, IKZ Berlin, Germany, October 2016, conference organizer
- 18th International Conference on Crystal Growth and Epitaxy (ICCGE), August 2016, Nagoya, Japan; member of program-committee

Appendix: **Guest Scientists at the IKZ**

01.01.2016 – 31.12.2016

Prof. Dr. Liu Feng
10.10. – 14.10.2016
China Electronics Technology Group
Corporation No. 46 Research Institute, Tianjin,
People's Republic of China

Prof. Dr. Kozo Fujiwara
08.11. – 26.11. 2016
Tohoku University Sendai,
Japan

Julia Pinina
01.08. – 23.09.2016
Moscow Institute of Physics and Technology,
Russia

Xiofang Qi
01.10. 2015 – 30.09.2016
School of Energy and Power Engineering, Xi'an, Shaanxi,
People's Republic of China

Prof. Dr. Petr G. Sennikov
14.07. – 30.08.2016
RAS – Institute of Applied Physics,
Russia

Sakari Sintonen
01.02.2015 - 31.12.2016
Aalto University, Department of Micro-
and Nanosciences,
Finland

Dr. Joel Varley
18.04. - 20.04.2016
Quantum Simulations Group Materials Science Division
Lawrence Livermore National Laboratory, Livermore,
Livermore
USA

Prof. Dr. Roger Wördenweber
29.11. – 02.12.2016
Forschungszentrum Jülich, Germany

Dr. Zhang Yingwu
10.10. – 14.10.2016
China Electronics Technology Group
Corporation No. 46 Research Institute, Tianjin,
People's Republic of China

Appendix: **Colloquia at the IKZ**

Prof. Dr.-Ing. Rainer Waser
RWTH Aachen, Lehrstuhl für Werkstoffe der Elektrotechnik II und Institut für Werkstoffe der Elektrotechnik
"Review of donor-doped $SrTiO_3$ – Redox kinetics and transient processes",
February 2016

Prof. Dr. Dr. h.c. Dietrich R. T. Zahn
Technische Universität Chemnitz, AG Halbleiterphysik
"Spectroscopic Characterisation of Surfaces, Interfaces, and Low-dimensional Structures",
February 2016

Dr. Ludwig Feigl
Karlsruher Institut für Technologie (KIT),
Institut für Photonenforschung und Synchrotronstrahlung (IPS)
"Domain control in tetragonal epitaxial ferroelectric thin films",
February 2016

Dr. Daniel Rytz
Forschungsinstitut für mineralische und metallische Werkstoffe – Edelmetalle/Edelsteine GmbH (FEE), Idar Oberstein
„Kristallzüchtung am FEE (Idar-Oberstein): Yb-dotierte Laserkristalle und NLO-Kristalle für UV-Erzeugung",
April 2016

Dr. Joel B. Varley
Quantum Simulation Group, Lawrence Livermore National Lab, USA
"Characterizing doping and defects in wide band-gap semi-conducting oxides from first principles",
April 2016

Dr. Rüdiger Schmidt-Grund
Universität Leipzig, Institut für Experimentelle Physik II
"Ellipsometry: From Electronic Properties to Surface Structures",
June 2016

Prof. Dr. Darrell G. Schlom
Cornell University, Herbert Fisk Johnson Professor of Industrial Chemistry,
Department of Materials Science and Engineering, and Kavli Institute at Cornell for Nanoscale Science, USA
"Thin-Film Alchemy: Using Strain and Dimensionality to Unleash the Hidden Properties of Oxides",
July 2016

Prof. Dr. Chang-Beom Eom
University of Wisconsin-Madison, Department of Materials Science and Engineering, USA
"Oxide Nanoelectronics",
July 2016

Dr. Nicolaj Moll
IBM Zürich, Department Cognitive Computing and Computational Sciences,
Quantum Technology Group, Switzerland
"Quantum Simulations with Superconducting Qubits",
October 2016

Prof. Dr. Elias Vlieg
Radboud University, Institute for Molecules and Materials, Nijmegen, The Netherlands
IKZ-Summer Course "Towards understanding crystal growth at the atomic-scale",
October 12-14, 2016

Prof. Dr. Kozo Fujiwara
Tohoku University Sendai, Japan
"In situ observations of crystal/melt interface during directional solidification of Si",
November 2016

Prof. Dr. Christian Pettenkofer
Helmholtz-Zentrum Berlin für Materialien und Energie GmbH (HZB), Institut für Silizium-Photovoltaik
"Chalcopyrite Interfaces: From Bandstructure to Bandalignment",
November 2016

Prof. Dr. Stefan Eisebitt
Max-Born-Institut für Nichtlineare Optik und Kurzzeitspektroskopie (MBI), Berlin
„Ultrafast Spin Dynamics",
December 2016

Dipl.-Ing. Michael Knetzger
Fraunhofer-Institut für Integrierte Systeme und Bauelementetechnologie, Erlangen
"V-pits in HVPE GaN – Where they come from, and how to (possibly) deal with them...",
December 2016

Appendix: **External Funding**

International programs

Cost-reduction through material optimisation and Higher EnErgy output of solAr pHotovolatics modules – joining Europe's Research and Development efforts in support of ist PV industry; EU, 2014–2017

Short Period Superlattices for Rational (In,Ga)N (SPRInG); EU, 2015–2018

Programs of Federal Ministry of Education and Research (BMBF) and Federal Ministry of Economics and Technology (BMWi)

Erforschung des human- und ökotoxikologisch relevanten Löslichkeits- und Reaktionsverhalens von GaAs sowie verwandter Arsenide und Phosphide im Verbundprojekt TEMPO: Toxikologische, physikalisch-chemische und gesellschaftliche Erforschung innovativer Materialien und Prozesse der Optoelektronik; BMBF, 2013–2016

InTerFEL: Zeitaufgelöste und nichtlineare Infrarot- und Terahertz-Spektroskopie mit einem FEL; BMBF, 2014–2017

Entwicklung einer Nitrid-Schaumkeramik als Graphitersatz; BMWi (Zentrales Innovationsprogramm Mittelstand ZIM), 2014–2016

ENOWA II: Entwicklung hoch- und kosteneffizienter PV-Si Wafer; BMBF, 2015–2016

Entwicklung von graphitfreien keramischen Halbzeugen für die Silizium-Kristallzüchtung (CleanSi); BMWi, 2015–2017

Entwicklung einer Plasmafackel für die Abscheidung von halbleiterreinem AlN zur Herstellung von Sputtertargets (PlasNiTar2.0); BMWi, 2015–2017

Advanced UV for Life – Verbundvorhaben: AlN-Substrate; BMBF, 2015–2017

KrisNet: Entwicklung, Umsetzung und Professionalisierung eines Verwertungskonzepts am Leibniz-Institut für Kristallzüchtung; BMBF, 2015–2018

EXIST-Gründerstipendium: Innovativer Beschichtungs-Prozess-Service mit induktivem Plasma; BMWi, 2015–2016

Erforschung und Qualifizierung innovativer Lasermaterialien und -kristalle; BMBF, 2016–2018

Leibniz Association

Growth of high perfection bulk SrTi03 single crystals; 2013–2016

Silizium Granulat Eigentiegelverfahren 2016–2019

Leibniz ScienceCampus: Growth and Fundamentals of Oxides for Electronic Applications (GraFOx) 2016–2020

DFG

Lösungsmittelgenerierte Phasenumwandlung zur Erzeugung kristalliner Si-Schichten; 2011–2014

Entwicklung einer Züchtungstechnologie für semi-isolierende GaN-Substrate und Untersuchung der in-situ Kohlenstoffdotierung; 2014–2017

Lokal gewachsene Cu(In,Ga)Se2-Mikroinseln für Konzentratorsolarzellen; 2015–2018

Züchtung von Delafossit-Substratkristallen; 2016–2019

Kontrolle der Domänen in verspannten, bleifreien Alkaliniobat-Dünnschichten zur Einstellung piezoelektrischer Koeffizienten; 2016–2017

Modellbasierte Steuerung und Regelung des Vertical-Gradient-Freeze-Kristallzüchtungsprozesses mit Hilfe verteiltparametrischer Methoden; 2016–2019

Funding by partners from industry and other institutions

Growth and characterization of new oxide single crystals; CrysTec GmbH, Berlin, DE; 2005–2016

Growth and characterization of new oxide crystals for piezoelectric sensors; Kistler Instrumente AG, Winterthur, CH; 2005–2019

KILOGRAMM-3; Physikalisch-Technische Bundesanstalt, Braunschweig, DE; 2015–2019

Germanium-Kristalle für das GERDA-Experiment; Max-Planck-Institut für Physik, München; 2013–2016

Plasmaabscheidung von GaN-Bauelementen PlanB – Elektronenmikroskopische Analyse und Modellierung der Wachstums- und Relaxationsprozesse von PSD In-AlGaN-Schichten auf Saphir und Silizium Substraten; Osram Opto Semiconductors GmbH; 2014–2017

Proof of Concept – VGF-Züchtung von 4'' InP-Kristallen zur Möglichkeit der Reduzierung der Zwillingsbildung im Heizer-Magnet-Modul; Freiberger Compound Materials GmbH; 2014–2015

Leibniz-Institut für Kristallzüchtung (IKZ)
Acting Director: Prof. Dr. Günther Tränkle
Max-Born-Straße 2
12489 Berlin
Germany

Phone +49 (0)30 6392 3001
Fax +49 (0)30 6392 3003
Email cryst@ikz-berlin.de
Online www.ikz-berlin.de

Annual Report 2016

Editor: Dr. Maike Schröder
Layout & typesetting: www.typoly.de
Cover photo: Felix Peschko
Photo p.2: © Katja Bilo

Berlin, September 2017

Leibniz-Gemeinschaft

Leibniz-Institut für Kristallzüchtung (IKZ)

Max-Born-Straße 2
12489 Berlin
Germany

Phone +49 (0)30 6392 3001
Fax +49 (0)30 6392 3003
Email cryst@ikz-berlin.de

www.ikz-berlin.de